MECHANICAL PERFORMANCE CHARACTERIZATION OF MANUAL WHEELCHAIRS USING ROBOTIC WHEELCHAIR OPERATOR WITH INTERMITTENT TORQUE-BASED PROPULSION

A Dissertation
Presented to
The Academic Faculty

by

Jacob P. Misch

In Partial Fulfillment
of the Requirements for the Degree
Doctor of Philosophy (Bioengineering) in the
George W. Woodruff School of Mechanical Engineering

Georgia Institute of Technology
December 2020

MECHANICAL PERFORMANCE CHARACTERIZATION OF MANUAL WHEELCHAIRS USING ROBOTIC WHEELCHAIR OPERATOR WITH INTERMITTENT TORQUE-BASED PROPULSION

Approved by:

Dr. Stephen Sprigle, Advisor
Schools of Mechanical Engineering & Industrial Design
Georgia Institute of Technology

Dr. Sharon Sonenblum
School of Mechanical Engineering
Georgia Institute of Technology

Dr. Aldo Ferri
School of Mechanical Engineering
Georgia Institute of Technology

Ramakant Rambhatla, MBA
Vice President of Engineering
Invacare Corporation

Dr. Frank Hammond III
School of Mechanical Engineering
Georgia Institute of Technology

Date Approved: November 12, 2020

ACKNOWLEDGEMENTS

"So many of our dreams at first seem impossible, then they seem improbable, and then, when we summon the will, they soon become inevitable."

– Christopher Reeve

I'd like to formally thank my advisor, Stephen Sprigle, for his guidance on nearly every aspect of my career. Day after day, he taught me by example that intelligence and wisdom are only worth as much as the motivation that drives them. I also thank the rest of my committee – Sharon Sonenblum, Aldo Ferri, Frank Hammond III, and Ramakant Rambhatla – for their valuable insight and inspiration. This project would not have moved past the 'ideation' and 'frustration' stages without them.

I share great appreciation for my lab mates, past and present, within the Rehabilitation Engineering and Applied Research (REAR) Lab. Never before have I been surrounded by such like-minded, kind-hearted, and capable individuals. I can humbly say that the students working with me have cumulatively taught me more than I ever thought I could learn. Finally, and of paramount sincerity, the friends and family that have tirelessly supported me for years deserve unmentionable gratitude. Each success was respectfully celebrated together with joy, but perhaps more importantly, every hurdle, delay, cancellation, and rejection were met with optimism and encouragement.

My inspiration is fostered by knowing each and every one of you.

TABLE OF CONTENTS

LIST OF TABLES

LIST OF FIGURES

LIST OF SYMBOLS AND ABBREVIATIONS

MWC	Manual Wheelchair
AMPS	Anatomical Model Propulsion System
HCPCS	Healthcare Common Procedure Coding System
CMS	Centers for Medicare and Medicaid Services
DW	Drive Wheel
CW	Caster Wheel
RR	Rolling Resistance
WD	Weight Distribution over the Drive Wheel Axle
DME	Durable Medical Equipment
KE	Kinetic Energy
PWM	Pulse-Width Modulation
CoV	Coefficient of Variation
CoM	Center of Mass

SUMMARY

Manual wheelchairs are separated into discrete categories based upon characteristics of the frame. Mass is the predominant "sorting" factor between classifications, with just 6 lbs. separating the 'standard' and 'ultra-lightweight' categories. This frame mass difference can drastically change chair cost by hundreds, if not thousands, of dollars. There is an underlying assumption that mass of the chair is an indicator of performance, with lighter chairs corresponding to greater efficiency and ease of use, yet the mass of the wheelchair frame is only a small percentage of the total system mass when the occupant is considered. Furthermore, users of the lower-end chairs have limited access to higher-end component options that are locked behind these dated, weight-based coding policies that are unrelated to performance, quality, or perceived value. Usability, ease of control, and maneuverability differences between categories cannot be objectively measured using human wheelchair users as subjects due to lack of repeatability or sensitivity to explore this complex issue. Non-human testing with system-level or component-level test methods have largely overlooked the context of use by fixating on the passive behavior of the system without active propulsion.

The objective of this research is to empirically characterize the cost of wheelchair propulsion, assess performance, and identify important design trade-offs through the use of a robotic apparatus with a novel cyclic propulsion control method. The main hypothesis of this work is that the measurements taken during the controlled robotic propulsion could be used to characterize quantitative parameters to differentiate between the mechanical

performance of groups of wheelchair components or configurations, with four specific aims:

1. Design, implement, and validate a torque-based propulsion system to emulate the intermittent human propulsion cycle with the existing robotic wheelchair tester

The first aim of this research was accomplished by integrating hardware and software changes to the existing wheelchair-propelling robot, the Anatomical Model Propulsion System (AMPS). Clutch-based decoupling between the AMPS motors and the wheelchair push-rims afforded novel intermittent robotic propulsion. Motor armature current-based torque control was developed for use in the voltage-based motor controller. Profiles of wheel torque applications were generated to produce straight and curvilinear motion on each tested wheelchair. These two distinct maneuvers were chosen to highlight the most prominent energy loss sources of rolling resistance and scrub torque acting on the wheels. The torque profiles for each maneuver endowed the system with unique distributions of energy and momentum that were used to distinguish between wheelchair components and configurations.

2. Investigate the influence of small, incremental additions to the wheelchair frame mass on the over-ground propulsion characteristics of an ultra-lightweight chair

The second research aim was accomplished via successful deployment of the straight and curvilinear maneuvers with the torque-based propulsion system. An ultra-lightweight frame was fitted with weights in five discrete configurations to explore the influence of frame mass on the over-ground propulsion behavior of the chair. Propulsion cost, rectilinear distance traveled, angular (yaw) displacement, and maximum attainable

kinetic energy were recorded for each maneuver. This study demonstrated the sensitivity of the AMPS over human subject testing and identified small but distinct differences between the five loading configurations.

3. Improve the propulsion characteristics of a representative high-strength lightweight wheelchair by utilizing existing component-level test results

The third research aim was accomplished by utilizing knowledge of common wheelchair component performances over interior flooring surfaces. An ordinary high-strength lightweight chair was loaded with the AMPS and tested with its manufacturer-default drive wheels and casters. These components were traded out for up-charged variants totaling less than $100 USD and the system was re-tested. This study clearly shows how impactful the choice of tire can be to the over-ground behavior of the wheelchair. The relatively inexpensive components greatly improved each outcome variable over both tested surfaces. These results are useful to clinicians and manufacturers to improve the prescription process and provide the best possible configuration to the user, regardless of wheelchair category.

4. Characterize the mechanical performance differences between representative folding and rigid ultra-lightweight frames

The fourth and final research aim was accomplished by deploying the AMPS maneuvers on a small selection of rigid and folding ultra-lightweight wheelchairs. Three of each frame style were tested and averaged together to generalize the impact of the frame type. No generalizable trends were present due to the relative equivalence of the mechanical performances and the narrow band of performances between all tested chairs.

This study quantified the trade-off, or lack thereof, between the frame types. The portability and rigidity of different frame types can reliably be left to the preference of the wheelchair user without any noticeable disadvantage in the energetic profile of the chair.

These outcomes provide insight to the mechanics of the system that were previously under-studied or confounded by variabilities within human subject testing. Mechanical testing with the AMPS definitively identifies differences between wheelchair configurations by means of repeatable, reliable, and controlled propulsion tests. The defined metric of propulsion cost numerically represents the energetic requirements of propelling each chair a given distance, with direct relevance to manufacturers, clinicians, and wheelchair users alike. Ultimately, these outcomes will inform clinicians and manufacturers about how configuration choices influence propulsive efforts, which can be used in turn to improve their classification techniques and generally improve their existing design processes. This knowledge empowers the wheelchair user to make informed choices in wheelchair selection based on objective mechanical performance metrics.

CHAPTER 1. INTRODUCTION

Manual wheelchairs serve multiple purposes for the user. Mobility, independence, postural support, and safety all need to be balanced for a wheelchair to become a functional extension of the user. Naturally, the process of manual wheelchair design involves a series of tradeoffs: comfort versus support, efficiency versus function, and cost versus performance. Ease of control and maneuverability are dictated by the mechanical efficiency of the vehicle; less efficient chairs require greater physical exertion with repetitive and intense loads on the upper extremities, which can ultimately lead to injuries from overuse. Essentially, mechanical efficiency is reflective of the energetic propulsion effort required from the user to travel over-ground against frictional and inertial resistances. The system resistance to motion can be improved by tuning the wheelchair, yet the 'optimal' wheel or frame choice is often unclear. Furthermore, users have limited access to higher-end component options that are locked behind dated coding policies. Financial coverage, as defined by Medicare, dictates that modern wheelchairs designs adhere to unempirical weight requirements of the wheelchair frames, and are unrelated to performance, quality, or perceived value.

To fill in the gap between manual wheelchair designs and expenses, this research is designed to analyze the impact of various configurations and components on the mechanical performance characteristics of manual wheelchairs. The research will emulate real-world use of each wheelchair through the use of a robotic apparatus with a novel cyclic propulsion control method. Data collected on the resulting motion of each wheelchair will be used to empirically characterize the cost of wheelchair propulsion and assess system-

level mechanical performance of each tested wheelchair configuration. Ultimately, this research will help clinicians and manufacturers understand how certain configuration options influence propulsive efforts, and empower wheelchair users with knowledge to make more informed design choices when selecting their manual wheelchairs.

1.1 Wheelchair Usage and Coding

In 2010, 3.6 million people above the age of 15 used a wheelchair in the U.S., and an additional 11.6 million used other ambulatory aids, according to the U.S. Census [1]. This number of wheelchair users increased to 5.5 million by 2014 [2]. By definition, a manual wheelchair (MWC) is a seat supported by wheels that is used as a mobility aid when walking is impaired by aging, illness, injury, or disability. The most common wheelchair type features two large drive wheels attached under the user and two small caster wheels located under the footrest. The manual wheelchair serves as a means of independent transportation and provides physical support during activities of daily living, which enables the users to participate in societal and vocational activities [3-6]. Movement is initiated by applying a forward-directed force on each drive wheel via the attached push-rim. The resulting torque about the wheel has to be used by the wheelchair to overcome frictional and inertial resistance to the motion before it can impart changes to the velocity of the chair. However, since MWC propulsion has an inherent mechanical efficiency of < 10% [7-10] and bouts of MWC mobility are typically short and slow [3, 4], users have to frequently supply large start-up torques to overcome these frictional and inertial resistances to motion [11]. A combination of these factors, alongside the navigation of various environmental conditions such as surface types and angles of incline, lead to increased

propulsion efforts. As a result, this repetitive and demanding propulsion cycle can culminate in pain [12, 13] and injuries [14-16] to the upper extremities.

To date, there are several ways to mitigate the risk of injury. First, one can change the propulsion mechanism to something more biomechanically suited to the human body, though this can cause unintended complications as it is even less efficient than the standard wheelchair push-rim mechanism. Second, multitudes of studies have shown that the wheelchair configuration itself significantly impacts the energetic effort of the user [17-22]. The user-to-seat interface may be adjusted [23]. Finally, users may just require practice with the chair, as more experience with propelling has high correlation with reduced energetic effort to maneuver the chair [24, 25].

1.1.1 Wheelchair Categorization

Reimbursement for durable medical equipment (DME) falls under the control of the Healthcare Common Procedure Coding System (HCPCS). Manual wheelchairs have been categorized into the 'temporary' K-series of codes, which have been largely unchanged since 1993 [26] and are largely non-descript: any MWC between 34 - 36 lbs is classified as a 'lightweight' (K0003) chair, followed by the range from 30 - 34 lbs as an 'high-strength lightweight' (K0004) chair, and under 30 lbs as an 'ultra-lightweight' (K0005) chair. A handful of additional features, such as an adjustable drive wheel axle position, are also distinct features of the higher-end K0005 classification. These features are vital to perfect the 'fit' of each user to the chair as users and clinicians can attest, to the point where there are reference guides on how to justify the apparent necessity of a K0005 prescription to a patient's funding source [27].

Table 1: HCPCS-assigned medical reimbursement codes for manual wheelchairs.

HCPCS Code	Description	Seat Height (inch)	Weight Capacity (lbs)	Warranty	MWC Weight (lbs)	Other Features
K0001	Standard	> 19	≤ 250	n/a	> 36	n/a
K0002	Standard Hemi	< 19	≤ 250	n/a	> 36	n/a
K0003	Lightweight	n/a	≤ 250	n/a	34 – 36	n/a
K0004	High-Strength Lightweight	n/a	n/a	Lifetime (frame)	30 – 34	n/a
K0005	Ultra-lightweight	n/a	n/a	Lifetime (frame)	≤ 30	Adjustable rear axle position

Local coverage determination for MWCs, as published by the Centers for Medicare and Medicaid Services, only briefly elaborates on the functional requirements needed for prescription of each type of chair [26]:

- K0001 - Limited mobility that cannot be overcome with use of a cane, walker, crutch, etc.
- K0002 – User requires lower seat height to use feet to propel
- K0003 – Cannot self-propel in K0001-02 in home, but can in K0003
- K0004 – Requires functionality (tied to activities of daily living), independent mobility, and / or sizing that cannot be accommodated in K0001-03
- K0005 – Full-time user, requires customized fitting that cannot be accommodated in lower categories

The chairs that populate each category can be disparate in terms of component material, objective quality, and manufacturing techniques, yet are treated as equivalents. The established DME coding protocol has no method to distinguish differences in the functional performance of MWCs and therefore fails to accurately address the needs of the community.

1.2 Methods of Wheelchair Testing

A substantial body of work in this research has been developed around the need to improve manual wheelchair mobility, with goals of reducing the risk of upper extremity injuries [14, 28, 29] and facilitating increased independence and community participation [30]. There are many possible approaches to collecting data on the performance of the MWC. The most common approach is to study the biomechanics of the human component of the propulsion, specifically the 'effort' or biomechanical exertion of the human user whilst propelling the wheelchair. This is typically done by measuring the MWC user's metabolic cost to assess items such as differences between frame types [31], propulsive stroke techniques [32], or mass and tire conditions [33, 34]. However, current methods of measuring metabolic costs are sub-optimal. The majority of these studies use simulated settings such as a treadmill which provide limited insight to real-world wheelchair use over common flooring surfaces. Sonenblum's work reports that real-world MWC use is in much shorter bouts [3] than a prolonged treadmill test. Multiple authors have expressed skepticism in extrapolating results from treadmills or dynamometers to over-ground settings [35, 36]. Furthermore, studies measuring metabolic effort have largely lacked sensitivity [34, 37] to the configuration changes of interest, hindering the generalizability of the results to inform clinical decision-making. A large part of this knowledge gap stems

from a lack of understanding in the relative contributions of the human user's biomechanical effort and the wheelchair's mechanical propulsion cost to the resulting motion [38].

Given the overwhelming diversity in human users and their unique propulsion biomechanics in different wheelchairs, the most efficient path is to first focus on developing standardized and representative measurements of the wheelchairs' mechanical propulsion cost. Isolating the wheelchair performance from the inherently high-loss human biomechanics offers a standardized measurement of the mechanical system's maximum efficiency capabilities, which provides valuable information for clinicians and users during wheelchair selection, and informs researchers how propulsion effort can be impacted by the overall mechanical design of the vehicle.

1.2.1 Component-Level Testing

Component-level testing is typically comprised of simple methodologies that quantify the resistive forces or losses associated with wheelchair drive wheels and/or casters, as well as key components that are widely considered the largest source of energy loss as described by Schuring [39], Pacejka [40], and Hofstad [41], among others [42, 43]. Researchers have pointedly studied frictional energy loss of the wheels to identify areas of improvement for MWC configuration and design. The rolling resistances of drive wheels have been directly measured using ramp coast-downs [44], treadmills [44, 45], and rollers [46]. Furthermore, Frank and Abel studied the impacts of caster size and shape on the caster rolling resistance [44]. In the same study, they also created a rotational scrub testing rib to investigate the turning resistance torque of each caster. Gordon, Kauzlarich, and Thacker

have also studied characteristics of caster and drive wheels including rolling resistance, static friction, and spring rate [45, 47, 48], which built a strong empirical foundation for the significance of component-specific test procedures.

Other methods include coast-down tests to study wheel styles, wheelchair mass and mass distribution, and tire inflation pressures [49, 50], as well as measuring swiveling resistance of drive wheels using a varying-radius load arm [51]. More recently, Silva has developed a benchtop methodology to characterize drive wheel corning forces that occur during combined rolling and turning, with various slip and camber angles [52]. Component-level tests are repeatable and offer a valid means to compare different components. However, they often cannot capture the complex interactions that take place at the system-level during over-ground maneuvering, which limits their direct clinical relevance.

1.2.2 System-Level Testing

Systems-level tests of MWC propulsion characteristics and energy losses expand on component testing to permit assessment of various wheelchair configurations in more realistic usage conditions. These include tests both with and without human operators. Systems-level testing with human operators has been dominated by focus on steady-state velocity often using treadmills and rollers [24, 29, 33, 37, 53, 54], which are not well positioned to assess the propulsion effort required to maneuver a wheelchair over-ground. Tests using human operators during over-ground maneuvers offer a much more realistic representation of propulsion forces and effort, as the system is endowed with changes in momentum and travels over common surface types. These studies have assessed the impact

of different surfaces [11, 55, 56], wheelchair mass [34, 55], weight distribution or axle position [55, 57, 58], and push forces at different speeds [59, 60]. Human-operated wheelchair performance has been assessed with a variety of techniques, many of which involve outfitting the human user with instrumentation to measure oxygen consumption [23, 33, 34, 61], kinetics of the body during motion [19, 54, 62, 63], propulsion cycle characteristics such as stroke patterns and stroke frequency [11, 57, 59, 61, 64, 65], and, more subjectively, perceived exertion [33, 34, 61]. In several of these studies, heavy instrumented push-rims were equipped to the test wheelchair. These wheels, though useful at capturing torques applied to each push-rim, added between 2 kg to 4 kg per side. This added weight naturally influences the inertial and frictional parameters of the wheelchair and has been reported to increase the rolling resistance. Therefore, claiming that propulsion kinetics are distinctly caused by the variables measured in the aforementioned studies may not be accurate with the confounding impact of the instrumented wheels [66].

Systems-level research without human operators affords a unique opportunity to investigate the mechanical behavior and performance of the vehicle with repeatable, reliable, and systematic methodologies. In 2004, Sawatzky used an inclined coast-down test to observe the impacts of various drive wheel styles and inflation pressures on the system-level rolling resistance of a lightweight wheelchair [49]. Similarly, to determine the system resistance to motion, Van der Woude measured the magnitude of external force applied to handlebars behind the seat that was required to roll wheelchairs at different constant speeds across multiple surfaces [56]. Systems-level testing, to date, has often been constrained to straight and steady-state conditions that lack representation in real-world wheelchair mobility [3], though there are a few notable exceptions. For example, Sauret

and Bascou measured the field rolling resistance of loaded MWCs using methods inspired by component test protocols [67]. By utilizing the actual MWC instead of a cart or test rig, they had the ability to expand into curvilinear coast-down tests and assess the turning resistances of various configurations [68]. Other examples include Lin's curvilinear coast-down testing [50] and Sprigle and Huang's wheelchair-propelling robot used to identify differences in propulsion torque to accelerate different MWCs [69]. These systems-level methodologies measure under discrete and curvilinear maneuver conditions but utilize complex, customized testbeds that are not easily reproducible [69].

1.2.3 Advanced Model Testing

The reviewed literature above suggests that MWC testing needs an objective mechanical performance assessment system to separate the human propulsion biomechanics from the vehicular mechanics. Measurements from human users are understandably married to the limitations and inefficiencies of the musculoskeletal system. Though it would be possible to objectively test MWCs with human users, the level of control and throughput needed to build a catalog of results would be exhaustive, and the repetition would be potentially harmful to the subjects. Component-level testing has experienced a surge of progress in recent years and will continue to grow its capabilities, but is not yet to a level where results can be directly translated into clinically-relevant outcomes. Rolling resistance force values or resistive scrub torque values of wheels can help differentiate between ‘good’ and ‘bad’ wheels for each test surface, but there is no direct connection between those values and what the human user will experience.

One solution to this is the use of the robotic MWC testing apparatus developed by Liles, Huang and Sprigle [69-71]. In this research, the proposed 'propulsion cost' metric [71] is analogous to the energetic effort exerted by human operators to propel the chair, without the complexity and confounders associated with metabolic cost differences between users. One single operator, immune to fatigue and capable of propelling thousands of times with mechanically identical propulsion characteristics, would be the most ideal experimental apparatus to differentiate between wheelchairs, especially in cases where the differences between chairs may be too subtle for a human subject to detect in 15-minute test sessions.

CHAPTER 2. SPECIFIC AIMS

The main hypothesis of this work is that an instrumented robotic propulsion device is capable of operating a manual wheelchair with torque profiles analogous to a human operator, and that the measurements taken during the driven motion could be used to characterize quantitative parameters that can differentiate between the mechanical performance of groups of wheelchair components or configurations. This hypothesis has been tested in separate studies with the following specific aims:

2.1 Development and Assessment of Intermittent, Torque-Based Propulsion Using Robotic Testbed

The pre-existing robotic testbed controlled the velocity of the motor-driven wheelchair wheels and measured the torque applied to each push-rim. The hardware, including the circuitry and interface configurations between the wheels and the robot, were redesigned to accommodate an intermittent propulsion behavior in the style of successive 'push' and 'coast' phases, much like the 'push' and 'recovery' phases of human wheelchair propulsion. Corresponding software changes were made to the user interface and the motor controller to utilize the magnitude of torque applied to each wheel as feedback. The resulting 'torque mode' controller was tuned and assessed through stationary torque measurements and over-ground propulsion trials. Finally, one parametric over-ground maneuver was established as proof of feasibility of the system. This straight-forward trajectory highlighted energy loss in the wheelchair from the casters and drive wheels. The generated torque profile closely resembled the torque applications and corresponding over-ground motion of human wheelchair operators in standard conditions.

2.2 Investigation of the Effects of Incremental Mass Additions on Ultra-Lightweight (K0005) Manual Wheelchair Propulsion

An underlying construct established by the HCPCS coding system is that wheelchair frame mass is indicative of performance, with wheelchair frame mass as the major factor separating the five main categories of manual wheelchairs. To objectively explore this point, the robotic testbed was used to evaluate the behavior of an ultra-lightweight wheelchair frame loaded with incremental mass additions of up to 4 kg. Torque profiles were generated for two maneuvers, straight and slalom, to assess the energy losses of the system in rectilinear and curvilinear motion. Wheelchair performance was assessed through measurement of total distance traveled, angular heading direction changes, maximum achievable kinetic energy, and the energetic cost of propulsion for each maneuver. Data was further examined with equivalence tests designed to compare the outcomes for each loading configuration. Equivalence intervals were informed by the literature from similar human-based wheelchair propulsion metrics.

2.3 Improvement of the High-Strength Lightweight (K0004) Manual Wheelchair Baseline Configuration with Component Selection

This study investigated the system-level effects of swapping out components (drive wheels and casters) based on results from energy loss testing at the component-level. To assess relative improvements or detriments compared to the default wheelchair configuration, this study utilized the robotic testbed to measure the performance of an 'off-the-shelf' K0004 chair with its standard wheels and casters. Three other configurations were measured using the same K0004 frame: standard drive wheels swapped with an 'up-

charged' tire variant, costing $50 per pair; standard casters swapped with 'up-charged' variants, costing $50 per pair; drive wheels and casters both swapped to their 'up-charged' variants. These four configurations were propelled with a straight and slalom maneuver over linoleum tile and low-pile carpet. Performance for each maneuver was assessed through measurement of distance, yaw, maximum achievable kinetic energy, and the energetic cost of propulsion of each configuration. These data were analyzed with ANOVA and non-inferiority tests.

2.4 Comparison of Performance Between Folding and Rigid Ultra-Lightweight (K0005) Manual Wheelchair Frames

Six frames were tested with the robotic propulsion system across linoleum tile in the straight and the slalom maneuver. Three of these frames had solid rear wheel axles rigidly fixed to the frame. The other three frames contained a folding mechanism to collapse the frame for storage and transport. The six frames were configured to the same seat height, dump angle, and weight distribution. A standardized selection of drive wheels and casters were used on each frame. Performance outcomes of distance, yaw, kinetic energy, and energetic cost of propulsion were assessed per maneuver for each configuration, as well as assessment via ANOVA and equivalence for the collection of folding and rigid frames.

2.5 Broader Impacts

These specific aims address the issues in current standards of wheelchair testing and categorization. The creation of a robotic wheelchair operator with repeatable, reliable, and configurable propulsion characteristics has been used to remove the direct influence of

human biomechanics and the variability therein from analyses of wheelchair performance. This was especially useful in cases where human wheelchair users have demonstrated difficulties maintaining repeatability or sensitivity to the parameters of interest, such as the mass of a wheelchair frame. The three study-based specific aims utilized this robotic wheelchair testbed to answer long-standing questions about the mechanical performance of wheelchair frames that have been obscured, disputed, or overlooked by leaders in the field, whether due to difficulties isolating the parameters or controlling for subject variability. Examining the impact of frame mass in an objective, repeatable format provides data to base improvements to the predominantly weight-based HCPCS medical reimbursement policies. Improvements to these categorical definitions may expand available wheelchair options to individuals in need of better chairs without the current means to obtain them. Furthermore, the improvements to the performance of a K0004 chair with the simple substitution of drive wheels or casters is a demonstrative examination of simple, inexpensive factors that can greatly revitalize inefficient chairs. This study provides scientific evidence to encourage manufacturers and clinicians to provide better default options to the end-user. Additionally, these results will help inform general wheelchair users that they may, in many situations, be less than $100 away from a significantly better configuration. Finally, the robotic examination of folding and rigid frame types provides valuable insight into one of the main design choices involved with selecting an ultra-lightweight frame. Folding frames imply portability and ease of storage compared to a traditional rigid frame, with some assumption that there is a trade-off between the frame types. Yet, with the prestige of the K0005 category, there are implications that both frame styles have equivalent performance. Clinicians, manufacturers, and especially the users

have every right to know if their frame type selection comes down to pure preference, or if it carries a trade-off on their over-ground performance.

Wheelchair selection (and design, in general) follows a series of compromises. These research aims have identified three of the major tradeoffs in the decision process for long-term or full-time wheelchair users. With the optimism of the phrase ‘knowledge is power’, these studies were conducted and are reported with every intention of further improving the health and quality of life of manual wheelchair users.

CHAPTER 3. ANATOMICAL MODEL PROPULSION SYSTEM

The Anatomical Model Propulsion System (AMPS) is a robotic wheelchair assessment device created within the Rehabilitation Engineering and Applied Research Laboratory. Its primary purpose is to operate MWCs with controlled, repeatable, and reliable propulsion in predefined over-ground maneuvers.

3.1 System Overview

The AMPS was designed as an expandable testbed for wheelchair testing. It features three main subsystems: (1) anthropomorphic skeletal aluminum construction; (2) propulsion system; (3) data acquisition system [70].

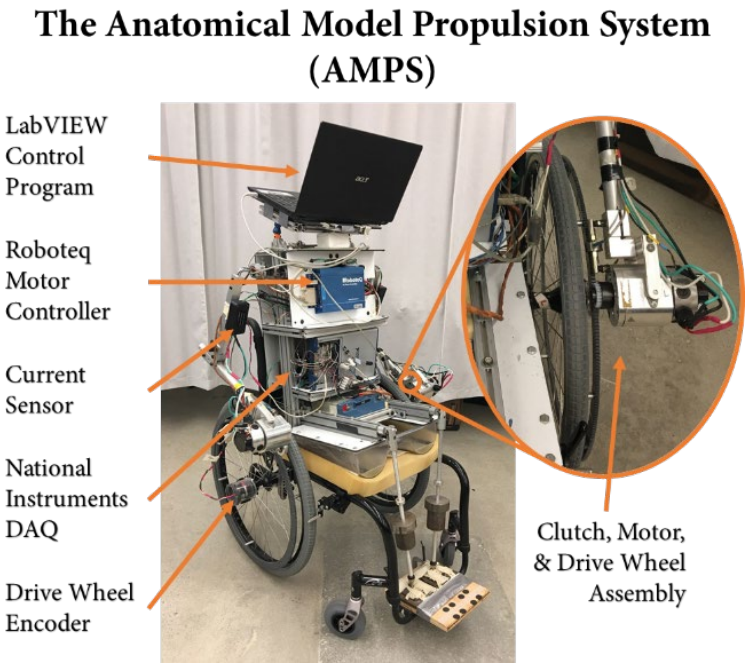

Figure 1: Overview of the AMPS subsystems.

3.1.1 Anthropomorphic Structure

The skeletal anthropomorphic structure intentionally resembles an abstracted human wheelchair user to replicate the loading on the wheels, frame, and bearings of an occupied wheelchair. The size of the AMPS were designed to be consistent with average body segment parameters of an American male at the 50th percentile in height [72, 73]. Total system weight, nominally at the 95th percentile of an American male, was originally based on the standardized 100 kg wheelchair test dummy specified in ISO 7176-11 [74]. The weights were reconfigured to a mass of 80 kg to match more closely with the 50th percentile of American male masses. The aluminum frame of the torso houses the batteries and electronics of the system, serving as the bulk of the weight of the mechanical body. Arms are connected to the torso via aluminum ball-and-socket joints to adjust alignment of each arm to the drive wheels. The elbow joints are likewise adjustable as a locking pin joint. The lower body comprises a hollow plastic buttocks mold with removable metal bar weights, and two aluminum rods representing the lower legs with attached metal feet. Removable split-collar weights are fixed to the aluminum rods to mimic the mass and general distribution of weight along the shank. Collectively, the adjustability of each sub-system of the AMPS offers unparalleled control over the total system mass and mass distribution of the occupied wheelchair.

Table 2. Body segment parameters used to inform the design of the AMPS.

	Body Segment Parameter	Referenced Value	Source
Segment Mass	Torso (head, arms, trunk)	61 (± 3) kg	ISO 7176-11: Test Dummies [74]
	Upper Legs (thighs, pelvic region)	31 (± 3) kg	
	Lower Legs (shanks, feet)	7 (± 1) kg	
	Total	100 (+5 / -2) kg	
Center of Mass	Trunk (fore-aft)	68 (± 10) mm	
	Trunk (vertical)	298 (± 10) mm	
	Upper Legs (fore-aft)	203 (± 10) mm	
	Upper Legs (vertical)	67 (± 10) mm	
	Lower Legs (vertical, from foot)	235 (± 3) mm	
Segment Lengths	Seated Shoulder Height (from seat)	561 (± 0) mm	Hybrid III (50th %ile Male) Dummy [72]
	Shoulder Breadth	455 (± 0) mm	CAESAR Database [73]
	Buttock to Knee	550 (± 0) mm	Hybrid III (50th %ile Male) Dummy [72]
	Knee Pivot Height (from floor)	498 (± 0) mm	
	Hip Breadth	414 (± 0) mm	CAESAR Database [73]

3.1.2 Propulsion System

The propulsion system utilizes custom hardware to emulate human propulsion forces applied to the drive wheel push-rims. Modifications to the wheelchair itself are minimal – the most drastic change is replacing the traditional cylindrical push-rim with a custom-made PVC ring gear. Each arm positions a motor 'hand' to the push-rim of the drive wheel at approximately the location where peak tangential forces are applied in human kinetic studies (40° forward from the top of the wheel) [75]. The 20-tooth pinion gear of the motor meshes with the teeth of the 340-tooth ring gear (Figure 2). As the ring gear and pinion gear are aligned within the same plane, the rotation of the motor causes a tangential force to act on the ring gear push-rim. This tangential force can be configured to

match the general force application of the average human user. The axial and radial forces applied by human users during the propulsion cycle [76, 77], however, are not replicated by the AMPS, as the motor itself does not move in relation to the push-rim.

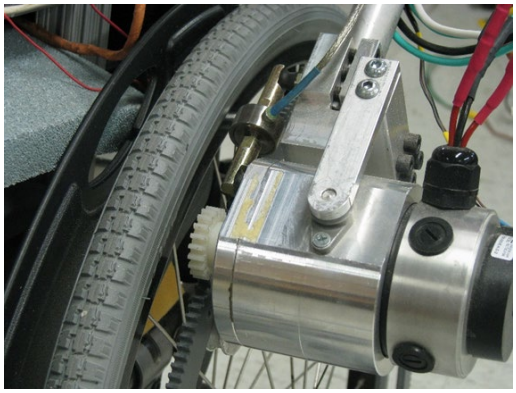

Figure 2: Motor 'hand' with shaft-mounted pinion gear and ring gear push-rim.

Typical torques applied by human operators on the push-rim vary based on travel speed [75], surface material [11, 55, 62], and incline. Literature suggests that steady-state propulsion at speeds of less than 1 m/s across smooth, flat surfaces necessitate an average of 81 N of tangential force, up to 100 N of force at start-up [75]. This translates to around 30 Nm of torque applied to the push-rim, which would be an excessive amount of torque from a small, lightweight motor. To accommodate for this, the tooth ratio between the motor pinion gear and the push-rim ring gear was set at 1:17 to act as a speed reducer and torque multiplier for the motor.

A pair of high-power brushed DC motors were selected (AmpFlow A28-150, Powerhouse Engineering, Inc.) based on the speed and torque requirements in combination with their small size factor. Brushed DC motors commonly feature high speed and torque outputs, as well as ease of control: the motor armature voltage correlates proportionally to the velocity output of the motor shaft. The most common motor controllers for brushed DC

motors use pulse-width modulation (PWM), or rapid gating of the output voltage to effectively deliver a prescribed percentage of total voltage.

The laptop positioned at the 'head' of the AMPS acts as a high-level central command interface for the system. A custom LabVIEW script (LabVIEW 2019, National Instruments Corp.) generates a velocity trajectory for each motor. These commands are sent out via the analog input/output ports on the data acquisition board (NI USB-6341, National Instruments Corp.) to the command input channels on the motor controller (RoboteQ HDC-2450, Nidec Motor Corporation) as analog voltage signals between 0 V and 5 V, with 2.5 V being the zero-point representing the motors at idle. The controller, fed by four individual 12 V SLA batteries, supplies each motor with separate channels of 24 V with 50 A of available current. Tunable parameters within the built-in motor controller interface (proportional gain K_p, integral gain K_i, derivative gain K_d) allow for customization of the proportional-integral-derivative (PID) control loop. The block diagram for the velocity-controlled system is shown in Figure 3.

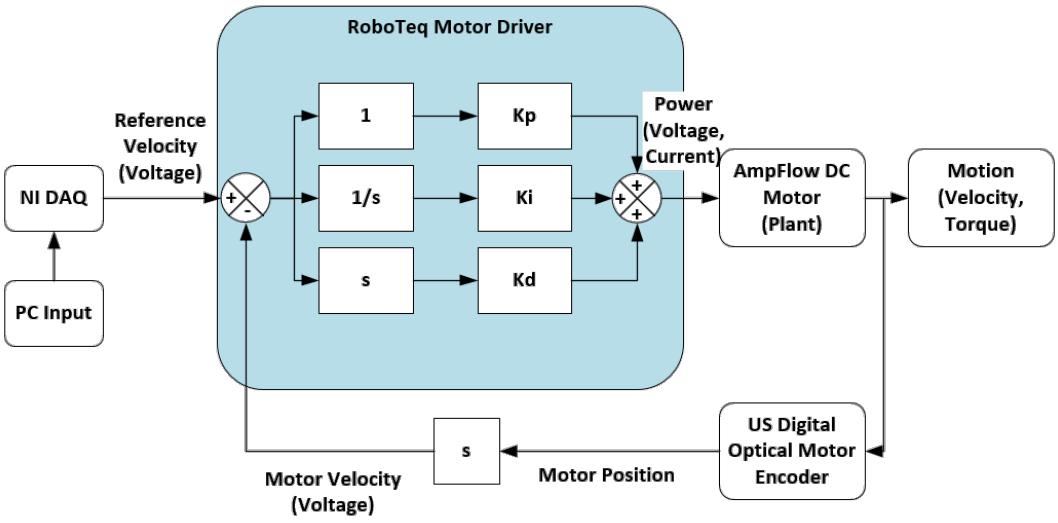

Figure 3: Control diagram for original velocity-control of AMPS motors.

The feedback to the system, rotational speeds of each motor, are measured with shaft-mounted optical encoders on each motor (Model E3, US Digital Corp.), at a resolution of 2500 counts per revolution. Performance of the controller was assessed by its ability to consistently match target motor velocities when propelling the wheelchair. Standard errors of the mean (SEMs) were ≤ 0.01 rad/s, and coefficients of variation (CoVs) of the wheel velocities were ≤ 2% for the left and right wheels at two separate target velocities [70].

3.1.3 Data Acquisition

Multiple sensors are integrated into the various subsystems of the AMPS. Motor commands, as voltage from the controller to the motor, run through passive voltage divider boards (P/N 1121, Phidgets Inc.). Similarly, the currents flowing to each motor are monitored by Hall Effect-based current sensor chips (ACS758xCB, Allegro MicroSystems, Inc.) on each arm. Wheel rotations are measured with hub-mounted encoders (Accu-Coder Model 260, Encoder Products Co.) fixed to the ends of the ½”-

diameter quick-release drive wheel axles, which have a resolution of 2540-count per revolution. Button-style load cells (LCFA-50, Omega Engineering, Inc.) are attached as the main interface between the motors and the arms, directly in alignment with the motor pinion gear, which record the tangential force transmitted to the push-rim of each side of the wheelchair. Each of these sensor signals are read by the centralized data acquisition board at a sampling rate of 40 Hz.

3.1.4 Data Processing and Analysis

Each channel of data (load cell force, supplied motor current, commanded motor voltage, wheel velocity) are post-processed in MATLAB (R2016b / R2019b, The MathWorks, Inc.) with a 3rd-order Butterworth filter designed with a cutoff frequency of 0.15 Hz to smooth over any high-frequency noise in the circuit. An example of the pre- and post-processed wheel velocity signals is shown in Figure 4.

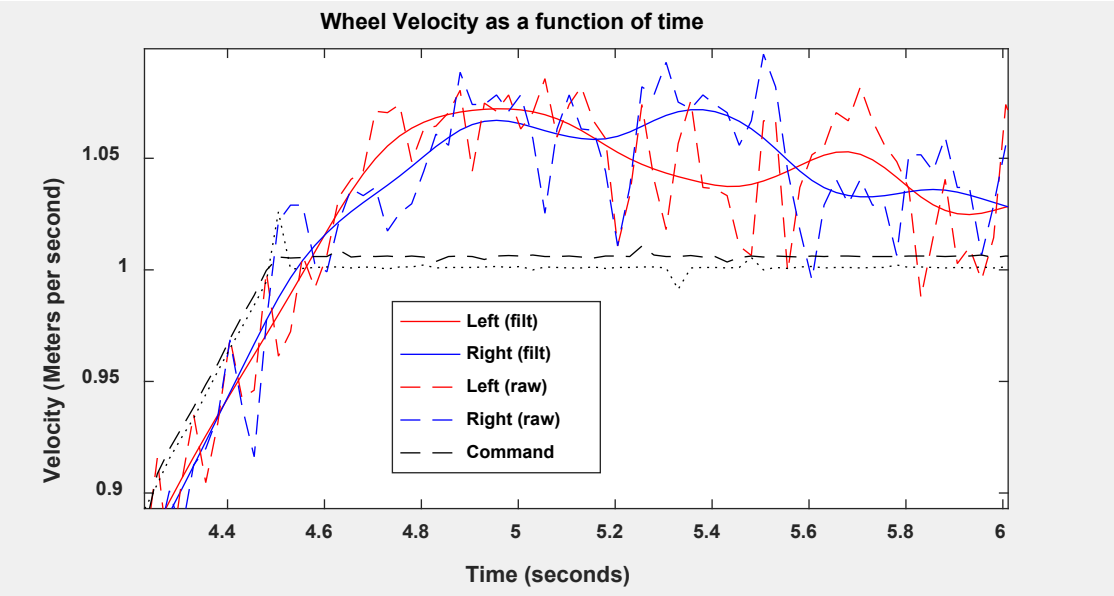

Figure 4: Detailed view of the signal pre- and post-Butterworth filter.

Filtered drive wheel velocities are and used in conjunction with measured geometry of the wheelchair frame to calculate the system kinematics and overall system kinetic energies [78] with the following equations:

$$KE_{translational} = \frac{1}{2} m_{sys} {v_G}^2 \tag{1}$$

$$KE_{turning} = \frac{1}{2} I^G_{ZZ,sys} \dot{\Psi}^2_{frame} + \frac{1}{2} I_{ZZ,LFLC} \dot{\Psi}^2_{LC} + \frac{1}{2} I_{ZZ,RFRC} \dot{\Psi}^2_{RC} \tag{2}$$

$$KE_{rotational} = \frac{1}{2} I_{YY,LD} \dot{\phi}^2_{LD} + \frac{1}{2} I_{YY,RD} \dot{\phi}^2_{RD} + \frac{1}{2} I_{YY,LC} \dot{\phi}^2_{LC} + \frac{1}{2} I_{YY,RC} \dot{\phi}^2_{RC} \tag{3}$$

$$KE_{total} = KE_{translational} + KE_{turning} + KE_{rotational} \tag{4}$$

m_{sys} represents the mass of the combined AMPS and wheelchair. I_{YY} and I_{ZZ} represent the rotational (yaw) and rotational (roll) inertias of the components, respectively. These terms are shown in the top-down schematic of a generalized MWC system (Figure 5). The motion of the drive wheels (*LD, RD*) and basic MWC geometry define the other terms.

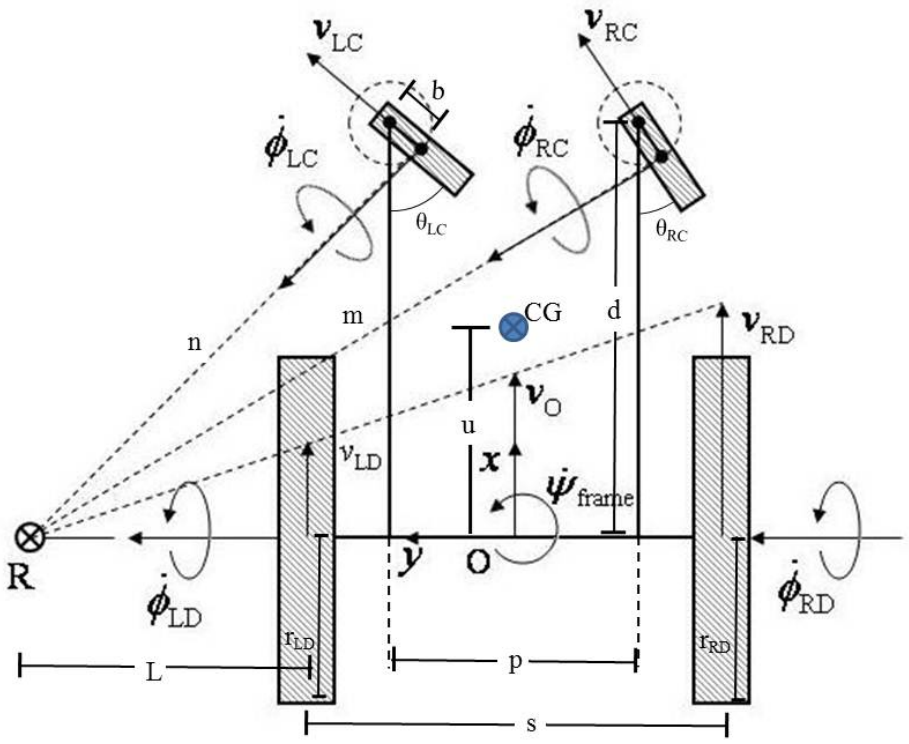

$\dot{\boldsymbol{\phi}} - Rotation\ (roll)\ rate;\ \dot{\boldsymbol{\psi}} - Rotation\ (yaw)\ rate;\ \boldsymbol{v} - Linear\ velocity;$

$\boldsymbol{s} - wheel\ center\ to\ center\ distance;\ \boldsymbol{p} - caster\ stem\ to\ stem\ distance;$

$\boldsymbol{u} - center\ of\ mass\ to\ drive\ wheel\ axle\ distance$

Figure 5: Top-down schematic of MWC used to derive system kinematics from drive wheel rotation, from [78].

The mass and inertia of the combined AMPS and MWC were measured with the iMachine, an inertial measurement device designed in the Rehabilitation Engineering and Applied Research Laboratory specifically for measuring occupied wheelchairs [79]. Rotational inertias of the smaller components (casters with and without forks, drive wheels) were measured instead with a trifilar pendulum method [80].

The main outcome variable from an over-ground trial with the AMPS is the cost of propulsion throughout the maneuver. Propulsion cost can be defined as the cumulative work put into the system over the displacement travelled by the center of mass. The theory behind this analysis is the fundamental work-energy principle, which states that the quantity of work supplied to a body or system must equal a corresponding change in the energy contained in the system. Theoretically, this would mean that each Joule of energy supplied by the motors would result in a summed combination of rotational, translational, and yaw-based turning kinetic energies of the system, as well as any potential energies contained within the system after climbing an elevated slope or from any stretched elastic components. In application, however, the AMPS is exposed to many non-conservative forces that consume portions of the applied work. Energy is lost at the contact points between casters, drive wheels, and the surface of the floor due to rolling resistance forces and resistive scrub torques [50, 81]. The adjusted equation for the work-energy relationship must therefore include a term representing the sum of any supplied energy that was not converted into motion. The amount of work, in Joules, can then be represented as the sum of the change in kinetic energy and the magnitude of energy lost:

$$Work_{in} = \Delta KE + E_{loss} \tag{5}$$

Work can also be expressed as the integral of the power supplied to the system over the time duration, from initial time t_i to final time t_f, of the maneuver. Mathematically, this can be written as:

$$Work_{in} = \int_{t_i}^{t_f} Power_{in}(t) \cdot dt \tag{6}$$

With respect to both the AMPS and human wheelchair operators, the source of work supplied to the wheelchair occurs at the push-rims. The rotational power, in Watts, is the product of the torque at the wheel (in Nm) and the angular velocity of the wheel in radians per second. The total power the AMPS supplies to the wheelchair is the summation of the rotational power applied to the left and the right wheels:

$$\begin{aligned} Power_{in} = &\left(\tau_{motor,l} \cdot \frac{N_{ring\ gear}}{N_{pinion}} \cdot \omega_{wheel,l}\right) \\ &+ \left(\tau_{motor,r} \cdot \frac{N_{ring\ gear}}{N_{pinion}} \cdot \omega_{wheel,r}\right) \end{aligned} \tag{7}$$

The power calculation cannot use the value of the torque at the wheel, τ_{wheel}, directly because is not measured by any of the instrumentation. It must be calculated from the measured torque at the motor multiplied by the 17:1 speed-reduction gear ratio, denoted by the fraction of the number of teeth N on the ring gear push-rim and the clutch-mounted pinion gear. The total supplied power is integrated over the maneuver duration to yield the total work supplied to the wheelchair, and propulsion cost is calculated by:

$$Propulsion\ Cost = \frac{Work_{total}}{\Delta s} \tag{8}$$

The numerator, $Work_{total}$, is the cumulative work supplied to the wheelchair by the AMPS. It is equivalent to the value calculated by Eqn. 6 when the t_i is set to 0 seconds (the beginning of the maneuver) and the t_f value is set to the final timestamp in the maneuver. The denominator for a rectilinear or almost any curvilinear maneuver is the distance travelled by the center of mass, Δs, in meters. For turning maneuvers such as a zero-radius turn, Δs could be substituted with $\Delta \psi$, the cumulative angular travel about the axis of rotation of the maneuver, in radians [71]. For a standard maneuver driving the wheelchair in a straight forward motion, the sensor signals would yield data such as the representative plots seen in Figure 6.

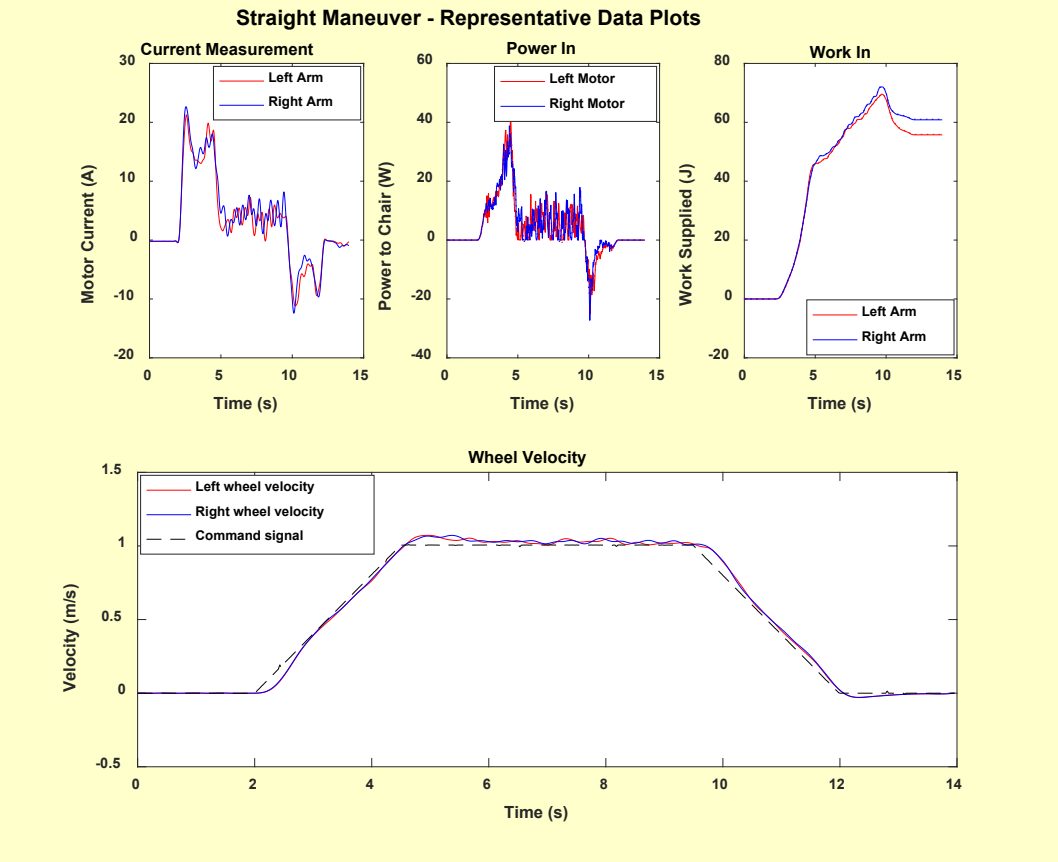

Figure 6: Representative data output of the 'Straight' maneuver in velocity-control mode.

In this illustrative example of a representative 'Straight' maneuver, the torques on each wheel would be interpreted as the product of the current (top-left plot) times the motor torque constant and the tooth ratio. The torques would be then multiplied by the wheel velocities (bottom plot) to generate the power values (mid-top plot) using Eqn. 7. This power curve would be integrated over time to generate the cumulative work (top-right plot) supplied to the chair, following Eqn. 6. Propulsion cost for the entire maneuver would be summarized as the end value of this plot divided by the total distance traveled by the chair. Other methods to parse the data are discussed in APPENDIX B and APPENDIX C. Propulsion cost of the entire maneuver was deemed to be the most direct metric of mechanical performance over the other options.

3.2 Prior Work

The precursor to the AMPS project stemmed from work with the standard wheelchair test dummy from ISO 7176-11 [74]. Wheel-mounted encoders were used to measure the velocity of a chair frame loaded with the dummy to study the changes on coast-down deceleration with and without heavily weighted instrumented wheels [66], and the turning resistance of chairs with different loading configurations [50].

Prior work using the AMPS include: the original AMPS design article, where the system design rationale and the propulsion system validation processes are discussed [70]; quantifying the impacts of loading configurations on the required propulsion torques in predetermined maneuvers [69]; the formulation of the propulsion cost metric (as in Eqn. 8) to describe differences between types of wheelchair motion, as well as the generation of 'canonical maneuvers' to prescribe a path-based trajectory to the wheelchair [70, 82]; an extensive study on propulsion cost differences between configurations and components [71]. Work tangentially related to the AMPS include: the development of component-level test methods to measure rolling resistance and scrub torque of casters and drive wheels [81]; statistical models of MWC motion to correlate the results of the component-level energy loss tests to system-level propulsion costs [83]. The efforts by Liles, Huang, and Sprigle to investigate the mechanical behaviors of disparate wheelchair configurations over the past decade have shaped the ongoing field of rehabilitation engineering and applied research – though the AMPS itself has yet to be recreated, researchers around the world have developed methods of testing energetic losses at the component-level [51, 52, 68, 84].

Recent studies with the AMPS [71, 83] rely on the construct of 'canonical maneuvers' – actions or trajectories that are identified to have unique energy distributions or sources of energy losses. The three canonical maneuvers used by Huang were Straight, Fixed-Wheel Turning, and Alternating Zero-Radius Turning, as they collectively

embodied unique combinations of rolling resistance and resistive scrub torque values at the casters and drive wheels. For example, the Straight maneuver started from rest, accelerated steadily to 1 m/s over 2.5 s, held constant velocity for 5 s, then steadily decelerated to a stop in 2.5 s. Under direct influence to drive in a straight line, the drive wheels and casters experienced rolling resistance exclusively. Conversely, the Alternating Zero-Radius Turning maneuver used a series of reciprocating clockwise and counter-clockwise turns. The wheels were driven in opposite directions for several seconds, then the motor polarities were inverted to turn the chair back towards the original orientation. Casters underwent swivel at the origin of each turn, and rolling resistance after they aligned with the trajectory radius. The drive wheels were under a combination of rolling resistance and scrub torque for the duration of the maneuver. The predetermined velocity trajectories for the canonical maneuvers were designed to control the path traveled by the center of mass. Each maneuver was able to endow the system with vastly different distributions of kinetic energies, split between the linear translation of the mass, rolling rotation of the wheels, and yaw rotation of the frame. The general motion of the three canonical maneuvers are shown in Figure 7.

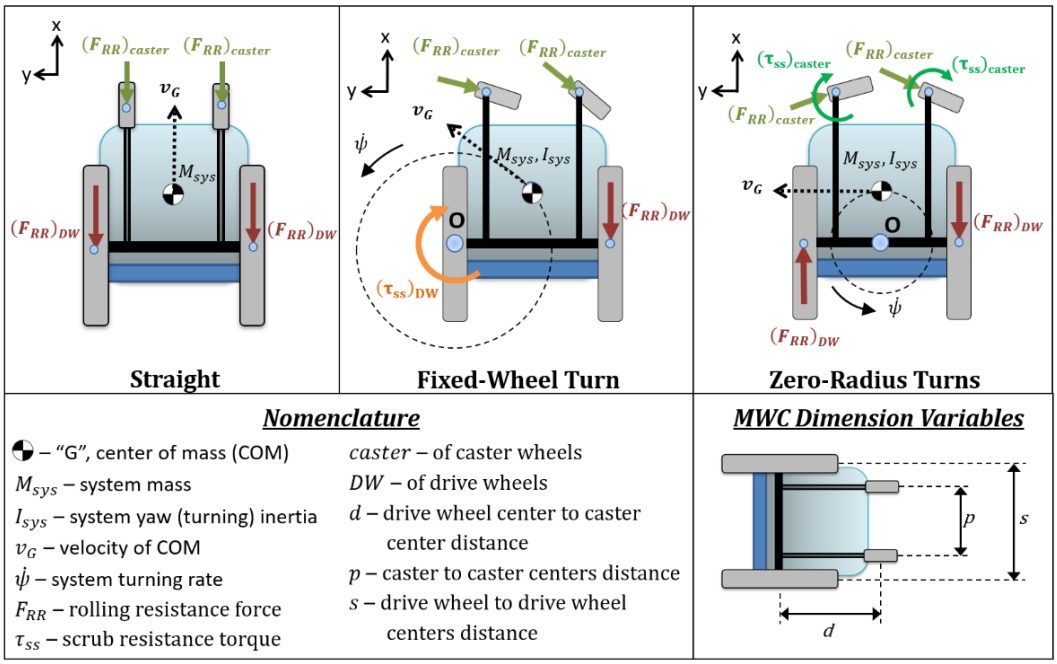

Figure 7: Simplified MWC diagrams with non-conservative forces and torques acting on the frame in each maneuver.

Representative kinetic energy distributions of each maneuver (Figure 8) were calculated with Eqns. 1-4 from [78] to highlight the disparities between each motion. The total kinetic energy in the Straight maneuver was dominated (over 90%) by the translational motion of the rectilinear inertia. The Fixed-Wheel Turn maneuver had much larger contributions of the turning energy, defined by Eqn. 2 as a representation of the change in heading direction of the chair, but was still dominated by the translation of mass. The Alternating Zero-Radius Turn maneuver is the only maneuver of the three that features a predominant turning-based energy distribution, due to the trajectory turning the chair about the drive wheel axle center, which minimizes any possible translation of the center of mass.

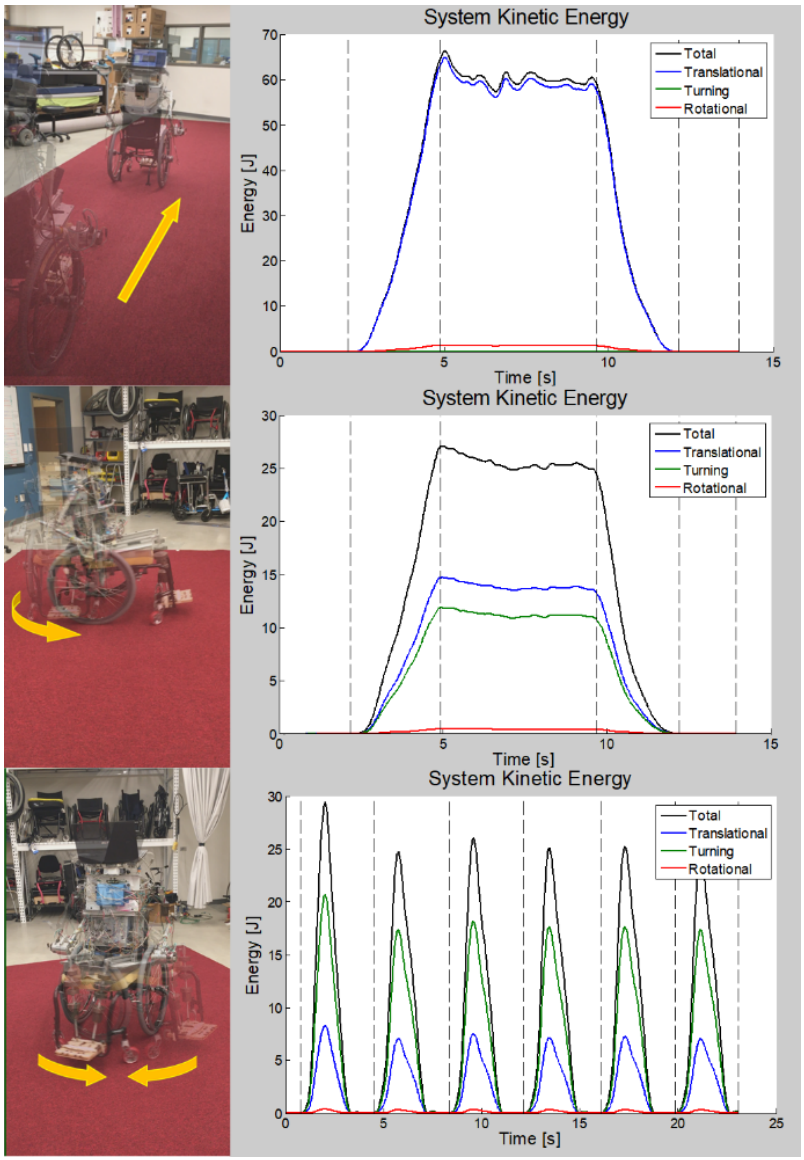

Figure 8: 'Canonical maneuvers' to replicate common aspects of wheelchair motion. (Top) Straight maneuver. (Mid) Fixed-wheel turn maneuver. (Bottom) Alternating zero-radius turn maneuver.

In other prior work, the interactions between the components (casters, drive wheels) and the ground were investigated to quantify the amount of energy that was lost during specific actions. These component-level empirical data collection procedures used a coast-down cart to measure rolling resistance and a materials-testing load frame to measure the resistive scrub torque of drive wheels and casters on common surfaces (tile, carpet).

Empirical data from these tests were used to assess the relative magnitudes of energy that are lost by the MWC system in each of the canonical maneuvers. These test methods are well-suited for simple testing of components at the manufacturer location, rehabilitation clinics, or in research labs, as the rigs themselves (Figure 9) are made from common lab equipment and relatively inexpensive instrumentation [81].

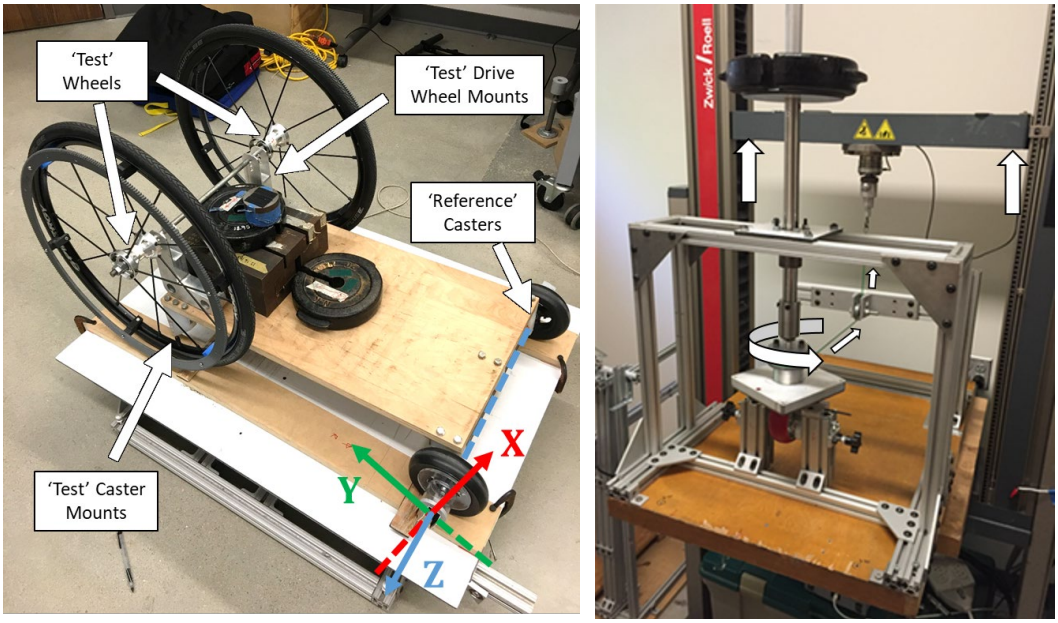

Figure 9: (Left) Instrumented coast-down cart. (Right) Scrub torque rig.

Furthermore, by assuming most or all of the energy lost by the MWC system is lost via these component-to-ground interactions, the empirical measurements can be combined to estimate the total system-level energy losses. These equations of total energy loss, referred to as 'System Loss', vary based on the types of motion that the MWC experiences. As such, System Loss terms were generated for each maneuver using the nomenclature of Figure 7. Many combinations of energy loss terms and geometric measurements exist. To find the combinations best-suited to predict system-level performance (i.e. propulsion cost), thousands of AMPS trials were run with multiple MWC configurations. The same configurations were tested on the coast-down cart and scrub torque test rig, and regression models were used to analyze the correlations between the outcome variable (propulsion

cost) and the predictor variables (rolling resistance, scrub torque, geometric measurements, weight distribution, system mass). The best models are presented below. More detailed descriptions and derivations can be seen in [83].

For the Straight maneuver, the MWC is propelled forward without any turning motion. The wheels undergo rolling resistance with minimal scrub torques and no heading direction changes. The System Loss equation, therefore, was constructed as a direct combination of the rolling resistance measurements of all the components (borrowing the terminology from Figure 7):

$$SysLoss_{\ straight} = 2 * (F_{RR})_{caster} + 2 * (F_{RR})_{DW} \tag{9}$$

Though seemingly oversimplified, this System Loss equation was the most influential predictor of propulsion cost for the Straight maneuver was the System Loss value of the summed rolling resistance of each wheel. For Fixed-Wheel Turning, the equation for System Loss involved a more complex combination of geometric measurements, scrub torques, and rolling resistances:

$$SysLoss_{\ FW\ turn} = (\tau_{ss})_{DW} + s * (F_{RR})_{DW} + \left((F_{RR})_{caster} * \sqrt{\left(\frac{s-p}{2}\right)^2 + d^2}\right) + \left((F_{RR})_{caster} * \sqrt{\left(\frac{s+p}{2}\right)^2 + d^2}\right) \tag{10}$$

Finally, the System Loss equation for the Alternating Zero-Radius Turning maneuver followed a similar format of rolling resistance and scrub torques:

$$SysLoss_{\ AZR\ turn} = 2 * (\tau_{ss})_{caster} + 2 * (F_{RR})_{DW} * \frac{s}{2} + 2 * \left((F_{RR})_{caster} * \sqrt{\left(\frac{p}{2}\right)^2 + d^2} \right) \quad (11)$$

These equations calculated values specific for each wheelchair configuration tested with the AMPS, which were then related to the system-level outcome parameter of propulsion cost through statistical modeling. Ultimately, the empirical data were collected over 2 surface types (tile, carpet), 2 occupant masses (80 kg, 100 kg), 3 drive wheels, 4 casters, 3 weight distributions (60%, 70%, and 80% over the drive wheel axle), and the 3 canonical maneuvers – over 4,000 AMPS trials. The modeling results showed that the predominant predictive factors for propulsion cost in each maneuver were the calculated System Loss values calculated from Eqns. 9-11. Yaw inertia and weight distribution did appear in the regression models for the turning maneuvers but had lower correlations with propulsion cost. High correlations between mass, weight distribution, and energy loss parameters suggest that the impacts of the loading conditions may be most directly caused by the increased losses at the wheels, rather than solely due to an increase in linear or rotational inertia [83].

3.3 Limitations of Velocity Control

To achieve motion, the user must first accelerate the chair by applying a force on the push-rim in the direction of travel and overcoming the inertial resistance to motion. Biomechanical limitations restrict the force and stroke length of the 'push' phase. The successive 'recovery' phase returns the users' hands to their point of contact (Figure 10). During the recovery phase, the wheelchair is subject only to resistive forces acting to decelerate the system. Thus, the next propulsive stroke must resupply the lost energy to maintain motion, as well as re-accelerate the mass of the system. These energy losses are exacerbated by the recovery phase when forward

propulsion stops and the MWC decelerates. Thus, the losses propagate during the short, slow, and infrequent bouts of human propulsion [3, 4].

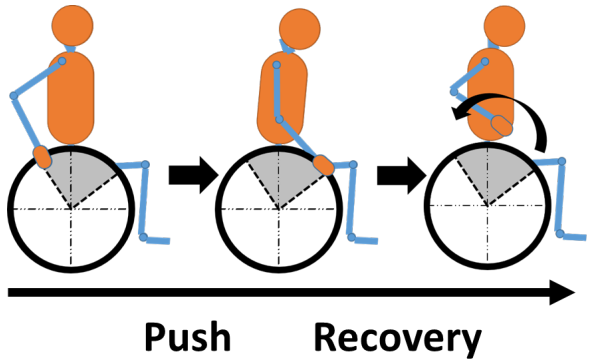

Figure 10: The 'Push' and 'Recovery' phases of the wheelchair propulsion cycle.

Energy losses between strokes are largely uncaptured by the AMPS. The Straight and Fixed-Wheel Turning maneuvers are limited to one continuous motion with well-defined acceleration, steady-state, and deceleration phases. These predefined trajectories endow the chair with kinetic energy along the prescribed path, but distinctly lack the intermittent propulsion and deceleration. As an example, the following figure shows the Straight velocity and torque:

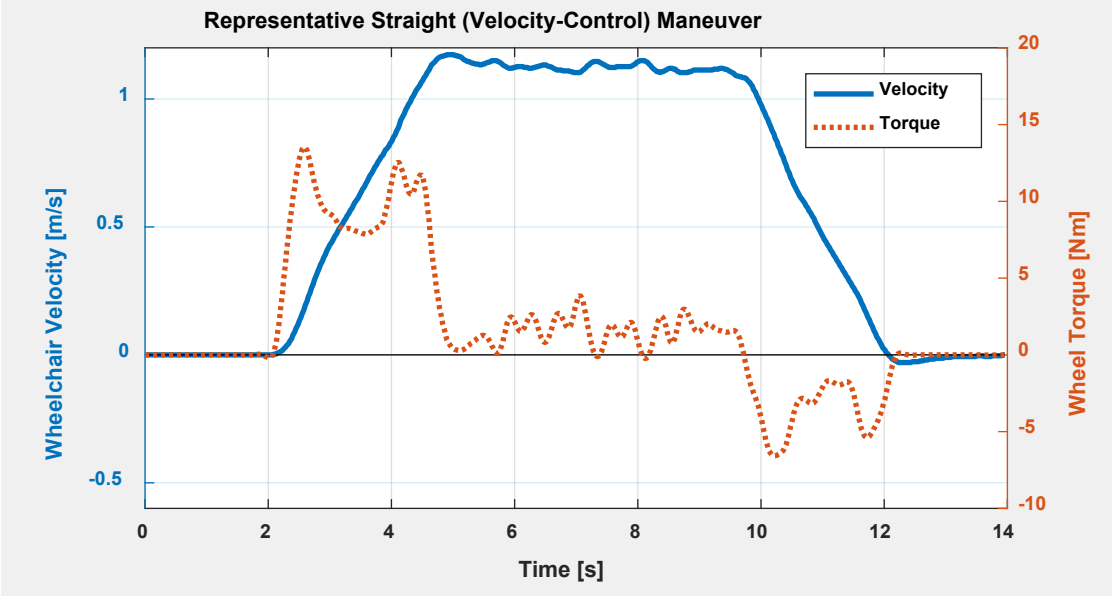

Figure 11: Representative velocity and torque of a straight over-ground AMPS trial in velocity-control mode.

The velocity may seem like it is attainable or even typical of a human user, but the torque data is irregular – the torques never fall to zero until the braking phase begins to decelerate the chair. Every motion is prescribed in Figure 11. The acceleration and the deceleration both follow the steady rate of 0.4 m/s^2. In reality, if the chair were released at the 1.1 m/s maximum speed and allowed to freely coast, the deceleration might be more gradual than the 0.4 m/s^2 slope. If the chair was poorly optimized and had poorer mechanical efficiency, it might even decelerate more rapidly than the deceleration in Figure 11. The point of the matter is that in velocity-controlled propulsion, the chair is never allowed to behave as it would in an organic environment – that is to say, the MWC is always absolutely under the control and influence of the motors driving it. In contrast, observe the representative torque and velocity profiles of a simulated human wheelchair user in a similar straight-forward motion in Figure 12, designed to emulate the torques and motion seen in [85].

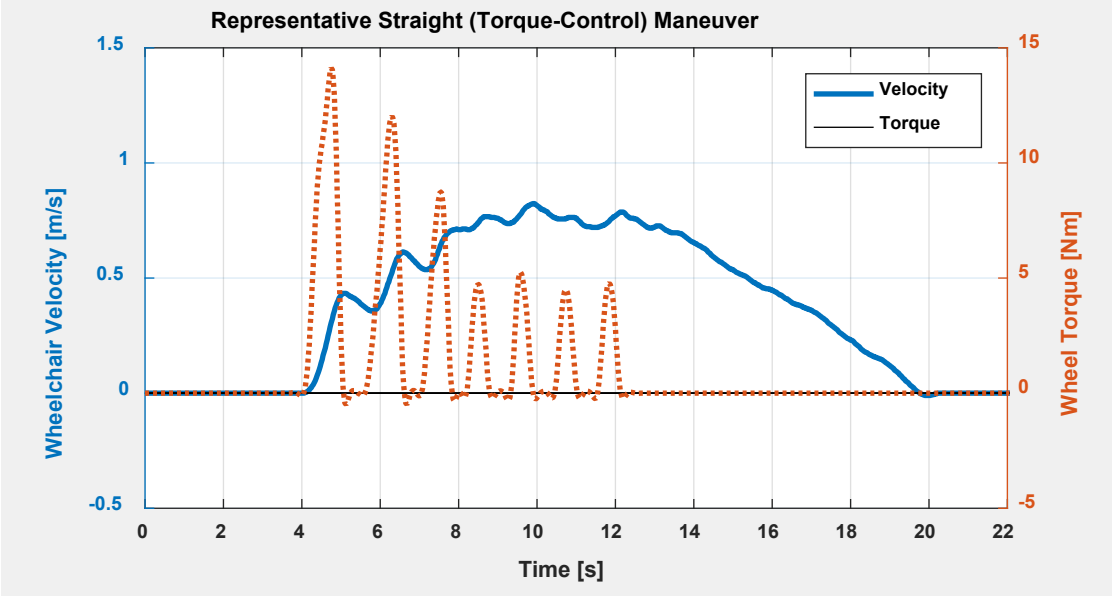

Figure 12: Representative velocity and torque of a straight over-ground trial as proposed for the AMPS.

There are discrete pushes, followed by segments of no torque where the chair experiences gradual deceleration as the user retracts his or her hands and prepares for the subsequent push. It is postulated that replicating this intermittent propulsion with the AMPS would magnify the impacts of inefficient ('lossy') components and add higher resolution to the comparative metric framework previously established in prior work [69-71, 83]. The new propulsion method should narrow the gap between testing with the AMPS versus human subjects, yielding more clinically-relevant data than previous AMPS studies.

Three major limiting factors prevent the optimal recreation of real-world motion using a velocity-based motor controller: (1) simplified parametric (trapezoidal) velocity profiles are impractical at recreating real-world wheelchair motions; (2) velocities may be disparate in challenging environments such as an incline or even carpeted surface; (3) intermittent decelerations would need to be prescribed within the maneuver file as a motor

command instead of as a result of the wheelchair configuration. The first of the two main limitations can be overcome by careful examination of the literature. Numerous studies on push-rim kinetics, kinematics, and biomechanics utilize both over-ground and treadmill or dynamometer trials to analyze the most common characteristics of the human propulsion cycle [7, 15, 75]. The velocities could be parameterized as simply as designing the first push to reach 0.3 m/s, the second to 0.6 m/s, the third to 0.7 m/s, and the fourth at 0.83 m/s to begin the steady-state velocity phase of the maneuver. However, the third main limitation prevents the use of this parameterized trajectory because the motor is directly engaged with the push-rim. The wheelchair would not be able to freely decelerate with the motors engaged, as the velocity-control would maintain the specified speed, or be back-driven by the momentum of the system. Furthermore, even with the motors powered off, the rotating wheels would back-drive the motors. 'True' deceleration in the recovery phase of wheelchair propulsion only occurs when the push-rims are released entirely via physical decoupling of the pinion and ring gears. The most effective method to augment the AMPS to better emulate human users was found to be recreating this highly repeatable and versatile torque profiles seen in the literature [7, 15, 75]. This involved rearranging the motor control scheme to control torque output, rather than speed, of the two motors.

3.4 Torque-Based Motor Control

The main goal of this aim is to prove feasibility and adequacy of the torque-based intermittent propulsion method. Velocity-control of MWC propulsion has been effective at differentiating between performances of wheelchair configurations [71, 83]. In velocity-control, the AMPS maintained wheel velocities within 0.1 m/s of the target value and demonstrated repeatability with coefficients of variation (CoVs) of < 2% during steady-

state motion, though the torque CoV was as high as 10% [70]. However, velocity-control of the motors caused irregular torques on the wheels that are unlike human propulsion forces (Figure 11), and the steady-state approach to propelling the wheelchairs does not match the context of use (Figure 12). There are no 'push' or 'recovery' phases in the velocity trajectories. Velocity-control mode lacked two features: (1) the ability to disengage from the wheel to emulate the coasting that happens when human operators release the wheel between pushes, and (2) the ability to directly apply a prescribed torque about the wheel axle. For any torque-based motor control method to adequately propel the AMPS, these two features have to be addressed.

3.4.1 Overview

Brushed DC motors feature the useful behavior of proportionally scaling output motion to the input of the armature (Figure 13, from [86]). The RoboteQ HDC-2450 voltage controller and many similar PWM-based voltage controllers leverage the relationship between armature voltage and output velocity to perform rudimentary velocity control. As an added feature, the simplicity of the encoder-based feedback loop integrated directly into the PID control loop to allow tuning of the system behavior and to compensate for external disturbances. The basis for each of these controllers is rooted in the fundamental, proportional relationship between input voltage and output velocity. In Figure 13, the value of torque in Nm increases linearly with increased current. Note, however, that the speed in RPM of the motor shaft decreases as the current increases. The standard 'DC Motor Power Curve', represented by the dark blue line, shows that the power maximizes where the torque and velocity lines intersect, approximately in the mid-range of the torque outputs.

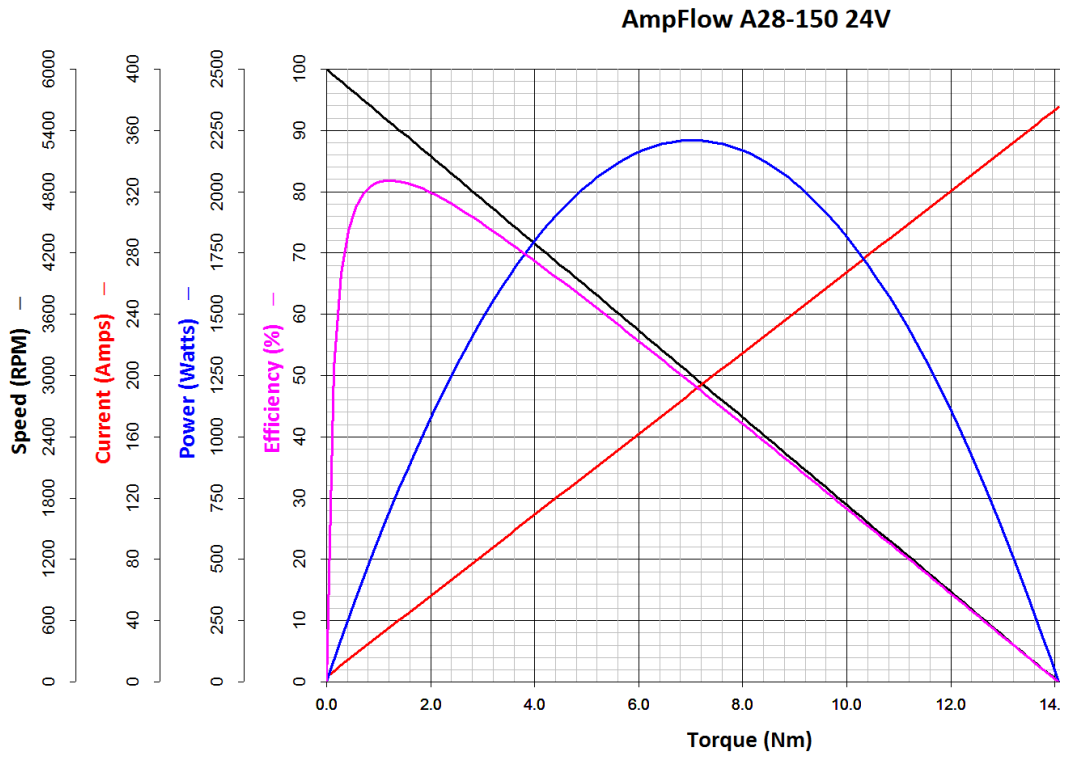

Figure 13: Brushed DC motor performance chart from manufacturer.

Brushed DC motor output torque is proportional to the amount of current flowing through the motor and can be measured, but few (if any) motor controller manufacturers supply a current-control mode. The market is saturated with the simple and inexpensive PWM-based voltage controllers, but the DC motor torque-speed curve (Figure 14) makes it difficult for the controller to provide the required torque if the speed of the motor is not carefully controlled. For example, if a PWM-based controller were to be used as a current-based torque controller, the current sensor signal would be sent to the processor to calculate the relative error between 'actual' and 'target' current. The typical solution is to boost the output voltage if the 'actual' is below the 'target'. In a PWM-based voltage controller, the voltage would therefore be increased, proportionally increasing the speed. As in Figure 14, the increased voltage/velocity would actually lower the effective torque output of the motor system, and the motor would have a 'run-away response' of rapid acceleration until the controller faults and shuts down.

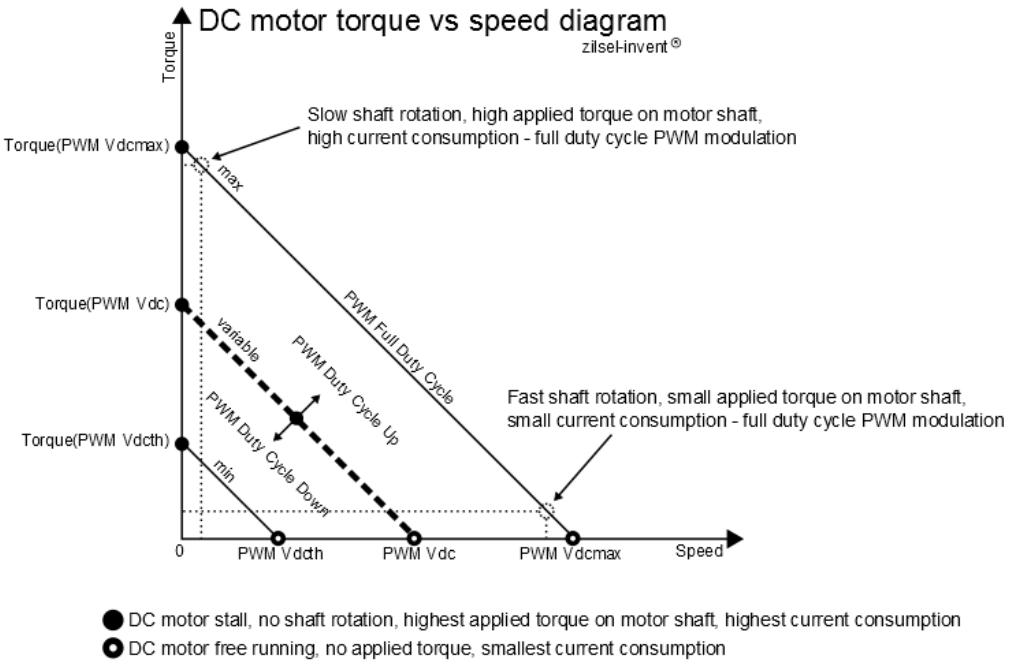

Figure 14: Torque-speed relationship of DC motors. From [87].

The few options for current-control that could be found were designed for low- to mid-power applications [88, 89] unlike the high throughput of the AMPS. Alternative options were briefly explored. Brushless DC motors were found to offer some degree of control over torque [89-91], specifically with 'field-oriented vector control'. The general obstacles with BLDC motors are the 'torque ripples' that are commonplace in BLDC output [92-94], and the complexity of instrumenting the motor to read the torque, voltage, and velocity of the system. The earliest model of the AMPS even had brushless motors for hybrid torque- and velocity-control, but were ultimately scrapped in favor of the simplicity and inexpensive brushed DC electromechanics. In 2014, the AMPS made a breakthrough in terms of torque-control: Teran and Ueda developed a method of implementing a free-wheeling or coasting behavior by applying a 'cancelling' torque on the motors to oppose any back-driven motion. Unfortunately, the multi-level control scheme required an entire inverse kinematic model of the chair and leaned heavily on existing knowledge of the mechanical behavior of the configuration [95]. Teran's work essentially needed a complete characterization of

the chair before the torque-controlled free-wheeling behavior would work. From the description of more recent projects with the AMPS, the aim has very clearly been to test any new chair, independent of configuration, without the hassle of generating such an extensive model.

Torque-to-current relationships were first measured using a stationary torque testing rig (Figure 15) to validate the use of wrist-mounted load cells within the original design. Each joint of the arm was constrained. A pully with a radius of 0.064 m was fixed to the exposed end of the motor shaft. Metal cables wrapped around the pulley were attached to metal disk weights. One ‘trial’ consisted of driving the motor at a commanded velocity of 0.1 m/s until the weights reached the end of their respective ends of the cable. The armature currents were measured by the 50A Hall Effect-based current sensors on each arm.

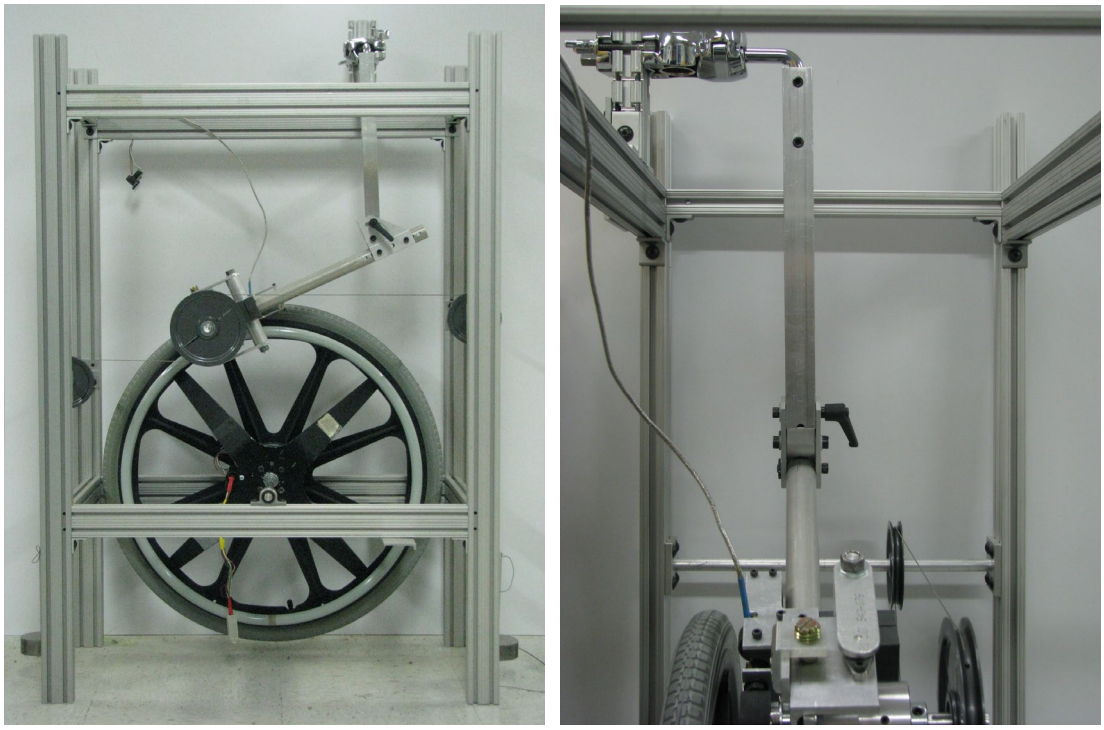

Figure 15: (Left) Motor torque calibration rig. (Right) Image of pulley attachment point and load cell position.

Current data points were averaged and multiplied by the torque constant provided by the manufacturer (5.32 oz-in per A). For reference, the conversion factor is 141.6119 oz-in per Nm of torque. The tension in the cable was multiplied by the radius of the pulley to get the effective or 'actual' torque on the motor, which was then plotted against the measured armature currents, as seen in Figure 16 and Figure 17, below.

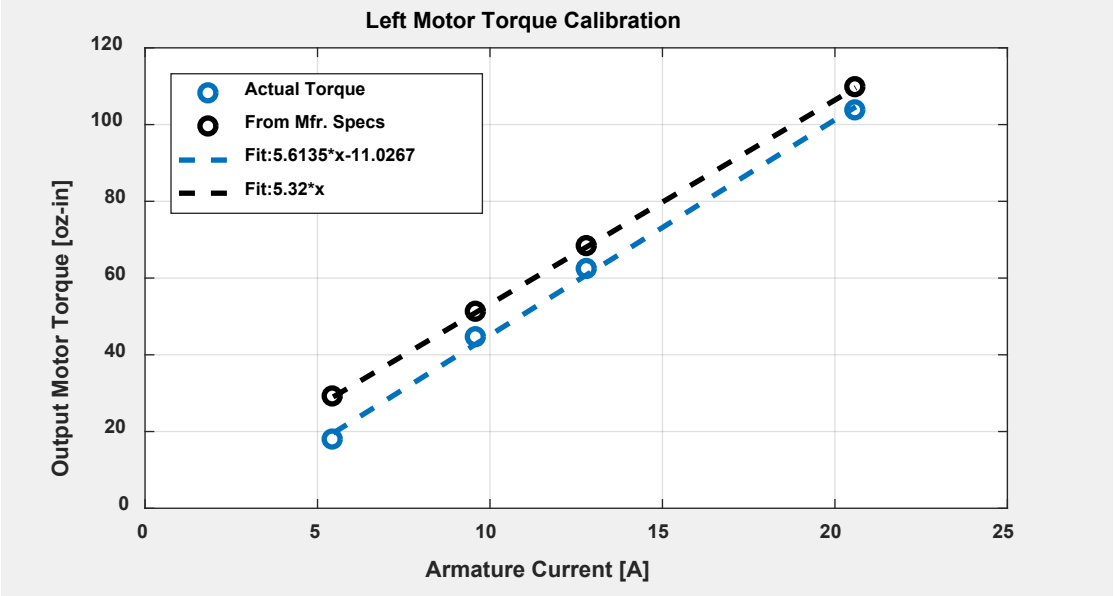

Figure 16: Calibration curve of the left motor comparing the torque constant of the manufacturer to actual torque outputs.

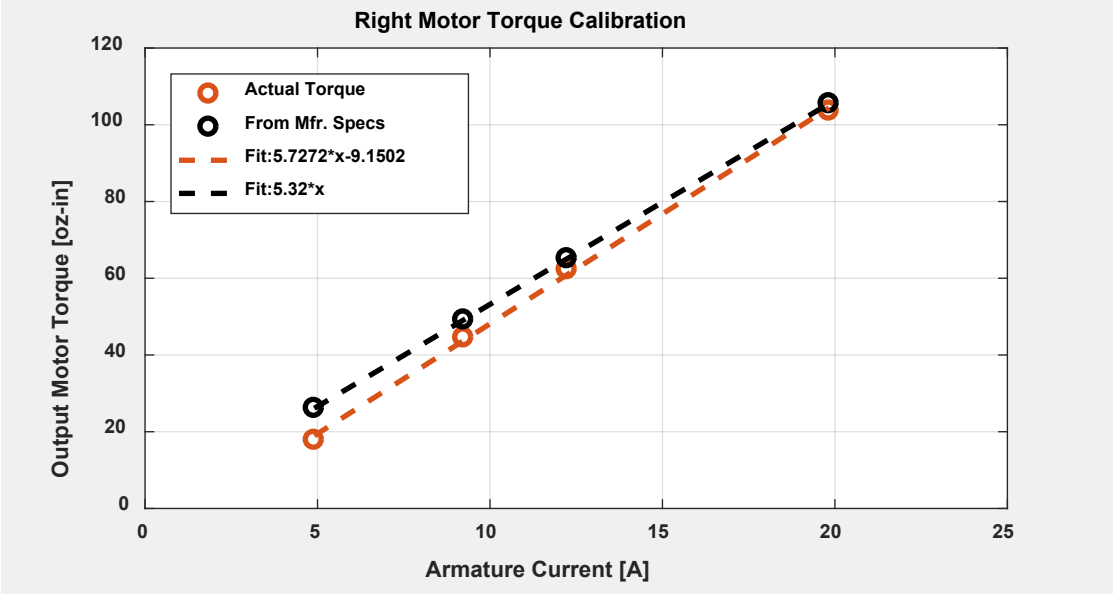

Figure 17: Calibration curve of the right motor comparing the torque constant of the manufacturer to actual torque outputs.

The manufacturer-supplied torque constant, or K_t, was intended to represent the slope between the current and actual torque output. From the empirical data, it was within 5-8%

of the derived 'actual' calibration slope. Both left (Figure 16) and right (Figure 17) motor calibration curves fit the data very well, with $R^2 \geq 0.99$.

Establishing the current-torque relationship was vital to the integrity of the data analysis. As in Eqn. 7, the 1:17 gear ratio at the motor-to wheel interface would drastically increase seemingly small 5-8% errors in motor torque to determine wheel torque, which could skew the work, power, and propulsion cost values. These calibration equations also permitted the prescription of torques at the wheel based purely on motor current, and served as the basic foundation for the creation of the torque-based motor controller.

3.4.2 Hardware Modifications

The hardware requirements to redesign of the AMPS propulsion system was limited mainly by the kinetic output of the testbed. The first requirement, and the most important feature of the drive system redesign, was the 'zero-impedance' functionality – the motors needed to be disengaged from the push-rims to prevent back-driving force between the wheels and motors. In the human propulsion cycle, recovery time between the point of push-rim release and the contact time at the beginning of the next push is characterized by a net push force of zero. A motor, together with its means of control, must be capable of providing a zero-force condition to mimic the recovery phase. This is typically executed via a combination of zero-force motors and clutches, the latter being the most appropriate to integrate with the AMPS mechatronics as the zero-force motor options were already explored by previous iterations of the AMPS.

Two types of clutches were chosen as viable candidates for the 'free-wheeling' augmentation of the motors (Figure 18). The first was an electromagnetic clutch, which

stood out due to passively disconnecting the physical contact between the input and output shafts entirely. The inner magnetic coil is designed to pull the two halves of the clutch together to establish a physical connection when the coil is energized, which gives the user full control over when the direct transmission of torque is permitted. The other option was a roller ramp clutch, or 'one-way' clutch. In this general class of clutches, the motor shaft connects to the inner face of the assembly and rotates. In the 'over-running' direction, the rotation of the input shaft pushes the internal ball or cylinder bearings to empty compartments to rotate freely. In the opposite direction, the bearings are forced to ascend specialized ramps by centrifugal force, where they contact the outer race and get 'locked' between the inner and outer faces by compressive force. In the locked position, the two faces are rotationally linked such that torques are directly transmitted from the input to the output shaft. Variations of this clutch model, known as bi-directional over-running clutches, have springs on either side of the bearing that are only engaged when the input shaft is driving. If the input shaft is idle, the output shaft is free to spin in either direction. Unfortunately, these are not readily available in the United States and the only reproducible model is sized for the wheel axle of All-Terrain Vehicles.

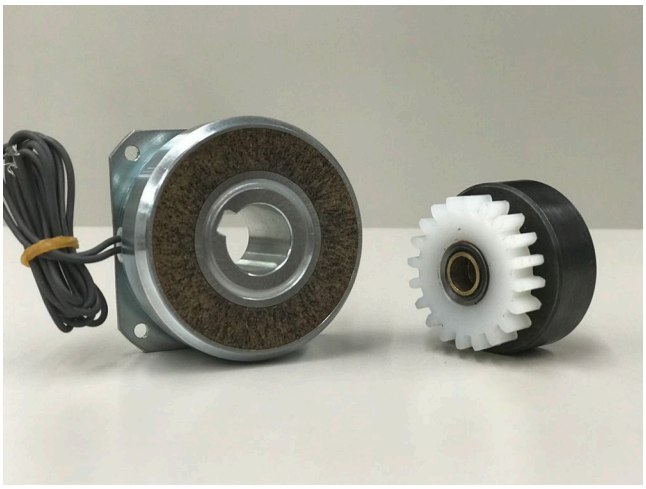

Figure 18: Relative size and shape of the electromagnetic clutch (left) and the mechanical over-running clutch (right).

One electromagnetic clutch and one over-running clutch were purchased. Due to the limited sizing options available, the selected electromechanical clutch (Miki Pulley EM 102-05-13, Zero Max, Inc.) the 3" length before the pinion gear attachment was incompatible with the motor shaft. The selected over-running clutch (TinyClutch D125-8-KW1/8, Helander Products, Inc.) was fitted with the output end of the 20-tooth pinion gear (P/N 57655K56, McMaster-Carr Supply Co.) at the manufacturer. The entire assembly, at 1" long and 0.12 kg, was designed to mount to the motor shaft with a through-hole (note: the version pictured in Figure 18 does not have the through-hole). A steel keyway and set screws prevented concentric rotation or slip. Assembled, the over-running clutch did not change the effective motor shaft length at all, and added minimal mass to the system.

3.4.3 Clutch Validation

The 'performance' of the clutch was evaluated by its impact on the coast-down of the system – configured with the AMPS at 80 kg, in the ultra-lightweight Sunrise Medical Quickie GT, with 70% of the weight distributed over the drive wheel axle. Three

configurations were used: 1) with motors entirely decoupled from the push-rims, 2) with the motors directly geared to the push-rims, and 3) with the clutches installed between the motors and the push-rims. The system, in each configuration, was manually pushed to a release velocity between 1.2 m/s and 1.6 m/s. The decelerations were measured with the hub-mounted encoders on the drive wheels. The data suggests that the clutches provide some drag to the wheelchair (i.e. steeper deceleration) in the form of back-driven torque or rolling resistance on the push-rim. However, the clutches are an improvement over the configuration with the motors directly geared to the push-rims.

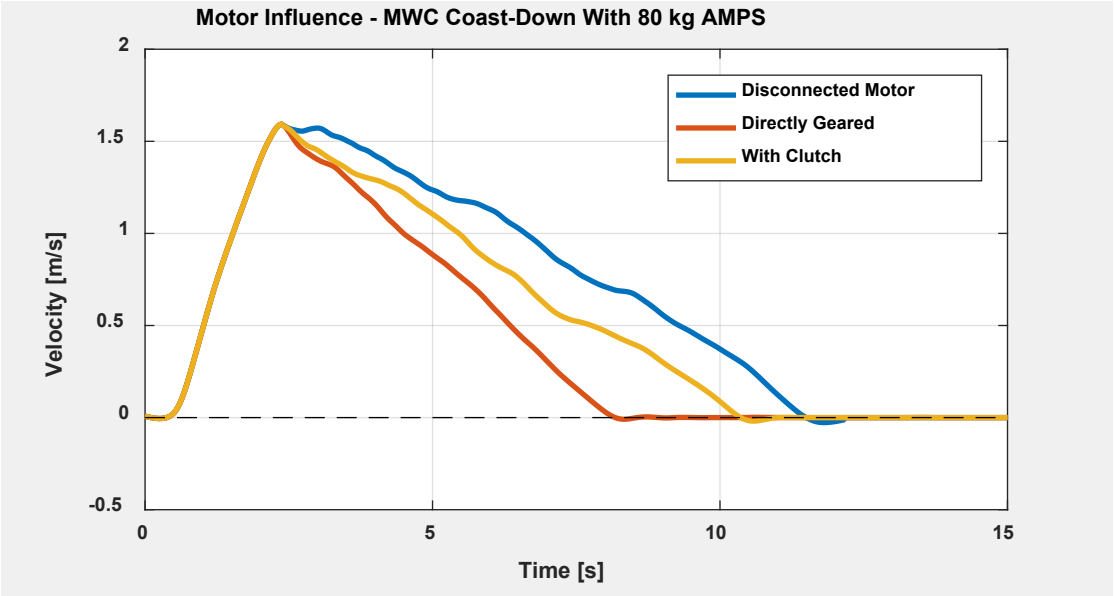

Figure 19: Demonstration of coast-down deceleration differences with and without the over-running clutch.

The data plotted in Figure 19 only shows one trial for each configuration. In this graphic, the optimal condition is the "Disconnected Motor" configuration, which has the most gradual deceleration. Visual inspection reveals that the configuration with the motors directly geared to the push-rims had the largest drag and caused the greatest deceleration

of the wheelchair. The slopes of the 'disconnected' and 'with clutch' lines are nearly parallel. The uppermost peak of the 'disconnected' line appears to be an irregularity, causing the blue line to appear steeper despite having an identical slope. For a better sample, five trials were taken of each configuration. The deceleration values for each trial were calculated as described in the component-testing paper [81] using the deceleration window between 0.8 m/s and 0.4 m/s. The average (N = 10) values are shown in Table 3.

Table 3: Deceleration values with and without clutch equipped.

	Deceleration (m/s^2)	**StDev. (m/s^2)**	**% Diff.**
Disconnected	0.0821	0.0062	-
Directly Geared	0.1366	0.0045	+ 49.8%
With Clutch	0.0959	0.0054	+ 15.5%

For proof of feasibility and preliminary testing of the 'coasting' upgrade to the mechanical system, the clutch performance was adequate. The installation of the clutches added only 15.5% deceleration to the wheelchair, versus 49.8% with the direct-geared configuration. Further testing to quantify the exact bearing resistance and potential effects of aging of the clutches is highly recommended, using methods as described in Varenberg's article [96]. This equipment is not currently available at the facilities of Georgia Institute of Technology at this time.

The final hardware updates to the AMPS were upgrades to the controller circuitry. Controlling torque via current sensor was impractical on the existing model of controller. The RoboteQ HDC-2450 motor controller was replaced by the upgraded RoboteQ HDC-

2460 with built-in torque mode, higher switching frequency, and the capability of running from larger custom-built controller scripts. A second current sensor was added to each arm in series with the existing current sensor to remove extraneous noise in the system (Figure 20). One of the sensors on each arm is used as feedback to the RoboteQ controller, and the other reports the current signal to the data acquisition board.

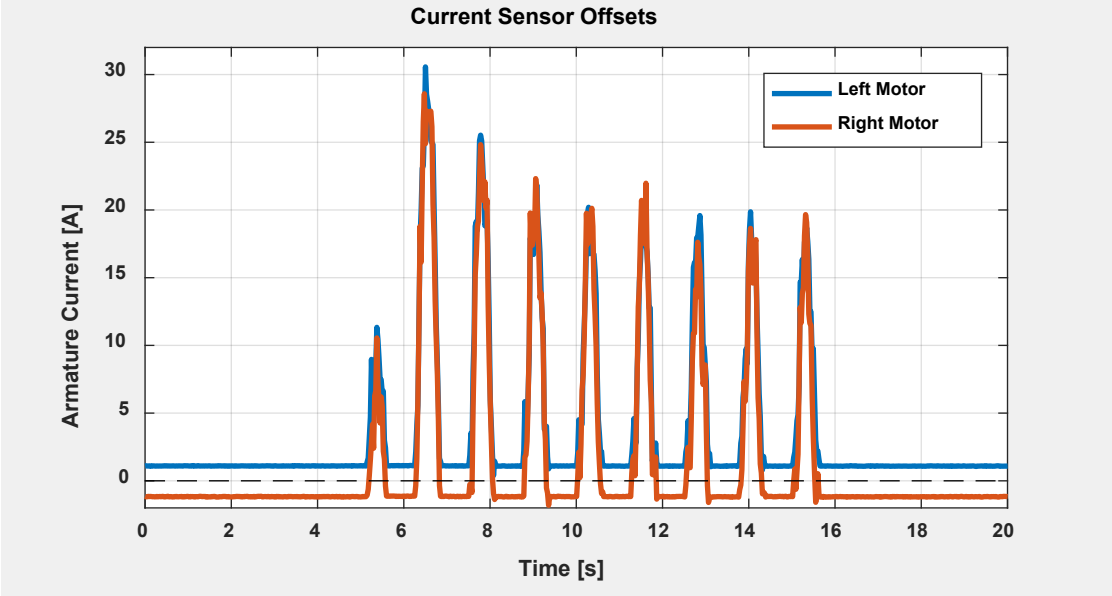

Figure 20: Current sensor offsets observed when linking data acquisition board with the motor controller, using single current sensor per motor.

The described hardware upgrades made it possible to move forward in designing a custom torque-based controller for the AMPS.

3.4.4 Theoretical Controller Derivation

A basic command-following system, like the velocity-based control diagram seen in Figure 3, uses a simple feedback loop and calculates error or deviation from the target value. This error term is manipulated in a PID loop to determine the output required to reach the desired output. A trajectory-following controller, while more complex, uses

measurements from the system to predict what the next output should be. Trajectory-following controllers tend to be smoother and more responsive. Brushed DC motors are electromechanically simplistic and robust, such that a trajectory-following controller can be made to control the output torque with the PWM output. First, the motor itself must be characterized, using the notation in Figure 21, reproduced from [97].

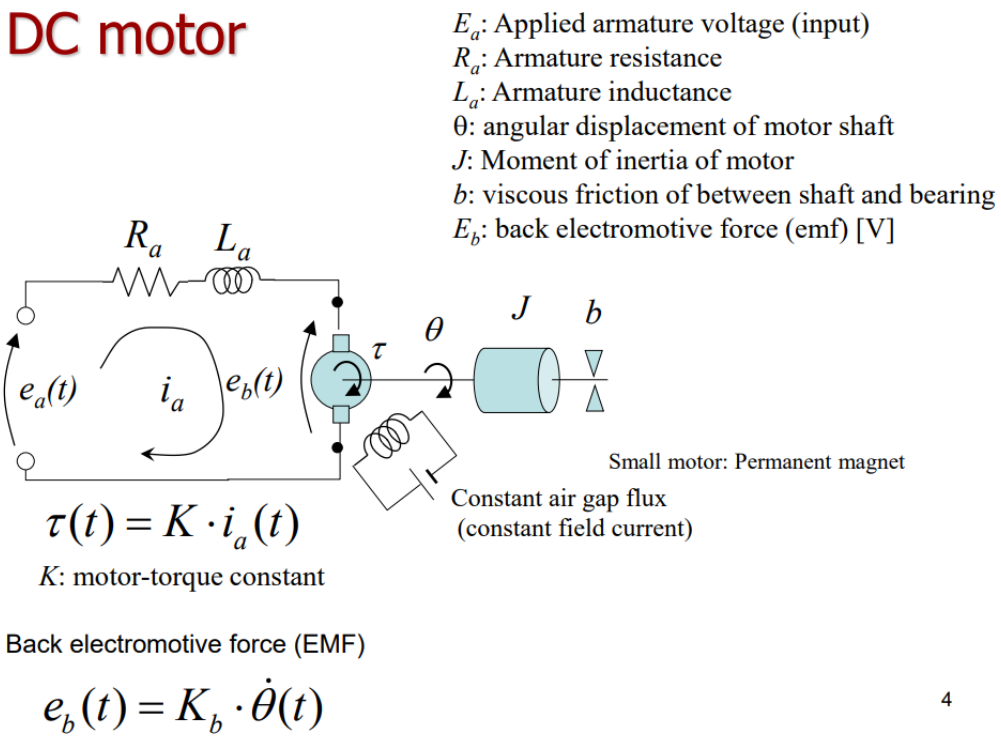

Figure 21: Electromechanical circuit diagram for brushed DC motors.

Some of the electromechanical parameters for the AmpFlow A28-150 motors were documented in the manufacturer specifications, such as the motor-torque constant, and were verified with empirical testing. Others were measured directly with a multimeter, like the armature resistance and inductance at various sample rates. Some terms in Figure 21 were left unmeasured – in the derivation of the current-based motor torque controller, they were seen to be either negligible to the overall equation and were left to be collected into

the ‘disturbance’ term, or they were dependent on the state of the system and could not be measured preemptively to a trial.

Table 4: Electromechanical parameters of the AMPS motors.

Parameter	Symbol	Value	Units
Input Voltage	$e_a(t)$	(input)	V
Armature Resistance	R_a	L = 0.430 R = 0.566	Ω
Armature Inductance	L_a	L = 111 μH R = 87 μH	H (kg-m^2 s^{-2} A^{-2})
Armature Current	$i_a(t)$	(dependent)	A
Back Electromotive Force (EMF)	$e_b(t)$	(dependent)	V
Motor Torque	τ	(dependent)	N-m
Motor Motion	θ, ω, α	(dependent)	rad, rad-s^{-1}, rad-s^{-2}
Rotor Inertia	J	(not measured)	kg-m^2
Rotor Damping	b	(not measured)	kg-m^3 s^{-1} rad^{-1}, or N-m rad s^{-1}
Motor Torque Constant	K_t	L = 0.03964 R = 0.04044	N-m A^{-1}
Back-EMF Constant	K_b	(same as K_t)	V-s rad^{-1}

To properly model and simulate the performance of a proposed motor controller, equations of motion should be derived from the fundamental equations of the circuitry and the system dynamics, and put into state-space form. Simply put, these estimate the motion of the motor and can be used as a ‘plant’ in subsequent controller model simulations. The initial state vector was chosen with variables of armature current and the angular velocity of the motor:

$$x = \begin{bmatrix} i_a(t) \\ \dot{\theta}(t) \end{bmatrix} \tag{12}$$

Note that $e_a(t)$ cannot be used as a state variable, as it is not linearly independent of the first state variable, $i_a(t)$. The goal is to find the array of values that satisfies the equation:

$$\dot{x} = \begin{bmatrix} A_{11} & A_{12} \\ A_{21} & A_{22} \end{bmatrix} x + U$$

$$\text{Assuming } y = \begin{bmatrix} 1 & 0 \\ 0 & 1 \end{bmatrix} x + [0] * U \tag{13}$$

The state-space equations of motion for the system, using the state variables of current and angular velocity, must be derived from Kirchhoff's Current and Voltage Laws [98]. In the case of a generic brushed DC motor using the notation in Figure 21, the voltage loop should be written as:

$$e_a(t) - R * i_a(t) - L * \frac{d}{dt}\big(i_a(t)\big) - e_b(t) = 0 \tag{14}$$

The relationship between back-EMF and angular velocity simplifies the equation to:

$$e_a(t) - R * i_a(t) - L * \frac{d}{dt}\big(i_a(t)\big) - K_b * \dot{\theta}(t) = 0 \tag{15}$$

which can be further rearranged to:

$$\frac{d}{dt}\big(i_a(t)\big) = \frac{1}{L} * \Big(e_a(t) - R * i_a(t) - K_b * \dot{\theta}(t)\Big) \tag{16}$$

Next, the equations of motion can be defined using the relationship between armature current and motor torque:

$$J * \ddot{\theta}(t) = \tau - b * \dot{\theta}(t) - \tau_m \tag{17}$$

In this equation, the motor is opposed by τ_m, which is the driven load at the end of the motor shaft. Once again, expanding this equation further using the relationships seen in Figure 21:

$$J * \ddot{\theta}(t) = K_t * i_a(t) - b * \dot{\theta}(t) - \tau_m \tag{18}$$

This equation can be resolved into its final differential form:

$$\ddot{\theta}(t) = \frac{1}{J} * \left(K_t * i_a(t) - b * \dot{\theta}(t) - \tau_m\right) \tag{19}$$

Now, the entire state-space equation can be written in matrix form:

$$\dot{x} = \begin{bmatrix} \dot{i_a}(t) \\ \ddot{\theta}(t) \end{bmatrix} = \begin{bmatrix} -R/L & -K_b/L \\ K_t/J & -b/J \end{bmatrix} \begin{bmatrix} i_a(t) \\ \dot{\theta}(t) \end{bmatrix} + \begin{bmatrix} e_a(t)/L \\ -\tau_m/J \end{bmatrix} \tag{20}$$

The first row is especially important in this modeling process – it describes the behavior of the current signal, given that the most recent state of the armature current is known, and the only other non-constant value is the command voltage, or $e_a(t)$, which is directly calculated and generated by the motor controller.

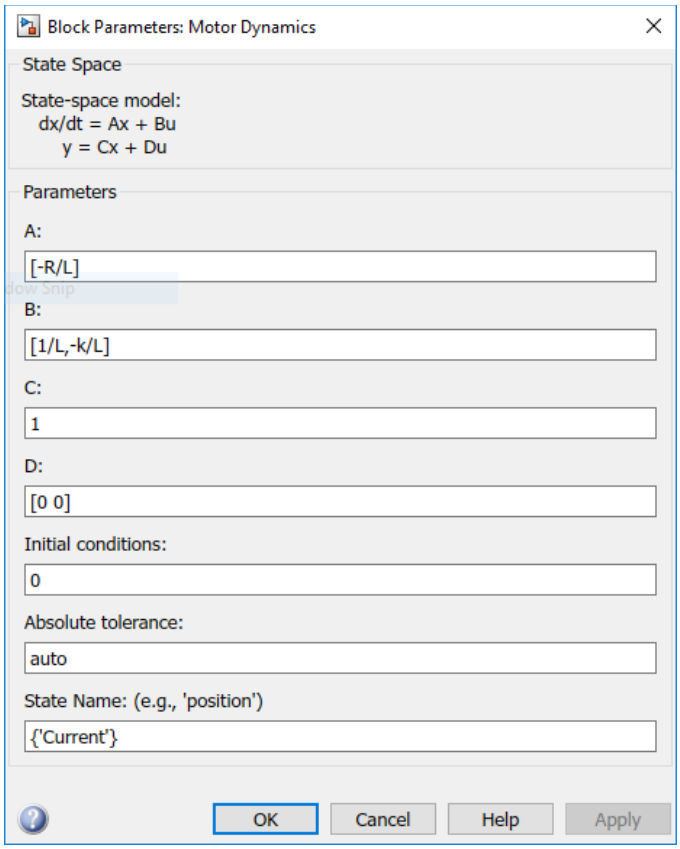

Figure 22: Example transfer function block from a Simulink model of the AMPS current-based torque controller simulation.

The goal of most state-space modeling tasks is to transcribe the equations into usable transfer functions summarizing the outputs and inputs of the system. The challenge with controlling the torque of a brushed DC motor is that the controllable output of the motor controller is voltage, not current. Moreover, the voltage is delivered via PWM. The constant flickering of the signal can be detrimental to the consistent estimation of the current, as it will have periods with the voltage off where the current cannot be drawn and will be discharged from the motor. However, assuming that the switching frequency is high enough to eliminate any transient drops in armature current, the focus of this theoretical model is to leverage the existing PWM-based PID voltage/velocity controller for the

motors and to estimate the necessary command to produce a desired torque. The unfinished block diagram in Figure 23 shows a simplified hybrid control system capable of indirectly controlling armature current via the standardized PWM voltage controller.

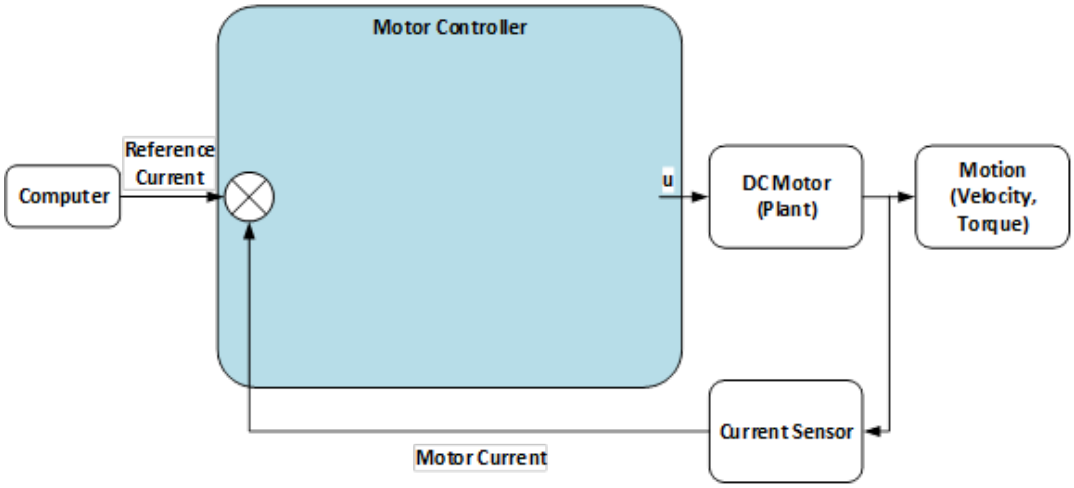

Figure 23: Partially-completed block diagram for torque controller.

A typical current-control scheme utilizes a PI-based controller rather than a PID, forgoing the derivative term for better performance. The PI controller output, or input to the plant that was established in the equations above, can be written as:

$$u = e_a(t) + K_i * \int (i_{error}) + K_p * i_{error} \tag{21}$$

where K_i is the integral gain and K_p is the proportional gain. For simplicity, it is assumed that there are no external loads and no damping on the motor. The armature current equation can thus be simplified from Eqn. 20 and written as:

$$\frac{d}{dt} i_a(t) = {}^{-R}/_{L} * i_a(t) + {}^{1}/_{L} * e_a(t) \quad (22)$$

Note that the external load and damping will be added in as disturbances in a more complex version of the model. The first step to resolve the equations above is to recognize that i_{error} in Eqn. 21 is equivalent to $(i_{ref} - i_{actual})$ and $e_a(t)$ can be re-written as $L * \frac{d}{dt} i_{ref} + R * i_{ref}$, which allows the entire u equation to be reframed as a function of the reference current and the measured 'actual' motor current:

$$u = L * \frac{d}{dt} i_{ref} + R * i_{ref} + K_i * \int (i_{ref} - i_{actual}) + K_p * (i_{ref} - i_{actual}) \quad (23)$$

The final step is to break each mathematical operation into its respective block diagram form, as seen in the filled block diagram in Figure 24, below. The s block acts as a differential and the ${}^{1}/_{S}$ block does the inverse – it integrates the incoming signal.

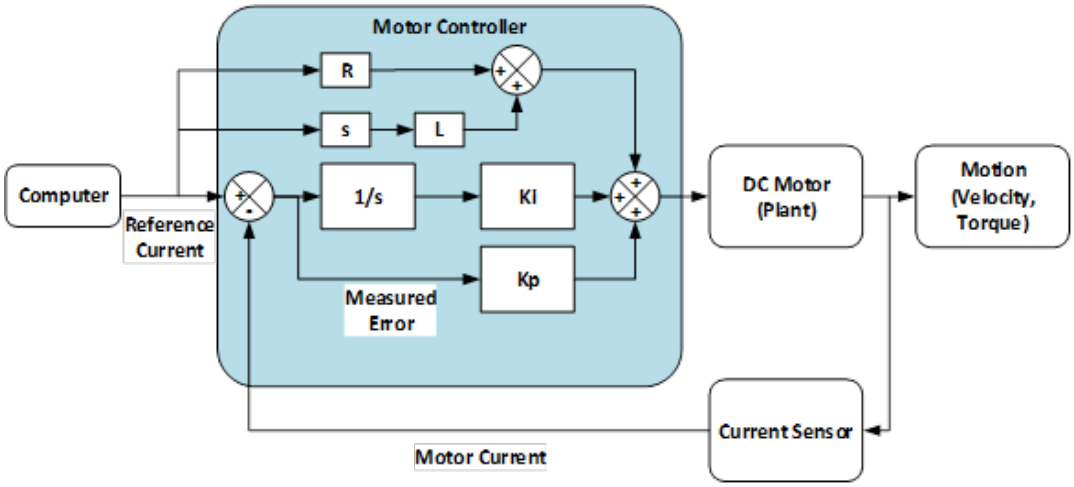

Figure 24: Simplified command-following torque controller diagram.

This solution could be simplified further by replacing the $e_a(t)$ term in the u equation with a reference voltage, u_{ref}, sent as a command directly from the computer acting as the high-level controller (Figure 25). In this situation, the user would be able to command a reference current to the motors, and the high-level controller would calculate the required voltage to achieve this current, rather than spending valuable computational power at the level of the actual motor controller.

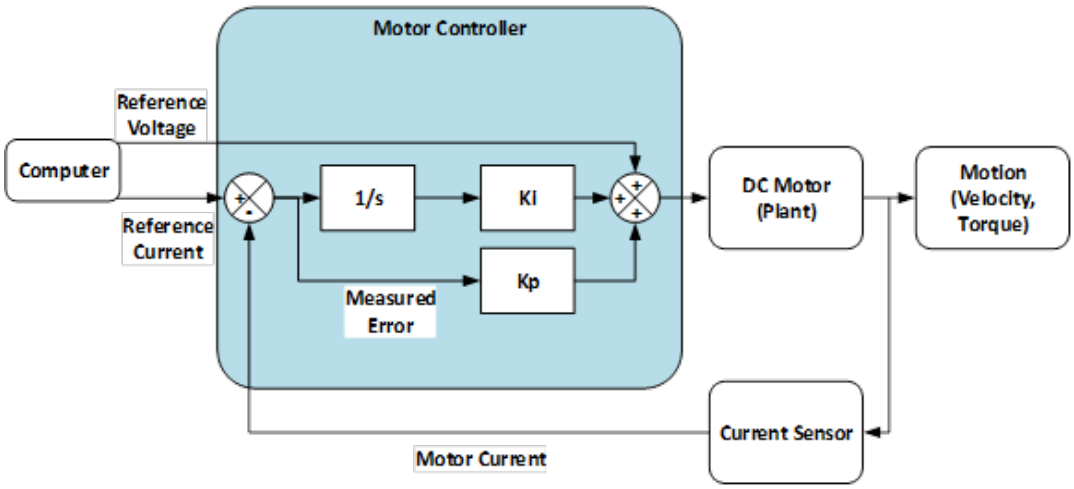

Figure 25: Simplified dual-input command-following torque controller diagram.

Unfortunately, the NI USB-6341 data acquisition board is limited to two analog outputs, and the RoboteQ HDC-2450 is similarly limited to two analog input commands, prohibiting this simplified control scheme from working with the AMPS hardware.

The assumptions made for the previous model unrealistically removed the influence of the motor shaft rotation from the equations to simplify the simulation. Building from the previous control diagrams and equations, the angular velocity of the system (and the back-EMF that it causes in the circuit) can be included as a disturbance. It must be normalized by the inductance to coerce it into voltage, and can be given the symbol ε:

$$\varepsilon = {K_b}/{L} * \dot{\theta} \tag{24}$$

Rearranging the basic equation from Kirchhoff's Voltage Law in Eqn. 14, the pre-plant system can be approximated as:

$$e_a(t) = R * i_a(t) + L * \frac{d}{dt}\left(i_a(t)\right) + K_b * \dot{\theta}(t)$$
$$= R * i_a(t) + L * \frac{d}{dt}\left(i_a(t)\right) + \varepsilon \tag{25}$$

A slight rearrangement of the terms shows that the new control output should be represented by:

$$u = L * \frac{d}{dt} i_{ref} + R * i_{ref} + \varepsilon + K_i * \int (i_{ref} - i_{actual}) + K_p * (i_{ref} - i_{actual}) \tag{26}$$

Therefore, the disturbance term should be added just before the u term is sent as the output to the plant. It can be approximated using a speed sensor such as a rotary encoder (optical or Hall-Effect). This additional motion-based feedback makes the controller behave more appropriately to account for the drop in voltage that occurs when back-EMF is introduced to the system.

To make the controller a trajectory-following system, rather than the more basic command-following system, the voltage necessary to attain the expected current is predicted. The compensation makes the controller more dynamic and responsive to actively cancelling the effects of the external disturbance and better follows the intended behavior, rather than single-mindedly tracking a value and ignoring the external influences skewing the output voltage. The implementation of the rotational compensation can be seen in Figure 26.

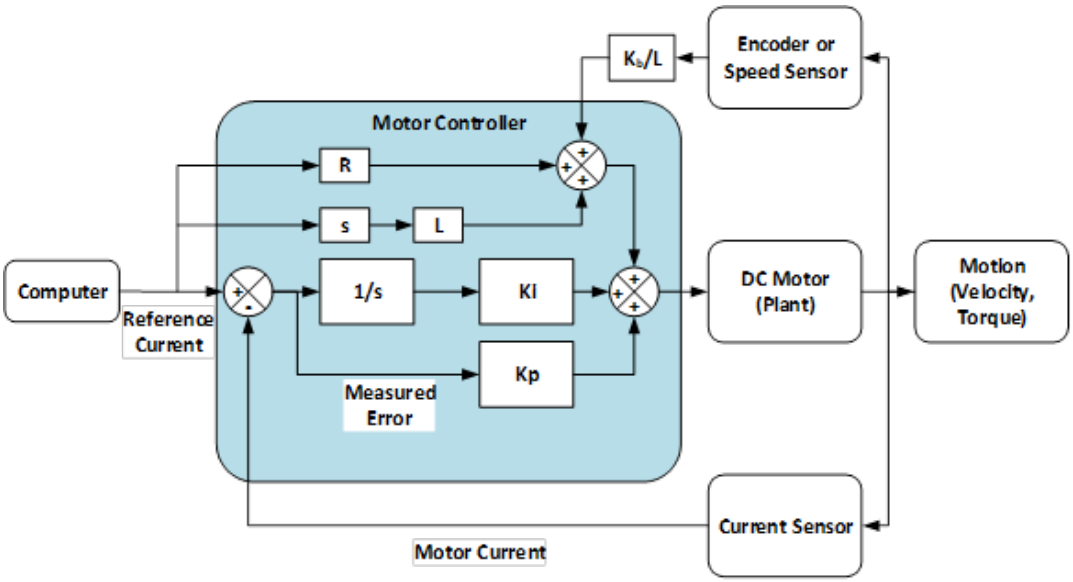

Figure 26: Diagram for proposed torque controller with PWM output.

This theoretical approach to modeling the motor system and the corresponding controller block diagrams follow similar logic to the derivation of an angular position-controlled DC motor system using PWM-based PID control [99]. In their work, the estimation of position was more simplistic than predicting voltage required to reach an output torque, yet the controller block diagrams are similar. Compensation of the back-EMF voltage in Figure 26 is the equivalent of the Coulomb friction compensation in the angular position-tracking PID controller diagram [99].

The trajectory-based controller was modeled in Simulink with the values seen in Table 4 and a variable driven load on the output shaft. Additionally, the same model was duplicated and the R, s, and L blocks connecting the 'Reference Current' input to the speed-based feedback node were removed. This devolved controller represented the command-following controller as it responded solely to changes in current without calculating the armature voltages needed to reach the current response. Both controller models were given

a pulsatile command to follow. The command had a target armature current magnitude of 13 A and a period of 2 s. The negative portion of the sinusoidal input was truncated to better emulate the conditions of use, which would never command a negative voltage due to the clutches preventing torque transmission to the wheels in the rearward direction. As Figure 27 shows, the trajectory-following controller deviated by less than 1% from the command for the duration of the pulsed input with low gains, whereas the command-following controller deviated significantly more and required much higher gains to respond to the input command.

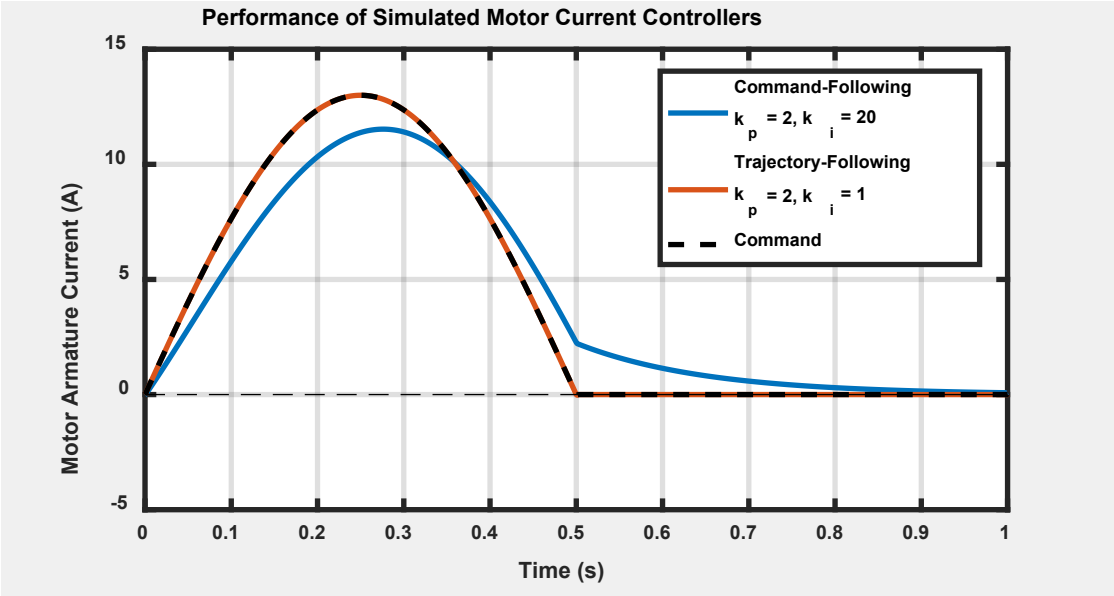

Figure 27: Comparison of command-following and trajectory-following torque control modes.

3.4.5 Software Modifications

Several changes were implemented in the AMPS software suite to create the torque-based propulsion controller. First, the existing high-level control of the AMPS utilized a custom LabVIEW program to interpret pre-made trajectories, send commands to the motor

controller, and collect data from the sensor arrays. The major adjustments to this program involved changing the way the code interpreted the pre-made trajectories. Instead of receiving desired over-ground speeds, converting to angular speed at the wheel, and calculating required motor speed, the program was modified to interpret a more generic '% Command' trajectory. This new setup removed the necessity of having exact geometric measurements of each drive wheel to produce desired motion.

Analog voltage output channels from the NI USB-6341 data acquisition panel have an output voltage between 0.00 to 5.00 volts. The new system maintained the dead-band in the middle of the voltage range to maximize the resolution of the output command around 0 to 50% output. Therefore, an analog voltage output of 2.50 V was set to represent the idle state (no velocity or torque output from either motor), with a ±1% dead-band. Commands had to exceed the dead range of (2.45, 2.55) V to enable motion of the system, with 5.00 V representing the 'full-current forward' command, and 0.00 V representing 'full-current backward'. The generic command interface is seen in Figure 28. Additional tuneable parameters in the 'Configuration' tab allowed the operator to finely adjust the ratio of output command between the left and right motor channels. These were coded in to accommodate for configurations where the driven chair might veer to one side or another – if the floor has a strong side-slope, for example, or if a drive wheel tire is slightly under-inflated, the user can bump up the effective torque to the motor on the affected side and help the AMPS propel in a straight forward trajectory down the test track.

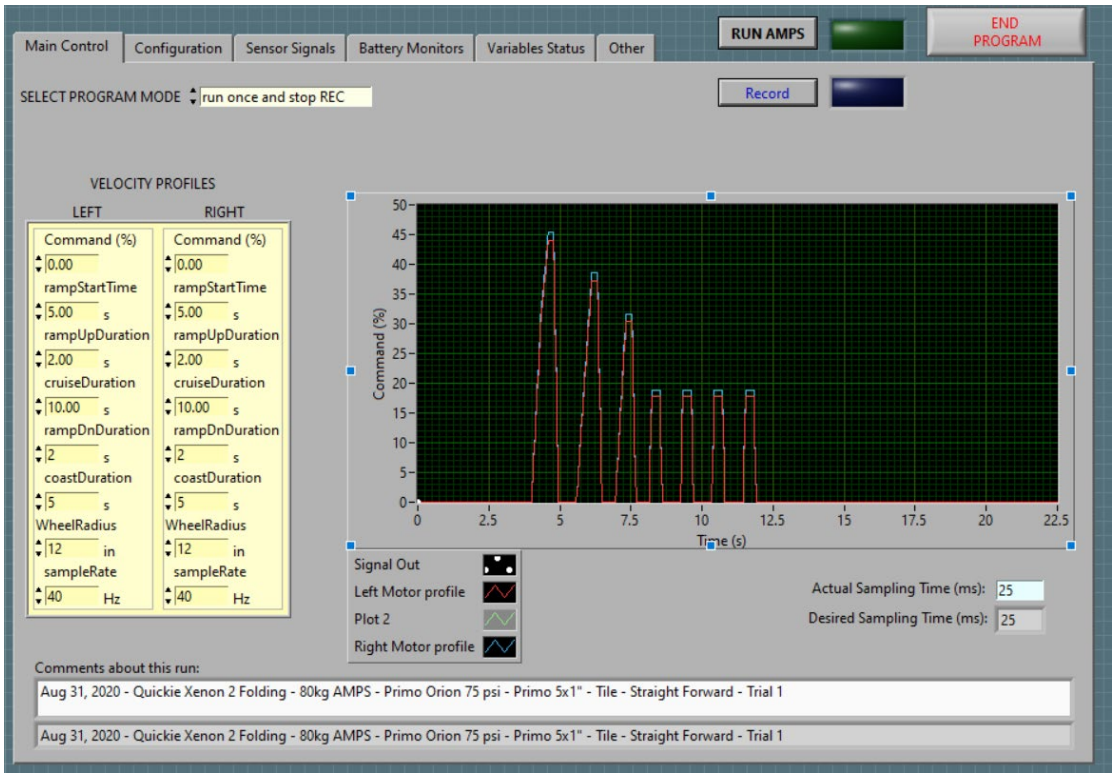

Figure 28: Command interface within LabVIEW for torque-based motor control.

The analog voltages sent from the data acquisition panel were already wired to the motor controller, but they were read as desired motor velocity values. The HDC2460 motor controller was modified to accept the new generic '% Command' voltages and convert them to desired current values for each motor. The built-in 'Torque Mode' of the HDC2460 did not provide the level of control required for the AMPS as it estimated motor current via average current flow from the battery power source, rather than having external current sensors on the motor cables. To account for this, the existing Hall Effect-based current sensors for each motor were wired into the controller as feedback channels. A custom code was developed in the MicroBasic scripting language (proprietary language by RoboteQ based on Visual Basic) built into the motor controller. The controller script is reproduced in plain-text in APPENDIX A. With assistance from RoboteQ representatives, this basic

controller script was implemented by setting the motors to use the 'Closed-Loop Position Tracking' mode with the Hall Effect-based current sensor as the main feedback component, as is now recommended by the manufacturer [100]. In this configuration, the built-in control features effectively replicate the trajectory-following command scheme within the RoboRun+ Motor Control Utility (v2.1, Nidec Motor Corp.) seen in Figure 29.

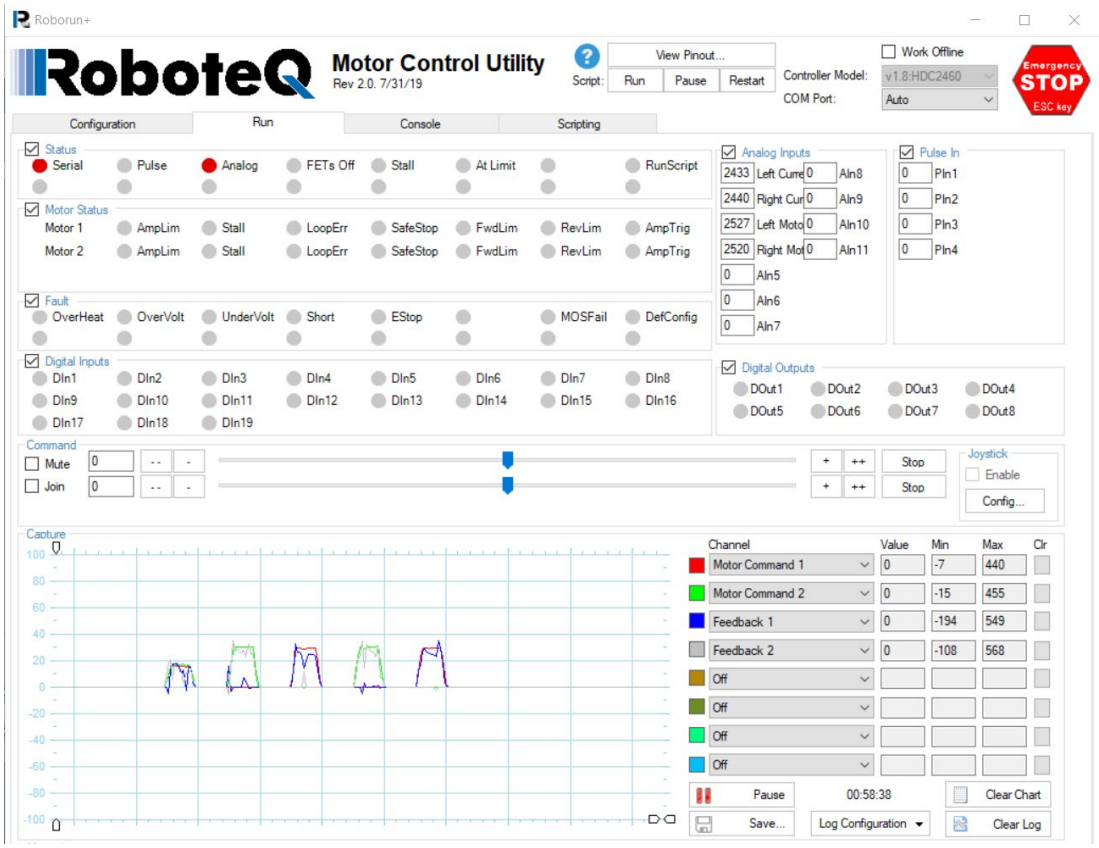

Figure 29: User interface within the RoboRun+ motor controller software, as seen during an alternating left- and right-side push ('slalom') maneuver.

The data visualization within the RoboRun+ interface shows the left and right motor commands from the NI USB-6341 and the corresponding levels of feedback from the in-line current sensors. RoboRun+ can also be configured to show power output, motor speed, motor current, and channel temperature for other applications. With the limited resolution

of the graphical interface and the inability to control start time and end time for each trial, the screen depicted in Figure 29 is used solely for quick verification that the channels were active, rather than being used for actual data logging and further analyses.

3.4.6 Torque Output Validation (Stationary)

Two main methods of calibration were used to characterize the relationship between motor armature amperage and output motor torque. Previous calibrations of the torque-current relationship for each of the motors used a weighted pulley system and commanded the motors to lift the weights in velocity mode (Figure 15). Regression fits of the armature current and effective motor torque yielded torque constants that matched the data more appropriately than the manufacturer-specified torque constant (Figure 16, Figure 17). The protocol is described in higher detail in [69]. A second method was adapted from a test rig originally designed to assessing the maximal tangential force output of human subjects, as described in [23]. The heavy wooden base platform acted as an anchor for a 110 lb-capacity digital force gauge (FG-3008, Shimpo Instruments Co.) and a yoked jack stand to lift the drive wheel axle by 1-5 mm (Figure 30).

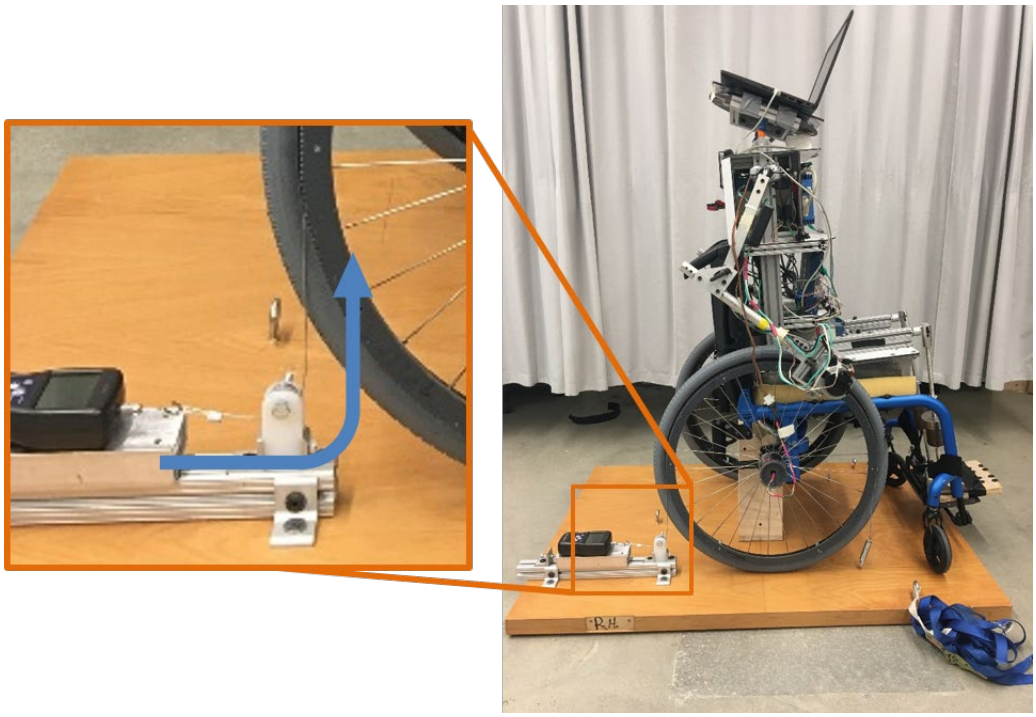

Figure 30: Stationary wheel torque measurement rig, with an inset detail view of the braided steel cable connecting the force gauge to the drive wheel.

In Figure 30, a braided steel cable connects the force gauge to the drive wheel push-rim standoff. A small pulley aligned with the load cell transmits tension in the cable from the horizontal orientation of the force gauge to the vertical orientation to run tangent to the drive wheel. A metal hook attached the cable end the standoff. To configure this rig to work with the AMPS, the opposite tangent point of the wheel was attached to a second cable, which grabbed the push-rim spacer and connected to the platform via a large tension spring (shown at the front-facing end of the drive wheel in Figure 30). With the cable attached, the spring was stretched to remove the slack of the cable and apply tension to the force gauge. This pre-load was zeroed out by the force gauge to remove any impact on the torque measurements from the spring.

Motor commands were designed as 5 second continuous applications at specific current outputs – 5 A, 7.5 A, 10A, and 12.5 A. The controller showed high repeatability across 5 trials at each command. CoVs were below 4% for each test configuration data set (e.g. left motor commanded to 5 A output).

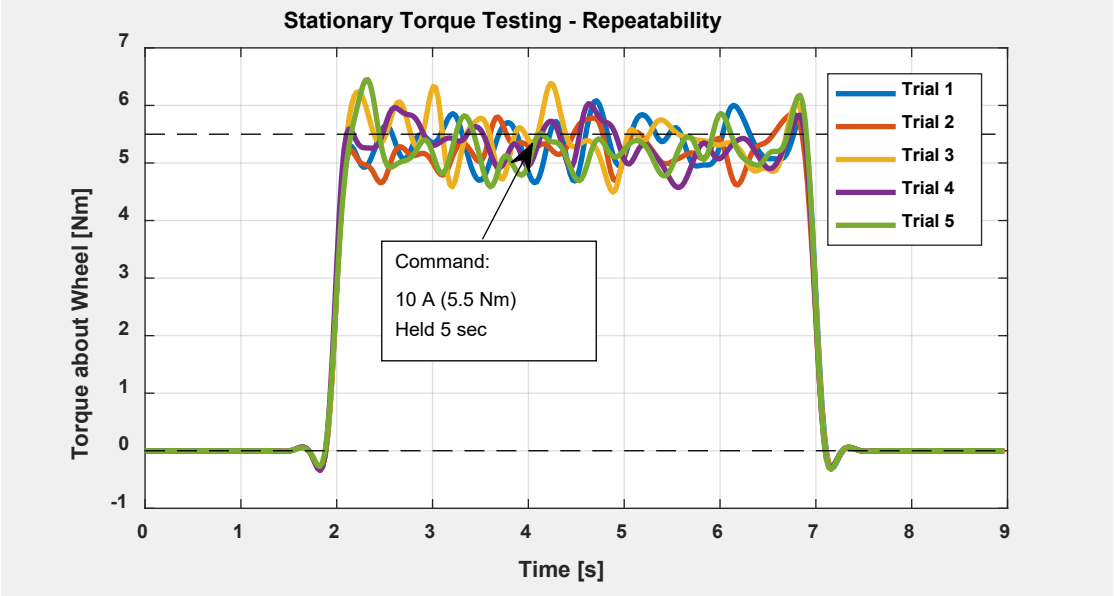

Figure 31: Repeatability of motor current control in stationary test rig.

The mean, standard deviation, and standard error of the mean (SEM) were calculated over the applied current range for each trial. SEM values never exceeded 0.05 Nm of torque within a trial (N = 200 samples over the 5 second duration). SEM values calculated across the trials of each configuration (N = 5 trials) remained under the same level. With these results, a total of 40 trials (5 trials per each of 4 command levels, with 2 motors) were taken. Forces from the Shimpo force gauge were multiplied by the measured radius of the push-rim to obtain wheel torques. The current-derived motor torques were plotted against the measured force-derived torques in Figure 32. Regression fits show high correlation

between desired and actual torques. As such, the AMPS was removed from the stationary torque testing rig and prepared for over-ground propulsion validation trials.

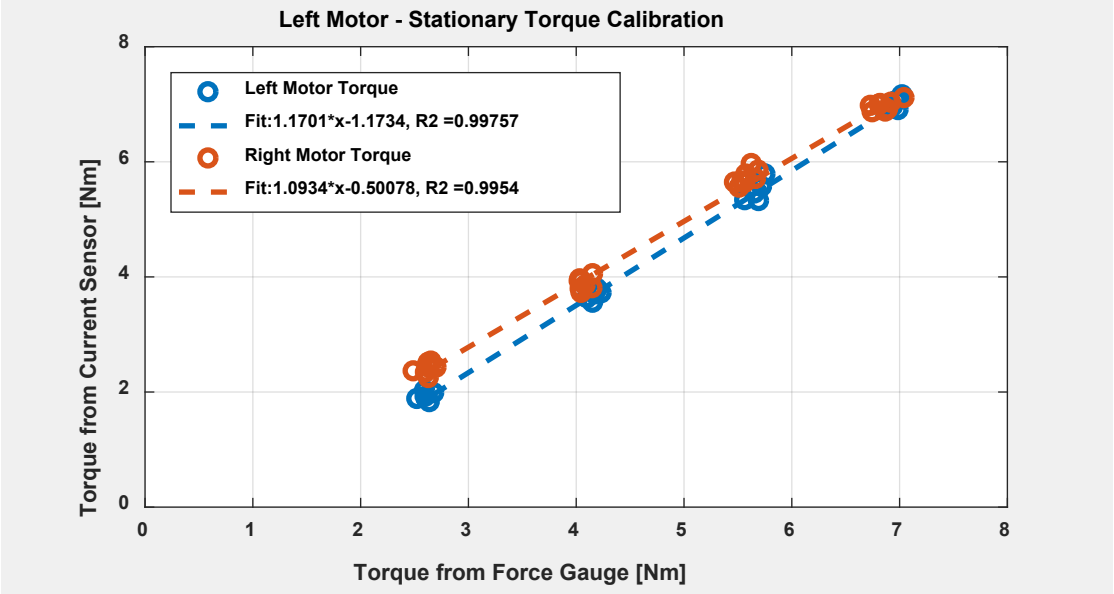

Figure 32: Motor torque validation from external force gauge.

3.4.7 Torque Output Validation (Over-Ground)

Part of the challenge with tuning the system in a stationary torque measurement rig is that the behaviour of the motor might look ideal without motion, then fail to meet expectations when applied in motion – as seen in Figure 13, the attainable torques drop as the motor shaft rotation rate increases. As a relevant example, the AMPS maintained a steady output on the stationary rig when given a 3 second command of 6 Nm, but dropped nearly 1.5 Nm over the exact same pre-generated torque command trajectory when allowed to travel over-ground (Figure 33).

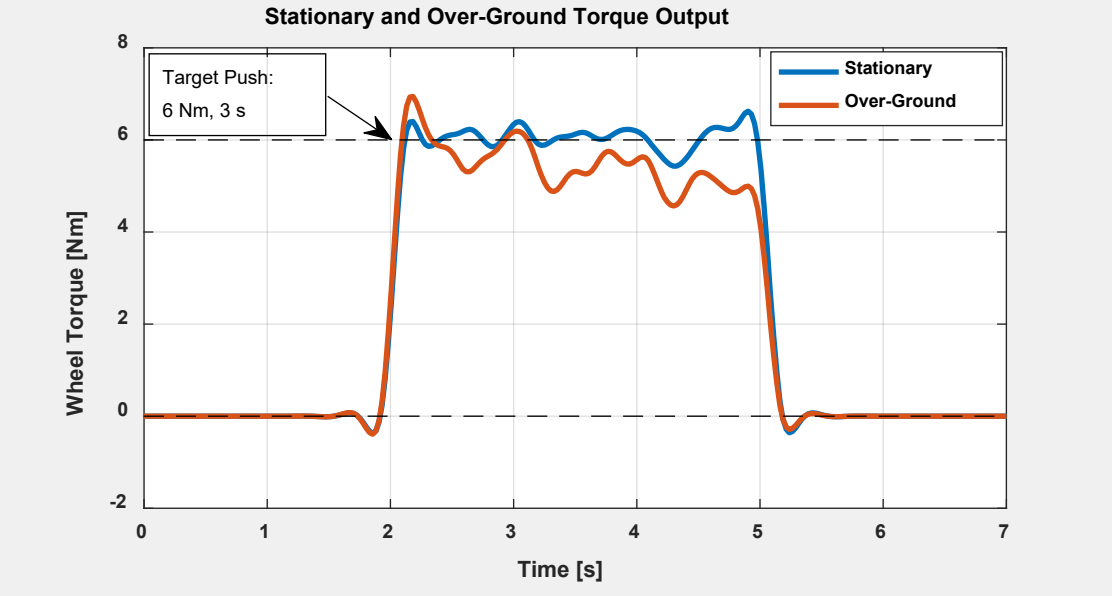

Figure 33: Discrepancy between stationary and transient torque output.

The differences are slight, but apparent: as the chair is allowed to roll under the influence of the applied torques on the wheels, the effective torque on the wheels decreases. This stems from the power curve (Figure 13) and the torque-speed relationship (Figure 14) of brushed DC motors. Fortunately, the speeds of human wheelchair bouts are typically less than 1.0 m/s [3, 4], and as seen in Figure 34, even elongated command torques were followed fairly consistently (up to 15% from target) at up to 1.5 m/s. What Figure 33 and Figure 34 fail to convey is that 'normal' torques from human users are short, at less than 0.6 seconds of push time. Within that time, the user accelerates their hand to match the speed of the wheel, accelerates even more to apply torque to the wheel, and quickly releases the wheel, creating a trapezoidal or even triangular torque profile about the wheel over the course of 0.6 seconds. By observation and MATLAB analysis, the first 1.0 second of the over-ground trial in Figure 33 (and dozens of similar trials at other desired torque values) stayed well within ± 10% of the target torque.

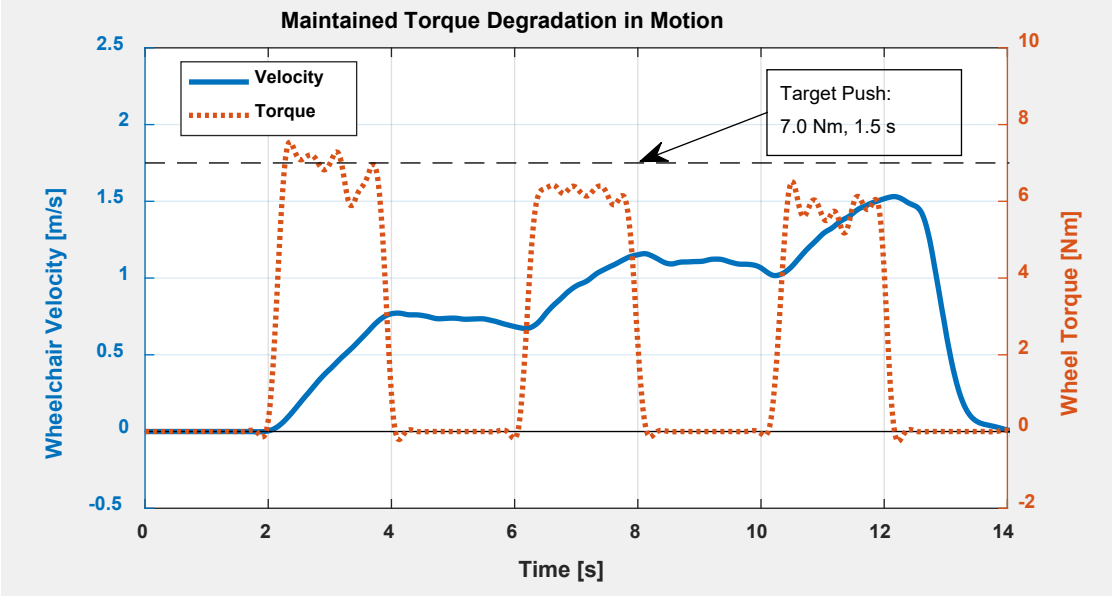

Figure 34: Degradation of maintained torque value due to motor rotation.

To more thoroughly address concerns over the possibility of the AMPS losing torque due to motion, the temporal parameters of the command propagation were examined. This was done by generating torque profiles with triangular or trapezoidal shapes of varying peaks and widths. It was found that purely-triangular pushes were never able to reach the target torque, regardless of push duration. The peaks of the triangular command signals were always truncated and the actual output motor torques resembled more of a parabolic shape. The cause of this timing issue was examined in two steps: the first step was to check if the LabVIEW program could actually output the command signal at the required speed (changing the analog output from 2.5 V to 4.0 V in 0.1 seconds in some cases), and the second step was to quantify how long the motor controller took to reach the target torque, after it was given the correct analog LabVIEW command.

Preliminary results from the triangular profile showed that the propagation of the signal through the LabVIEW-to-DAQ-to-output process required nearly 0.1 second – a

significant delay for the signal to generate and reach the desired value. The subsequent trapezoidal profiles were thus made using 0.25 second ramps on the rising side of the plateau to account for the signal delay. The width of each trapezoid was varied from 0.1 seconds to 0.7 seconds to investigate the rise time and settling time of the output motor torque. From visual inspection of Figure 35, it can be seen that none of the trapezoidal shapes of the command input were preserved in the 'Actual Torque' output signal. Further analysis showed that the desired peak torques were most often reached around 0.2-0.3 seconds. The 'ideal' output, where deviation from the command was minimized, occurred at a total push time of 0.55 seconds. This remained true for repeated tests with torques other than 12 Nm (profiles with the same temporal pattern at 5 Nm, 7 Nm, and 9 Nm were also tested).

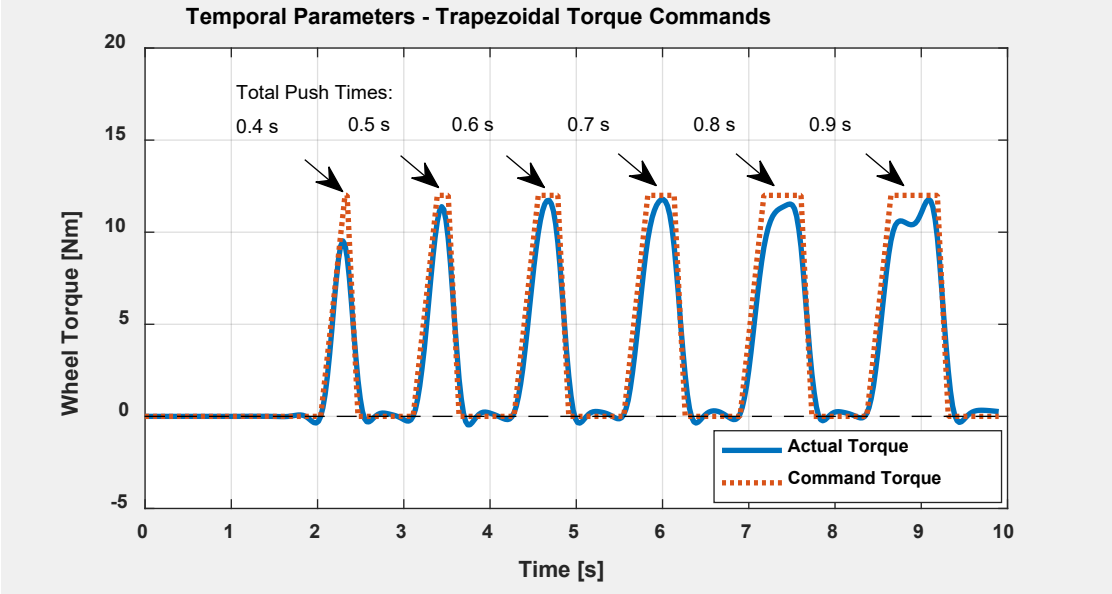

Figure 35: Temporal parameters used for torque mode trajectory generation.

Note that the torque profiles in Figure 35 were applied to each wheel of the MWC unrestrained – by the last push, the AMPS was traveling at over 1.5 m/s, whilst still

maintaining torques within ± 10% of the desired signal. This behavior, in addition to the cumulative validation testing results described above, showed that the AMPS was capable of producing torques on command, and it produced a general set of guidelines to follow to make pre-determined torque trajectories that could be followed by the AMPS.

3.4.8 Maneuver Generation

Several pieces of literature were used to inform the design of the torque trajectory. Torques about the wheel axle during straight forward motion have been measured with instrumented push-rims such as the SMART^{Wheel} system[36, 55, 60, 62, 101] and the OptiPush rim[102]. Though the added mass from the heavy instrumented wheels may have impacted the mechanics of the system[66], the torque trajectories from multiple studies were collected and considered when designing the appropriate torque profile for the AMPS. Some common characteristics from these study results showed the typical straight, forward maneuver to have an accelerating ramp-up phase consisting of three or four initial high-intensity pushes to rapidly accelerate the wheelchair, followed by a steady-state phase where the torque peaks are much lower and wheel velocities stay fairly constant. From a review of 22 studies and papers written on human wheelchair propulsion observations, there were key characteristics that were common amongst empirical data sets: start-up torque, steady-state torque, push time, and cycle duration or frequency, several of which are represented in Figure 36. The start-up and steady-state phases were analyzed separately when possible, as the torques, speeds, and push times within these two phases of motion are drastically different. Floor surfaces also changed the measured inputs – linoleum tile and carpet, for example, require different torques to reach the same speeds or maneuver along the same path tracks. The preliminary over-ground propulsion trials with the AMPS

mimicked these characteristics, and were adjusted accordingly to limit the resulting steady-state velocities to less than 1.0 m/s for most chair configurations, with a target of 0.8 m/s to align with the upper range of average wheelchair propulsion speed among the general population[3, 4].

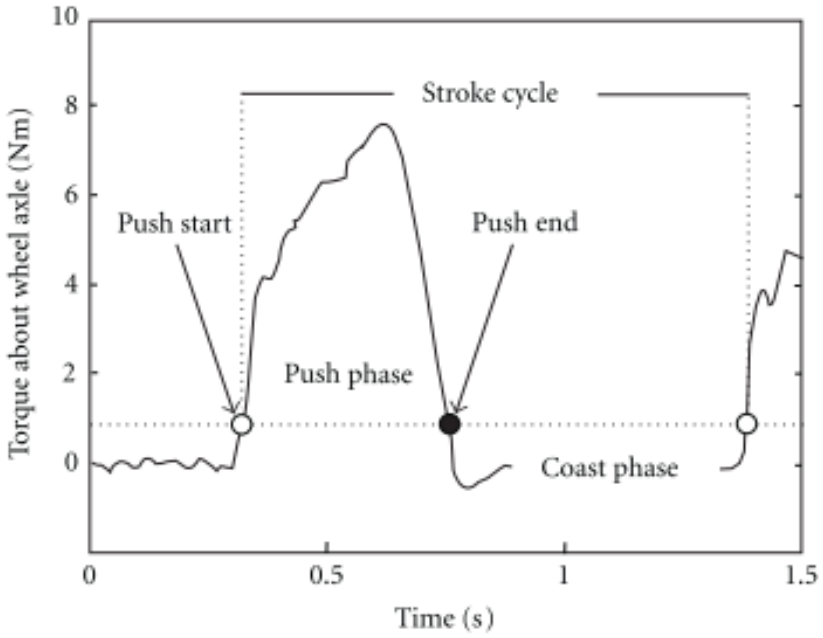

Figure 36: Typical propulsion cycle with nomenclature. From [102].

Generic maneuvers were already selected – as in previous iterations of AMPS studies, the most important aspects of MWC motion have already been identified via kinetic energy [78], and the canonical maneuvers showcased the efficacy of the AMPS at propelling with various trajectories [81] and discerning differences from the resulting MWC behavior [83]. The difficult task was to determine how to generate a torque profile to result in the desired motion without direct control over the velocity. Searching the literature produced articles from researchers like Koontz [11, 62, 103], Hurd [104], and Cowan [55, 105]; these published studies establish a precedent for expected over-ground

human propulsive torques for certain surfaces, from the initial start-up to steady-state velocity. The multitude of results from simulated environments (dynamometer, treadmill, ergometer) [7, 15, 75, 101, 106-108], though more numerous, did not always closely align with over-ground propulsion [35, 64, 103].

The timing of each push was especially hard to design. Crichlow's work reported cycle durations of 1.33, 0.94, and 0.78 seconds for the first three pushes and steady-state durations of 0.74 seconds, with push-to-cycle percentage of 65%, 42%, 30%, and 22%, respectively [85]. Koontz, on the other hand, reported 1.33, 1.03, 1.10, and 1.22 seconds for the same strokes, with push-to-cycle ratios of 68%, 59%, 45%, and 35%, respectively [62] – a great deal longer and slower than Crichlow's push parameters. Careful attention to the details in the 22 reviewed papers was taken to inform the temporal parameters. Sources like Ojeda's article [109] formed a solid basis to design each profile with a 1 push/sec frequency, as it showed that humans might employ more frequent strokes on more challenging surfaces like inclines, but the extent of the frequency ranged from 0.95 Hz to 1.06 Hz, with a fairly tight grouping. Cowan's study using the instrumented Smart^{Wheel} push-rims similarly reported cycle frequencies of about 1 Hz [60]. More specific timing was found in Robertson's article [75] which defined a 0.3 second time-to-peak for each push and a max tangential force of 100N. Finally, van der Woude's study went through 4 different speeds (0.55, 0.83, 1.11, and 1.39 m/s) and recorded average peak moments, push times, and rest times [7] – it was one of the few studies that utilized slower and more realistic travel speeds, despite being done on an ergometer. Koontz suggests that ergometer and over-ground are similar enough for consistent torque and force measurements [103], as does Kwarciak [64], with the caveat that the treadmills may actually require higher

torque. Typical push patterns show the first three pushes being slow and forceful, gradually becoming quicker and lighter pushes into the steady-state phase [60, 62, 85]. Other useful push cycle characteristics were identified and are presented in Table 5.

Table 5: Push-rim propulsion characteristics from reviewed literature

Source	Tang. Force (N)	Wheel Torque (Nm)	Speed (m/s)	Cycle Freq (Hz)	Push Time (s)	Surface or Environ.	MWC +Instr.
Asato, K.T., et al. (1993) [101]	30.0	-	1.3-1.8	1.2	0.5	Dynamometer	K0005 +SmartWheel
Boninger, M.L., et al. (2000) [20]	70.9-102.7	7.9-10.9	1.0-1.7	1.0-1.3	-	Dynamometer	Personal +SmartWheel
Cooper, R.A., et al. (1992) [108]	-	16.0	1.3-1.8	-	90° along rim	Dynamometer	Quickie +SmartWheel
Cowan, R.E., et al. (2008) [60]	72.3, 87.5, 126.2	-	0.7, 1.0, 1.2	1.0	-	Over-Ground, Assorted	Varied +SmartWheel
Koontz, A.M., et al. (2005) [62]	-	25.2 (peak), 13.0 (steady)	0.8-1.4	1.0	0.5	Over-Ground, Assorted	Varied +SmartWheel
Koontz, A.M., et al. (2012) [103]	-	15.0 (peak)	-	-	-	Over-Ground vs Dynamometer	Varied +SmartWheel
Kotajarvi, B.R., et al. (2004) [57]	-	8.3-12.3	1.5	0.9	0.3	Treadmill	K0005, custom rim
Kwarciak, A.M., et al. (2011) [64]	58.1 (peak), 38.9 (steady)	10.9	1.1	0.9	-	Treadmill, over-ground	Personal +OptiPush
Vegter, R.J., et al. (2013) [106]	65.8	-	0.77	0.4		Treadmill	K0005 +SmartWheel +OptiPush

The literature had disparate results, as seen in Figure 37. No common trends were established between target steady-state velocity and applied wheel torque from the body of literature reviewed. In general, wheel torques increased as the human operator traveled at faster velocities, though some flooring surfaces caused the opposite behavior. Similar plots were made comparing torque, push frequency, surface type, test type (simulated environment versus over-ground), with even less informative trends.

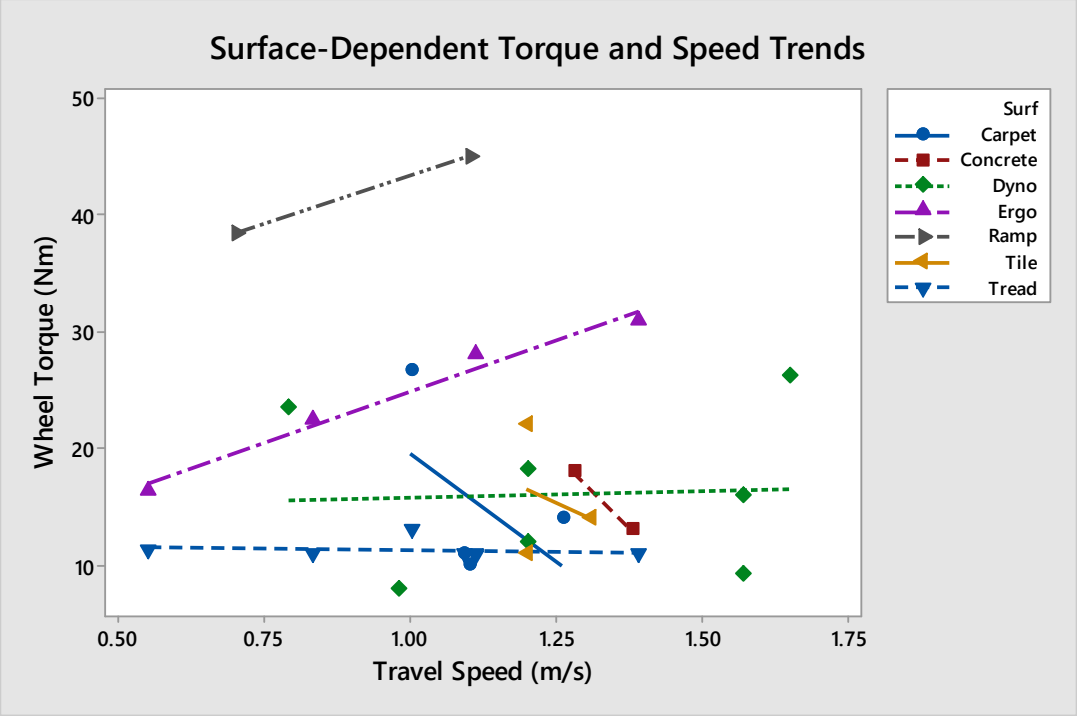

Figure 37: Average wheel torques versus the MWC velocity, grouped by floor surface.

Out of these disparate results, the literature search was narrowed to focus on studies measuring propulsion characteristics with travel velocities of around 0.65-0.95 m/s [57, 61, 62, 64, 75, 107] to mimic the most common speed in MWC bouts of mobility [3, 4]. From these sources, the finalized specifications for the original system maneuvers were chosen based on five commonly-identified push cycle characteristics: (1) Slower and heavier first

push; (2) Acceleration phase of three pushes in straight-forward motion; (3) Steady decrease in the push time and intensity of the latter two acceleration pushes; (4) At least four 'steady-state' pushes; (5) Consistent temporal parameters and torque magnitudes over the steady-state phase. A generic over-ground straight maneuver for straight forward motion over a linoleum tile hallway floor was generated (Figure 38) using the criteria above, with peak values and temporal parameters informed by the literature. To prove feasibility of the system and maneuver, a total of 13 pushes were applied to the push-rims. After the peak of the third push of the acceleration phase, the chair reached its steady-state velocity of around 0.83 m/s, which was maintained for the rest of the steady-state pushes. In Figure 38, the AMPS was loaded at 80 kg with a weight distribution of 70% on a K0005 (ultra-lightweight Quickie GT) frame. Out of 40 trials with the same maneuver, the applied torques for both motors had RMS deviations of less than 3% of the maximal torque and the SEM was 0.05 Nm of wheel torque.

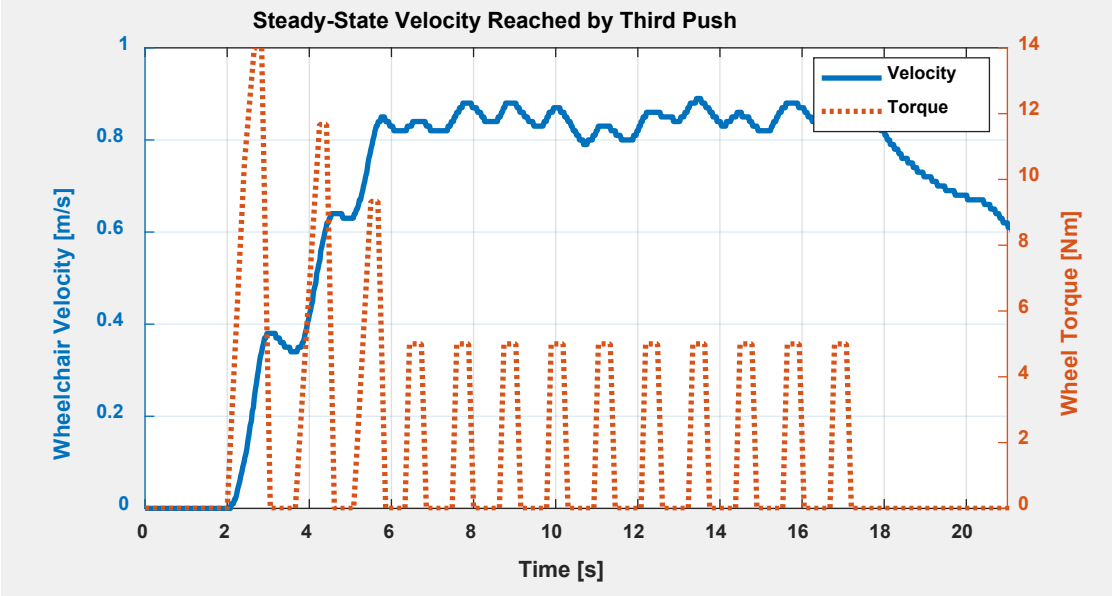

Figure 38: Example of extended straight maneuver torque profile with resulting MWC velocity.

These preliminary trials proved feasibility of the overall torque mode as well as the validity of the torque profile push characteristics.

3.5 Data Collection Procedure

The following three chapters investigate various aspects of common manual wheelchairs using the AMPS as a standardized wheelchair operator and test device. A single methodology was developed to collect data from each wheelchair configuration in an identical format. The data processing and analysis could therefore be standardized across studies. Data collection consisted of loading the body of the AMPS into a chair of interest, installing the necessary components to the chair frame and equipping the motors to the push-rims, and running over-ground AMPS trials with pre-defined maneuvers. The sensors onboard the AMPS collected speed and torque data to use for further processing.

3.5.1 Over-Ground Maneuvers

The preliminary over-ground propulsion trials with the AMPS were designed to parametrically mimic the propulsion characteristics of wheelchair users traveling along common indoor surfaces, specifically on tiled linoleum floor, as previously measured with the instrumented Smart^{Wheel} [11, 55, 60, 62, 101] and OptiPush [102] drive wheel systems. As in [78] and [71, 83], multiple types of motion exist in everyday MWC use. Straight (rectilinear) motion, such as propelling the chair forward in a straight line, is a very common component of MWC travel. This motion endows the system with kinetic energy dominated by the linear translation of the system mass [78] and the major sources of energy loss are from the rolling resistances of the casters and drive wheels [81, 83].

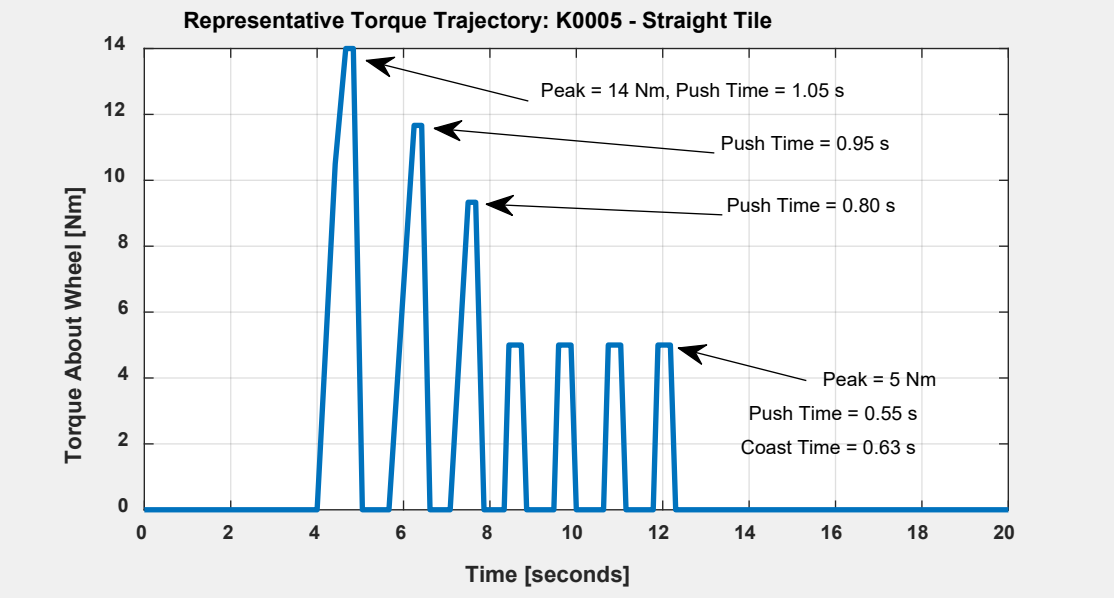

Figure 39: Torque trajectory – Straight on tile for ultra-lightweight frames.

The Straight maneuver utilized the same parameters as the torque profile generated for Figure 38, except with fewer pushes – the preliminary trials on the default K0005 frame

tended to accelerate past the expected steady-state value and reach maximum speeds of nearly 1.6 m/s. At those high speeds, the distance travelled by the MWC tended to quickly exceed the available stretch of tile hallway, and the motor speeds would exceed the reliable range of RPMs that could supply desired wheel torques, as in Figure 34.

Another main component of MWC travel is turning, or curvilinear motion. This motion endows the system with kinetic energy that is dominated by the linear translation of the system mass [78], but also has energetic contributions from the turning (i.e. angular travel of the system about the vertical 'yaw' axis). The major sources of energy loss in curvilinear motion are the rolling resistances of the casters and drive wheels as well as the scrub torque of swivelling the tires against the floor as the system turns [81, 83]. A slalom or serpentine-like trajectory was selected as the best representation of curvilinear motion with the AMPS. The Slalom maneuver featured longer torque applications with correspondingly longer coast times between each push. This maneuver had to first apply a small bilateral push (both arms simultaneously) to give the AMPS an initial velocity and align the casters to a path facing straight ahead, followed by a series of unilateral pushes to force the MWC to turn left, then right, then left, etc.

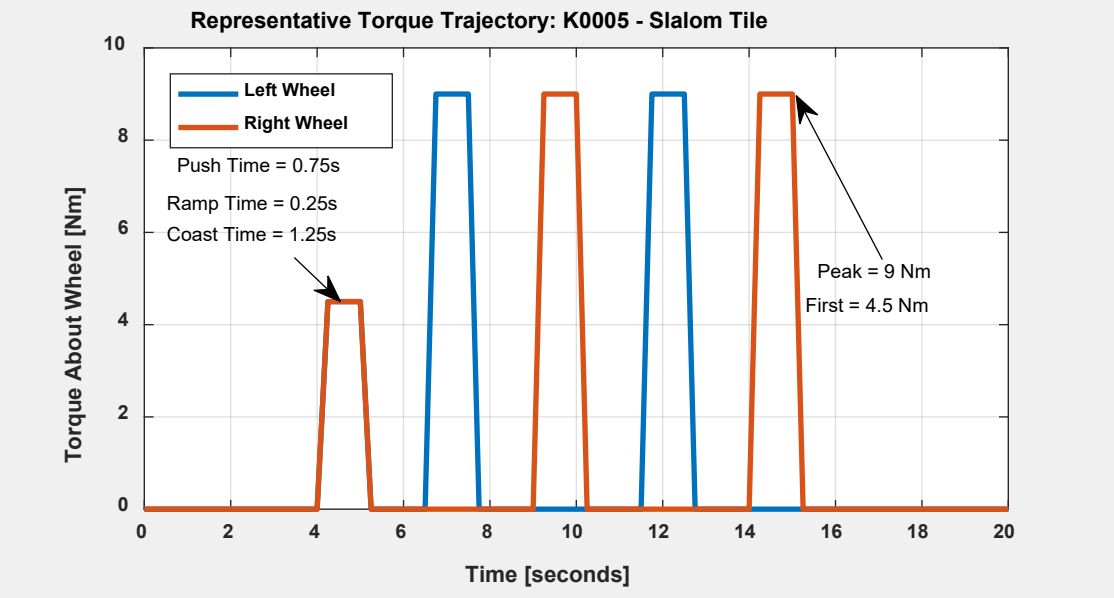

Figure 40: Torque trajectory – Slalom on tile for ultra-lightweight frames.

Both trajectories were tuned by adjusting the timing of the pushes and coasts, the peak torque amplitudes, and the overall number of pushes. The default 80 kg, 70% weight distribution was used for the initial testing; the expected torques from the literature review on human propulsion characteristics suggested that the torque peaks would be much higher than those seen in Figure 39, but deploying the AMPS with torques of nearly 10 Nm at the fourth push and beyond caused rapid acceleration of the system and was generally not a stable maneuver. The Slalom torques were similarly reduced from the initially-expected values because torques of 12 Nm would rotate the chair rapidly, to the point where the AMPS could have potentially been ejected out of the wheelchair seat. The torque profiles seen in Figure 39 and Figure 40 were the most viable and stable profiles.

3.5.2 Analysis of Over-Ground Data

Three outcome variables were reported for each Straight maneuver trial: propulsion cost; total distance traveled by the center of mass; maximum attainable kinetic energy by the MWC system. A fourth outcome variable was reported for the Slalom maneuver: cumulative (total) angular displacement of the MWC system about the vertical 'yaw' axis of the chair. These outcome variables were calculated using the following analysis:

In each of these over-ground maneuvers, the AMPS endowed the MWC with motion by applying torques to the wheels. Optical encoders on the wheels recorded the wheel position and angular velocity for every maneuver. The current sensors measured armature current on each motor, which was directly converted to output motor torque using the proportionality constant and further converted to wheel torques via the gear ratio between the motor and the push-rim. Wheel velocities and wheel torques were multiplied together to calculate the power supplied to the wheelchair by the AMPS (Eqn. 7). This power curve was integrated to yield the cumulative work over time for the duration of the maneuver (Eqn. 6). Angular velocities of the wheels were integrated over time and multiplied by the wheel radius to calculate the total distance traveled by the MWC over the maneuver. Propulsion cost, the dominant outcome variable representing mechanical performance, was reported as the ratio of total work supplied by the AMPS divided by the total distance traveled by the center of mass (Eqn. 8). Angular yaw displacement was found by recording the change in heading direction over time as a function of the wheel velocities and frame geometry, as in [78]. Kinetic energy was calculated as a sum of the various kinetic energies seen in Eqns. 1-3, and the maximum value throughout the maneuver was reported.

3.5.3 Equivalence Testing

Equivalence testing was used as a means to evaluate 'equivalent performance' of multiple configurations compared to a single baseline configuration. This style of analysis is well suited for a multi-faceted comparative study and is technically more appropriate than inferring a lack of a difference when assessed by traditional statistical means [110, 111]. Operationally, equivalence tests are a two-sided evaluation of differences using confidence intervals. They can be thought of as similar to a Student's t-test, but instead of assessing if the differences between groups of values are 0, equivalence tests assess if the 95% confidence interval of that same difference between groups is within a specified threshold. Take, for example, the two cases in Figure 41, below. The equivalence band in this example was arbitrarily set to ±5% of the control group mean value. The "Case 1" data shows that the 95% confidence interval, represented with horizontal error bars, is around 0 and both ends of the interval are within the threshold from -0.5 to +0.5 (arbitrary units). The two groups in "Case 1" would be equivalent.

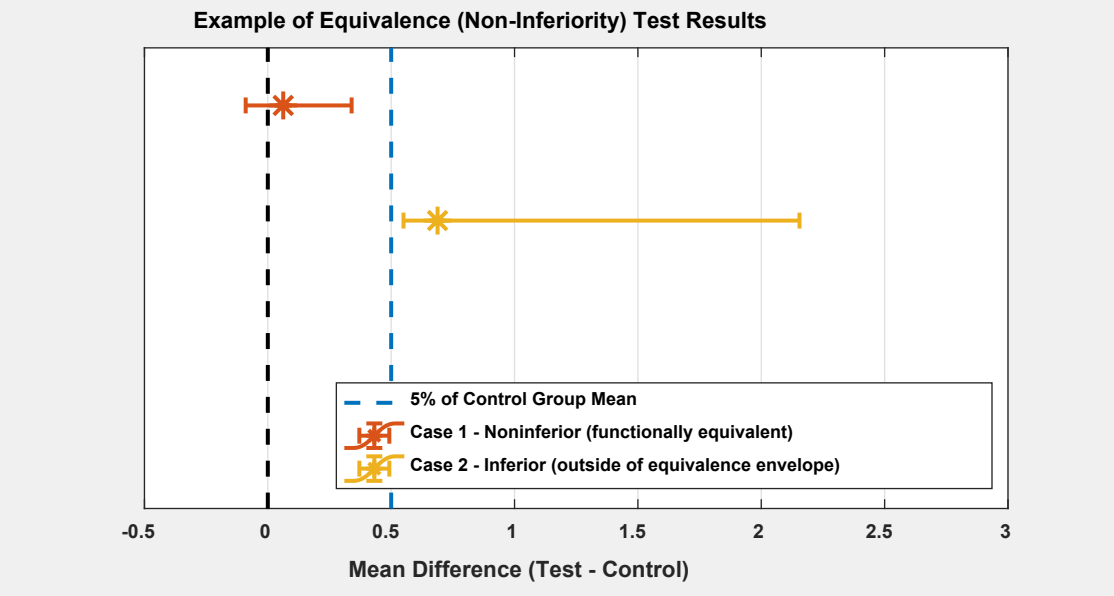

Figure 41: Equivalence testing, with two example cases showing the main types of outcome (equivalence and inferiority).

A subset of equivalence testing, called non-inferiority, is a one-sided version of the equivalence testing analysis. Non-inferiority assesses the absence of a relevant difference between performances of a test device to a reference device. In Figure 41, "Case 2" is a demonstrative example. Instead of setting the bounds of the threshold to ±5% of the control group mean, one of the bounds is set to either +∞ or -∞. Figure 41's bounds for non-inferiority were set to -∞ and +0.5, in this case, to see if the test group values were statistically higher than the control group values. Now, any groups with confidence interval differences completely above that threshold demonstrate that the control has an inferior value, definitively.

Within the following studies, propulsion cost values were compared between configurations with one configuration as the 'baseline' or 'reference' dataset. The assessment of non-inferiority was defined by:

$$H_1: \theta > \theta_0 + \varepsilon \quad (27)$$

where θ_0 is the mean of the reference or baseline condition, θ is the test mean, and ε is the equivalence interval value for which non-inferior performance is defined.

Non-inferiority can be claimed if the confidence interval of the difference between groups falls entirely above the lower bound of a one-sided equivalence interval [110, 111]. In the field of pharmaceuticals, the two-sided equivalence interval is normally defined as ±20% of the mean of the reference drug results – a very wide berth for a field as sensitive as medicine. In the following studies, non-inferiority bound values were based on a number of factors including the precision of measurement and human subject measurements from the reviewed literature. To define noticeable or meaningful differences, published studies of propulsion effort were reviewed to identify differences that were deemed *non-significant* in the respective analyses. A focus on non-significant differences was used to identify a judicious equivalence interval that reflected differences in propulsion effort obtained across manual wheelchair comparisons that did not result in a conclusion of a significant difference. Therefore, the defined equivalence interval would be realistic but also minimized within this study.

To inform the practically-important bounds of the non-inferiority analysis, literature from human wheelchair propulsion effort studies were examined, with various interventions and test configurations. Propulsion effort via metabolic cost measurement was chosen as it seemed to be the closest standardized wheelchair metric to the propulsion cost measured by the AMPS. The magnitudes of statistically significant differences versus

insignificant differences in metabolic cost measures were insightful. For example, Lui et al. compared lever-driven propulsion mechanisms versus typical push-rim propulsion via mass-normalized VO_2 measurements (mL min^{-1} kg^{-1}). VO_2 readings were significantly different between the spring-lever (5.78±0.66) and hand-lever (6.32±0.73) mechanisms (mean differences of 9.34% of the reference mean), but not between the roller-lever (5.91±0.86) and roller-hand (6.34±0.86) mechanisms (mean differences at 7.3% of the reference mean) [112]. Between standard manual push-rim propulsion and powered motor-assisted propulsion, Pavlidou reportedly found that the difference between energy expenditure (J kg^{-1} s^{-1}), 7.6%, was not statistically significant [113]. de Groot reported differences in VO_2 measurements (mL min^{-1}) of 4.9% across drive wheel tire inflation values (879±93 versus 838±135) that were not deemed significant [33]. Similarly, Sawatzky's distance- and body mass-normalized energy expenditures (mL kg^{-1} m^{-1}) were not significantly different between 100% tire inflation and 75% tire inflation (3.0% change in expenditure), but differences were significant between 100% and 50% tire inflation (12.0% change) [49]. Hilbers and White measured oxygen consumption (L min^{-1}) and reported differences between propelling a standard wheelchair (0.70±0.05) and a sports wheelchair (0.58±0.06); despite a difference of nearly 21% of the baseline mean, the differences were not statistically significant [114]. From Sagawa's incremental mass study, the reported metabolic effort values measured via VO_2 integral visually showed few differences between tests with incremental mass additions of 1 kg, 2 kg, and 5 kg, and it was ultimately concluded that mass had no significant effect in propulsion tests over sidewalk, slalom, flat treadmill, or 5% inclined treadmill, despite slalom costs increasing between 4% and 12% depending on added weights [34]. Another point of reference was

found in a different metric: Cowan's measurements of propulsion forces before and after adding 9 kg to the tested wheelchair frame while propelling over tile reported statistically significant differences of approximately 4% of the reference mean [55]. These reportedly non-significant differences in the propulsion effort values are shown in Table 6, below, to summarize these results.

Table 6: Reported insignificant differences used to inform equivalence and non-inferiority tests.

Source	Studied Comparison	Propulsion Effort Parameter	Non-Sig. Difference in Prop. Effort Param. Means
Lui, J., et al. (2013) [112]	Lever-based propulsion versus hand-rim propulsion	Oxygen consumption ($\dot{V}O_2$ in L/min)	7.3%
Pavlidou, E., et al. (2015) [113]	Standard push-rim versus power-assist wheels	Energy expenditure (J/kg/s)	7.6%
de Groot, S., et al. (2013) [33]	Tire pressure inflation, 100% versus 75% of recommended	Oxygen consumption ($\dot{V}O_2$ in mL/min)	4.9%
Sawatzky, B.J., et al. (2004) [49]	Tire pressure inflation, 100% versus 75% of recommended	Energy expenditure (J/kg/s)	3.0%
Hilbers, P.A. & T.P. White. (1987) [114]	Standard versus sports-designed wheelchair	Oxygen consumption ($\dot{V}O_2$ in L/min)	21%
Sagawa, Y., et al. (2010) [34]	Added 5 kg of mass to frame during slalom	Oxygen consumption ($\dot{V}O_2$ in L/min)	~12%

The statistically insignificant differences were found to be, on average, 9.4% of the reference mean from each of the reviewed literature. Based on the assumption that mechanical testing is more precise at capturing the mechanical system performance than the reviewed human subject performance measurements, the non-inferiority bounds in the following studies were defined as approximately half of the value identified as the average

insignificant, yet noticeable, difference. Functionally, if studies with human subjects could not detect significant differences at even 10% of the reference mean (depending on the intervention or independent study variable), it is assumed that the AMPS robot should be a more sensitive data collection tool; any effect that a dependent variable would have on mechanical propulsion cost would be recorded by the AMPS. If no differences are found at the robotic level, then it would reinforce and explain why no differences were reported at the human level. In other words, if the AMPS propulsion cost results show equivalence, then the propulsion cost differences between configurations for all intents and purposes can be considered negligible to the human user, from a functional standpoint considering the context of use. The resulting equivalence bounds for the following three studies, therefore, were set at 5% of the baseline mean value, or 0.05 times the propulsion cost mean of the default configuration.

CHAPTER 4. INCREMENTAL MASS ADDITIONS TO FRAME

The purpose of this study was to (1) evaluate the extent to which incremental additions to the wheelchair frame mass has influence on the mechanical propulsion characteristics and (2) compare the influence of proximal loading under the CoM to distal loading on the footrest, in both straight and curvilinear maneuvers. Additionally, a simple coast-down deceleration test was used to approximate the system-level rolling resistance of each loading configuration.

4.1 Overview

The topic of wheelchair frame mass in the literature is often misguided and controversial [27]. It is an accepted fact that increased system mass causes an increase in the rolling resistance of the drive wheels and casters, as clearly shown in several sources ranging from classical tire and vehicle dynamics [40] to more specific wheelchair-related studies [56, 81, 115, 116]. However, when discussing the range of frame masses that separate the HCPCS K-codes, humans are notably insensitive to the mass increases [33, 34, 55]. In fact, outside of professional wheelchair athletes [117], wheelchair users showed no performance detriments between unweighted and chairs loaded with up to 10 kg, which would nearly double the mass of a typical K0005 wheelchair. Why, then, is it so heavily relied upon in the medical reimbursement coding system?

In general, very few studies relate measurements of human propulsion characteristics to system mass or wheelchair mass for analysis. From the few existing articles, one reported that the position of the shoulder relative to the drive wheel axle and

weight distribution have the most significant influence on propulsion effort, whereas system mass and muscle strength had the least influence [23]. These conclusions are corroborated by articles comparing the position of the seat to propulsion characteristics [19, 58, 69]. Likewise, de Groot et al. designed an experiment to assess the relative contributions of system mass (0 kg, 5 kg, or 10 kg added) versus tire type on the power output, heart rate, VO_2, mechanical efficiency, and propulsion technique of 11 human subjects on a treadmill at a fixed speed of 1.11 m/s. The extra mass did not increase any of the measured outcome variables [33]. In fact, simply changing the tire type from pneumatic to solid had a greater impact on physiological measurements than adding up to 10 kg of mass to the frame, though the added mass magnified the disadvantage of the solid tire type [33]. In a similar manner, Bednarczyk and Sanderson also added masses in discrete 0 kg, 5 kg, and 10 kg loading conditions but did not find mass to have an impact on the propulsion efforts exerted by the subjects [118]. In contrast, Cowan et al. used two chairs differing by 9 kg frame mass, and observed that increased mass was linked to decreased velocities and increased tangential push forces on the push-rims [55], though the apparent effects on propulsion characteristics should likely be attributed to incidental changes between the two tested wheelchairs, rather than directly correlated to the mass [119]. Similarly, Hilbers and White compared propulsion characteristics when traveling in a sports-designed wheelchair versus a 9.1 kg heavier standard ‘conventional’ wheelchair, and reported a 17% reduction in metabolic cost with the lighter chair [114], though they made it apparent that the cost difference was likely due to alternate design choices and should not be attributed to the frame mass exclusively.

With disparate conclusions on the effects of mass even at increased loads of 10 kg, it is difficult to deduce the impact of sub-5 kg additions. To more appropriately address this question, Sagawa et al. designed a study focused solely on the effect of small, incremental additions of 0, 1, 2, and 5 kg on the propulsion performance of wheelchair users versus able-bodied subjects on the physiological parameters, perceived exertion, and performance during completion of specific tasks. None of the loading conditions had any significant impact on energy expenditure, heart rate, or task completion rate [34]. The margin of error in the results are too high to draw any meaningful conclusions between the results; high variability between human subjects is not unexpected, yet it does diminish the gravitas of the reported results. There is too much variability between studies to have any statistical power to draw conclusions about frame mass and its relation to propulsion.

Following the results of several specific studies [23, 33, 34] would seem to suggest that adding mass to the wheelchair frame, at least to an extent of 5 kg, plays little to no role in the performance or efficiency of the wheelchair under human operation. The placement of the weight, however, may make a difference. Specifically with respect to turning maneuvers, adding weights far away from the drive wheel axle or center of mass increases the required propulsion forces and is generally more physically demanding [120]. This is due to a combination of reasons: shifting mass from a larger-radius wheel to a smaller-radius wheel increases the rolling resistance and scrub torque acting on the wheelchair [51, 81], and the rotational inertia of the system will increase, which correspondingly increases the system resistance to turning [69, 79, 121].

Nevertheless, with no mention of weight distribution, the HCPCS-defined “standard” (K0001) and “ultra-lightweight” (K0005) MWCs are simply separated - among

other criteria - by differences of less than 3 kg. It would be a great benefit to this field of research if the respective contributions of system mass and weight distribution to overall wheelchair performance could be quantified in a repeatable and expandable manner. The AMPS has demonstrated the required sensitivity in the preliminary mass and weight distribution study [69] and an extensive study of 'propulsion cost' with respect to multiple wheelchair design factors [71]. However, in the efforts to model the relationship between propulsion cost and simple wheelchair measurements, the mass and weight distribution factors were drastically overshadowed by the factors of energy losses at the wheels. Wheelchair mass and weight distribution can and should be further investigated using this concept of propulsion cost, which is a relevant and useful outcome measure that can be directly translated and understood by manufacturers, clinicians, and users themselves. Thus, the objective of this study was to isolate the effects of mass placement and weight distribution on wheelchair propulsion cost using the wheelchair-propelling AMPS robot.

4.2 Hardware and Configurations

Two main factors were considered in this study: frame mass and weight distribution. The main focus was placed on adding incremental mass to the tested wheelchair frame, in increments of +0, +2, and +4 kg. Distribution of the weight took a secondary focus because it has already shown importance in previous studies [19, 57, 69], and has significant correlation to the system mass in terms of the loads applied to the casters and drive wheels [81]. Weight distribution was included as a secondary factor as it is demonstrative to showcase how the placement of any added mass might be as important as the added mass itself to the outcome performance. Both parameters were measured by placing the AMPS and wheelchair together on the iMachine [79]. The chosen 'default'

configuration included the AMPS configured to an occupant mass of 80 kg with approximately 72% of the total system weight distributed over the drive wheel axle (nominally 70%WD), in accordance with reported average weight distributions for ultra-lightweight wheelchair users in a recent study [23].

4.2.1 Weight Support

To accommodate incremental mass additions to the frame without fundamentally changing the weight distribution, a lightweight metal shelf was fastened underneath the seat of the wheelchair (Figure 42), similar to the shelf used by Sagawa et al. to keep added weights out of sight of the human subjects [34]. Weights added to this shelf were secured at approximately the same fore-aft location as the drive wheel axle.

Figure 42: (Left) Platform to support up to 4 kg of added mass to the K0005 frame. (Mid) Platform loaded with 4 kg of disk weights. (Right) Footrest loaded with same stack of 4 kg disk weights.

Weights were placed on either the footrest or the axle (via the Dibond weight support shelf) in a total of 5 configurations, seen in Table 7. The default arrangement, termed the “0A” configuration to represent +0 kg on the axle, was measured at a weight distribution of 72%

over the drive wheel axle. This distribution was preserved by adding weights to the axle around the CoM location. Placing weights at the more distal footrest location shifted the CoM forward and reduced the weight over the drive wheel axle by 3-6%.

Table 7: Mass and weight distribution of incremental mass configurations.

Config. Name	Placement	Added Mass	System Mass	Weight Distribution over Drive Wheel Axle
"0A"	Axle (Default)	+0 kg	93.6 kg	71.9%
"2A"	Axle	+2 kg	95.6 kg	72.0%
"4A"	Axle	+4 kg	97.6 kg	72.0%
"2F"	Footrest	+2 kg	95.6 kg	68.7%
"4F"	Footrest	+4 kg	97.6 kg	65.7%

4.2.2 Frame Selection

Only one single chair was used in this study to control for geometric factors that vary between makes and models. The wheelchair frame selected for this study was the Quickie GT (Sunrise Medical, LLC), a rigid ultra-lightweight (K0005) with customizable axle and caster fork positions. The 16"x17" seat was set to have a floor-to-seat height of 18" and the front edge, with a seat dump of 1" (from the front edge to the rear edge, the seat has an angle of approximately 3.5° below horizontal). The AMPS was loaded to 80 kg. Precise weight distribution values of each configuration are in Table 7.

4.2.3 Component Selection

Components were selected based on examination of the industry standard. Primo Orion 24”x1-3/8” tires were used on metal spoked rims. The tires were inflated to the suggested pressure of 75 psi. Primo 5”x1” solid casters were used in this study. These components are common options for similar ultra-lightweight wheelchairs. The total mass of the unloaded wheelchair with the front footrest, casters, drive wheels, and anti-tip bars was 13.6 kg.

4.3 Experimental Design

A single K0005 frame was used with one pair of standard drive wheels and casters. Two maneuvers were selected: a 7-push straight trajectory and a 5-push slalom trajectory, both over a waxed linoleum tile surface. Each maneuver is tested with 5 trials in each opposing heading direction (forwards, backwards, as well as left and right starting pushes for the slalom) to normalize any irregularities in the hallway. With 30 total trials per configuration and 5 configurations, this experiment required 150 over-ground AMPS trials.

4.3.1 Maneuver Selection

The preliminary over-ground propulsion trials with the AMPS were designed to propel the MWC test configurations in a Straight and Slalom motion, respectively. The Straight maneuver utilized the same pre-generated torque trajectory seen in Figure 39. Likewise, the Slalom maneuver utilized the pre-generated torque trajectory in Figure 40. This maneuver featured a series of reciprocating turns that repeatedly changed the direction

of travel to induce a swivelling motion on the interface between the flooring surface and the tires.

4.4 Methods

4.4.1 Data Collection

First, a simplistic coast-down deceleration method was used to characterize the typical coasting behavior of each configuration. The motors were disconnected from the ring gear push-rims to decouple the propulsion system. The wheelchair was centered in the hallway. From rest, the wheelchair was manually pushed via the rear handles to accelerate the chair to approximately 1.0 m/s. Upon reaching the target speed, the wheelchair was released and permitted to roll down the hallway until it naturally decelerated to a stop. Wheel velocities were recorded by the wheel encoders. 10 trials were taken in the forward and backward hallway directions (the AMPS was always facing the direction of travel) to account for any slopes or inconsistencies in the tiled floor for each configuration, resulting in 100 total coast-down trials. The coast-down deceleration tests were used to demonstrative a rapid test method to detect differences between the configurations without deploying the entire AMPS protocol. Though the AMPS was loaded on each configuration, the same test could have taken place with the ISO 7176-11 wheelchair dummy [74] and some form of inertial measurement unit or accelerometer on each drive wheel. This analysis was expanded to a simple investigation of rolling resistance force acting on the system, much as is done with the coast-down cart deceleration test protocol [81], by multiplying the mean deceleration value by the mass of the system (93.6 kg for 0A, 95.6

kg for the +2 kg configurations, and 97.6 kg for the +4 kg configurations). The product of those terms yields the average force acting against the motion of the chair.

Next, the experimental protocol consisted of 30 over-ground propulsion trials for each of the five configurations, totaling 150 AMPS trials in all. Any additional incremental weights on the under-seat platform were tightened into place. The pneumatic drive wheels were inflated to 75 psi as per the manufacturer recommendations. The torque trajectory was loaded into the LabVIEW interface and the AMPS was set up along a 30 meter length of clean, flat linoleum tile hallway. To normalize for surface inconsistencies such as slope or intermittent bumps, 5 forward-heading trials were run in each of the forward and backward hallway directions along the same length of tile for the Straight maneuver. Similarly, the Slalom maneuver was tested with 5 trials in each of the left and right slalom maneuvers in both the forward and backward hallway directions, resulting in a total of 20 slalom trials altogether. The collection of trials for each configuration were averaged together by maneuver ($N = 10$ for Straight, $N = 20$ for Slalom) and the repeatability for the set of trials was assessed. The inclusion criteria for each set of trials was that the CoV of each outcome variable (nominally distance, as it was the easiest to assess visually and with a rapid post-trial MATLAB analysis) remained $\leq 10\%$.

4.4.2 Data Analysis

The four main outcome variables of this experiment were: 1) propulsion cost (Eqn. 8), 2) distance travelled by the center of mass, 3) yaw distance travelled as the wheelchair changed heading direction, and 4) the maximum attainable kinetic energy of the system, as calculated utilizing Eqns. 1-4 and nomenclature from Medola [78]. Data from the current-

based motor torque sensors, motor encoders, and wheel-mounted encoders were collected at 40 Hz during the over-ground trials. These data were processed in MATLAB. Butterworth filters were used to smooth each sensor signal before calculating the input power to the system from each motor. Coast-down data, represented as the value of the deceleration slope as the MWC slowed from 0.95 m/s to 0.35 m/s, were analyzed as per [81]. The collected data from the 150 individual over-ground trials were used to calculate the propulsion cost and overall distance traveled by the center of mass.

Basic descriptive statistics for each outcome variable, including coast-down deceleration, were first assessed across the trials for each loading configuration. Cohen's d effect sizes were calculated for each group with the +0 kg (0A) configuration as the baseline. Effect sizes of $d = 0.2$ indicated that the group means differed by less than 0.2 of the baseline standard deviation and were therefore considered small, $d = 0.5$ were considered medium, and $d = 0.8$ were considered large [122]. Percent change of the means between groups was calculated to tease out the relative contributions of incremental mass and weight placement to the outcome variables. Paired t-tests were used to determine statistically significant differences between configurations for each of the outcome variables, including coast-down deceleration values. Normality of propulsion cost data were assessed with Kolmogorov-Smirnov goodness-of-fit tests. Both Straight and Slalom propulsion costs were found to have normal distributions ($p > 0.150$). Further analyses were run with ANOVA tests with propulsion cost as the outcome variable and the configuration as a categorical predictor. Tukey's significant difference test was used for post-hoc analysis with a comparison rate of 5.

To assess when the performances differed by more than a practically-important amount, equivalence tests were conducted within Minitab (Minitab 18, Minitab Inc.). The α, or risk level of claiming inferiority when inferiority should be rejected, was set to 0.05 to calculate the location of the 95% confidence interval of the difference. Propulsion cost values for the baseline configuration were entered as the reference sample group and the values for each modified loading case were selected as the test sample groups. The null hypothesis was that the differences (test mean – reference mean) would fall above the lower bound (0.05 times the mean of the reference sample). The alternative hypothesis was that the difference would remain within the boundaries, and the sample groups would be claimed equivalent, which places a greater burden of proof on proving the groups are equivalent than a standard paired or 2-sample t-test.

4.5 Results

4.5.1 Coast-Down

Table 8 shows that both mass and weight distribution had large effects on the deceleration and force acting on the wheelchair.

Table 8: Descriptive statistics of coast-down results for each incremental mass configuration.

		0A	2A	4A	2F	4F
Mean Decel. (m/s^2)	Mean (± StDev)	-0.0596 (±0.0015)	-0.0572 (±0.0011)	-0.0589 (±0.0014)	-0.0601 (±0.0018)	-0.0622 (±0.0009)
	Effect Size	-	1.81	0.48	0.29	2.16
	% Change	-	- 3.98%	- 1.18%	+ 0.81%	+ 4.47%
	p-value	-	0.00*	0.13	0.43	0.00*
Mean Force (N)	Mean (± StDev)	5.58 (±0.14)	5.47 (±0.11)	5.75 (±0.14)	5.74 (±0.17)	6.07 (±0.09)
	Effect Size	-	0.87	1.22	1.06	4.27
	% Change	-	- 1.93%	+ 3.04%	+ 2.96%	+ 8.93%
	p-value	-	0.01*	0.23	0.01*	0.00*
*Significantly different ($p < 0.05$) from the mean of the 0A configuration.						

In both coast-down deceleration and the simplistic rolling resistance force test, the 2A configuration had a statistically significant ($p < 0.05$) difference from 0A. Out of 10 forward and 10 backward coast-down trials, the chair experienced a more gradual deceleration by adding 2 kg to the axle. This was not a general trend, however, as adding a second 2 kg mass to the axle increased (i.e. worsened) the deceleration and added more

rolling resistance. Every other configuration experienced greater rolling resistance force, and the deceleration values were higher for both of the footrest-loaded configurations. As expected, as the weight was placed on the distal footrest, the deceleration was increased and the approximated resistive force on the wheelchair likewise increased.

4.5.2 Straight

Basic descriptive statistics for the three major outcome variables (Table 9) show that there were noticeable and statistically significant differences between the configurations. Effect sizes ranged from small to very large, with greater emphasis under the footrest-loaded configurations.

Table 9: Descriptive statistics for cost, distance, and kinetic energy of incremental mass configurations in the Straight maneuver.

		0A	2A	4A	2F	4F
Cost (J/m)	Mean (± StDev)	8.89 (±0.53)	8.95 (±0.37)	9.25 (±0.27)	9.27 (±0.29)	9.43 (±0.34)
	Effect Size	-	0.14	0.87	0.89	1.21
	% Change	-	+0.71%	+4.11%	+4.28%	+6.06%
	p-value	-	0.77	0.08	0.07	0.02*
Distance (m)	Mean (± StDev)	8.76 (±0.40)	8.45 (±0.44)	7.90 (±0.10)	8.01 (±0.11)	7.65 (±0.12)
	Effect Size	-	0.76	2.97	2.56	3.76
	% Change	-	-3.64%	-9.86%	-8.60%	-12.68%
	p-value	-	0.11	0.00*	0.00*	0.00*
Max. Kinetic Energy (J)	Mean (± StDev)	34.27 (±2.09)	32.99 (±2.28)	30.87 (±0.86)	31.39 (±1.08)	29.73 (±1.10)
	Effect Size	-	0.58	2.13	1.73	2.72
	% Change	-	-3.73%	-9.91%	-8.42%	-13.26%
	p-value	-	0.21	0.00*	0.00*	0.00*
*Significantly different ($p < 0.05$) from the mean of the 0A configuration.						

Statistically significant differences between the group mean propulsion costs were reported ($F(4,45) = 3.79$, $p = 0.010$). Tukey's post-hoc assessment showed significant differences between the 4F configuration cost and both the 0A and 2A configuration costs. Overall, even the most extreme changes in propulsion cost were small, but non-negligible – 2 kg on the axle had a small effect size and did not vary by even 1%, whereas the 4F (i.e. worst-case) loading had less than 6% change in propulsion cost. The distance traveled by the CoM showed more drastic differences. Effect sizes were large to very large for all groups,

and the paired t-test determined that the differences between each group to the 0A configuration were statistically significant. The percent change from the 0A mean is the most demonstrative of the distinct differences between incremental mass and weight placement – adding 2 kg decreased the distance by only 4% with careful arrangement of the weight, and nearly 9% with the same extra weight on the footrest. In fact, 4 kg on the axle has very nearly the same impact on the distance as just 2 kg on the footplate. For the maximal kinetic energy, every group showed statistically significant differences, and groups 4A, 2F, and 4F had very large effect sizes. It is important to keep in mind that the most basic kinetic energy equation for the rectilinear (forward) translation of the mass, $KE_{translate} = mv^2/2$, increases proportionally with the mass of the system. The +2 kg and +4 kg configurations, therefore, achieve lower velocities than the 0A configuration and ultimately have poorer utilization of the torque supplied to the wheels despite having a slight advantage from the extra mass term.

Propulsion costs were plotted in Minitab with their representative 95% confidence intervals (Figure 43). Though the ranges seem disparate between the 0A and 4F configurations, the entire vertical span of the plot is only ~1.75 J/m of cost, which is a tight group of propulsion costs compared to prior cost studies with the AMPS [71, 82].

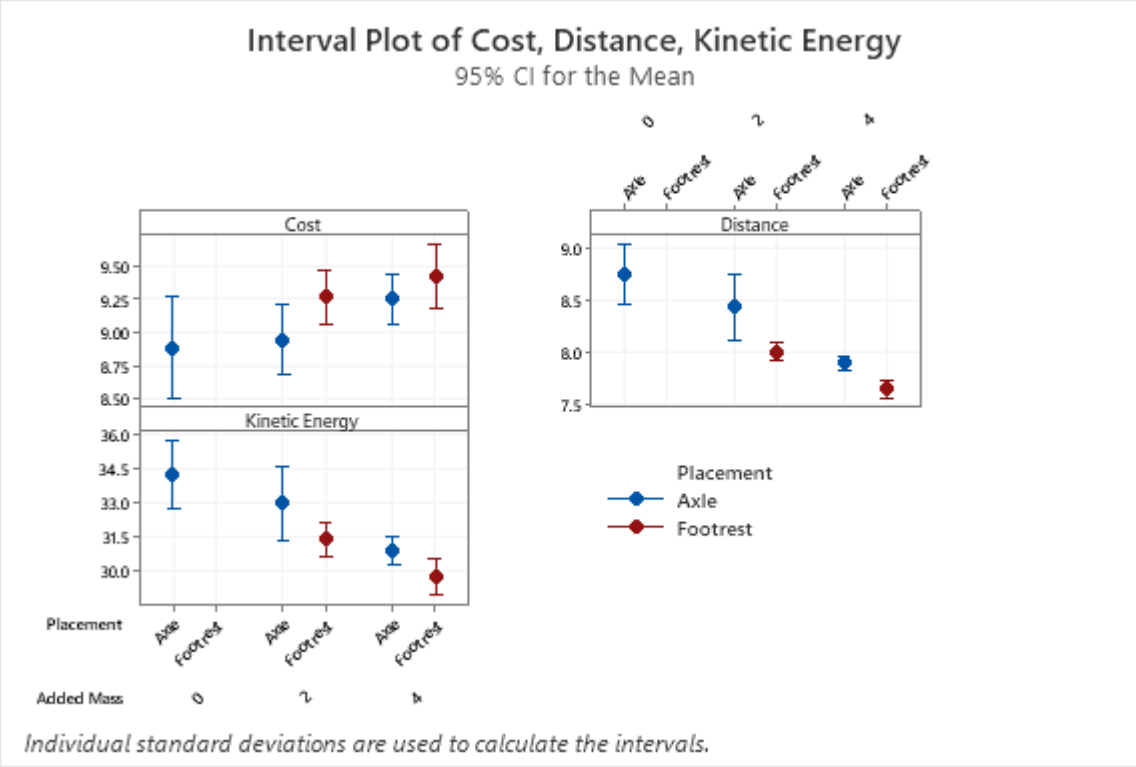

Figure 43: Interval plots of each outcome variable (Straight maneuver) across incremental mass configurations.

The distances were plotted in a similar manner. Again, the range of the y-axis makes the differences appear drastic between groups. Confidence intervals around each of the means are very small for the 2F, 4A, and 4F configuration data. Finally, the general trend seen in the kinetic energy plot is apparent that the added masses reduce the attainable kinetic energy, and moving the weights to the footrest exacerbates the effect.

Equivalence bounds and the mean differences were plotted (Figure 44) to visualize the mean differences in propulsion cost values between configurations. The 95% confidence intervals are shown for each propulsion cost difference (Test – Ref). As this involved a one-sided test, only the lower bound of the confidence interval is shown. The established equivalence criteria specified that if the lower bound is greater than the

specified +5% threshold, then the cost of that tested group is statistically greater than the control group. In this test, the lower bounds of all configurations are less than 5% of the reference mean. No cases were statistically 'inferior' to the 0A baseline configuration.

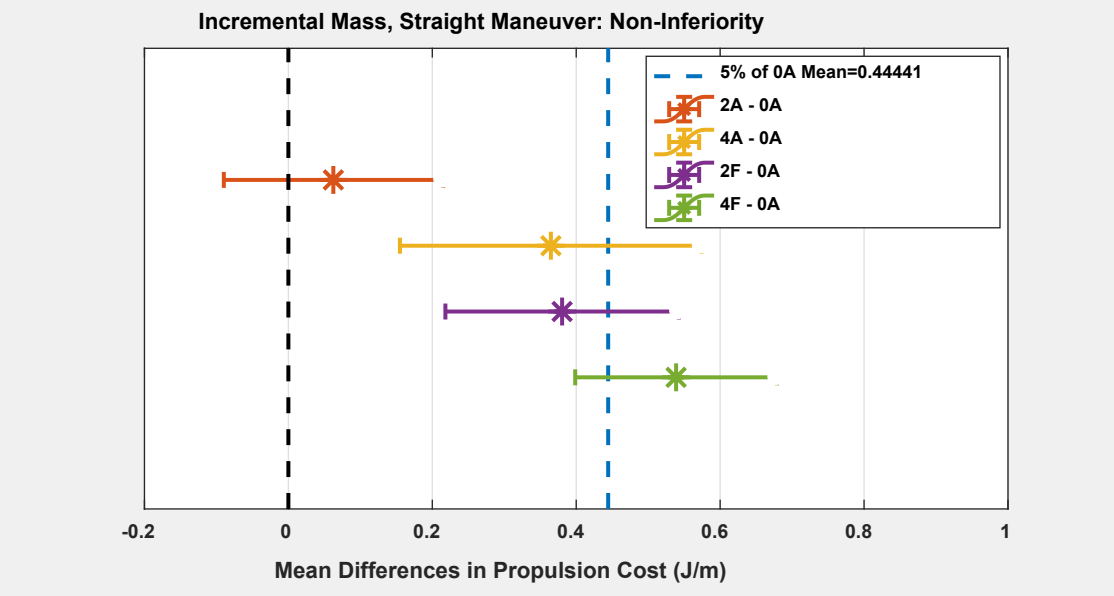

Figure 44: Non-inferiority testing of propulsion costs (Straight maneuver) across incremental mass configurations. No cases were statistically inferior (>5%).

4.5.3 Slalom

Descriptive statistics of the Slalom maneuver outcome variables (Table 10) show essentially the same trends as the Straight maneuver results (Table 9) – overall, proximally-placed masses had less of an impact on the wheelchair than the distally-placed masses. Compared to the Straight maneuver results, the distances traveled in Slalom were less, as more time and effort was spent by the AMPS to turn the wheelchair heading direction instead of propelling in a straight line. The maximal kinetic energies were less than the Straight maneuver because linear translation of the large (~93-98 kg) linear inertia

dominates the kinetic energy distribution [78]. In comparison, the magnitude of rotational inertia (~8 kg m^2) and the rotational speed are small.

Table 10: Descriptive statistics for cost, distance, yaw, and kinetic energy of incremental mass configurations in the Slalom maneuver.

		0A	2A	4A	2F	4F
Cost (J/m)	Mean (± StDev)	9.98 (±0.18)	10.11 (±0.20)	10.10 (±0.17)	9.95 (±0.19)	9.98 (±0.19)
	Effect Size	-	0.72	0.67	0.16	0.01
	% Change	-	+1.33%	+1.17%	-0.28%	-0.01%
	p-value	-	0.03*	0.04*	0.62	0.99
Distance (m)	Mean (± StDev)	5.54 (±0.15)	5.43 (±0.13)	5.31 (±0.13)	5.20 (±0.12)	4.90 (±0.08)
	Effect Size	-	0.75	1.66	2.45	5.30
	% Change	-	-1.89%	-4.13%	-6.02%	-11.50%
	p-value	-	0.02*	0.00*	0.00*	0.00*
Yaw (rad)	Mean (± StDev)	2.01 (±0.09)	2.02 (±0.10)	1.96 (±0.13)	1.78 (±0.14)	1.62 (±0.06)
	Effect Size	-	0.08	0.44	2.03	5.00
	% Change	-	+0.38%	-2.36%	-11.61%	-19.54%
	p-value	-	0.80	0.18	0.00*	0.00*
Max. Kinetic Energy (J)	Mean (± StDev)	15.93 (±0.78)	16.05 (±0.79)	15.53 (±0.72)	14.33 (±0.49)	13.22 (±0.51)
	Effect Size	-	0.16	0.54	2.46	4.12
	% Change	-	+0.77%	-2.54%	-10.03%	-17.04%
	p-value	-	0.62	0.10	0.00*	0.00*
*Significantly different ($p < 0.05$) from the mean of the 0A configuration.						

Within the propulsion cost analysis, 2A and 4A show statistically significant (p-value < 0.05) differences from 0A with less than 2% change from the 0A mean, and the footrest-loaded configurations do not. ANOVA analysis showed statistically significant differences between the group mean propulsion costs ($F(4,95) = 3.33$, $p = 0.013$). However, Tukey's post-hoc assessment only showed significant differences between the 2F configuration cost and the 2A configuration cost. This is partially explained by visual inspection of the plotted data (Figure 45) due to significant overlap between groups and generally close proximity of the means.

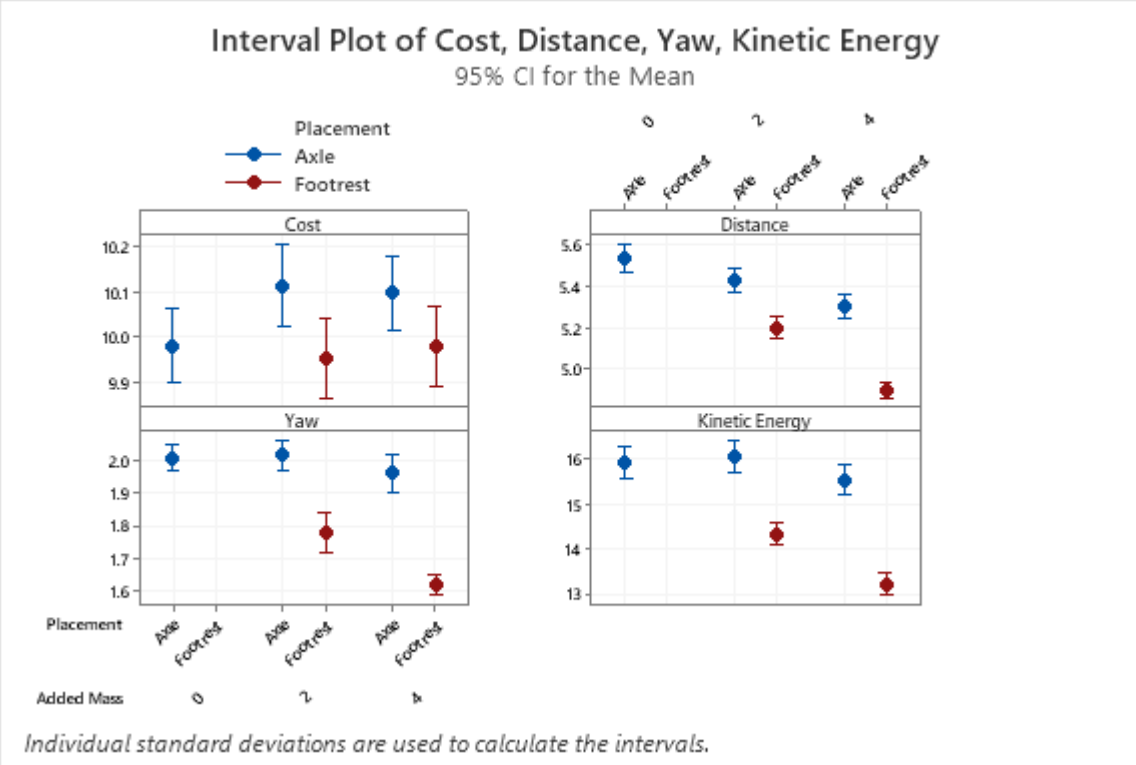

Figure 45: Interval plots of the outcome variables (Slalom maneuver) across incremental mass configurations.

Distance values were more distinctly different than propulsion cost. The plot of distances in Figure 45 shows two very different trends between proximal loading on the

axle and distal loading on the footrest. Though mass has a clear effect and causes 2% (+2 kg) and 4% (+4 kg) decrease in the distance traveled, the same weights on the footrest cause 6% (+2 kg) and 12% (+4 kg) decreases in the distance versus the 0A configuration. Angular yaw distance traveled by the system was even more disparate than the linear distance. In Figure 45, the effect of proximal (axle) loading was hardly noticeable, even at +4 kg, yet the distal footrest-loaded configurations stop much sooner. This likely is a combination of the added weights directly over the casters causing increased rolling resistance and scrub torque, as well as the increased system yaw inertia due to the addition of large distal loads. For the maximal kinetic energy attained by each configuration under the influence of the Slalom torque trajectory, the axle-loaded configurations appear similar to the 0A configuration with significant overlap of confidence intervals, whereas the footrest-loaded kinetic energy values show a steep decline from the baseline.

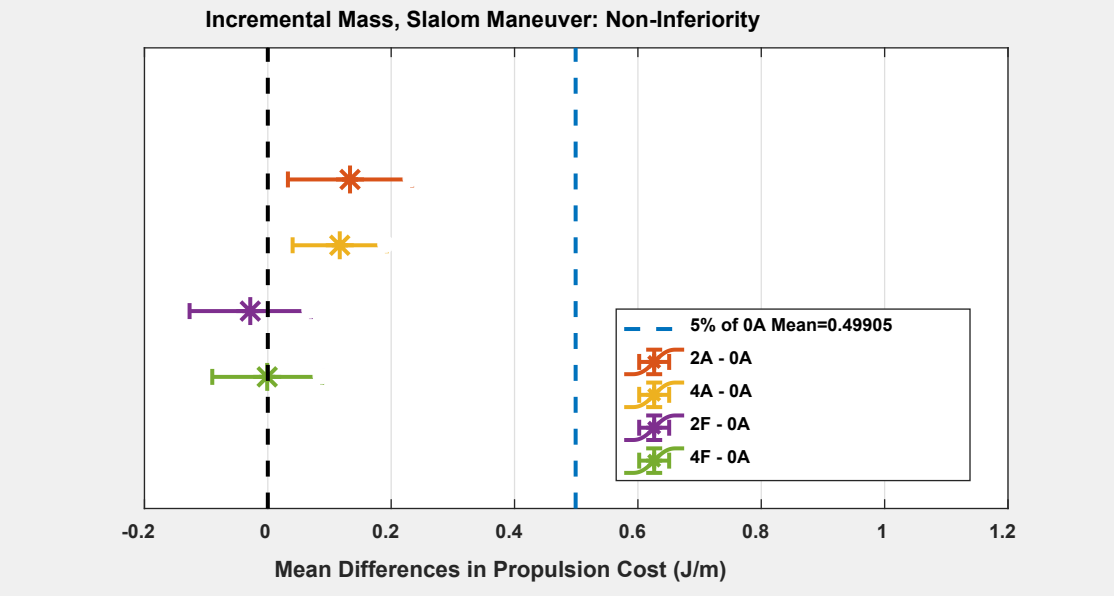

Figure 46: Non-inferiority testing of propulsion costs (Slalom maneuver) across incremental mass configurations. No cases were statistically inferior (>5%).

The non-inferiority test shows that none of the configurations fell outside of the threshold. In fact, almost all of the propulsion cost differences were within 2% of the reference mean. In other words, each of the weight configurations functionally demonstrated equivalent propulsion cost performance as the baseline configuration in the Slalom maneuver.

4.6 Discussion

The main objective of this study was to use the new torque-controlled AMPS to investigate the effects of incremental mass, as well as the secondary effect of weight placement, on wheelchair propulsion cost, with the assumption that repeatedly re-accelerating and decelerating with the phases of the propulsion would highlight the influence of any added system mass, if any differences were to exist. The results presented above show that the AMPS was capable of detecting differences in the mechanical behavior

of the wheelchair under slightly different loading conditions. The small standard deviations of the means demonstrate the high repeatability of the AMPS. Coefficients of variation of the propulsion costs are below 6% within each configuration data set for the Straight maneuver, and under 2% for the Slalom maneuver. The greatest variability in the data showed up in the yaw and the kinetic energy measurements. Both of these metrics can be highly influenced by inconsistencies in the floor – simple uncontrollable and nearly-imperceptible imperfections such as a slight slope or a gradual incline could cause the AMPS to deviate from the expected path trajectory and introduce variability to the measurements. This was monitored closely and any trials that drastically veered off-course were retested. As a result of the careful control of the AMPS starting point and initial caster alignment, the expected travel path was almost always followed, and all outcome variables had under 8% coefficients of variation for each configuration.

Human subject studies often lack the sensitivity and precision necessary to separate the energetic effects of biomechanics from mechanical differences in manual wheelchairs. A flat tire might be noticeable, but strands of hair caught by and wrapped around a caster axle may go unnoticed until a scheduled maintenance appointment. Incrementally adding mass to the frame should unsurprisingly go unnoticed by the user. Consider adding +5 kg to an unloaded 10 kg wheelchair, which would be a 50% increase in system mass, versus adding the same mass to the same chair loaded with an 80 kg occupant. That 50% increase shrinks to a 5.6% increase in system mass. It is not unexpected that Sagawa et al. [34], de Groot et al. [33], Bednarczyk and Sanderson [118], and Cowan et al. [55] reported little to no change in the human propulsion characteristics under the influence of such small (typically < +5 kg) additions to the system mass. Other studies that *did* report significant

differences between chairs with varying masses tended to compare across categories such as standard versus ultra-lightweight chairs in Beekman's study [31] and standard 'conventional' chairs versus sports-designed chairs in a study by Hilbers and White [114]. Picking chairs from disparate categories can cause readers to conflate the effects of frame mass with other design aspects of the chairs, such as the caster, drive wheel, and weight distribution configurations – these aspects were properly addressed by both sets of authors [31, 114], but this point deserves to be re-established every time the association of 'frame mass versus efficiency' begins. Mechanical testing portrays this more clearly: multiple studies have shown that adding mass to the system can impact the rolling efficiency [56, 68, 115, 116] but that weight distribution is far more influential on the mechanical propulsion cost of the chair [71, 81, 83]. Wheelchair assessment without influence of human biomechanics often improves the accuracy of the data and isolates the behavior of the wheelchair under controlled test environments.

Starting with the coast-down test results, it is evident that the mass of the wheelchair frame is not the most influential factor when compared to weight distribution. The incremental mass addition of 4 kg to the axle had more gradual deceleration values than the footrest-loaded case with only half the added weight. Moving the entire stack of 4 kg weights to the footrest instead caused the deceleration to increase drastically, and had a similarly detrimental effect on the approximated rolling resistance force. Mechanically, it should be apparent that the loading configuration of the wheelchair defines the forces that are transmitted through each wheel. From previous component-level [81] and system-level [71] testing, it has been shown time and time again that weight distribution has a major role influencing the mechanical system performance, and recent statistical modeling has

shown that the energy losses at the wheels are highly indicative of system-level propulsion cost [83]. Within the range of expected weights and weight distributions on a manual wheelchair, the 24”-diameter drive wheels are just generally better suited to handle larger loads without suffering the same dramatic increase in rolling resistance or scrub torque that are characteristic of 4”-, 5”-, or 6”-diameter casters [81, 82]. The coast-down testing was included in this study as a simplistic framework to assess the loaded configurations mechanically, yet it arrived at the same conclusions as the more advanced testing: adding mass at this incremental scale only really matters when it is placed in a poorly-chosen location that shifts more weight over the casters. However, coast-down testing did not capture the full story of the mechanical performance of the MWC, which was further assessed via over-ground propulsion trials with the AMPS.

The data collected with the torque-controlled AMPS showed some general trends: travel with higher system mass increased the propulsion cost of the chair, reduced the linear distance traveled, and decreased the kinetic energy that was endowed to the system via the supplied wheel torques. However, this trend was typically overshadowed by the effect of distal placement of the added weights. The footrest-loaded configurations had the highest propulsion costs, the shortest distances traveled, the least amount of angular turning in the Slalom maneuver, and the lowest kinetic energies, despite having the exact same torque profiles applied to the wheels of each configuration.

Propulsion cost, the most clinically-relevant of the outcome variables, has been used in prior work to compare wheelchair performance differences between drive wheels and casters [71] and to generate several statistical models of cost during various maneuvers [83]. The concept is similar to gas mileage in automobiles, except that the ratio is inverted;

the energetic expenditure of the system is normalized by the distance traveled to present a potential user with an idea of how efficient the vehicle performs over common surfaces. In an article by Sprigle et al. [71], propulsion costs for a straight forward maneuver over a tiled hallway ranged from 20 J/m to 32 J/m depending on the equipped drive wheels, casters, and weight distribution. Lower costs are associated with better performance. From the data collected for this study, the costs were considerably lower (8.89 J/m to 9.43 J/m). The reason for this discrepancy is a shift from the velocity-controlled trajectory to a more human-like torque application. Under this new control system, energy is only supplied to the wheelchair during the push-phases of the propulsion cycle instead of the 10 s duration of the continuous propulsion in velocity mode. Additionally, the target velocity of the velocity-controlled Straight maneuver was 1.0 m/s in [71]. Under the torque-controlled propulsion cycle, the velocities typically only reached 0.83 m/s. Understandably, propelling at a lower speed requires less work from the AMPS. One other major reason for the difference in cost values is that velocity-controlled trials assessed the cost from the beginning of the acceleration phase to the end of the steady-state phase, but did not include the deceleration phase at all. The kinetic energy remaining in the system was not accounted for in the propulsion cost calculation. In the present study, the wheelchair freely coasts to a stop without direct impedance from the motors such that every Joule of work supplied is normalized by every meter traveled by the system – a more holistic approach to determining the propulsion cost in a realistic context of use.

Overall, changes in the calculated propulsion cost displayed small but appreciable differences between the tested configurations. The data collected in Table 9 and Table 10 show Cohen's *d* effect sizes ranging from small (< 0.2) to very large (> 1.30). These sizes

imply that some of the configurations have distinctly grouped propulsion cost values that are appreciably separate from the baseline 0A configuration cost, yet the percent differences are less than 5.89%. Non-inferiority tests were used to investigate the extent of similarity between the propulsion costs. All configurations were found to have cost differences compared to the 0A configuration that extended below the non-inferiority lower bound, specified as 5% of the baseline (0A) mean. As the burden of proof is placed on the conclusion of non-inferiority, none of the incremental mass configurations could be claimed to have statistically higher costs than the baseline 0A mean – this means that each mass configuration had functionally equivalent propulsion costs, which supports the findings of many human subject studies showing insensitivity to added masses.

Isolating the effect of mass: Adding +4 kg to the axle increased the frame mass from 13.6 kg to 17.6 kg, a 30% jump in mass for the wheelchair itself, but only a 4% increase in system mass (93.6 kg to 97.6 kg). The added mass increased the rolling resistance by 3%, the Straight cost by 4% and the Slalom cost by 1%, decreased the Straight distance by 10% and the Slalom distance by 4%, and decreased the maximal Straight kinetic energy by 10% (but Slalom by only 3%). A glance through Table 8, Table 9, and Table 10 would suggest that most of these differences are significant, from the perspective of standard statistics. But what do these differences really represent? A 4% increase in cost is a relatively small difference. Consider that the average wheelchair user travels between 1.4 km [4] to 1.6 km [3] per day. If even 50% of that travel is straight forward motion over linoleum tile, the total cost in the 0A configuration would be 8,890 J of energy for 500 m of straight forward motion, versus 9,250 J of energy in the 4A configuration. That 360 J difference is the energetic equivalent of nearly 38 full bicep curls with a 1 kg dumbbell, or

simply propelling the 4A-configured chair an extra 40 m per day. To most users, this change might seem insignificant, especially when other studies report increases of 54% in propulsion cost by changing from pneumatic tires to solid polyurethane tires [71], or increases in gross efficiency of 15% just by changing propulsion cycle frequency from the typical rate [59].

Adding in the additional influence of weight distribution by assessing the 4F configuration compared to 4A: coast-down deceleration worsened by 5%, as well as the apparent rolling resistance force; propulsion costs for the Straight maneuver increased by an additional 2%, as well as 4% less distance and kinetic energy; the Slalom cost was relatively unchanged by the weight distribution but the distance decreased by 8%, the yaw decreased by 19%, and the kinetic energy decreased by 16%. The results and trends seen here are conceptually supported by mechanical energy loss test results of the wheelchair system [52, 67, 81, 123]. As in most studies at the component level, casters are very sensitive to loading, and extra weight over the casters can result in steep increases in the rolling resistance and scrub torque experienced by the wheelchair [52, 67, 81, 123]. In many ways, these results also reinforce prior findings that incremental mass has a nearly-negligible impact on the energetic exertion during propulsion in human studies [33, 34, 55, 118], and weight distribution seems to have a larger impact on the overall mechanical behavior [124].

4.7 Conclusion

Out of 100 coast-down deceleration trials, mass as an isolated factor was not significantly detrimental to the wheelchair performance. Moving weights from the center

of mass to the footrest, however, caused significant increases to the severity of the deceleration and apparent rolling resistance forces by up to 9%. Under the robotic propulsion of the AMPS, the results were more pronounced: incremental masses on the frame caused noticeable increases to the propulsion cost (< 4%), decreases to the distance traveled (< 10% Straight, < 4% Slalom), and decreases to the overall attainable kinetic energy of the system (< 10% Straight, < 3% Slalom), most of which were worsened by moving the same masses to the footrest. Notably, propulsion cost itself was not increased by more than 6% in any configuration, nor was the propulsion cost of any configuration identified as non-inferior to the mean of the baseline configuration. More demonstrative measurements showed severe differences due to weight distribution – adding 4 kg on the axle decreased the angular displacement in the Slalom maneuver by 4% and the kinetic energy by 3%, but the same mass on the footrest decreased those by an additional 19% and 16%, respectively. Thus, both the mass and weight distribution parameters are evidently optimized at lower masses with the bulk of the weight loaded predominately over the rear wheels. Faced with the compromise of moving something like a loaded backpack from the footrest to the rear of the seat, these results suggest that the propulsion cost would be similar in either case, but the propulsion cycle may seem much more effective with the weight centralized over the drive wheel axle due to the increased distance traveled per push and the greater attainable kinetic energy, given the same torques on the wheels in both cases.

This work demonstrates the value and importance of examining the manual wheelchair system as an independent unit from the human occupant. Mechanically, the chair can be tested and assessed with much greater sensitivity than human users, as evidenced by the non-inferiority testing of the Straight propulsion cost. Though ultimately

the differences in the clinically-relevant cost assessment were slight, this controlled propulsion technique has objectively investigated the effect of frame mass, and provided some insight as to how it *could* seem important to propulsion characteristics, *if* it was poorly balanced along the wheelbase.

CHAPTER 5. IMPROVING HIGH-STRENGTH LIGHTWEIGHT WITH COMPONENTS

The purpose of this study was to investigate the extent of improvement on the performance of a K0004 (high-strength lightweight) manual wheelchair by replacing the manufacturer-default components with up-charged alternatives, purchased for $100 or less. This goal of this study was to compare the mechanical propulsion characteristics of a K0004 (high-strength lightweight) manual wheelchair in two configurations: (1) as configured by the manufacturer, and (2) with up-charged casters and drive wheels, in both straight and curvilinear maneuvers. Additionally, coast-down deceleration tests were used to approximate the system-level rolling resistance of each component configuration.

5.1 Overview

As reported in 2017 Centers for Medicare and Medicaid Services data [125], the distribution of allowable services ranged from a mere 11,000 allowed K0005 prescriptions to nearly 600,000 K0003's, and well over 1,000,000 K0001's (Table 11). K0004 chairs had only 96,000 allowed prescriptions in 2017 [125], down from 708,000 in 2010 [126].

Table 11: Amount of allowed services and charges from 2017 CMS data

	Allowed Services (in 1,000s)	Allowed Charges (in $100,000s)	Average Charge Per Service ($/Unit)
K0001	1,374	263	$19.14
K0002	99	35	$35.35
K0003	579	165	$28.50
K0004	96	33	$34.38
K0005	11	186	$1,690.91

The data represents the average use-cases of each category – K0001 through K0003 chairs are typically for short-term rehabilitation (< 3 months, < 2 hours per day), and are therefore not designed to be used as long-term, full-time medical devices. In contrast, the Local Coverage Determination and Policy published by the CMS [26] states the "…high strength lightweight wheelchair is rarely reasonable and necessary if the expected duration of need is less than three months (e.g. post-operative recovery)." As a further division between groups, the K0004 is the first to include self-propulsion as one of its criteria; the specifications for K0001-K0003 do not actually require self-propulsion, and instead rely on a caregiver to travel. Moving forward, the major separation between the two 'self-propelled' categories, K0004 and K0005, is that the beneficiary must either be a full-time manual wheelchair user, or the beneficiary requires accommodations in the form of customization or adjustment points that are not available on K0001-K0004 frames. At face-value, this also makes sense – not every user requires full customization, but may struggle with the standard or lightweight frames and need more than a K0003. However, reserving the ability to customize components, seating configurations, axle positions, or caster sizes behind a clinical evaluation [127] of 'necessity' is arbitrary at best, and harmful to the beneficiary at worst.

Competitive bidding, in effect currently with systems like the current Medicare structure, is an idealized effort to reduce the cost of necessary products for the beneficiary, and it works conceptually by forcing suppliers to competitively price their items, but it tends to leave gaps. For example, by undercutting prices on K0004 frames to secure a contract (currently at $34 per month for reimbursement), suppliers give manufacturers much less incentive to supply features on K0004 frames that are not absolutely mandated

by CMS. As a direct result, the entire category is drained of any optional benefits that could be reserved for the more expensive frames, as discussed by Mobility Management authors and correspondents since 2014 [27, 127, 128]. In many cases, a professional may read the 'lightweight' title and assume the best-case scenario without realizing that a K0004 may be 34 lbs (or more with components) and may have little to no adjustment to custom-fit the user. In contrast, ultra-lightweight chairs are specifically required to be under 30 lbs and have customization options to accommodate a wide variety of users, or at least provide adjustment points at points of interest on the frame (e.g. drive wheel axle height position, or caster fork angle and height) to match specialized dimensions for each individual [27]. K0004 chairs are typically used 'as-is', or as supplied direct from the manufacturer, with little to no adjustment. As they are significantly less expensive than their K0005 counterparts, they are often the more accessible and affordable option for individuals in need of wheeled mobility assistance. Do they, however, meet the same performance-based needs of the beneficiary?

Studies have shown that lightweight (K0003, K0004) chairs could be propelled faster and farther than standard (K0001) chairs without changing cardiorespiratory levels [129], likely due to the posterior placement of the user mass over the drive wheel axle [130]. When compared to higher-tier ultra-lightweight (K0005) chairs, though, users tended to propel lightweight chairs slower and for shorter distances [6, 31] at higher energetic costs – in fact, push-rim forces, energetic expenditure per meter, and shoulder and elbow flexion were all negatively influenced by using the K0004 frame instead of the K0005 frame [131]. These may be mitigated by changing the weight distribution via the drive wheel axle position, though it's an increasingly rare feature to see on a K0004 frame.

It is important to understand and publicize these performance tradeoffs; the additional cost of K0005 wheelchairs acts as an obvious deterrent from buying out-of-pocket, and the cost is also an obstacle to the DME reimbursement process, which may ultimately prevent some beneficiaries from getting the level of comfort and care they require. Considering the financial restrictions at play, what can be done to offset these performance tradeoffs and improve quality-of-life for individuals using K0004 wheelchairs, especially when the common adjustment points to shift weight distribution are locked to one configuration? The simplest solution, according to predictive models of wheelchair mechanics, is to address the energy losses occurring within the system [83, 132-134]. System-level energy losses may vary per maneuver (Eqns. 9-11) but can reliably be used to predict the propulsion cost [83] with linear combinations of simplistic energy loss measurements at the component level [81]. Fortunately, many wheelchair components are designed to be interchangeable (e.g. 24”x1” or 24”x1-3/8” drive wheels all use the same axle size, and caster forks have multiple settings to accommodate casters with diameters from 4” to 6” or 8”). Armed with the knowledge from the extensive library of empirical component-test results, it is hypothesized that the performance of an out-of-the-box K0004 chair could be significantly improved with a simple change of drive wheels and casters.

The steps taken to assess this hypothesis were: (1) identify ‘off-the-shelf’ components that would fit a generic K0004 frame; (2) utilize the results from prior component-level tests to select a set of drive wheels and casters with performance benefits over the manufacturer-configured components; (3) empirically assess system-level parameters with the default and ‘up-charged’ components to quantify differences in performance across use-cases (tile and carpet surfaces, straight and curvilinear motion).

This study was not aimed to make a K0004 behave like a K0005, but rather to leverage existing knowledge to propose feasible changes that could improve the quality of life for K0004 users within their context of use (short and slow bouts of turning and straight motion, inside the home and workplace).

5.2 Hardware and Configurations

This study did not require external hardware on the wheelchair frame except the custom ring gear push-rims and the hub-mounted drive wheel encoders for the AMPS.

5.2.1 Frame Selection

A convenience sample of a Drive Medical MWC frame (MSRP: $1690) was selected for this study – the seat dimensions met the size requirements of the AMPS, the quick-release drive wheel axle receptacles were adjustable between hemi-height (for foot propulsion) and standard (for push-rim propulsion), and the caster forks could accommodate the most common 6”- and 8”-diameter casters available for K0004 wheelchairs. Before testing with the AMPS, the arm rests, heel straps, and anti-tip bars were removed from the frame. The original configuration utilized 12 mm-diameter quick-release axles for the default drive wheels. The axles, axle housings, and the drive wheels themselves were replaced with ½”-diameter equivalents for integration with the AMPS hardware. The mass of the wheelchair in its original unloaded configuration was 13.48 kg, including the front riggings. These detachable footrests, commonly removed before taking ‘frame mass’ measurements, weighed 1.30 kg. The removed hardware (arm rests, anti-tip bars) weighed an additional 2.62 kg.

5.2.2 Component Selection

The Viper Plus GT frame came equipped with the standard component offerings from Drive Medical: solid 24”x1” polyurethane tires with a trapezoidal cross-sectional profile equipped on 8-spoked composite plastic ‘Mag’ wheel rims, and a set of unlabeled 8”x1” casters with wide bearing housings at the hubs. According to the official Drive Medical order form, these components are the only ones available for this particular chair, which is uncommon. Order forms typically include at least the choice of pneumatic versus non-pneumatic drive wheel tires at no cost. As stated in the previous section, the original drive wheels were replaced with equivalent wheels and tires that could interface with the AMPS – the ring gear push-rim was designed for the 9-spoke variant of the Mag wheel and the axle-mounted optical encoder is threaded to fit the ½”-diameter quick-release axle.

Up-charged replacement parts were selected from common components that are used as standard options in many K0005 wheelchairs, and are readily available. Knowledge from the library of energy loss parameters (rolling resistance, resistive scrub torque) compiled from empirical component-level test results [81] were used to further narrow the selection. Most caster choices (Primo 6”x1”, Frog Legs Narrow Court 6”x1”, and Primo 6”x1” pneumatic) demonstrated varied performance across the surfaces and exhibited better in either rolling resistance or scrub torque [81]; the Primo 6”x1.5” casters were selected based on their versatility and efficiency in both rolling and scrubbing across the tile and carpet surfaces of interest. Similarly, Primo XPress 24”x1-3/8” non-pneumatic tires were chosen due to their performance across the test configurations. The selected components were relatively inexpensive compared to the cost of the chair: out-of-pocket costs to the user for a set of Primo 6”x1.5” casters tops out around $47, and for the Primo

XPress 24”x1-3/8” tires, around $50 per pair. The prices shown were aggregated from popular online retailers (enableyourlife.com, dmehub.net, southwestmedical.com). The extra 3/8” width of the XPress tires did not prohibit their use on wheel rims with equivalent size as the default wheels. Regardless, it is suggested that the wheel rims do not impact the performance of the overall system [135].

5.2.3 Chair Configurations

Four configurations were established to investigate the performance changes at the system level (Table 12). The single Drive Medical Viper Plus GT frame was used as acquired from the manufacturer (configuration “A”). The 8”x1” casters were replaced with the Primo 6”x1.5” casters (configuration “B”) in a lower hole on the caster fork to maintain the floor-to-seat height at the front of the seat. The 8”x1” casters were re-equipped and the default Solid Mag wheels were replaced with the Primo XPress wheels (configuration “C”). Finally, the last configuration replaced the default drive wheels and casters with their up-charged counterparts (configuration “D”). Inertial parameters of the AMPS were controlled to be as consistent across configurations as possible: occupant mass was nominally 80 kg and the target weight distribution was 65% over the drive wheel axle.

Table 12: Overview of configurations used to assess performance of the high-strength lightweight wheelchair.

Config. Name	Drive Wheel	Caster	System Mass	Weight Distribution over Drive Wheel Axle
"A"	Solid Mag 24"x1"	Drive Medical 8"x1"	96.1 kg	63.8%
"B"	Solid Mag 24"x1"	Primo 6"x1.5"	95.8 kg	63.5%
"C"	Primo XPress 24"x1-3/8"	Drive Medical 8"x1"	95.8 kg	64.9%
"D"	Primo XPress 24"x1-3/8"	Primo 6"x1.5"	95.5 kg	64.0%

5.3 Experimental Design

This study was designed to investigate propulsion cost and over-ground kinematics of the high-strength lightweight wheelchair with four discrete configurations over two common surfaces. Two maneuvers were selected: a 7-push straight trajectory and a 5-push slalom trajectory. Maneuvers maintained common temporal parameters between surfaces but the torque peaks were adjusted for the waxed linoleum tile and low-pile carpet surfaces. Each maneuver was tested with 5 trials in each opposing heading direction (forwards, backwards, as well as left and right starting pushes for the slalom) to normalize any irregularities in the hallway. With 30 total trials per configuration and 4 configurations, this experiment required 120 over-ground AMPS trials.

5.3.1 Maneuver Selection

Ultimately, the maneuvers employed in this study are very similar to the maneuvers from the incremental mass study. The coast-down deceleration tests were used for each configuration over the tile and carpet surfaces to capture the representative system energy

losses. The Straight (tile) maneuver utilized the same parameters as the torque profile generated for Figure 39, except with larger torques to maintain steady-state velocity – preliminary trials with the default "A" configuration tended to decelerate to a complete stop by the fifth or sixth push with the 5 Nm peaks used in the incremental mass study.

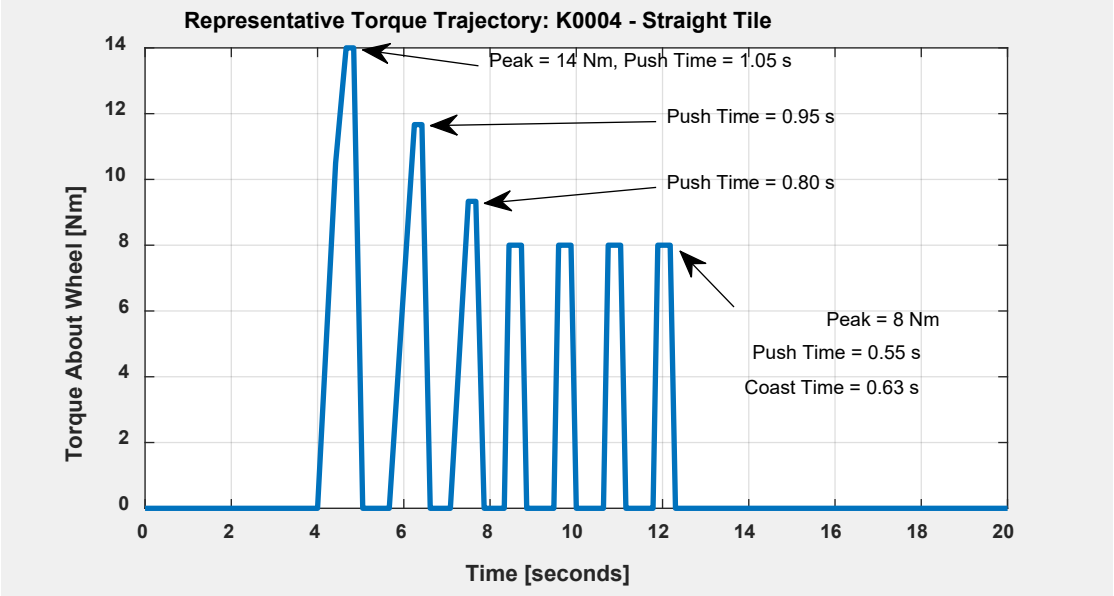

Figure 47: Representative torque profile for the Straight maneuver on tile for the K0004 configurations.

To accommodate for the extra energy losses introduced by the low-pile carpet, the torques seen in Figure 47 were exaggerated even further. For the initial push, the peak was increased from 14 Nm (tile) to 18 Nm (carpet). To maintain a steady-state velocity, the default configuration required peaks of at least 12 Nm throughout the steady-state phase.

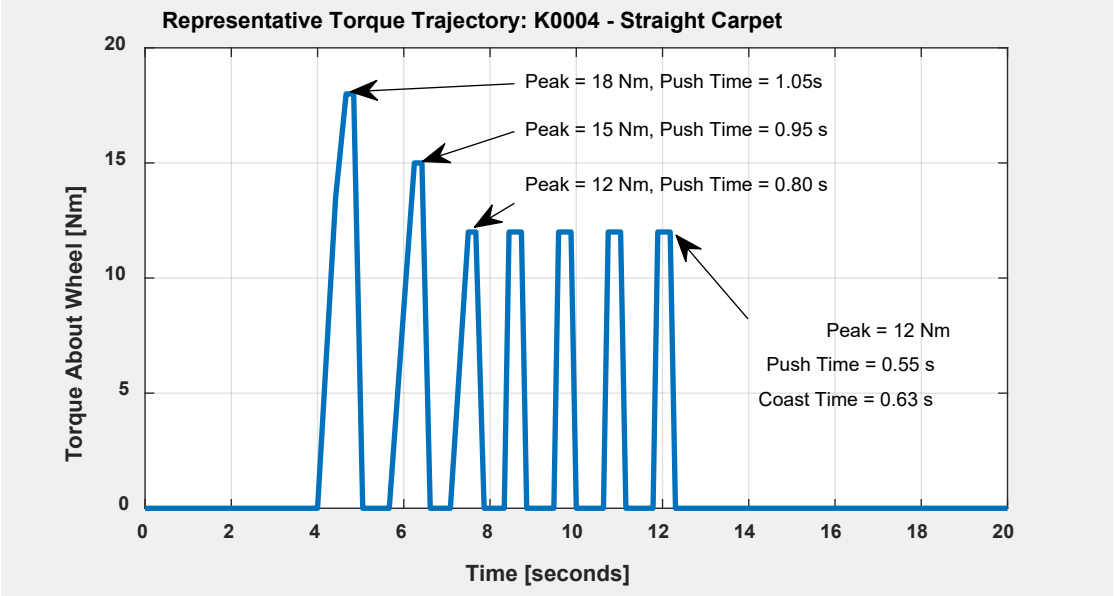

Figure 48: Representative torque profile for the Straight maneuver on carpet for the K0004 configurations.

The Slalom maneuver featured longer torque applications with correspondingly longer coast times between each push. This maneuver had to first apply a small bi-lateral push to give the AMPS an initial velocity and align the casters to a path facing straight ahead. Next, a series of unilateral pushes were applied. The reciprocating turns were reminiscent of the Alternating Zero-Radius Turning maneuver from the velocity-controlled testing, with the exception that the new clutches prevent the AMPS from propelling one wheel in reverse. Peak torques were increased by around 30% from the profiles used in the incremental mass study (Figure 40) to maintain similar motion. Preliminary trials suggested that the K0004 in the default configuration was highly resistant to any turning motion.

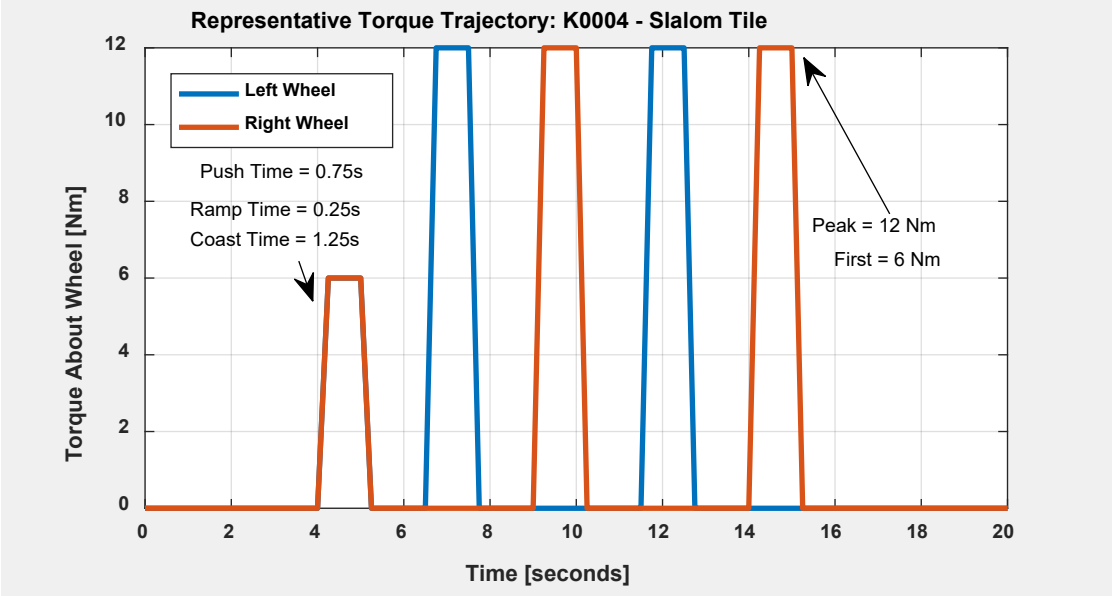

Figure 49: Representative torque profile for the Slalom maneuver on tile for the K0004 configurations.

Torques were raised to 16 Nm to perform the Slalom maneuver over carpet. Peak torques were raised incrementally from 12 Nm to 20 Nm to identify the most repeatable and steady trajectory for the default configuration. Peaks over 16 Nm caused slight mechanical issues within the context of the Slalom maneuver itself – rapid application of that amount of unilateral torque caused an abrupt change in heading direction that would shift the bar weights within the AMPS. It was hypothesized that this would be especially inhibitive for data collection using the up-charged drive wheels and casters because the abrupt change in heading direction would occur even more rapidly.

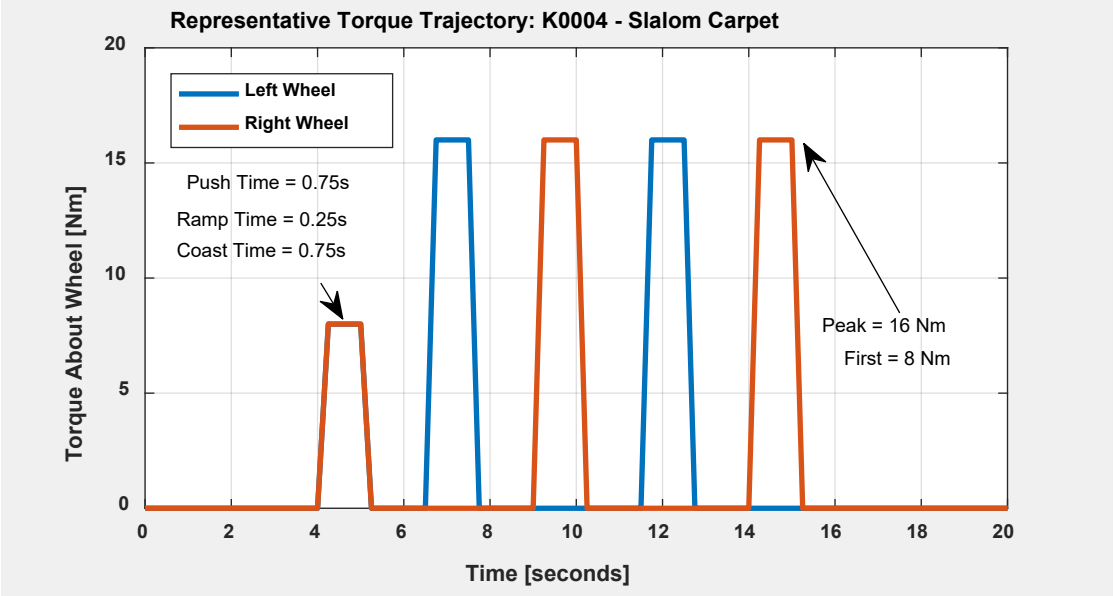

Figure 50: Representative torque profile for the Slalom maneuver on carpet for the K0004 configurations.

5.3.2 Test Surfaces

K0004 chairs are designed for use inside and out of the home. Typical environments include carpeted and bare wood or tile flooring, as well as sidewalk, pavement, and inclines. Two surfaces were chosen (Figure 51): linoleum tile floor which is commonplace inside stores, hospitals, and schools, and low-pile carpet designed for highly-trafficked areas.

Figure 51: (Left) The linoleum tile hallway testing area. (Right) The low-pile carpeted testing area.

5.4 Methods

5.4.1 Data Collection

First, a simplistic coast-down deceleration method was used to characterize the typical coasting behavior of each configuration. The motors were disconnected from the ring gear push-rims to decouple the propulsion system. The wheelchair was centered in the hallway. From rest, the wheelchair was manually pushed via the rear handles to accelerate the chair to approximately 1.0 m/s. Upon reaching the target speed, the wheelchair was released and permitted to roll down the hallway until it naturally decelerated to a stop. Wheel velocities were recorded by the wheel encoders. 10 trials were taken in the forward and backward hallway directions (the AMPS was always facing the direction of travel) to

account for any slopes or inconsistencies in the tiled floor for each configuration. 20 trials were taken for each configuration over each surface for a total of 160 coast-down trials.

Next, the experimental protocol consisted of 30 over-ground propulsion trials for each of the four configurations. The wheels were lightly wiped with a microfiber cloth prior to testing to remove dust and debris. The torque trajectory was loaded into the LabVIEW interface and the AMPS was set up along a 30 meter length of clean, flat linoleum tile hallway. To normalize for surface inconsistencies such as slope or intermittent bumps, 5 forward-heading trials were run in each of the forward and backward hallway directions along the same length of tile for the Straight maneuver. Similarly, the Slalom maneuver was tested with 5 trials in each of the left and right slalom maneuvers in both the forward and backward hallway directions, resulting in a total of 20 slalom trials. This protocol was replicated for the carpeted surface. In total, 240 over-ground AMPS trials were collected. Tile and carpet trials were collected and in separate sessions to allow the AMPS batteries to charge to full capacity before each trial set. The trials for each configuration were averaged together by maneuver ($N = 10$ for Straight, $N = 20$ for Slalom) and the repeatability for the set of trials was assessed. The inclusion criteria for each set of trials was that the CoV of each outcome variable (nominally distance, as it was the easiest to assess visually and with a rapid post-trial MATLAB analysis) remained $\leq 10\%$.

5.4.2 Data Analysis

The four main outcome variables of this experiment were propulsion cost (Eqn. 8), distance travelled by the center of mass, yaw distance travelled as the wheelchair changed heading direction, and the maximum attainable kinetic energy of the system, (Eqns. 1-4

and nomenclature from Medola et al. [78]). Data from the current-based motor torque sensors, motor encoders, and wheel-mounted encoders were collected at 40 Hz during the over-ground trials. These data were processed in MATLAB. Butterworth filters were used to smooth each sensor signal before calculating the input power to the system from each motor.

Coast-down data were assessed as a regression fit of the MWC velocity. The normal window of analysis was expanded to 0.95-0.35 m/s instead of 0.95-0.65 m/s to average over some inconsistencies at the release velocity. Goodness of fit was improved from $R^2 \leq 0.8$ to $R^2 \geq 0.98$ by expanding the window. Decelerations were derived from linear regressions of each coast-down velocity. From the AMPS-based propulsion testing, collected data for each of the 240 trials were used to calculate the propulsion cost, overall distance traveled by the center of mass, and maximal kinetic energy of the system. For each Slalom trial, the additional outcome variable of yaw displacement was calculated from wheel velocities and geometric parameters of the chair to track the angular change in heading direction over the course of the maneuver. Descriptive statistics were tabulated and 2-sample t-tests were performed across each outcome variable.

Analysis included assessment of differences across configurations and calculating the magnitude of differences. In a strict sense, configuring the same wheelchair with multiple components may not fully meet the assumption of independence required of ANOVA, but it does control for any variance across frames as a confounder, and isolates the main factors. However, in deference to convention, ANOVA was run to assess the four configurations for each maneuver. An *a priori* decision was made to report all p-values and discuss results at the $p \leq 0.1$ levels. Normality of the dependent measures were assessed

using Kolmogorov-Smirnov analysis. Cost values were found to violate the assumption of normality during 3 of the maneuvers, straight tile, slalom tile and slalom carpet. ANOVA was run using a Box-Cox transformation of this data.

Differences in cost across the four configurations are represented using effect size. Effect size, as calculated using Cohen's *d* is a measure of the magnitude of difference between two samples. Cohen's *d* is calculated using the differences in the means and the pooled standard deviations of the parameters of interest [122]. Effect size provides the most direct evaluation of differences with the ability to judge meaningfulness. Cohen suggested general guidelines that d=0.2 be considered a 'small' effect size, 0.5 represents a 'medium' effect size and 0.8 a 'large' effect size. The reference level for calculation was the K0004 wheelchair frame configured with its standard components of a mag wheel with solid tires and 8" x 1" casters.

Equivalence testing was used to assess when device performance differs by more than a practically important amount following the same analysis procedure discussed in the prior study. Within this project, comparison of propulsion cost with various drive wheels and casters used the standard K0004 configuration as the reference device as defined above. To evaluate whether non-standard configurations resulted in lower propulsion cost, the tests determine whether the ratio of the means is less than an upper limit, and evaluates the hypothesis seen in Eqn. 27. A confidence interval is constructed from the difference in propulsion costs between configurations, and non-inferiority is concluded if the confidence interval falls entirely below the bounds of a one-sided equivalence interval [110, 111]. The prior review of six studies (Table 6) was used as a basis to define the equivalence threshold to be ε = 5% of the control group ("A" configuration) propulsion cost mean. This ε value

signifies that any differences in propulsion cost would have to exceed 5% of the "A" configuration cost to be reported as significantly different. This ratio was based upon the assumption that mechanical testing is more precise than human subject investigation, where even 9.4% mean differences were insignificant, while exhibiting an interval that could be considered 'clinically meaningful'.

5.5 Results

5.5.1 Coast-Down

The deceleration values are shown in Table 13. On tile, the deceleration was reduced by 30% by replacing the casters, only 20% by replacing the drive wheels, and nearly 50% by replacing both. On carpet, the difference was less drastic. The deceleration was reduced by less than 6% with just casters, 15% with just drive wheels, and almost 20% with both replaced. Effect sizes are all very large and the p-values suggest significant differences for each configuration compared to the default "A" configuration.

Table 13: Descriptive statistics of coast-down deceleration values for the lightweight frame configurations, over linoleum tile.

		A	B	C	D
Mean Decel. (m/s^2) Tile Surface	Mean (± StDev)	-0.1557 (±0.0186)	-0.1095 (±0.0098)	-0.1233 (±0.0098)	-0.0795 (±0.0099)
	Effect Size	-	3.12	2.19	5.13
	% Change	-	+29.72%	+20.84%	+48.97%
	p-value	-	0.00*	0.00*	0.00*
Mean Decel. (m/s^2) Carpet Surface	Mean (± StDev)	-0.2290 (±0.0118)	-0.2155 (±0.0140)	-0.1947 (±0.0233)	-0.1866 (±0.0071)
	Effect Size	-	1.05	1.86	4.35
	% Change	-	+5.92%	+15.00%	+18.53%
	p-value	-	0.00*	0.00*	0.00*
*Significantly different ($p < 0.05$) from the mean of the "A" configuration.					

5.5.2 Straight (Tile)

Propulsion cost, distance, and kinetic energy values are shown in Table 14. As expected from the coast-down testing, the up-charged casters and drive wheels improved the over-ground travel behavior – propulsion costs were reduced, distances were increased, and the kinetic energies increased. Swapping both components out concurrently for the up-charged variants had the greatest change over all outcome variables, by a large margin.

Table 14: Descriptive statistics for cost, distance, and kinetic energy of K0004 configurations in the Straight (Tile) maneuver.

		A	B	C	D
Cost (J/m)	Mean (± StDev)	22.80 (±1.82)	17.23 (±0.67)	17.57 (±0.89)	13.51 (±1.14)
	Effect Size	-	4.10	3.70	6.10
	% Change	-	-24.40%	-22.94%	-40.72%
	p-value	-	0.00*	0.00*	0.00*
Distance (m)	Mean (± StDev)	2.11 (±0.63)	4.10 (±0.41)	4.28 (±0.39)	6.98 (±0.07)
	Effect Size	-	3.73	4.13	10.82
	% Change	-	+93.99%	+102.37%	+230.17%
	p-value	-	0.00*	0.00*	0.00*
Max. Kinetic Energy (J)	Mean (± StDev)	6.88 (±2.82)	14.78 (±2.22)	16.34 (±2.94)	32.19 (±0.70)
	Effect Size	-	3.12	3.29	12.33
	% Change	-	+114.90%	+137.53	+368.06%
	p-value	-	0.00*	0.00*	0.00*
*Significantly different ($p < 0.05$) from the mean of the "A" configuration.					

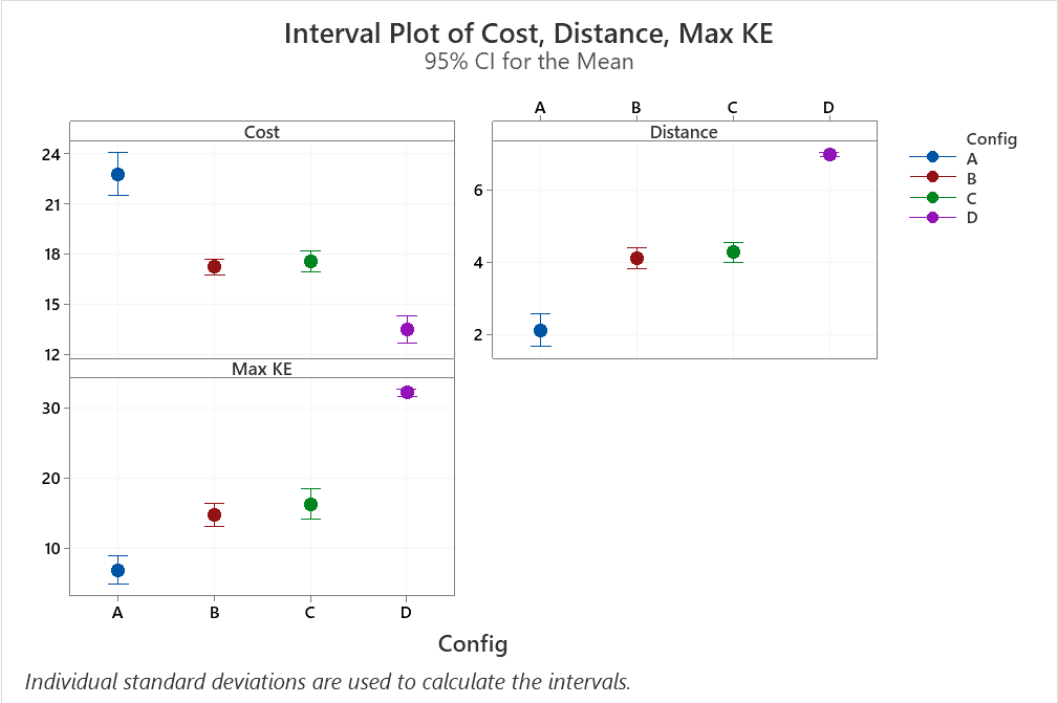

Figure 52: Interval plots of each outcome variable for the Straight (Tile) maneuver across K0004 configurations.

From the ANOVA analysis (original output: F(3,36) = 99.81, p=0.000; output with transformed data: F(3,36) = 103.82, p=0.000), the propulsion costs between groups had statistically significant differences. Post-hoc analysis with Tukey's test reported that the only non-significant difference was between the "B" and "C" configurations. Every other interaction was significant. Visual inspection of the minimal overlap and distinctly grouped costs in Figure 52 supports these findings.

Non-inferiority test results show that all propulsion cost differences were below the threshold (established as -5% of the "A" configuration mean propulsion cost). This indicates that, statistically, all up-charged configurations had lower propulsion costs.

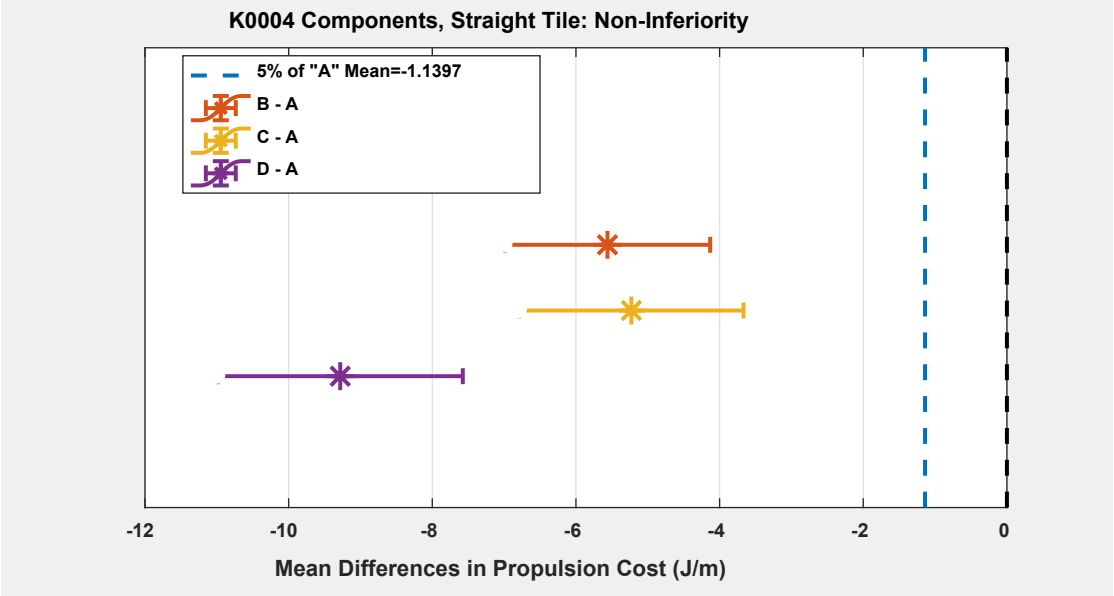

Figure 53: Non-inferiority test results between K0004 component configurations, Straight maneuver over tile.

5.5.3 Slalom (Tile)

Outcome variables for the Slalom maneuver over tile highlighted considerable improvements in the turning maneuverability of the chair with the up-charged components. Yaw displacement, measured in radians of angular heading direction change, was increased by nearly 500% between configurations "A" and "D" without any performance trade-offs. In general, configuration "D" had the lowest cost, traveled the farthest linear distance, and reached the greatest kinetic energy out of all four configurations.

Table 15: Descriptive statistics for cost, distance, and kinetic energy of K0004 configurations in the Slalom (Tile) maneuver.

		A	B	C	D
Cost (J/m)	Mean (± StDev)	19.56 (±0.20)	17.00 (±0.25)	16.75 (±0.29)	14.54 (±0.83)
	Effect Size	-	11.48	11.35	8.31
	% Change	-	-13.08%	-14.38%	-25.69%
	p-value	-	0.00*	0.00*	0.00*
Distance (m)	Mean (± StDev)	1.24 (±0.07)	2.89 (±0.18)	2.96 (±0.23)	5.78 (±0.27)
	Effect Size	-	12.32	10.28	23.04
	% Change	-	+133.68%	+138.99%	+367.64%
	p-value	-	0.00*	0.00*	0.00*
Yaw (rad)	Mean (± StDev)	0.45 (±0.05)	1.69 (±0.10)	1.42 (±0.15)	2.66 (±0.17)
	Effect Size	-	15.65	8.80	17.26
	% Change	-	+278.36%	+217.14%	+495.06%
	p-value	-	0.00*	0.00*	0.00*
Max. Kinetic Energy (J)	Mean (± StDev)	2.69 (±0.30)	6.83 (±0.76)	6.99 (±0.84)	18.53 (±1.80)
	Effect Size	-	7.12	6.80	12.29
	% Change	-	+153.41%	+159.39	+587.47%
	p-value	-	0.00*	0.00*	0.00*
*Significantly different ($p < 0.05$) from the mean of the "A" configuration.					

From the ANOVA analysis (original output: $F(3,76) = 386.32$, $p = 0.000$; output with transformed data: $F(3,76) = 836.27$, $p = 0.000$), the propulsion costs between groups had

statistically significant differences. As in the Straight (Tile) analysis, the Tukey's test reported that the only non-significant difference was between the "B" and "C" configurations. Every other interaction was significant.

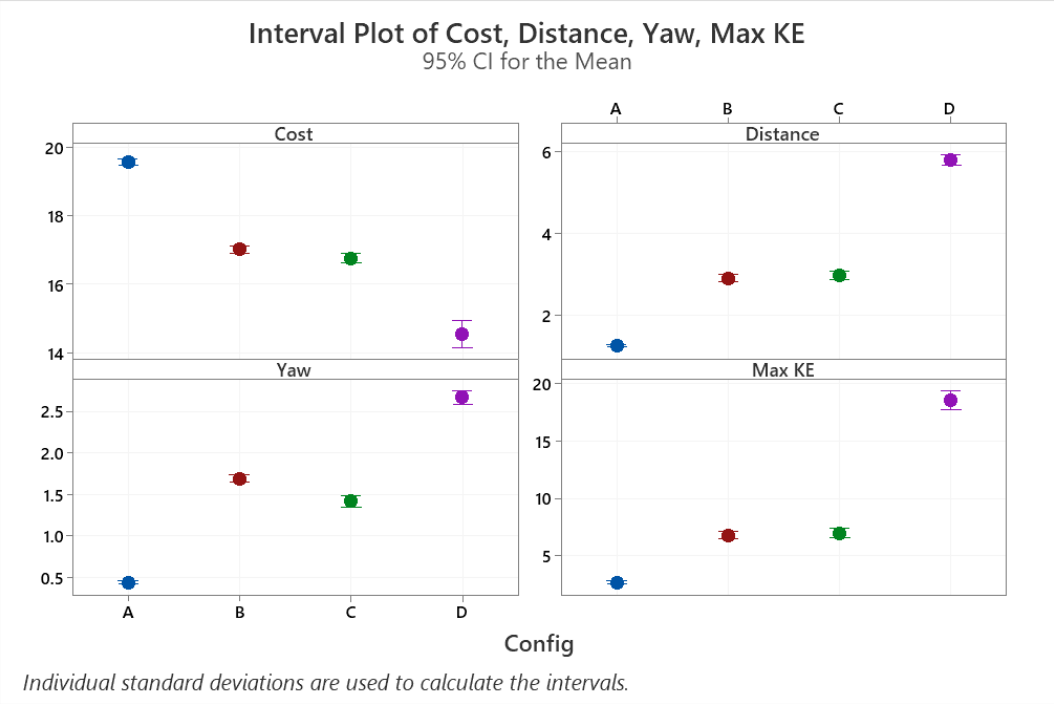

Figure 54: Interval plots of each outcome variable for the Slalom (Tile) maneuver across K0004 configurations.

Non-inferiority test results for the Slalom maneuver over tile had the same general trends as the Straight results on tile, with tighter groupings. The "B", "C", and "D" configurations all statistically showed costs that were lower than the "A" configuration costs by more than 5%.

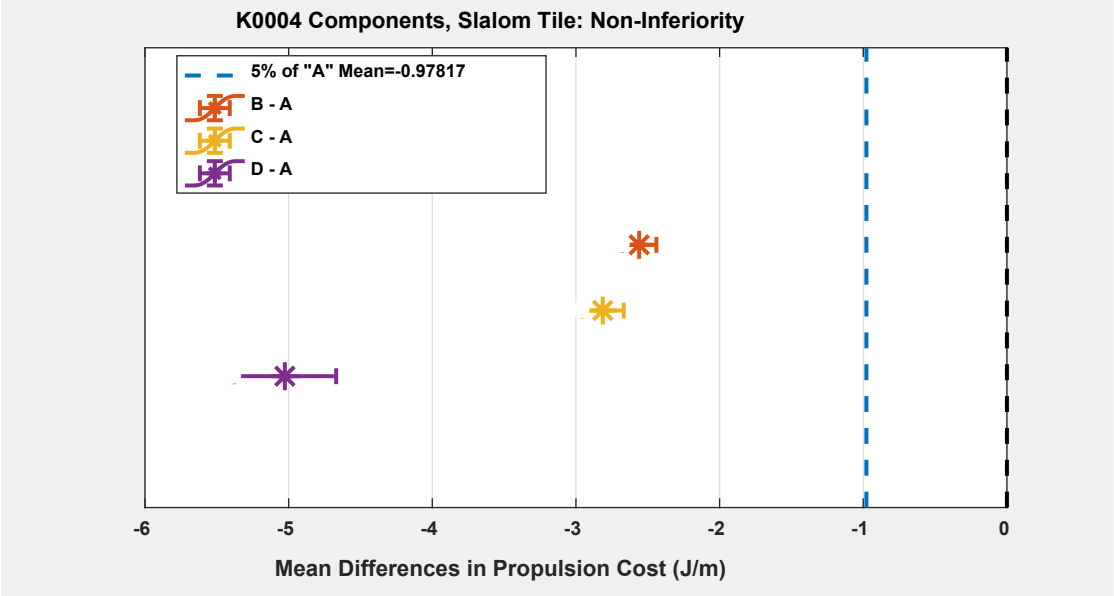

Figure 55: Non-inferiority test results between K0004 component configurations, Slalom maneuver over tile.

5.5.4 Straight (Carpet)

Carpeted flooring increased the propulsion cost for every configuration, even though the torques supplied to the wheels were much greater than the torques for the tile-based maneuvers. Variability within each configuration data set increased as well. Effect sizes remained large to very large.

Table 16: Descriptive statistics for cost, distance, and kinetic energy of K0004 configurations in the Straight (Carpet) maneuver.

		A	B	C	D
Cost (J/m)	Mean (± StDev)	28.04 (±1.32)	26.84 (±1.05)	24.52 (±1.07)	23.13 (±1.05)
	Effect Size	-	1.00	2.93	4.12
	% Change	-	-4.28%	-12.57%	-17.53%
	p-value	-	0.04*	0.00*	0.00*
Distance (m)	Mean (± StDev)	3.52 (±0.45)	4.30 (±0.70)	5.52 (±0.62)	6.21 (±0.72)
	Effect Size	-	1.33	3.67	4.50
	% Change	-	+22.15%	+56.70%	+76.38%
	p-value	-	0.01*	0.00*	0.00*
Max. Kinetic Energy (J)	Mean (± StDev)	13.66 (±2.46)	18.02 (±4.99)	26.67 (±5.00)	31.79 (±5.61)
	Effect Size	-	1.11	3.30	4.19
	% Change	-	+31.96%	+95.30	+132.79%
	p-value	-	0.03*	0.00*	0.00*
*Significantly different ($p < 0.05$) from the mean of the "A" configuration.					

From the ANOVA analysis (original output: $F(3,36) = 38.75$, $p = 0.000$; Kolmogorov-Smirnov assessment did not prove non-normality so the data did not require Box-Cox transformation), the propulsion costs between groups had statistically significant differences. Post-hoc Tukey's test reported that "A" and "B" configurations did not have significant differences. Every other interaction was significant.

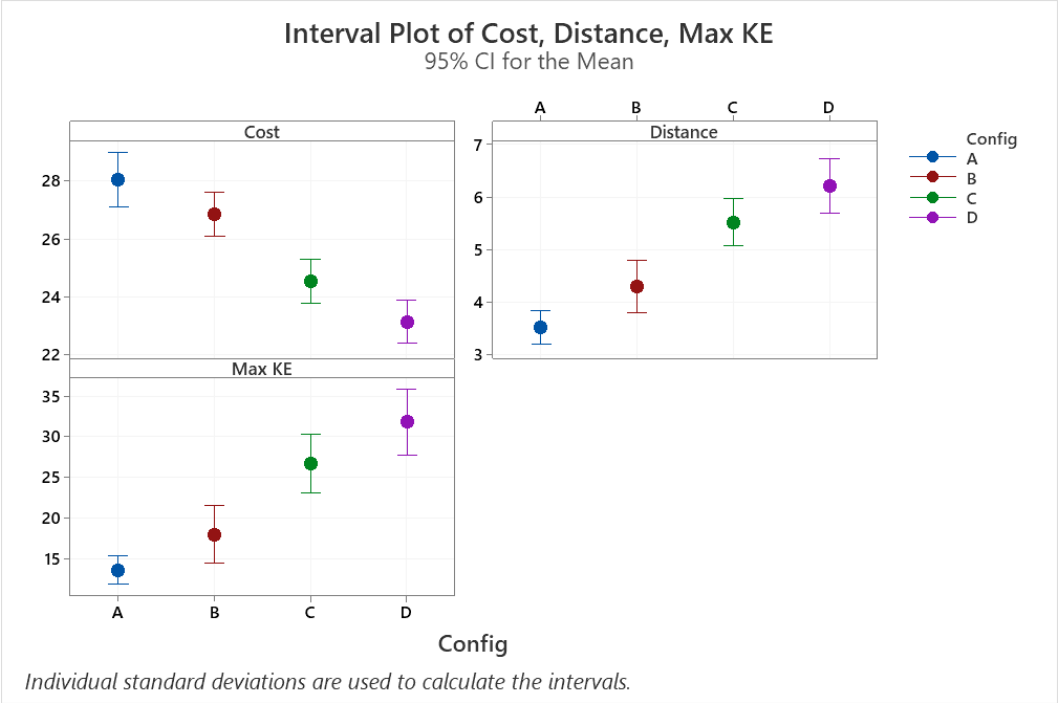

Figure 56: Interval plots of each outcome variable for the Straight (Carpet) maneuver across K0004 configurations.

Non-inferiority test results for the Straight maneuver over carpet (Figure 57) indicated that the propulsion cost of the "B" configuration was *not* statistically less than the cost of the "A" configuration by more than 5%, whereas the "C" and "D" configurations were. Just swapping the casters with the up-charged variant did not reduce the propulsion cost enough to prove inferiority, and though there is a difference of over 1 J/m between the "A" and "B" configuration costs, the "B" configuration cost did not differ by more than 5%.

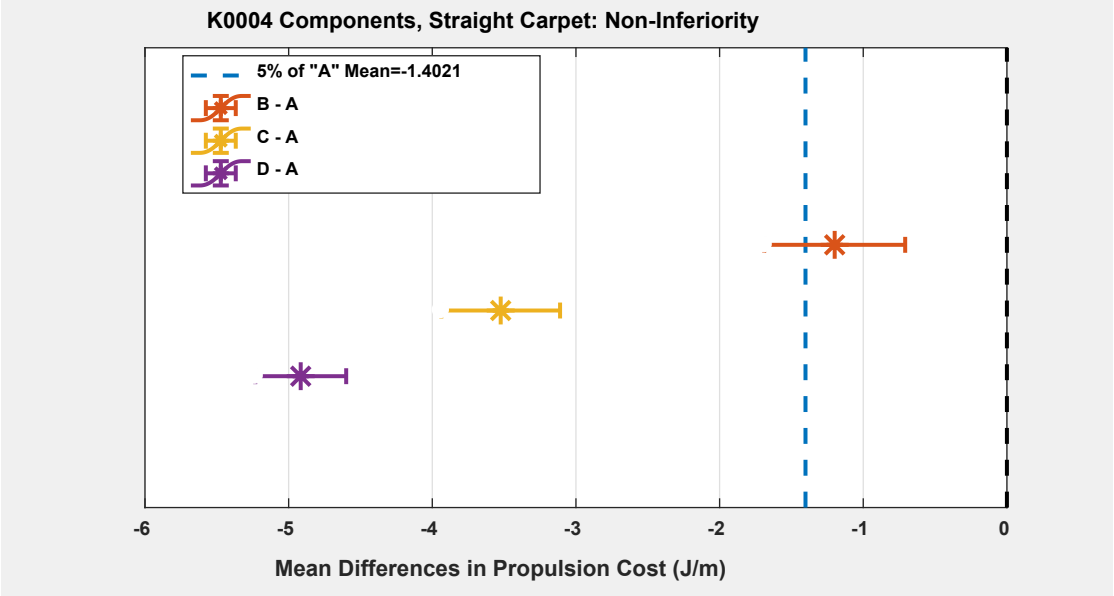

Figure 57: Non-inferiority test results between K0004 component configurations, Straight maneuver over carpet.

5.5.5 Slalom (Carpet)

Trials over carpet decelerated quickly and had difficulty turning with the alternating unilateral pushes. Therefore, the propulsion costs were high and the distances were fairly short. High variability within groups caused reductions in the effect sizes compared to other tested maneuvers.

Table 17: Descriptive statistics for cost, distance, and kinetic energy of K0004 configurations in the Slalom (Carpet) maneuver.

		A	B	C	D
Cost (J/m)	Mean (± StDev)	27.94 (±1.85)	28.74 (±2.59)	26.43 (±2.75)	26.38 (±2.59)
	Effect Size	-	0.35	0.64	0.69
	% Change	-	+2.85%	-5.40%	-5.57%
	p-value	-	0.27	0.05*	0.04*
Distance (m)	Mean (± StDev)	1.47 (±0.32)	1.96 (±0.68)	2.41 (±1.05)	2.98 (±1.11)
	Effect Size	-	0.93	1.21	1.85
	% Change	-	+33.30%	+63.67%	+102.53%
	p-value	-	0.01*	0.00*	0.00*
Yaw (rad)	Mean (± StDev)	0.89 (±0.23)	1.72 (±0.46)	1.68 (±0.65)	2.64 (±0.45)
	Effect Size	-	2.29	1.61	4.87
	% Change	-	+93.18%	+88.24%	+196.55%
	p-value	-	0.00*	0.00*	0.00*
Max. Kinetic Energy (J)	Mean (± StDev)	3.71 (±1.13)	6.03 (±2.94)	8.05 (±4.50)	10.53 (±5.48)
	Effect Size	-	1.04	1.32	1.72
	% Change	-	+62.46%	+116.92%	+183.75%
	p-value	-	0.00*	0.00*	0.00*
*Significantly different ($p < 0.05$) from the mean of the "A" configuration.					

From the ANOVA analysis (original output: $F(3,76) = 4.42$, $p = 0.006$; output with transformed data had same values), the propulsion costs between groups had statistically

significant differences. Interestingly, Tukey's test results reported significant differences between the "B" configuration and both the "C" and "D" configurations. The up-charged casters improved the distance, yaw, and kinetic energy of the system, but only did so at the expense of increased propulsion cost. Adding the up-charged drive wheels reduced the propulsion cost and further improved the distance and attainable kinetic energy.

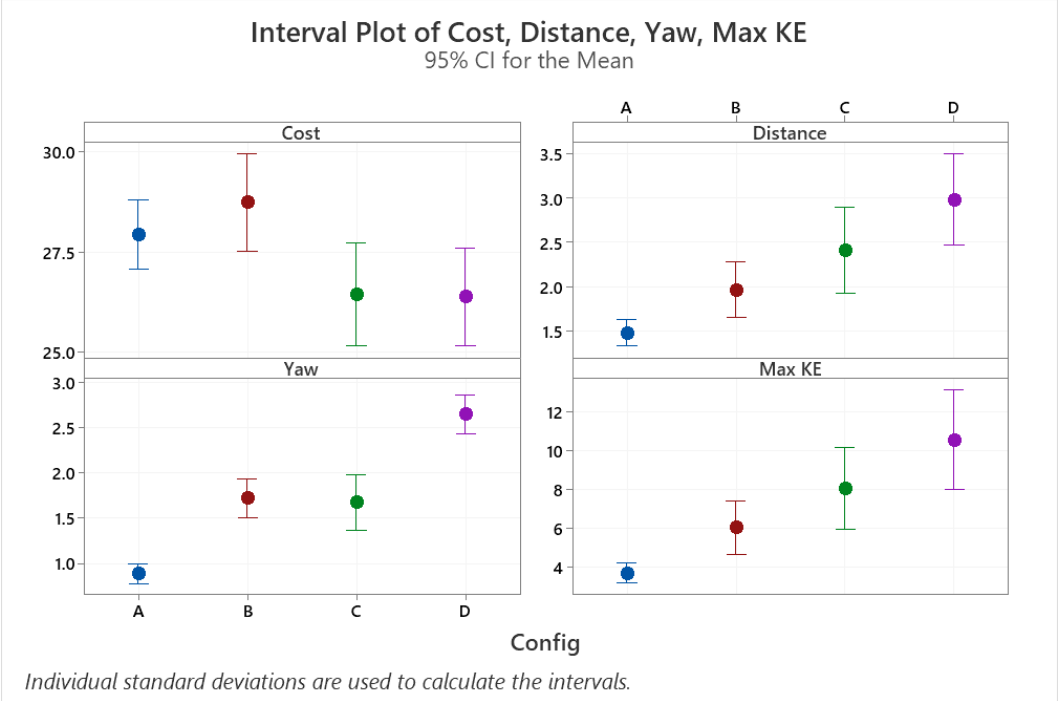

Figure 58: Interval plots of each outcome variable for the Slalom (Carpet) maneuver across K0004 configurations.

Non-inferiority test results for the Slalom maneuver over carpet (Figure 59) showed that all of the configurations had tails of the 95% confidence interval within the equivalence threshold (set at 5% of the mean propulsion cost of the "A" configuration). Therefore, they all had functionally-equivalent propulsion costs.

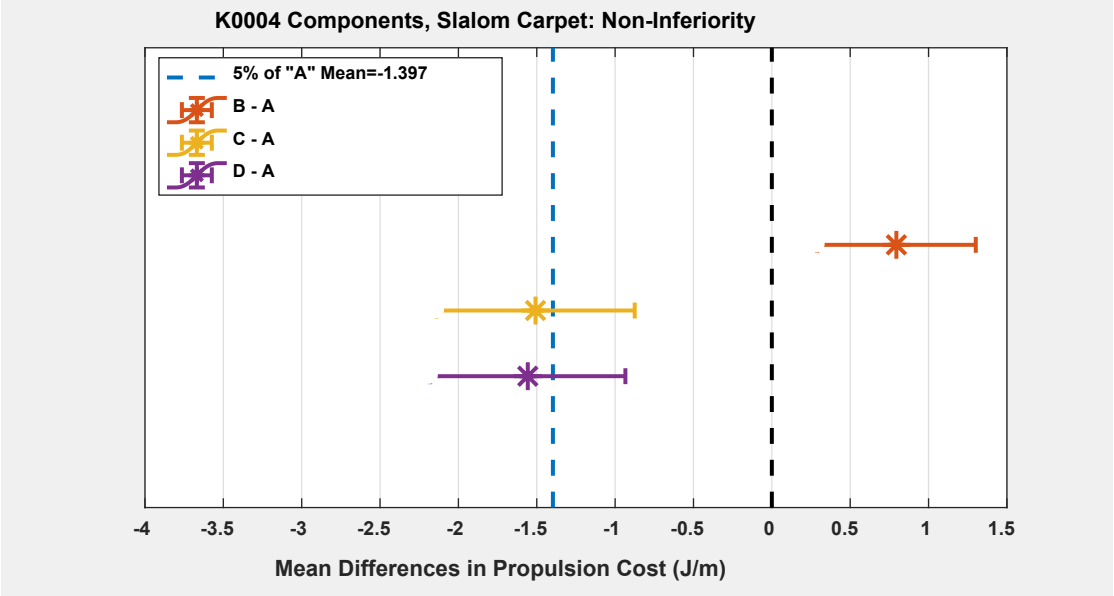

Figure 59: Non-inferiority test results between K0004 component configurations, Slalom maneuver over carpet.

5.6 Discussion

Few studies have investigated the over-ground performance of lightweight wheelchairs. Out of these reports, the findings were limited to show that lightweight chairs can be propelled farther and faster than standard wheelchairs [129] but are surpassed in performance by ultra-lightweight wheelchairs in drag tests [116], over-ground propulsion tests [31], and general usage monitoring [6]. Only one study specifically investigated the K0004 category: Oliveira et al. compared high-strength lightweight and ultra-lightweight wheelchair performances by measuring the biomechanics of adolescent wheelchair users [131]. In all reported metrics (push-rim forces, upper body kinematics, and a biomechanically-measured equivalent of propulsion cost), Oliveira's report shows that K0004 chairs need larger forces and travel at a slower natural pace than K0005 chairs, and

they demand a higher propulsion cost over two of the three surfaces. Though the reported human-based propulsion costs (15.3±5.78 versus 19.7±7.86 J/m on tile, 105.6±27.3 versus 85.2±20.1 J/m over polyfoam mat, and 82.4±21.8 versus 73.4±23.6 J/m up a 5° ramp for K0004 and K0005, respectively [131]) do not directly align with the propulsion cost values measured by the AMPS, the general trends between studies are similar.

The K0004 frame required higher torque profiles (Figure 47 through Figure 50) than those defined for the K0005-dependent incremental mass study (Figure 39 and Figure 40). For the default K0004, the speed (represented via kinetic energy) was significantly lower than the speed of any tested K0005 configuration despite the higher torques applied to the wheels. The highest kinetic energy attained by the K0004 frame in configuration "D" was similar to those seen in the incremental mass study, but that was attained at a significantly higher propulsion cost. By upgrading both casters and drive wheels, the K0004 chair had similar over-ground motion to a K0005 chair, but at a higher propulsion cost.

The aim of this study was to improve the performance of the chosen K0004 wheelchair through careful consideration of the components. Though K0004 chairs are expected to be used as a full-time device, they are commonly only equipped with low- to no-maintenance components from the manufacturers. Therefore, solid or non-pneumatic components were selected to maintain this low-maintenance context of use. Up-charged component selections were informed from existing knowledge of the energy losses exhibited by each component, as measured by the component-level rolling resistance and scrub torque test methods [81].

Primo 6”x1.5” casters were chosen because out of all the casters in the energy loss ‘library’, they demonstrated the most ideal characteristics of the solid caster options at the 6”- to 8”-diameter range. They had nearly the lowest scrub torque out of every tested caster on tile and carpet, comparable rolling resistance on tile, and lower rolling resistance on carpet than the other non-pneumatic 6”-diameter casters [81]. Ideally, large tires and wheels tend to handle increased load better than smaller-diameter counterparts [67, 81, 115]. Specifically, increased caster diameter directly correlates to better (decreased) rolling resistance, with all other wheelchair parameters held constant [136]. The present findings are in slight contradiction – according to the outcome variables from the coast-down and AMPS tests, the 6”-diameter casters rolled considerably better than the 8”-diameter casters over tile and carpet. However, the 6”-diameter casters did appear to hinder the Slalom maneuver on carpet compared to the larger 8”-diameter casters.

Non-pneumatic 24”x1-3/8” Primo XPress tires were selected because they had the lowest scrub torque by a large margin over every tested drive wheel tire including pneumatic variants, and had the lowest rolling resistance on both surfaces out of any non-pneumatic tire [81]. If the user were to explore higher-maintenance options, it is highly suggested that pneumatic tires would further reduce rolling resistance and improve efficiency [33, 45-47]. The Primo XPress tires were seated on steel-spoked wheels, in contrast to the composite plastic ‘Mag’ wheels used in the default configuration, though it is suggested that the style of wheels does not impact the rolling characteristics of the chair [135], unless there is a notable difference in the rigidity of the wheel or quality of the internal bearings. This up-charged component swap from Solid Mag wheels to the steel-

spoked Primo XPress wheels was universally beneficial across all surfaces and maneuvers, with up to a 23% reduction in propulsion cost.

Propulsion cost seemed to be the most appropriate measure to rate the system-level performance differences between configurations. Out of all four outcome variables, it is uniquely structured as a metric of energy input versus the functional output (travel distance) of the MWC. The up-charged configurations very clearly outperformed the default configuration in almost all maneuvers. Propulsion costs were reduced by up to 41% by swapping both components. This difference was most noticeable in rectilinear motion over the linoleum tile surface, where all of the configurations had their best performances – tiled surfaces feature a lower drag and scrub resistance than the carpet, and straight motion without any turning has the fewest sources of energy loss because there aren't any resistive scrub components in the system loss equations [83]. The caster swap had more of an effect on cost than the drive wheel swap on tile, but the opposite trend was reported on carpet. The caster swap even raised the propulsion cost in the Slalom maneuver.

The other outcome variables (deceleration, distance, yaw, kinetic energy) demonstrate similar observable changes in the system output. Deceleration values, the most 'quick and simple' test method in this study, aligned nicely with the Straight results – up-charged casters had a higher advantage than drive wheels over tile, whereas drive wheels were much more advantageous over carpet. "B" improved deceleration by nearly 30%, "C" by 21%, and "D" by 49% over the tile surface. The carpeted flooring reduced this effect by exaggerating the deceleration values for all configurations, but the drive wheels provided the most benefit (15% improvement) instead of the casters (6% improvement). The same trends are noticeable in the distance and yaw outcome variables, as well: solely replacing

the casters more than doubled the distance and yaw of the "A" configuration in Slalom over tile. Replacing the default casters and upgrading the drive wheels slightly improved the distance and reduced the yaw (2.96 m and 1.42 rad), though this configuration still demonstrated over double the displacement of the default configuration. Configuration "D" with up-charged casters and drive wheels doubled the distance and nearly doubled the yaw angular travel yet again (5.78 m and 2.66 rad). In that same Slalom over tile maneuver, the kinetic energy differences showed massive discrepancies between groups, with the "B" and "C" configurations having over 150% increases in kinetic energy over the "A" configuration, and the "D" kinetic energy at almost 600% higher than the "A" value. These percent differences are more extreme than those seen in propulsion cost data, but they are dependent on the maneuver – if another trial were to use higher torques on the wheels, the speeds would increase and the distance, yaw, and kinetic energy values would all increase accordingly. The propulsion cost metric would be the only outcome variable that would remain relatively stable, which is why it was selected as the main performance predictor.

The general concept of this study was to 'raise the floor' of the K0004 category. Competitive bidding has partially undermined the ingenuity of the market and brought the K0004 down to level dictated by the lowest bidder. However, by quantifying the improvements of just switching out some tires, this study has unveiled that even the lowest bidder can significantly boost the performance for minimal cost. The cost for the manufacturer to replace the components would be a fraction of the $100 cost from the consumer to a third-party accessory vendor.

The direct societal impact of this study is hindered by the K0004 category seemingly phasing out. The amount of K0004 approvals has fallen drastically in the past

decade, from 708,000 in 2010 [126] to only 96,000 in 2017 [125]. As the definitions of the wheelchair coding evolves, the K0004 category may – or perhaps, should – be divided into segments of K0003 and K0005. The 2-lb. weight limit difference is not the defining factor between K0004 and K0005, as shown in the incremental mass assessment, but there *does* exist a performance difference between the groups. The discussion about where this performance difference comes from is only partially explained by the results of this study, but there is an abundance of evidence showing that the default K0004 components are largely the limiting factor of the K0004 mechanical performance. The torque profiles defined for the K0005 frame would not propel the K0004 at all in the "A" configuration, and the only configuration with similar performance to the K0005 (the "D" configuration) required up-charged components that were not even offered by the manufacturer. It should be obvious that the tested chair was not intended to compete with the ultra-lightweight category. However, for current K0004 users, there are simple and inefficient options to boost performance by a wide margin at the component-level.

5.7 Conclusion

The results presented above show ample evidence that the 'as-is' configuration of the K0004 could be significantly improved for less than $100. Propulsion cost can be reduced, travel distances can be increased, and the overall kinetic energy of the system can be raised by trading out the default components with slightly more expensive variants. If only one set of components can be replaced, it is highly recommended to change the drive wheels, solely due to their increased performance over a carpeted surface. The generalizable knowledge from this work informs users and clinicians, as well as manufacturers, of the energetic differences of various component options with physically-

and clinically-relevant parameters. Additionally, this study shows that coast-down deceleration tests are informative and largely aligned with more advanced system-level propulsion tests. Simplistic tests methods like the coast-down deceleration test can be modified to use lower levels of technological instrumentation. With a lower bar of entry, more researchers and clinicians can contribute to this shared wealth of knowledge.

CHAPTER 6. COMPARING RIGID AND FOLDING FRAMES

6.1 Overview

Generally speaking, the portability of each individual wheelchair is dependent on the capabilities of the user. A first-time wheelchair user is much less likely to have custom hardware in their house or automobile that enables them to stow a full-size rigid K0005 frame. Instead, this user will likely rely on the frame to fold into a compact form before stowing the chair in a car or around the house. For this particular user, portability of the chair is defined by how compact the frame can be, how many components must be removed, and how heavy the frame is, if lifting is required to stow the chair. Though it varies case-by-case, some users will greatly benefit from the use of folding frames over rigid frames to facilitate transport and/or storage. However, rigid and folding frames may differ with respect to propulsion cost due to frame flexion or vibration [137]. Since a folding frame has more moving parts, the quality of the design and manufacturing can impact durability [138, 139] and lead to abandonment of the device [140]. Whether a folding frame adds to the cost of propulsion, however, has not yet been determined.

K0005 wheelchairs are used for long durations and undergo a wide range of uses and stressors during everyday mobility. If certain folding frames offer the same durability as rigid frames with a similar cost of propulsion, then they deserve to be considered as equivalent across these two important parameters. Conversely, if some folding frame chairs do not offer similar performance – either new or after use – then users and clinicians will be able to weigh the tradeoff of a folding frame in relation to performance. Similarly, public

policy officials should benefit from this new information to better reflect whether or not folding and rigid frame chairs can and should be considered as equivalent K0005 options.

As of contemporary HCPCS requirements [26], the only substantial requirements for K0005 chairs are: (1) the frame weight with or without front riggings, depending on the model, is less than 30 lbs.; (2) the drive wheel axle position is adjustable; (3) the side frames and cross-braces have a lifetime warranty. There are chairs in this category that range from 18 lbs. to 29 lbs. and though the incremental mass study concludes that frame mass should not be a major factor in propulsion cost or performance, it seems counterproductive to separate K0004 and K0005 chairs by 2-4 lbs. if the K0005 category alone has a range of over 10 lbs. The drive wheel axle position requirement does not specify direction nor amount of adjustment, so a drive wheel axle that has a single discrete 1" fore-aft adjustment will meet the same specification as one that can move continuously over a vertical and fore-aft range of 6". This may be irrelevant if the chair is custom-made with measurements to properly fit the user, however for a first-time K0005 user, the adjustability can make up for some errors in their ordered dimensions. With the range of offerings within the K0005 category, the three major requirements do not seem to adequately describe one particular group of chairs, but rather a highly-variable assortment of chairs that lack commonality. Categories can and should be divided into more discrete groups based on their clinical application with some metric of performance, or at the very least by the available features and options on each frame to improve the shared characteristics of each group.

To this end, the aim of this study was to utilize the AMPS to assess the propulsion cost and other performance characteristics of several K0005 rigid and folding frames. Three chairs of each frame style were selected for testing and equipped with components (24”x1-3/8” Primo Orion drive wheels and Primo 5”x1” casters) standardized across all chairs. Weight distribution and general geometric measurements were controlled to isolate the impact of the frame style from other prominent confounding factors.

6.2 Hardware and Configurations

6.2.1 Frame Selection

Several popular wheelchair models were chosen for this study based on product characteristics, options, accessories, and adjustability of the frame. Seat sizes were limited to 16”-18” depth and width to accommodate the AMPS. Floor-to-seat heights were constrained to 16”-19” at the front of the seat, with a target height of 17” for all adjustable frames. Drive wheel camber was limited to $\leq 3°$. In the case of two frames, the axle housings were swapped with alternate housings from the manufacturer to reduce the camber angle to within the specified range. A small convenience sample of brand-new chairs were sourced from the nearby Shepherd Center seating clinic and rehabilitation equipment stock room (Quickie Xenon^2, Motion Composites Helios A6). Other chairs were sourced directly from the manufacturer (Ki Rogue, Ki Catalyst 5).

Table 18: Rigid-frame K0005 wheelchair selection.

Rigid Frame Selection		
		
Quickie (Sunrise Medical)	***Ki Mobility***	***Tilite (Permobil)***
GT	***Rogue***	***Aero Z***
"R1"	"R2"	"R3"

The two remaining chairs were already available in the REAR Lab from previous studies. The Quickie GT was used in the extensive configuration-based propulsion cost study [71] incremental frame mass study. The TiLite Aero Z was used in a similar mass-based wheel torque investigation [69].

Table 19: Folding-frame K0005 wheelchair selection.

Folding Frame Selection		
		
Motion Composites	***Quickie (Sunrise Medical)***	***Ki Mobility***
Helios A6	***Xenon²***	***Catalyst 5***
"F1"	"F2"	"F3"

The wheelchairs in Table 18 and Table 19 were chosen by convenience, but represent a fair cross-section of some popular makes and models of chairs with both frame types. Advertisements for these chairs often feature statements indicating performance benefits of the chair model. Take the following examples: From the Sunrise Medical website for the Quickie 5^R (the latest Quickie GT replacement), they write that the rigid K0005 frame is "…designed to deliver superior rigid wheelchair performance day after day." Ki Mobility's rigid Rogue is said to have "…state-of-the-art design innovation that lends itself to the highest level of responsiveness and rigidity than has ever been felt before." The TiLite Aero Z is advertised to feature a "…minimal design with unmatched adjustability and performance." The folding frames have very similar marketing. The Motion Composites Helios A6 has a vague statement about performance, suggesting that the "…symmetrical cross brace ensures remarkable mobility and ease of propulsion." The Sunrise Medical Xenon^2 states that the "…streamlined design maximizes your speed and efficiency with every push". The Ki Mobility Catalyst 5 is even bolder, saying that "with a more rigid design than its competitors, Catalyst 5 offers the best performing ride in its class." Each of these claims should be demonstrable via AMPS testing. 'Ease of propulsion' or 'best performance' may be terms that comprise many definitions, but propulsion cost at the very least should be a decent metric for 'performance' or 'efficiency'. The goal is to investigate equivalence between the frame types – does a rigid chair, regardless of make/model, have a distinct advantage over folding chairs in terms of propulsion cost, travel distance, angular yaw travel, or attainable kinetic energy under the same torque application?

6.2.2 Component Selection

Components were standardized across all six chairs, and were selected based on examination of the industry standard and prior knowledge about component-level test results [81]. At the K0005 level, there are often two 'no-cost' options for drive wheels: 24"x1-3/8" pneumatic tires or airless, solid polyurethane tires. Both options are typically mounted on steel-spoked wheels. A pair of pneumatic Primo Orion 24"x1-3/8" tires were used on metal spoked wheels. The tires were inflated to the suggested pressure of 75 psi. Similarly, the default option for casters are 1" wide solid plastic wheels with polyurethane tires, and the 'no-cost' variants normally only vary in diameters ranging from 3" to 6". In this study, a pair of Primo 5"x1" solid casters were used on each of the selected frames.

6.2.3 Chair Configurations

Each chair was measured individually on the iMachine [79] to determine unloaded chair mass including the frame, drive wheels, and casters. Optional attachments such as arm rests, anti-tip bars, seat belts, and leg straps were removed on each frame. Drive wheel axle positions and caster stem orientations were adjusted on each frame to reach a weight distribution of 70% over the drive wheels in each chair to better emulate the average ultra-lightweight user configuration [23]. For several of the chairs, this process involved shifting the drive wheel axle position and aligning the caster fork stems to be vertical. Additionally, this process involved shifting 5.5 kg bar weights between the abdomen-region of the AMPS and the hollow cavities in the thighs of the plastic buttock shell.

Table 20. Mass and weight distribution of folding and rigid K0005 frames.

Config. Name	Chair Make and Model	System Mass	Weight Distribution over Drive Wheel Axle
"R1"	Sunrise Medical Quickie GT	93.6 kg	69.9%
"R2"	Ki Mobility Rogue	93.1 kg	69.5%
"R3"	TiLite Aero Z	93.6 kg	70.9%
"F1"	Motion Composites Helios A6	94.7 kg	69.2%
"F2"	Sunrise Medical Quickie Xenon^2	96.4 kg	69.3%
"F3"	Ki Mobility Catalyst 5	94.4 kg	70.3%

6.3 Experimental Design

This experiment, in summary, was designed to isolate the effects of only the wheelchair frame type (folding, rigid). Three K0005 chairs from each group were used with one pair of standard drive wheels and casters. One coast-down deceleration procedure was used for general rolling resistance measurement. Two AMPS-based propulsion maneuvers were selected: a 7-push straight trajectory and a 5-push slalom trajectory, both over a waxed linoleum tile surface. Each maneuver was tested with 5 trials in each opposing heading direction (forwards, backwards, as well as left and right starting pushes for the slalom) to normalize any irregularities in the hallway. With 20 coast-down trials and 30 AMPS trials per each of the six configurations, this experiment required 120 coast-down trials and 180 over-ground AMPS trials.

6.3.1 Maneuver Selection

As in the previous studies, coast-down deceleration tests were used to demonstrative a rapid and low-tech test method to detect differences between the frame types. The AMPS-based propulsion testing utilized identical maneuvers from the incremental mass study (Figure 39 for the Straight maneuver, Figure 40 for the Slalom maneuver). Since both studies were designed to propel ultra-lightweight wheelchairs across linoleum tile flooring, it seemed logical and reasonable to keep the same torque profiles.

6.4 Methods

6.4.1 Data Collection

First, a simplistic coast-down deceleration method was used to characterize the typical coasting behavior of each configuration. The coast-down procedure followed the same steps outlined in the incremental frame mass and K0004 studies: first, the AMPS was loaded onto the wheelchair seat with the motors decoupled from the wheels. The tires were inflated to the specified 75 psi. The wheelchair was centered in the hallway. From rest, the wheelchair was manually pushed via the rear handles to accelerate the chair to approximately 1.0-1.2 m/s. Upon reaching the target range of speeds, the wheelchair was released and permitted to roll down the hallway until it naturally decelerated to a stop. Wheel velocities were recorded by the wheel encoders. 10 trials were taken in the forward and backward hallway directions (the AMPS was always facing the direction of travel) to account for any slopes or inconsistencies in the tiled floor for each configuration, resulting in 120 total coast-down trials.

Next, the experimental protocol consisted of 30 over-ground propulsion trials for each of the six configurations, totaling 180 AMPS trials in all. The pneumatic drive wheels were inflated to 75 psi as per the manufacturer recommendations. The torque trajectory was loaded into the LabVIEW interface and the AMPS was set up along a 30 meter length of clean, flat linoleum tile hallway. To normalize for surface inconsistencies such as slope or intermittent bumps, 5 forward-heading trials were run in each of the forward and backward hallway directions along the same length of tile for the Straight maneuver. Similarly, the Slalom maneuver was tested with 5 trials in each of the left and right slalom maneuvers (Figure 40 shows a "right" slalom, as the first unilateral push is on the left wheel and would turn the chair to the right first) in both the forward and backward hallway directions, resulting in a total of 20 slalom trials altogether. The collection of trials for each configuration were averaged together by maneuver ($N = 10$ for Straight, $N = 20$ for Slalom) and the repeatability for the set of trials was assessed. The inclusion criteria for each set of trials was that the CoV of each outcome variable (nominally distance, as it was the easiest to assess visually and with a rapid post-trial MATLAB analysis) remained ≤ 10%.

6.4.2 Data Analysis

The four main outcome variables of this experiment were propulsion cost (Eqn. 8), distance travelled by the center of mass, yaw distance travelled as the wheelchair changed heading direction, and the maximum attainable kinetic energy of the system, (Eqns. 1-4 and nomenclature from Medola [78]). Data from the current-based motor torque sensors, motor encoders, and wheel-mounted encoders were collected at 40 Hz during the over-ground trials. These data were processed in MATLAB. Butterworth filters were used to

smooth each sensor signal before calculating the input power to the system from each motor.

Coast-down data were assessed via linear regression fit of the system linear velocity. The normal window of analysis was shifted to 0.75-0.45 m/s instead of the default 0.95-0.65 m/s window to average over some inconsistencies at the release velocity. Goodness of fit was improved to $R^2 \geq 0.80$. Unfortunately, many of the configurations were prone to following the curvature of the floor, and the deceleration trials had high variation due to the subtle accelerations and decelerations of the chairs riding over slight dips and hills. Shifting the window minimized the influence of these bumps in the velocity data, but the results show notably poorer precision than previous iterations of coast-down testing. Deceleration values were averaged for each chair, as well as over the entire group (folding, rigid).

From the AMPS-based propulsion testing, collected data for each of the 180 trials were used to calculate the propulsion cost, overall distance traveled by the center of mass, and maximal kinetic energy of the system. For each Slalom trial, the additional outcome variable of yaw displacement was calculated from wheel velocities and geometric parameters of the chair to track the angular change in heading direction over the course of the maneuver. Descriptive statistics were tabulated across each outcome variable for each chair as well as the collective statistics for each group. Effect size, percent change, and p-values from 2-sample t-testing were reported between the folding- and rigid-frame groups, using the rigid-frame as the baseline.

Analysis included assessment of differences across frame types, as well as a more direct comparison across each individual frame. The experimental design served to control the components (drive wheels, casters) and general loading characteristics of each frame to isolate the main factor of frame type. One-way ANOVA tests were run to assess the differences between folding and rigid frame types for each maneuver. An *a priori* decision was made to report all p-values and discuss results at the $p \leq 0.10$ levels. Normality of the dependent measures were assessed using Kolmogorov-Smirnov analysis. Cost values were found to violate the assumption of normality during both of the maneuvers. ANOVA was run using a Box-Cox transformation of this data. Post-hoc analysis included Games-Howell pairwise comparisons with $\alpha = 0.100$, otherwise known as an error rate of 10. Kruskal-Wallis tests, which do not require data normality, were used to assess differences in the medians of the data sets. Finally, 2-sample (not paired) equivalence testing was used to assess the relative differences between the mean propulsion costs of the folding and rigid groups. A two-sided equivalence window of ±5% of the rigid propulsion cost was established. Though there were no 'control' and 'test' cases in this study, the rigid group was selected as the control group and the folding frame was used as the test group.

6.5 Results

6.5.1 Coast-Down

Results from the coast-down tests are shown in Table 21. The range of the deceleration means across groups (folding, rigid) is tightly grouped, much like the deceleration values from the incremental mass study. Despite disparities within each group, this data shows folding chairs to have slightly lower deceleration values in comparison to

the rigid chairs. The 2-sample t-test returned a p-value of 0.054 indicating that the group means had statistically significant differences. The within-group variance hinders the group-wise comparison. Though the folding frame group has the lowest average, it also features the single highest deceleration value from any of the six frames.

Table 21: Descriptive statistics of coast-down deceleration values for the folding and rigid K0005 frame configurations, over linoleum tile.

		Mean Deceleration (m/s^2)	
		Mean (±StDev)	**Group Mean (±StDev)**
Rigid	**R1**	-0.0517 (±0.0140)	-0.0605 (±0.0174)
	R2	-0.0651 (±0.0205)	
	R3	-0.0646 (±0.0141)	
Folding	**F1**	-0.0491 (±0.0187)	-0.0544 (±0.0199)
	F2	-0.0461 (±0.0136)	
	F3	-0.0681 (±0.0198)	
	Effect Size		0.51
	% Change		+3.26%
	p-val		0.054*
	*Significantly different ($p < 0.100$) from the Rigid group.		

6.5.2 Straight

The Straight maneuver outcome variables (Table 22) show a performance benefit of the rigid frames, on average, over the folding frames. Propulsion cost is significantly lower ($p = 0.054$). No other statistically significant differences were reported. The effect

size between the groups is small to medium for each variable, and the percent changes are very small (< 4% difference between folding and rigid). The average values of cost, distance, and kinetic energy imply that the rigid frames have a slight advantage to cost and distance, and have nearly equivalent maximal kinetic energies to their folding counterparts.

Table 22: Descriptive statistics of each outcome variable (Straight Tile maneuver) for the folding and rigid K0005 frame configurations.

		Cost (J/m)		Distance (m)		Max. Kinetic Energy (J)	
Rigid	**R1**	8.89 (±0.53)	9.12 (±0.64)	8.76 (±0.40)	8.59 (±0.63)	34.27 (±2.09)	32.96 (±2.58)
	R2	8.69 (±0.41)		9.16 (±0.29)		34.19 (±2.42)	
	R3	9.79 (±0.30)		7.83 (±0.12)		30.43 (±0.75)	
Folding	**F1**	9.76 (±0.26)	9.42 (±0.53)	8.26 (±0.46)	8.36 (±0.59)	33.96 (±2.40)	33.22 (±2.60)
	F2	8.82 (±0.37)		8.95 (±0.43)		34.95 (±2.14)	
	F3	9.68 (±0.30)		7.86 (±0.24)		30.76 (±0.87)	
	Effect Size		0.51		0.37		0.10
	% Change		+3.26%		-2.64%		+0.78%
	p-val		0.054*		0.156		0.701
	*Significantly different ($p < 0.100$) from the mean of the Rigid group.						

Figure 60 shows a clearer visualization of the outcome variable differences between rigid and folding frames. There are distinctions between group cost and distance means, but the 95% confidence interval bars show a large margin of overlap.

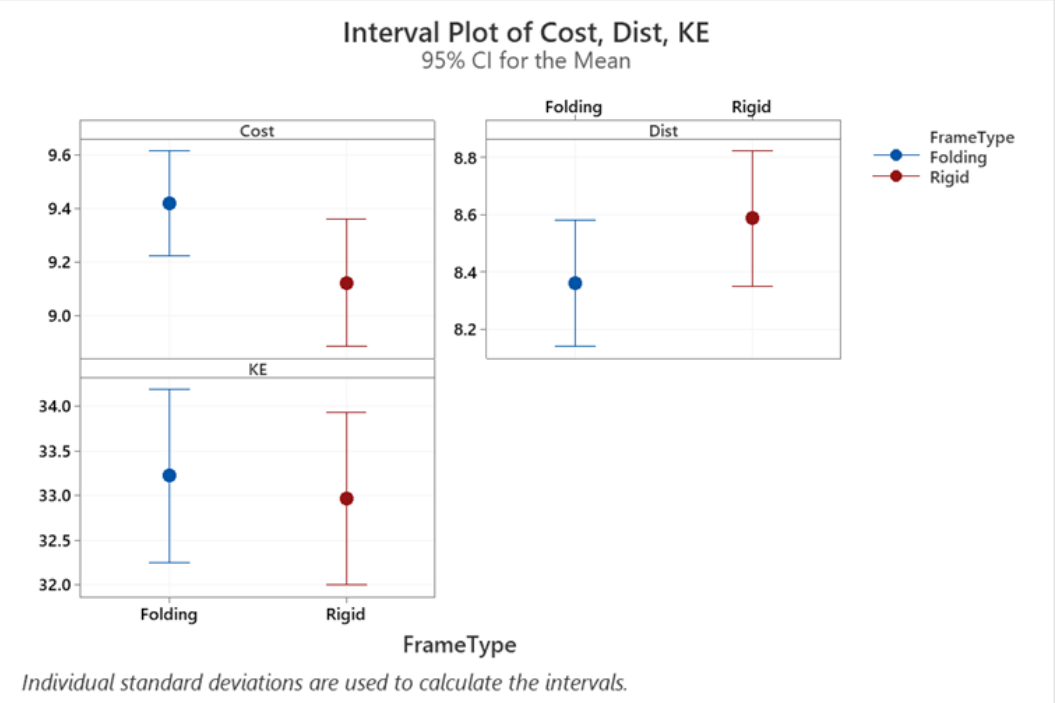

Figure 60: Interval plots of each outcome variable for the Straight (Tile) maneuver across folding and rigid K0005 wheelchairs.

One-way ANOVA results with the Box-Cox transformed propulsion cost reported a significant ($F(1,57) = 3.57$, $p = 0.064$) difference between the groups, and the means of the groups were identified as different by the Games-Howell method with an error rate of 10 for the comparison. The Kruskal-Wallis test results ($H = 3.98$, $p = 0.046$) also reported differences between the medians of the groups. Rigid frames had two distinctly grouped costs (R1 and R2 around 8.69 to 8.89 J/m, and R3 at 9.79 J/m, almost a full 1 J/m higher), as did the folding frames (F2 with 8.82 J/m, versus F1 and F3 around 9.68 to 9.76 J/m). Propulsion cost data was plotted in a histogram (Figure 61) to further investigate the distribution of these costs.

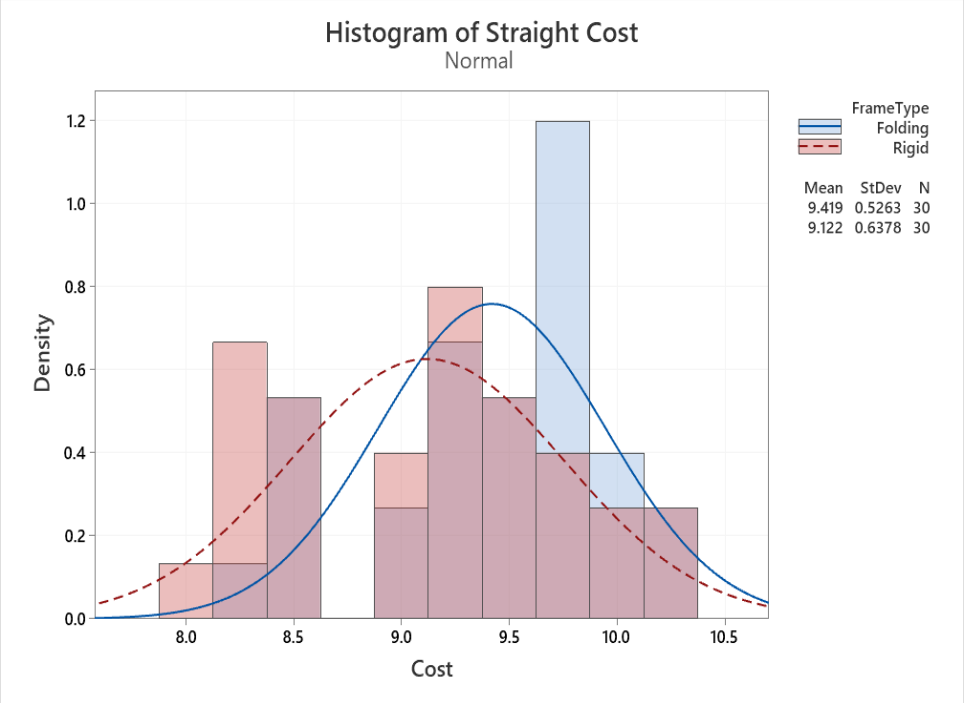

Figure 61: Histogram showing distribution of Straight (Tile) costs for folding and rigid K0005 wheelchairs.

This non-normal distribution of the data implies that the propulsion costs are not solely dependent on the frame type, as both frame types share an equivalent range and similar distribution of propulsion cost values. The fitted curves nicely illustrate the effect size by showing that there is significant overlap between the distributions, despite having different spreads. The bins within this histogram may show a slightly misleading trend of a slightly lower-leaning propulsion cost of the rigid chairs. If these small bin widths (~0.25 J/m as presented in Figure 61: Histogram showing distribution of Straight (Tile) costs for folding and rigid K0005 wheelchairs.Figure 61) were increased to even 0.5 J/m widths, the folding and rigid bins would almost entirely overlap one another and these bin-based trends would disappear.

Equivalence test results (Figure 62) show that the propulsion costs differed between the groups by ±5% of the baseline (mean propulsion cost of the rigid group). Statistically, this implies that the groups did not have equivalent propulsion costs, and the folding frame group had a slightly higher cost on average.

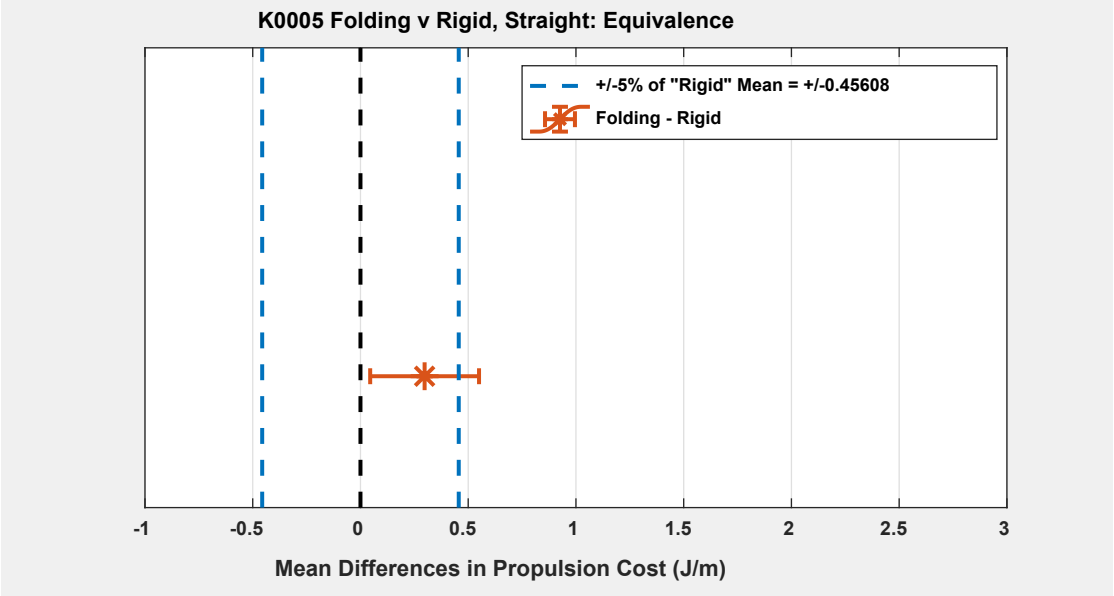

Figure 62: Equivalence test results for propulsion costs of the folding and rigid frame types, Straight maneuver over tile.

6.5.3 Slalom

The Slalom maneuver outcome variables (Table 23) show near-equivalent performances between the rigid and folding frames, on average. Translational distance and maximal kinetic energy differences were reported as significant ($p = 0.066$ and $p = 0.074$, respectively), with rigid frames at a slight advantage. Effect sizes were small to medium for each variable, and the percent changes are very small (< 4.5% difference between folding and rigid).

Table 23: Descriptive statistics of each outcome variable (Slalom Tile maneuver) for the folding and rigid K0005 frame configurations.

		Cost (J/m)		Distance (m)		Yaw (rad)		Max. Kinetic Energy (J)	
Rigid	**R1**	9.98 (±0.18)	9.68 (±0.48)	5.54 (±0.15)	5.68 (±0.38)	2.01 (±0.09)	1.93 (±0.46)	15.93 (±0.78)	16.59 (±1.33)
	R2	9.54 (±0.50)		6.00 (±0.34)		2.44 (±0.09)		17.84 (±1.47)	
	R3	9.51 (±0.53)		5.51 (±0.37)		1.34 (±0.06)		16.00 (±0.52)	
Fold.	**F1**	10.27 (±0.44)	9.80 (±0.66)	4.55 (±0.34)	5.47 (±0.81)	2.03 (±0.14)	1.93 (±0.17)	13.08 (±0.90)	15.89 (±2.69)
	F2	9.47 (±0.65)		6.32 (±0.34)		1.80 (±0.14)		19.04 (±0.98)	
	F3	9.66 (±0.60)		5.53 (±0.43)		1.96 (±0.15)		15.55 (±1.36)	
	Effect Size		0.21		0.34		0.00		0.33
	% Change		1.26%		-3.80%		-0.03%		-4.21%
	p-val		0.245		0.066*		0.992		0.075*
	*Significantly different ($p < 0.100$) from the mean of the Rigid group.								

The interval plots below (Figure 63) show, in general, that the folding chairs have a higher cost and travel shorter distances with less kinetic energy endowed to the system via the motor torques.

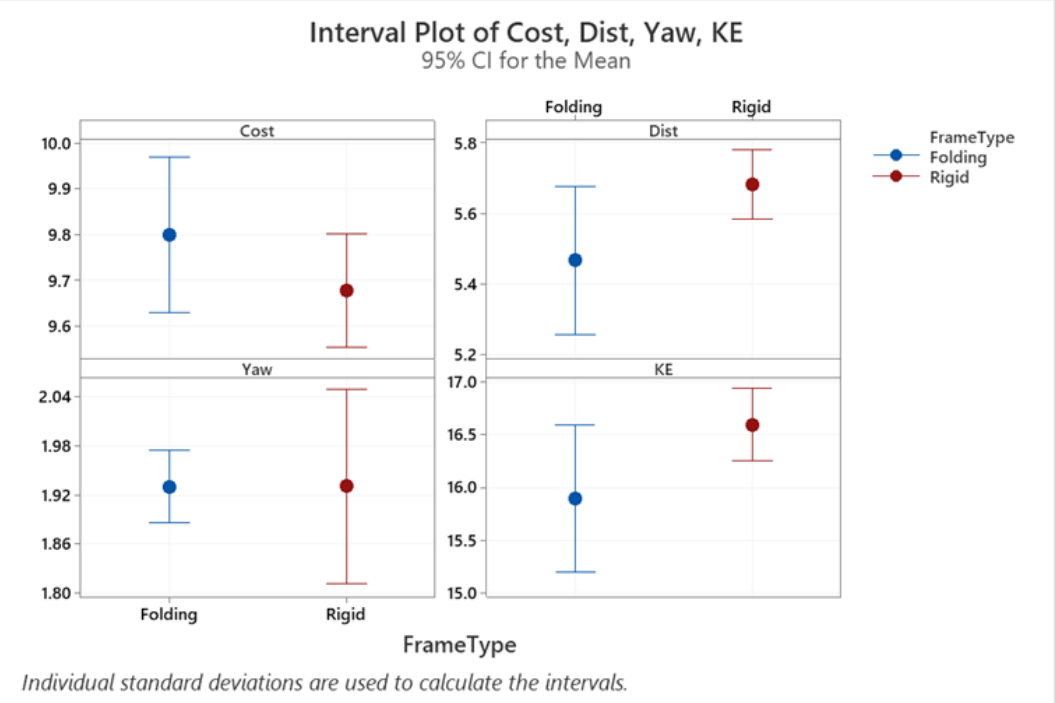

Figure 63: Interval plots of each outcome variable for the Slalom (Tile) maneuver across folding and rigid K0005 wheelchairs.

The histogram plot of the Slalom propulsion cost showcases the bimodal distribution of the data (Figure 64). As in the Straight propulsion cost histogram, there are two distinct groupings that are not tied to a frame type – both folding and rigid frames exhibit propulsion costs between 8.4 and 11.2 J/m, though the folding frame costs tend to lean towards the upper end and the rigid frame costs tend towards the lower end of the cost range. However, much of this apparent trend comes from one outlier – the "F1" (Motion Composites Helios A6 folding frame) cost is 10.27 J/m, versus the 9.47 and 9.66 J/m of the "F2" and "F3" chairs. Without the "F1" data included, the folding chairs would appear to be even more equivalent to the rigid chairs.

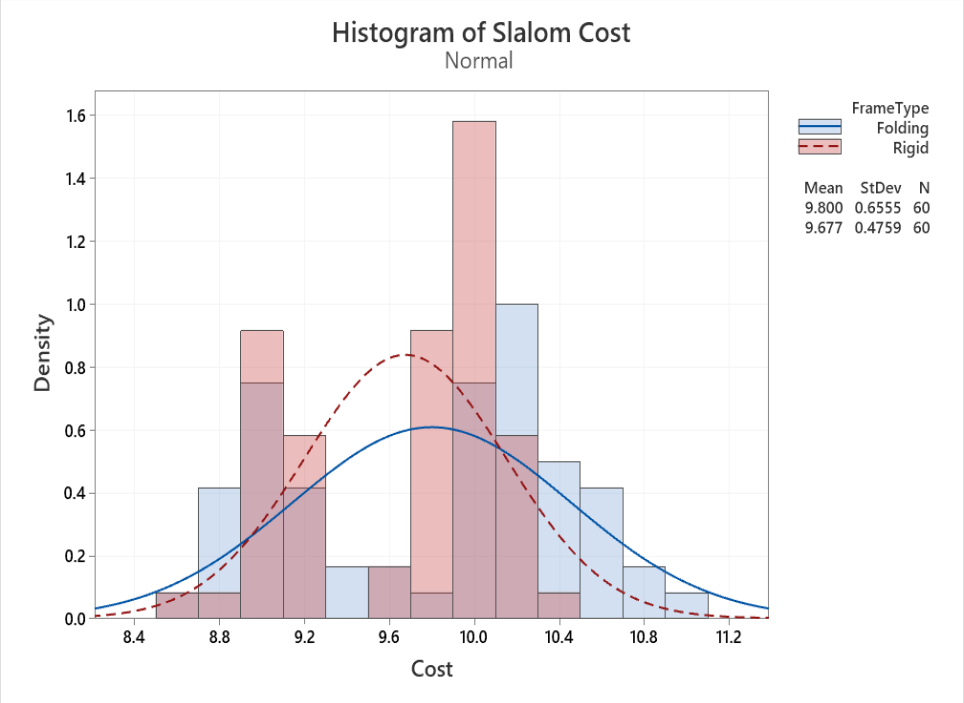

Figure 64: Histogram showing distribution of Slalom (Tile) costs for folding and rigid K0005 wheelchairs.

One-way ANOVA results with the Box-Cox transformed propulsion cost values did not report a significant ($F(1,105) = 2.24$, $p = 0.138$) difference between the groups, and the means of the groups were not reported to differ by the Games-Howell method comparison. In contrast, the non-parametric Kruskal-Wallis test results ($H = 3.11$, $p = 0.078$) report differences between the medians of the grouped propulsion costs.

Finally, equivalence testing was used to determine if the two frames had equivalent propulsion costs in each of the two maneuvers. Figure 65 shows that the folding and rigid frames had propulsion cost differences firmly within the equivalence band (±5% of the mean cost of the rigid group). Therefore, statistically and functionally, the two groups had equivalent performance in the Slalom maneuver.

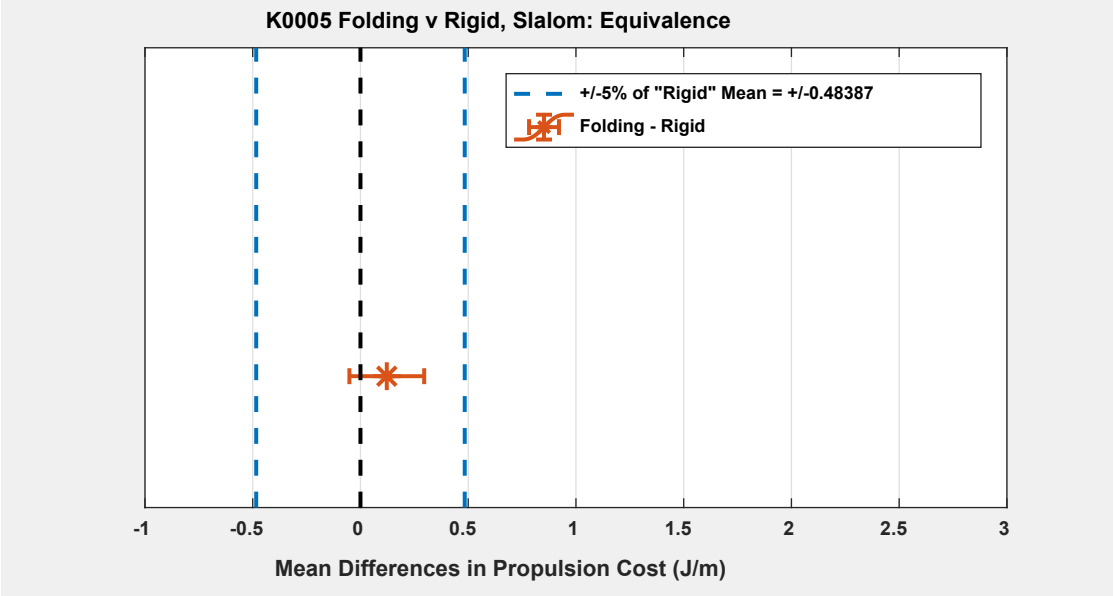

Figure 65: Equivalence test results for propulsion costs of the folding and rigid frame types, Slalom maneuver over tile.

6.6 Discussion

The contemporary HCPCS requirements [26] for the K0005 category are ambiguous and notably devoid of performance-based metrics. Frames weighing under 30 lbs., drive wheel axle adjustability, and lifetime warranty on the side frames and cross-braces are all features that can be offered on frames with poor production quality as easily as they can be offered on state-of-the-art frames, and they will be branded with the same classification. This leads to an important question: How would a new full-time wheelchair user properly select a new K0005 frame, out of all the available options on the market? Without relevant performance-based studies, clinicians are often informed solely by the manufacturers and dealers, who may be biased by their own interests. Wheelchair users themselves are unlikely to have access to numerous wheelchairs for extended-length trials, making the chance of finding the illusive 'perfect fit' near-impossible. Therefore, the

selection process would follow a series of need-based questions, and at the top of the list would be a question about the main dividing characteristic of the K0005 category: the option of folding versus rigid wheelchair frames. If there was a clear divide between the performances of folding and rigid wheelchair frames, that would be useful knowledge to the world of rehabilitation. The truth of the matter – at least, as evidenced by the AMPS testing – is that no such clear divide exists. There are 'better' and 'worse' wheelchairs in both categories, though relatively speaking, the performances are so tightly grouped that they might effectively be equivalent from the perspective of a human user. Furthermore, the results show that both frame types had low propulsion costs, far distances, and high kinetic energies, which are all reflective of the high performance expected of K0005s.

From coast-down testing, the deceleration values showed the folding frames, in general, exhibited 10% more gradual decelerations ($p = 0.076$), which implies that the folding frames lose less energy by passively rolling down the tiled hallway floor. As each chair was configured with the same components with the same inflation values and loading configurations, the only observable differences between the tested chairs were the system masses due to slight variations in frame mass and the frame type. To assess 'performance' of each chair, the propulsion work exerted by the AMPS via torque on the push-rims is compared to the distance traveled by linear translation of the center of mass. These energy-by-distance ratios ranged from 8.69 to 9.79 J/m across each chair in the Straight maneuver, though the combined grouping of folding chairs and rigid chairs had mean costs of 9.42 and 9.12 J/m, respectively. At face-value, the rigid frame group looks to have a small (3.26%) but significant ($p = 0.054$) cost reduction over the folding frame group. The same story appears in the Slalom maneuver cost: 9.80 versus 9.68 J/m for the folding and rigid

groups, respectively, which shows a cost advantage of 1.26% for the rigid frames ($p = 0.245$). Compare these values to the propulsion costs seen in the incremental mass study: 8.89 to 9.43 J/m in Straight and 9.95 to 10.11 J/m for Slalom between the 0 to 4 kg loading configurations. Nominally speaking, these generalized performances over the folding and rigid categories span the same range as adding weights directly to the footrest. Travel distances, angular yaw distances, and attainable kinetic energies show < 5% differences between folding and rigid frames.

Mechanisms to fold the frames add small amounts of mass to the frame, and according to the incremental mass study (Table 8) and component-testing results [71, 81], this additional mass should manifest as additional (albeit slight) rolling resistance at the wheels. However, the slightly heavier folding frames demonstrated better decelerations. This suggests that the flexibility of the frame may actually improve the passive rolling characteristics of the chair, but did not manifest within the actual over-ground propulsion study. The most reasonable explanation for this is that each chair followed a similar path along the tile surface, but reacted differently to minor bumps or imperfections along the track. It is possible that the minor flexibility in the frame afforded by the folding mechanism was advantageous in dissipating the shocks from the small dips and rises in the floor, which could have made the deceleration data between 0.75 to 0.45 m/s appear more gradual. Flexibility of the frame material has been explored through the concept of 'vibration transmissibility', which suggests that the vibrations at the floor-to-wheel interface are passed through the frame to the user and may result in long-term health detriments [137] but there is no clear link between vibration transmissibility and system-level performance.

Gebrosky et al. reported ‘performance’ in the form of results from ANSI/RESNA tests designed to assess longevity and durability of wheelchair frames [139] and showed that folding ultra-lightweight wheelchairs have greater durability and are more cost-effective than rigid ultra-lightweight counterparts. These tests have previously been used to differentiate between ‘survivability’ ratings of standard, lightweight, and ultra-lightweight wheelchairs [138] with clear divisions between the HCPCS K-series codes. With the more recent additions of the folding ultra-lightweight frames, a new division can be seen within the K0005 category alone. Folding frames are shown to survive, on average, more than three times the amount of simulated-use cycles that rigid aluminum and 70XX-alloy aluminum frames could withstand before failure [139]. This alone should be enough to call into question the current rating system.

There is merit to combining simulated-use testing with AMPS-based propulsion testing that would augment the findings from the present study. Folding frames may be able to survive thousands of cycles more than rigid frames, but how does the over-ground propulsion behavior change throughout this process? If rigid and folding frames were both tested with the AMPS in their new out-of-box state and again after 300,000 cycles on a double-drum or carousel-mounted durability test track, would their performances degrade at the same rate? To tie this discussion back to the results from the current study, two of the rigid frames (“R1” = Quickie GT, “R3” = TiLite Aero Z) were obtained several years ago by the REAR Lab and have been used in multiple propulsion studies with the AMPS [50, 66, 69, 71]. For example, the Quickie GT was the single wheelchair frame used in the component-based propulsion cost study [71], meaning it withstood at least 4,320 over-ground propulsion trials in recent years. It performed admirably in the Straight and Slalom

maneuvers in this study but was clearly outperformed by "R2" (Ki Mobility Rogue), a brand-new chair direct from the manufacturer. "R2" had a better cost by 0.20 J/m, a better distance by 0.40 m, and only slightly lower kinetic energy by 0.08 J in the Straight maneuver. In the Slalom maneuver, the cost difference increased to 0.44 J/m, with 0.46 m more distance travelled, 0.43 rads more yaw rotation, and 1.91 J more maximal kinetic energy. It is uncertain from the results on hand if these differences are due to the usage and general aging of the Quickie GT frame, or differences in the material and manufacturing techniques between the chairs.

Finally, each of the selected chairs were advertised with some marketing phrases that heavily implied some performance benefit over their competitors. This study has afforded some values that can validate or disprove their claims. The original Quickie GT advertisement made no claims about performance, but the newest iteration of the GT series (Quickie 5^{R}) says it delivers "…superior rigid wheelchair performance day after day." From the data, the GT was never the most superior rigid frame for cost or distance, but was at least mid-range in every metric. Ki Mobility's Rogue ("R2") claims to have "…the highest level of responsiveness and rigidity that has ever been felt before," which is not necessarily a claim of performance benefit – however, the results from the Slalom trials do show the Rogue with the highest yaw travel and the second-highest maximal kinetic energy. Furthermore, it had the second-highest deceleration value, which would support the concept of frame rigidity hindering passive coast-down behavior if the claim of 'rigidity' is true. The last rigid frame, the TiLite Aero Z ("R3"), was said to have "…unmatched adjustability and performance," which was true for Slalom but hard to prove for Straight, as it had the highest cost by a slight margin. It also had a surprisingly low yaw

travel in Slalom, which suggests that it would not perform as well in a test that prioritized frequent changes in direction.

The folding frames can be scrutinized in a similar format. Motion Composites Helios A6 ("F1") boasts that the cross-brace folding mechanism "…ensures remarkable mobility and ease of propulsion," yet had the highest cost of any chair for the agile Slalom maneuver. To be fair, it also had high average yaw values that would have boosted its apparent performance if the cost metric was normalized by angular displacement instead of linear translation. Sunrise Medical's Quickie Xenon^2 ("F2") was designed to maximize the "…speed and efficiency with every push." This claim is demonstrably true within the confines of this study – it consistently had the lowest cost, highest distance, and greatest maximal kinetic energy for both maneuvers out of the folding chairs, and was the highest or second-highest performing chair for all metrics (except yaw) out of all six tested chairs. Lastly, with the boldest claim out of all tested chairs, the Ki Mobility Catalyst 5 ("F3") is claimed to offer "…the best performing ride in its class." Depending on how you define 'its class', this may not be untrue, but generally speaking, its performance placed it solidly mid-range, and demonstrated the worst coast-down deceleration of any of the tested chairs.

K0005 chairs have many configuration options that make the selection process difficult. Components like drive wheels and casters matter [33, 71, 81, 116, 136]. Weight distributions matter [23, 69, 117]. The tire inflation [33] and frame material [137] have even shown performance differences. When articles are published with results showing differences in standard versus lightweight, or lightweight versus ultra-lightweight categories [31, 129, 131], it is nearly impossible to sift out which variables are responsible. The AMPS-based propulsion testing has demonstrated within-group and between-group

differences regarding folding and rigid ultra-lightweight frames using the same components, weight distributions, general frame geometry, and overall category of frame, but ultimately under the operation of human users, these differences are likely to be negligible. Cost differences would be more evident by switching components than by switching from rigid to folding frames.

6.7 Conclusion

Out of 120 coast-down deceleration trials, folding and rigid wheelchair frames showed a significant ($p = 0.076$) difference in measured deceleration values, with the folding frames generally appearing 10% better than the rigid variants. Under the robotic propulsion of the AMPS, the results from 180 over-ground trials showed an opposing trend: rigid frames appeared to have slightly better propulsion costs (< 4%) and travel distances (< 4%) in the Straight and Slalom maneuvers. Propulsion cost values were equivalent in Slalom but exceeded the ±5% equivalence window in the Straight maneuver. Individual wheelchairs within both groups had disparate performances – despite the average costs and distances showing the folding frames to be at a slight disadvantage, one folding frame consistently had the lowest propulsion cost and highest distance traveled out of all six chairs, and one rigid frame had the worst cost and distance values. Faced with the choice of selecting a folding or a rigid frame, these results suggest that the performance depends more on the quality of each individual frame, and less on the category of frame type.

Furthermore, this work once again highlights the utility of mechanical propulsion testing of manual wheelchairs without the human occupant. The sensitivity of the AMPS and the repeatability of the propulsion profile yield close-knit groupings of propulsion

costs, distances travelled, and kinetic energies endowed to each of the six tested frames. From a clinical viewpoint, there is no great divide separating rigid and folding frame performances, as the cost and distance assessments show the same range of values within both frame type groups. Even so, even at the maximum observed propulsion cost, these ultra-lightweight frames had significantly less cost than the high-strength lightweight chair in any of its configurations by a comfortable 50% margin, which should put the general proximity of the folding and rigid frames into better perspective. The literature reviewed and discussed in this study also raised a new research question that can be uniquely assessed by the AMPS in a future study – How do the propulsion costs of brand-new folding and rigid chairs compare with each other, and how do the propulsion costs of each group change after subjecting each chair to simulated-use durability tests?

CHAPTER 7. CONCLUSIONS

7.1 Generalizable Knowledge

7.1.1 Frame Mass

Mass *can* be important. Newton's Second Law of Motion directly states that an object of greater mass requires more force to achieve an equivalent acceleration as an object of lesser mass. However, wheelchair frames need strength and rigidity to support the occupant and maintain durability across months to years of daily use. Construction of wheelchair frames should *never* sacrifice these factors for the sake of meeting arbitrary weight restrictions and, for the most part, the lighter categories of wheelchairs do not. In fact, durability testing shows that contemporary ultra-lightweight frames have better longevity and survivability in simulated-use environments [138, 139]. As more advancements are made in manufacturing techniques and material development, it is likely that wheelchairs will become even lighter and more efficient due to the nature of scientific progress.

With all that said, the AMPS-based propulsion study reported that frame mass was *not* found to impact the over-ground performance characteristics within the range of human sensitivity. Propulsion costs increased by just over 4% with the addition of 4 kg (8.82 lbs.) of metal disk weights to the drive wheel axle. That 8.8 lbs. range of frame weight spans the entire range of wheelchair categories: the requirement for K0005 frames is < 30 lbs., whereas K0001 frames can be > 36 lbs. without restriction. Adding this mass to the frame of a K0005 chair did not drastically alter the energetic cost of travel. Other outcome

variables (travel distance, angular yaw displacement, and maximum attainable kinetic energy) experienced greater detriments (< 11%) just from the added weights to the axle. Yet, when the same weights were added to the footrest, the weight distribution showed the casters taking a greater percentage of the load, and the same performance detriments nearly doubled in some cases (< 22%) with an increased propulsion cost (< 6% over the unloaded chair). What does this mean for the rest of the rehabilitation engineering field? Studies with human subjects often rely on heavy instrumented push-rims like the SMART^{Wheel}, though a pair of these wheels can add 6 kg of distally-distributed mass to the system over standard drive wheels. The frictional energy losses increase by 40% in straight forward motion and 30% in turning motion [66] with a pair of SMART^{Wheel} wheels over standard pneumatic tires on spoked wheels. From the present incremental mass results, it can be interpreted that these additional energy losses are not all from the mass of the wheels. Mass is, however, certainly a factor that should be considered if the SMART^{Wheel} is being used to assess mass-based differences in configurations [33].

Frame mass can be important in certain scenarios, like manually lifting the chair frame to load it into a vehicle. However, users lift or load their chairs much less frequently than they propel the chair, and the impacts of frame mass are very unlikely to show up in the propulsion performance, even after 1.2 to 1.6 km daily travel [3, 4]. Therefore, perhaps it is time that frame mass is re-examined and given less importance by HCPCS and the K-code assignment policy. Instead, it is advised to categorize chairs by the configuration adjustment options, and/or the component selection available to the user.

7.1.2 Component-Based Improvements

The high-strength lightweight (K0004) category is the first tier of wheelchair that requires the user to self-propel and use the chair for more than two hours a day. The only other type that has these requirements is the more expensive ultra-lightweight K0005 category. Unlike the K0005 class, the manufacturers of high-strength lightweight frames have no obligation to provide additional options for components or configurations, as there are little to no incentives for manufacturers to provide these options for the reimbursement cost. Some frames may have multiple wheel options, or even the drive wheel axle position adjustment capabilities that are only required of K0005 chairs, but this is not the industry standard. In fact, as competitive bidding further drives down the price of K0004 frames, it seems likely that these options will largely disappear. The research question that spurred this study into existence was a simple premise: How far can we improve a representative K0004 chair for less than $100?

This study used existing knowledge from simplistic coast-down and scrub torque tests on drive wheels and casters [81]. The selected K0004 frame came equipped with 8”x1” casters and 24”x1” solid polyurethane tires on plastic composite wheels. To remain consistent to the low-maintenance non-pneumatic components, two ‘up-charged’ variants were purchased: Primo 6”x1.5” solid casters and Primo XPress 24”x1-3/8” non-pneumatic tires on metal spoked wheels. The casters and tires collectively cost less than $100 from several online retail stores. The metal spoked wheels were re-used from previous wheelchairs but could have been placed on the original plastic composite wheels. Coast-down decelerations improved by 30% with the up-charged casters, 20% with the drive wheels, and 50% with both equipped when tested on tile. In the AMPS-based propulsion

trials, propulsion cost was reduced by up to 41% with both up-charged components. Travel over tile had the most pronounced effects. Carpeted flooring introduced systematic inefficiency in all configurations and maneuvers. Consequently, the propulsion cost improvements were subtler (< 15%) with the up-charged components. Distances, yaws, and kinetic energies were all greatly improved (22% to 580%) by the simple change of components.

The main takeaway message from this study is that the ability to drastically improve a chair may be 'locked' behind a few simple changes. A caster is normally held on by a single bolt, and drive wheels normally attach with a quick-release axle. The main barrier to the astounding performance changes is the cost of purchasing the components. In a perfect world, the cost of supplying these better wheels would be shouldered by the manufacturer as demanded by the 'informed clinician', and would not fall upon the wheelchair user. Alas, K0004 wheelchairs are not bad by design. Instead, they are bad by disinterest, competitive bidding, and a general lack of understanding about what makes a 'good' and 'bad' wheelchair. Better drive wheels and casters can make a world of difference. Weight distribution adjustments can dramatically alter performance. Not having access to this knowledge is detrimental to the well-being of wheelchair users. Not demanding *more* from manufacturers is even worse. If this study can impact anything, it should be to point the finger of blame at manufacturers for not striving to make the best product for their consumers, and to motivate them to search for better options for their wheelchairs.

7.1.3 Frame Type

Selecting a new wheelchair configuration is difficult, especially at the K0005 level. The order forms require specific measurements of the intended user to provide the best possible 'fit' and many choices are intended to be made by trained clinicians. First and foremost, selecting the frame style is one of the most prominent design choices that can be made. Folding the wheelchair reduces the overall footprint of the chair in a storage location and can make the frame easier to transport. However, there are no known literature that discuss the over-ground performance trade-offs between folding and rigid chairs. The only 'performance' metric that directly compare the frame types is the durability under simulated-use testing conditions [138, 139] in which recent folding chairs demonstrate excellent performances. However, for curb-descent (a common task for an active full-time manual wheelchair user), the folding chair frames transmit more of the shock through the frame [141] to the detriment of the user health. These trade-offs are presented but are not witnessed in everyday travel. The AMPS-based propulsion testing was used to rate performances of a representative swath of chairs with each frame type to quantify the general propulsion quality of each frame type.

Coast-down testing highlighted the folding chairs as advantageous from a passive 'energy loss' standpoint, contrary to the hypothesis that folding frame flexibility would introduce more energy loss to the system. Propulsion cost showed a general favorability to the rigid frames with a slight < 4% better distance per Joule of energy supplied to the wheels. Between frame types, ±5% equivalence could not be established universally for propulsion cost. Anecdotally, a greater difference would be seen if the tire pressures were reduced by 10%, or if the frame height adjustment points were improperly aligned.

Demonstrably, even just adding 4 kg to the drive wheel axle had a greater impact, despite being too insignificant to be detected by any human operator [33, 34]. A closer look at the means of cost, distance, yaw, and kinetic energy show that the differences between frames of the same type easily exceed the differences between the grouped means – for example, the third rigid frame had the worst performance in slalom out of any of the chairs, and the second folding chair was consistently high-performing in every metric. The disparities between chairs do not discredit the close grouping of the means. Propulsion cost differences were often below 1 J/m, distances were all within 1.5 m, and kinetic energies stayed within 6 J, yet both categories spanned the same ranges. In fact, the story may become more interesting with more details to dig into – does the performance vary by manufacturer, or by frame material, or even by the structure of the frame members?

From the current results on hand, the most impactful takeaway message is that folding-versus-rigid, at the K0005 level, does not seem to correspond to a discrete change in over-ground performance. A closer look should be taken regarding performance over time for rigid and folding frames. Simulated-use environments have demonstrated the durability of contemporary folding and rigid K0005 frames to ANSI/RESNA standards [139]. The propulsion cost and over-ground metrics presented in this study compared three brand-new folding frames to two used rigid frames that were in good condition with visible signs of age. No significant differences could be seen between the used and new rigid frames, and the cited durability study implies that no differences would be expected from folding frames pre- and post-simulated-use. Yet, the world of rehabilitation engineering and wheelchair mechanics involves so many variables already – definitively establishing

equivalence between folding types would go a long way towards clearing up the convoluted 'science' of wheelchair prescription.

7.1.4 Performance of the AMPS

The AMPS was augmented from velocity-control to torque-based motion control with intermittent propulsion and free-wheeled coasting. The software and hardware modifications to the AMPS subsystems were modular to allow for future tuning and tinkering with the configuration. Custom control schemes were derived from essential electromechanical equations for current-based torque control of the brushed DC motors using pulse-width modulation of the armature voltage. Diagrams and simulations were developed to rationalize trade-offs between controllers. The finalized controller script (APPENDIX A) was translated into the motor controller software and torque outputs were assessed with an external force gauge. Clutch integration on the motor shaft afforded a simple decoupling mechanism between the AMPS and the wheelchair push-rims to mimic the 'recovery' phase of human wheelchair propulsion. To overcome the one-way directionality of the clutches, the Slalom maneuver was produced as a means to assess curvilinear motion. Both Straight and Slalom trajectories were performed on a wide range of wheelchairs and two distinct surfaces (tile, carpet).

Three studies were conducted with this current-based motor torque controller and the intermittent propulsion technique. Standardized wheelchair parameters (height, frame angles), occupant parameters (mass, weight distribution), and component selection (drive wheels, casters) were controlled across each study to isolate variables of interest. The AMPS captured differences in propulsion cost, distance, angular yaw displacement, and

attainable kinetic energy between each level of the control variables (frame mass, component changes, frame type). The measured outcome variables stayed beneath 10% coefficient of variation within data sets for nearly all cases. Kinetic energies tended to vary by the largest margin due to the slight differences in speeds across trials. The torques applied to each wheel – the vital output of the current-based motor torque controller in the first specific aim – were applied in a repeatable and reliable manner. As seen in Figure 66, the commanded torque profile was followed very closely and deviations typically remained under 1 Nm. The largest deviations occurred at points of rapid change, such as when the controller commanded the motors to reduce the applied torques on the tail-end of a push.

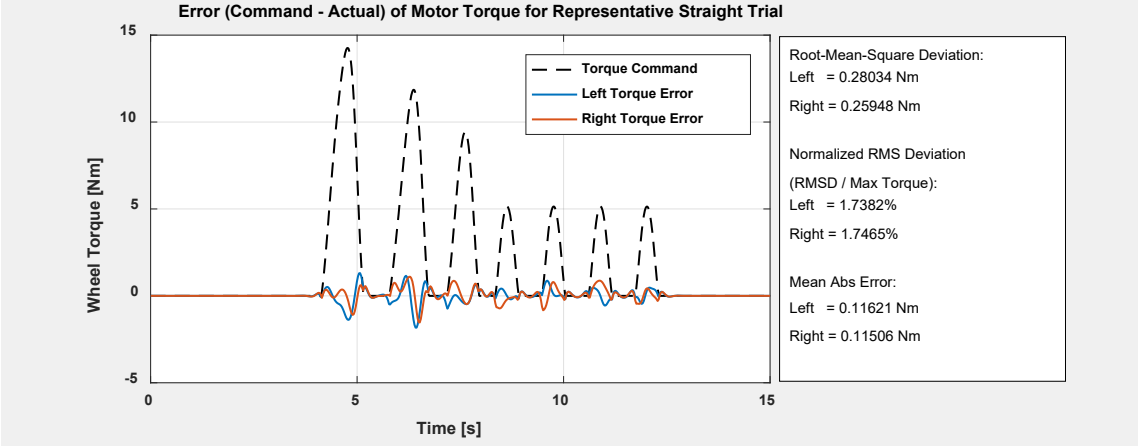

Figure 66. Deviations between commanded torque output and actual torque output of each motor for the Straight (K0005, Tile) maneuver.

From a mechanical standpoint, the three studies (incremental frame mass, casters and drive wheels, and frame type) have collectively proven the validity and sensitivity of the measurements of energetic input and kinematic output of a manual wheelchair via the AMPS in the new torque-based propulsion mode. The controller maintained the desired torques within a mean absolute error of 0.2 Nm and with < 3% root-mean-square error

throughout the duration of each over-ground trial. The data acquisition system demonstrated sensitivity across all control variables. The value of the system, as it is used as a modular manual wheelchair testbed, it that it can clearly discern differences between 3 non-disparate variables (mass, components, frame type). This is a stark improvement over utilizing human users and having to account for variance between trials, days, or geometric configurations. The AMPS is a complex but definitive wheelchair tester that is impartial to the wheelchair or test environment. Repeatability and reliability of the measurements should always be the utmost concern in mechanical assessment of equipment, including durable medical equipment. Actual wheelchair user input is important to the testing and design of wheelchair frames, but should not be the primary assessment tool – objective mechanical testing should take priority, using a suitable mechanical tester like the AMPS. Repeatable and reliable test results can then be supported or supplemented with results from human studies.

Correlations between the outcome variables from the incremental frame mass study were assessed by calculating Pearson correlation coefficients. From 100 over-ground Straight maneuver trials, the coefficients were: -0.818 for propulsion cost and distance; -0.873 for propulsion cost and kinetic energy; 0.969 for distance and kinetic energy. These high coefficients imply that these variables are very likely to show repeated trends, especially in the case of distance and kinetic energy – if a tested configuration traveled very far, the kinetic energy was likely to be very high, and vice-versa. Angular (yaw) displacement was less correlated to the other outcome variables. Correlation coefficients fell in the range of 0.5 to 0.7, indicating that weak to moderate correlations exist between all of the variables.

7.2 Limitations

There are several limitations to the current AMPS. First, the torque profiles for each maneuver could not be used across all tested configurations. Straight and Slalom had to be modified from the initial torque values used in the incremental frame mass study to the increased torques in the K0004 study. Therefore, the outcome variables of propulsion cost, distance, yaw, and kinetic energy cannot be directly compared between the two studies. Special adjustments had to be made to accommodate for the higher losses on carpeted surfaces, as well. Secondly, the established torque profiles did not always propel the wheelchairs over a repeatable path. There was a strong tendency for the chairs to veer off-course (Figure 67) instead of following the intended straight forward path under the Straight maneuver torque profile, and the Slalom path depended greatly on the surface near the start of the maneuver. Veering was determined not to be a systematic issue, though, because different chairs veered towards different directions, implying that other factors may have caused the chair to have greater resistance on one side. The established current-based motor torque control scheme was unable to account for this over-ground behavior. Outputs from the NI USB-6341 could be tuned within the LabVIEW interface to increase the torque of one motor and decrease the other proportionally, but the chair would still veer during the final coast-down phase of each maneuver. Path deviation for the Straight maneuver in Figure 67 appears to stay closely adhered to a straight-forward path, but a deviation of one full meter basically represents moving from the center of the hallway to the right-hand side of the hallway, accounting for the width of the wheelchair and the extended width of the motor. Trials were aborted and re-tested if the motors were at risk of scraping along any wall or doorway.

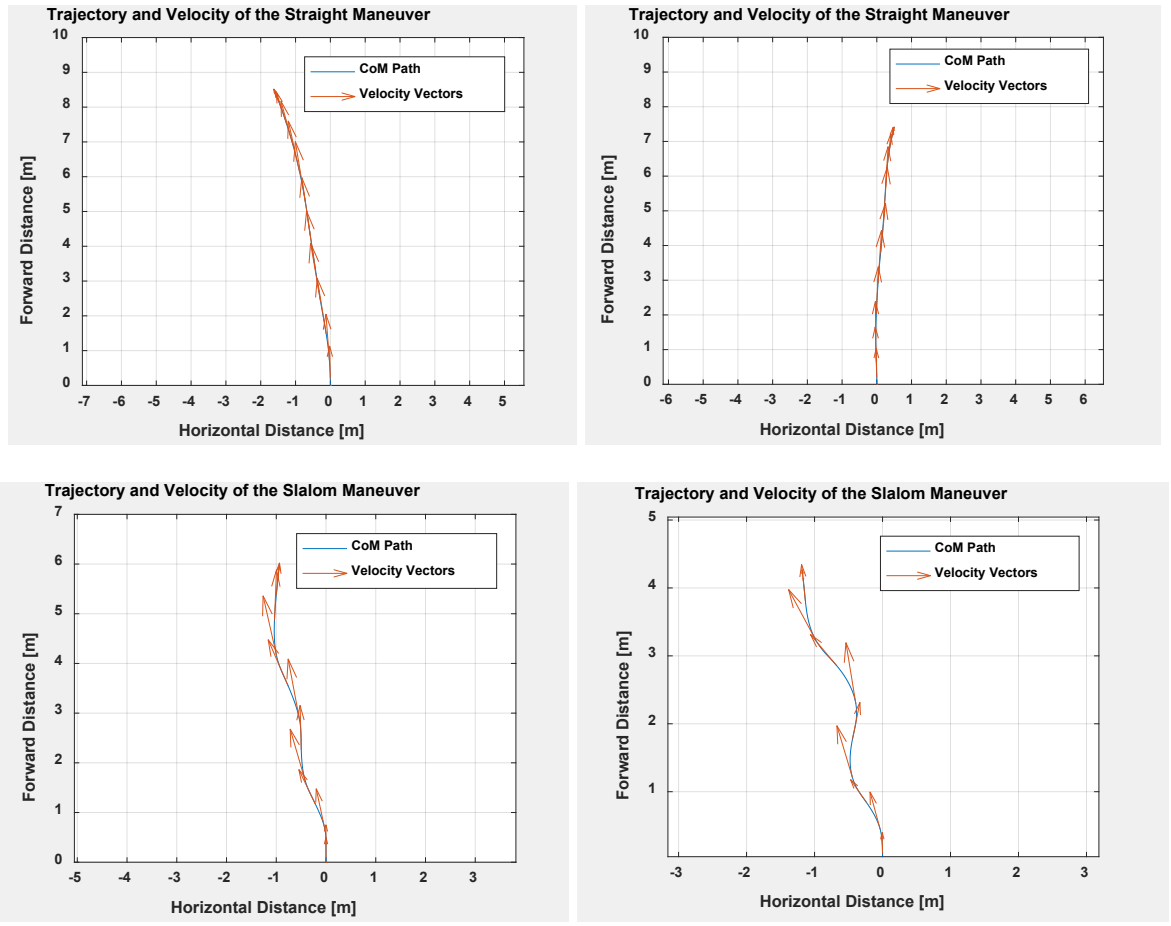

Figure 67. Over-ground trajectories of the Straight and Slalom maneuvers from two different chairs.

7.3 Future Directions

The 'next steps' for the AMPS project will span multiple 'big picture' concepts, to the benefit of the general rehabilitation engineering community. These steps will address further questions that have been raised by the presented studies, or other ideas that were spawned from the current work. There are multiple projects that have been proposed and discussed in detail within the REAR Lab:

(1) Upgrade the AMPS with intermittent velocity-based control

(2) Improve the capacity to represent real-world use

a. Including potential energy in the test maneuvers

b. Simulated-use testing to explore wear-related differences

c. Adding more real-world use surfaces to the maneuvers

(3) Vibration-based assessment of MWC frames

(4) Investigating other K-series differences, like K0003 versus K0004

The most logical solution to the limitations presented above is to integrate the intermittent propulsion system with the previous velocity-based motor control scheme. Feedback from high-resolution optical encoders mounted on each motor shaft would permit close monitoring of the motor speeds, which can be used to control the wheel speeds and overall system velocity. Veering is a solvable issue within the construct of velocity-based motor control, even with the clutches installed. Unlike torque mode, where the tuning may cause disproportionate torque applications to the wheel and lower the overall speed of the system, the same tuning in velocity mode would leave the speed of the center of mass unaffected and only tackle the directionality of the system. Furthermore, velocity mode would draw as much current as needed to reach a given speed. Torques may not be absolutely identical between pushes in the acceleration or steady-state phases. However, this means that the same exact Straight and Slalom maneuvers could be used across tile and carpet for both K0004 and K0005 wheelchairs. The propulsion cost assessment will consequently become easier – in torque mode, both the numerator (propulsion work supplied to the chair) and the denominator (distance traveled by the center of mass) change based on the configuration, because more efficient chairs require less torque to reach the same or greater speeds, and thereby cover greater distances. Lower torques would normally imply lower propulsive work, but in this case tend to get cancelled out by the proportionally greater

speeds. This should explain, in part, why the differences in propulsion costs within the three studies were so proportionally small compared to the distance, yaw, or kinetic energy differences. With velocity mode, the distance each chair travels will be relatively constrained, so only the numerator is expected to change. Propulsive work will be lower for more efficient chairs because they require less torque to reach the same system velocity. Velocity mode, therefore, should show even greater differences in propulsion cost between configurations than the torque mode.

The implementation of this 'Hybrid Intermittent Velocity Mode' would be fairly straightforward: (1) remove Hall Effect-based current sensors from the feedback channels of the HDC-2460 motor controller; (2) re-install optical motor encoders to the feedback channels; (3) replace existing 'Command Output' calculation in the LabVIEW interface with the legacy 'Drive Wheel Velocity' calculation, which uses the drive wheel radius to determine the desired motor RPM; (4) generate new velocity trajectories based on literature from human wheelchair propulsion, much like what was done to determine the torque profiles.

It seems logical that the human wheelchair user acts as both a torque- and velocity-controller for the manual wheelchair. As seen in reports by Cowan [55] and de Groot [25, 32, 33] with instrumented push-rims, the torque profiles for each push tend to look relatively identical between sides or within a particular phase of motion, but there are nuances that may not be detected by their instrumentation. The user may push at a slightly faster frequency (push per second) to maintain speed over rougher terrain, or make marginal adjustments between the left and right wheels to steer the wheelchair along a desired path. These changes happen during the trial and are difficult, if not impossible, to

quantify with contemporary instrumentation. Furthermore, even if they were picked up by the instrumented push-rims, it would be difficult to generalize the human response, as different users may react with a wide range of adjustments to their propulsion cycle. The human user learns these techniques through experience and can enact changes to the push rate, push time, push time-to-peak, peak torque, and coast (or recovery) time, all without much fore-thought. In fact, it is possible that the user may not even fully realize that they are making these on-the-fly changes. Over 500 AMPS trials in torque mode have shown that the AMPS is not yet advanced enough to autonomously enact these types of ad hoc changes to pre-generated trajectories. The torque mode accomplished the task of controlling torque, and much insight was gained about the wheelchairs that were tested. The hardware changes that enabled intermittent propulsion will be more long-standing and will carry into the foreseeable future iterations of the AMPS design.

AMPS-based mechanical performance testing has been proven capable of answering the question: “What differences, if any exist, are there between components and configurations of manual wheelchairs?” The more important questions, arguably, are the ones that are raised by wheelchair users and clinicians: “Do these differences matter within their context of use? Can we use these differences to establish trade-offs between configuration options?” The three presented studies aimed to address all of these questions in a useful manner for manufacturers, users, and clinicians, but there remains a near-endless amount of possibilities for the future directions of the project.

The first avenue of investigations will explore things that had insignificant or marginal impacts on mechanical performance in the three included studies, and determine where they begin to matter. For example, the incremental frame mass study did not show

much of a difference in propulsion cost out of the five tested configurations over flat tile, but a much greater difference is expected to be seen when traversing ramps (e.g. ADA-compliant slopes of up to 4.8°), where the incline would elicit potential energy changes and mass would take a more important role. Another example is expanding the folding-versus-rigid comparison to include pre- and post-simulated-use propulsion cost data, which would provide insight on the durability, robustness, and general quality characteristics of the two frame types. The simulated-use environment would be provided by Invacare Corp. in the form of a carousel-style test rig (Figure 68). Once attached to the test arm, the wheelchair would be loaded with an ISO-style weighted test dummy and driven along the obstacle-laden floor. This test would be punishing to the wheels and frame whilst simultaneously applying realistic side-loading to the axles and bearings from traversing the circular path.

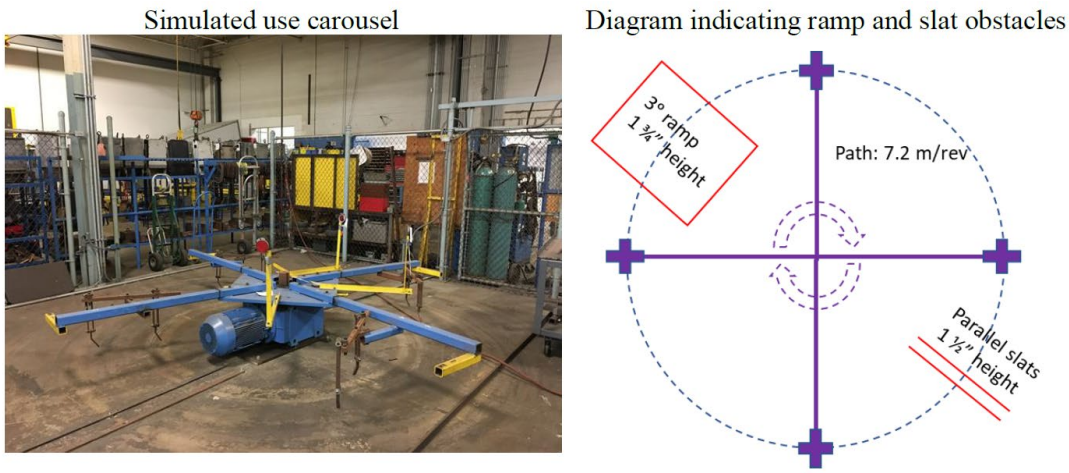

Figure 68. 'Carousel' apparatus for simulated-use testing of manual wheelchairs, as used by Invacare Corporation.

The second avenue of projects is to use the AMPS to address bigger-picture items, such as the growing divide between 'good' and 'bad' chairs (loosely defined and currently

very subjective, but the current work suggests this to be strongly related to the configuration options provided for each chair) within the most common extended-term wheelchair types, K0003 and K0004 (see Table 11). The AMPS is not exclusively tied to the higher tiers of wheelchair. In fact, because the vast majority of wheelchair users are given K0001-K0003 chairs, and though these categories do not have any self-propulsion requirements, it is necessary to ensure that the users are being given equipment that supports proper rehabilitation. Manual wheelchairs are predominately intended to provide independent mobility. Poorly-designed chairs that cannot meet this loose definition should not be marketable as durable medical equipment. AMPS-based testing could be useful to characterize the base propulsion cost of several default options from these categories. Trends should be identifiable that make the 'good' stand out from the 'bad', whether the factors are the components, frame material, or frame style. The goal of this type of testing is to 'raise the floor' of these categories by simultaneously pointing out factors that can boost performance of the chairs, and encouraging clinicians and manufacturers to design or configure new chairs with this newfound knowledge in mind. These steps will improve mechanical performance of the chairs that the vast majority of wheelchair users are supplied with, and would go a long way towards reducing the shoulder pain and immobilizing damage that comes with overuse.

Vibration transmissibility is an emerging focus of wheelchair-related research. Vibrations incurred at the interface between the tires and floor are transmitted through the components, through the frame, and up through the cushion into the user [137, 142, 143]. These vibrations can accumulate and pose as health risks to long-term or high-intensity wheelchair users [144, 145]. In ultra-lightweight frames, which do not always have the

mass leniency to add in sacrificial or viscoelastic damping components, vibration transmissibility may be an uphill struggle. The Ethos frame by Ki Mobility is a notable exception. Beyond the wheelchair frame itself, vibration-damping components have come on the market, but as components have been identified as the main sources of energy loss in the wheelchair system [83], it remains to be seen if the energy-absorbing (or energy-dissipating) features of these components would be of any net benefit to wheelchair users, especially to those that do not frequently drop off curbs or perform other drastic vibration-inducing actions.

The last major vein of investigation will introduce more surfaces to the testing protocol. Up to the contemporary studies, the only two surfaces that have been used in AMPS trials are linoleum tile and high-traffic carpet, which were selected due to being common interior flooring options. Active wheelchair users traverse across many different surfaces outside of the office or home as well. Sidewalk, pavement, and even the ADA-compliant tactile surfaces seen at curb-cuts on busy intersections would be included for over-ground propulsion testing to expand the library of mechanical performance outdoors. Any of the aforementioned studies would be applicable for these new surfaces, though particular interest is on the performance of energy-absorbing components across relatively bumpy, inconsistent surfaces.

Prior to any of these further studies, the Hybrid Intermittent Velocity Mode will be developed and implemented on the AMPS. This will provide a more suitable testing technique for comparisons between chair types. The specific methods used to measure propulsion variables (torque, velocity, power, work, and cost) will be deployed within each assessment. New velocity-based canonical maneuvers will replicate the intermittent propulsion

outlined by the torque-controlled propulsion mode, and will subject each tested wheelchair system to similar types of momentum changes and energy losses – one straight maneuver and one (or more) curvilinear maneuver, depending on how much caster swivel can be elicited from velocity-based slalom. The various test environments (tile, carpet, outdoor surfaces, inclines) would be presented separately in the results of each study to identify the behavior of each configuration in different contexts of use. Propulsion cost would serve as the main outcome variable for each assessment and will be used as the representation of system performance.

APPENDIX A. CUSTOM MICROBASIC TORQUE CONTROLLER SCRIPT

This script was written in RoboteQ-proprietary MicroBasic coding language. The Basic-like syntax is direct and literal, which has strong similarities to common written English for ease of communication. The language is limited with the data types it can process and the functions it can run on the data. Only signed 32-bit integers and binary true/false Boolean variables may be used in any script.

```
' Implementing Torque-Based Motor Controller Architecture
' Created by S.B.Ghorbel and J.Misch
' mischjp@gatech.edu
' October 15 2019
' Version 1.5
'
'''''''
```

```
45 Dim lURef as Integer                    ' Required armature voltage to achieve target current
46 Dim lUStar as Integer                   ' UStar required armature voltage, after PI gains
47 Dim lU as Integer                       ' U is the output voltage after saturation (-100, +100% output)
48 Dim lDutyCycle as Integer               ' Duty cycle is the % PWM output needed for U
49 Dim lOmega as Integer                   ' Omega is the encoder value to determine motor speed
50
51 ' Variable Declarations - RIGHT Motor
52 Dim rIRef as Integer
53 Dim rIRefOld as Integer
54 Dim rIMeas as Integer
55 Dim rSigma as Integer
56 Dim rSigmaOld as Integer
57 Dim rURef as Integer
58 Dim rUStar as Integer
59 Dim rU as Integer
60 Dim rDutyCycle as Integer
61 Dim rOmega as Integer
62
63 ' Control Parameters
64 Dim Kp as Integer                       ' Proportional Gain, Kp = 1
65 Dim Ki as Integer                       ' Integral Gain, Ki = 5
66 Dim A as Integer                       ' From transfer function, A = -33.7 (1/s)
67 Dim B as Integer                       ' From transfer function, B = -526.3 (A/V/s)
68 Dim lK as Integer                      ' From inverse of torque constant, K = 0.0041511 (V/RPM)
69 Dim lL as Integer                      ' Measured inductance, L = 0.111 (mH)
70 Dim lR as Integer                      ' Armature resistance, R = 0.43 (Ohms)
71 Dim rK as Integer                      ' K = 0.00423518 (V/RPM)
72 Dim rL as Integer                      ' L = 0.087 (mH)
73 Dim rR as Integer                      ' R = 0.566 (Ohms)
74
75 ' Control Constants
76 A = -33700                            ' in 1/ms
77 B = -526300                           ' in mA/mV/ms
78 Kp = 1
79 Ki = 5
80 lK = 4151                             ' in microVolt/RPM
81 lL = 111                              ' in microH
82 lR = 430                              ' in mOhms
83 rK = 4235                             ' in microVolt/RPM
84 rL = 87                               ' in microH
85 rR = 566                              ' in mOhms
86
87 ' Wiring Parameters
88 Dim lMotor as Integer                  ' Left Motor is on Channel 1
89 Dim rMotor as Integer                  ' Right Motor is on Channel 2
90 'Dim lSensor as Integer
91 'Dim rSensor as Integer
92 Dim lEncoder as Integer
93 Dim lEncoderA as Integer
94 Dim lEncoderB as Integer
95 Dim rEncoderA as Integer
96 Dim rEncoderB as Integer
97 Dim rEncoder as Integer
98
99 ' Reference Input Pins from DAQ
100 Dim lIDAQ as Integer                   ' Target current value for LEFT from DAQ
101 Dim rIDAQ as Integer                   ' Target current value for RIGHT from DAQ
102 Dim jj as Integer                      ' Loop number
103
104 lMotor = 1                            ' Left Motor on Motor Channel 1
105 'lSensor = 2                          ' Wiring: Left Current Sensor is AIn2 (Pin 16 in RoboteQ cable)
106 lEncoder = 1                          ' Define encoder directly by motor number
107 lEncoderA = 12                        ' Two pins - Encoder A is on RoboTeq cable pin 12
108 lEncoderB = 24                        ' Encoder B is on RoboTeq cable pin 24
109
110 rMotor = 2
111 'rSensor = 1                          ' Wiring: Right Current Sensor is AIn1, (Pin 15 in RoboteQ cable)
112 rEncoder = 2
113 rEncoderA = 11
114 rEncoderB = 23
```

```
115
116 ' Reference Input Channels from DAQ - Target Current Signals
117 lIDAQ = 3                                   ' Pin 4 in RoboteQ cable (ANA3) (Pin 15 on the LabDAQ)
118 rIDAQ = 4                                   ' Pin 17 in RoboteQ cable (ANA4) (Pin 31 on the LabDAQ)
119
120 ' Define offsets such that the system initializes every time it starts.
121 ' This makes sure the inputs do not have a steady-state offset,
122 ' unlike the original plan to hard-wire in an offset to subtract
123 Dim lSensorOffset as Integer
124 Dim rSensorOffset as Integer
125 Dim lIDAQOffset as Integer
126 Dim rIDAQOffset as Integer
127
128 ' Make moving average of several data points to smooth current sensor signal
129 Dim lCurrentOld as Integer
130 Dim rCurrentOld as Integer
131 Dim lMovingAverage as Integer
132 Dim rMovingAverage as Integer
133
134 ' Ensure motors are stopped upon startup of the script
135 Setcommand(_GO, lMotor, 0)                  ' Sends command to motor channel 1, stopped
136 Setcommand(_GO, rMotor, 0)                  ' Sends command to motor channel 2, stopped
137
138 ' Keep armature current in Safe range
139 setconfig(_ALIM,lMotor,200)                 ' Set current limit to 20A (Default: 50A)
140 setconfig(_ALIM,rMotor,200)                 ' Set current limit to 20A (Default: 50A)
141
142 ' Define safe voltage range for input batteries
143 setconfig(_OVL,0,400)                       ' Set overvoltage limit to 40V
144 setconfig(_UVL,0,50)                        ' Set undervoltage limit to 5V
145
146 ' Define controller parameters
147 setconfig(_CLERD,lMotor,2)                  ' Closed Loop Error Detection Set to medium
148 setconfig(_CLERD,rMotor,2)                  ' Closed Loop Error Detection Set to medium
149 setconfig(_PWMF,0,240)                      ' Set PWM Frequency to 24.0 KHz
150
151 ' Define max speed of each motor, in percentage
152 setconfig(_MXRPM,lMotor,100)                ' Set rpm at 24v to be 6000 (View Motor SpecSheet)
153 setconfig(_MXRPM,rMotor,100)                ' Set rpm at 24v to be 6000 (View Motor SpecSheet)
154
155 ' Define dead-band
156 setconfig(_AMOD,0,1)                        ' Set all analog inputs to absolute
157 setconfig(_ADB,0,1)                         ' Set Dead-band for all analog inputs to 1%
158
159 ' Initialize the encoders to start at position of 0
160 setconfig(_EPPR,lEncoder,2500)              ' Set encoder PPR value
161 setconfig(_EPPR,rEncoder,2500)              ' Set encoder PPR value
162 setcommand(_C, lEncoder,0)                  ' Initialize encoder counter
163 setcommand(_C, rEncoder,0)                  ' Initialize encoder counter
164
165
166 ''''''
```

```
185         wait(50)
186
187 ' Loop back up to the top of the Security loop, unless both command voltages are 'safe'
188 goto Security
189
190
191 '''''''
```

```
254     'print(" rOM: ", rOmega,"\n")
255
256     ' Get reference values from DAQ for Current on each motor
257     lIRefOld = lIRef
258     lIRef = iMax*(GetValue(_ANAIN, lIDAQ)-lIDAQOffset)/2500 ' in mA (50A corresponds to 5000 from getValue)
259     rIRefOld = rIRef
260     rIRef = iMax*(GetValue(_ANAIN, rIDAQ)-rIDAQOffset)/2500 ' in mA (50A corresponds to 5000 from getValue)
261
262     ' Calculate the voltage output needed by each motor to get the correct armature current
263     lURef = (lL*(lIRef - lIRefOld)/T + lR*lIRef )/1000 + lOmega*lK/1000          ' in mV
264     rURef = (rL*(rIRef - rIRefOld)/T + rR*rIRef )/1000 + rOmega*rK/1000          ' in mV
265
266     ' These legacy lines of code were used to take in another set of analog inputs from the LabDAQ
267     ' but the LabDAQ only has one set of analog output pins, and current command takes priority
268      'lURef = uMax*(GetValue(_ANAIN, lUDAQ)-2530)/2500 + lOmega*lK/1000  ' in mV (24V = 5000 from getValue)
269      'rURef = uMax*(GetValue(_ANAIN, rUDAQ)-2530)/2500 + rOmega*rK/1000 ' in mV (24V = 5000 from getValue)
270
271     '''''''
```

APPENDIX B. METHODS TO PARSE OVER-GROUND PROPULSION DATA

This appendix was included to demonstrate a selection of data processing techniques. The main propulsion cost metric used in the three study-based specific aims is included in this selection. In the following example calculations, the most generic straight-forward maneuver was used (seen in Figure 38) with 13 total pushes: 3 'acceleration phase' pushes that propel the chair from rest to the steady-state velocity, then 10 identical 'steady-state phase' pushes to maintain velocity and travel over a long stretch of the chosen test surface.

1. **Basic 'Work In' Calculation**

- Equation:
  - $Work_{total} = \int_{t_i}^{t_f} (Power_{total})\ dt = \int_{t_i}^{t_f} \left((\tau_L \omega_L) + (\tau_R \omega_R) \right) dt$
- Requires:
  - Wheel torque τ (Nm)
  - Angular velocity ω (rad/s)

The generic Straight maneuver features a torque profile with 13 pushes. 5 trials were run with the AMPS loaded on an ultra-lightweight frame and propelling down the linoleum tiled hallway, and averaged together. The Hall Effect-based current sensors captured the motor amperage, which was converted to motor torques and multiplied by the torque ratios between the motor pinion and the push-rim to get the following torque plot:

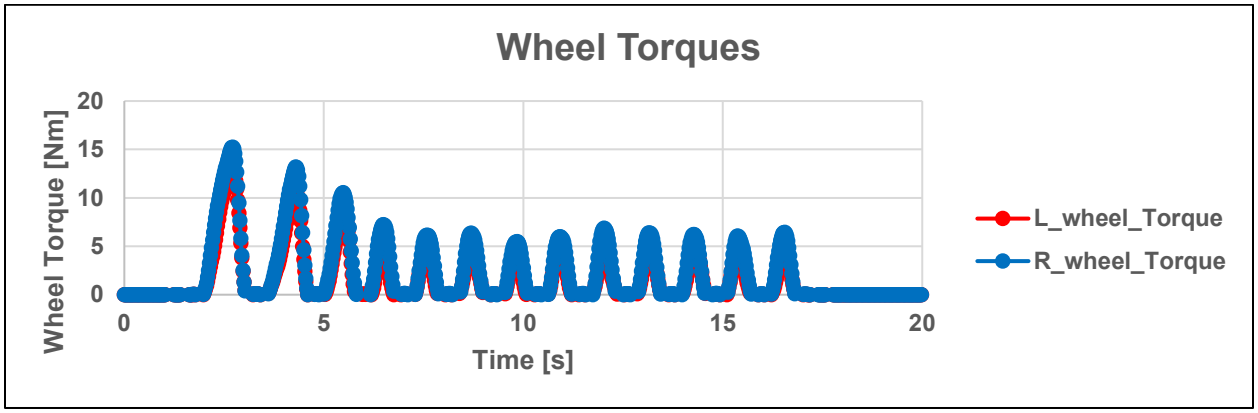

Under this torque application, the wheelchair accelerated and reached an arbitrary 'steady-state,' of sorts – despite the consistent acceleration from 7 sec to 16 sec, this period of time only featured the identical low-intensity pushes that were defined as the 'steady-state phase.' The wheel velocities are fairly equivalent between sides. The slight discrepancies can be attributed to inconsistencies in the floor including bumps, dips, and side-slopes:

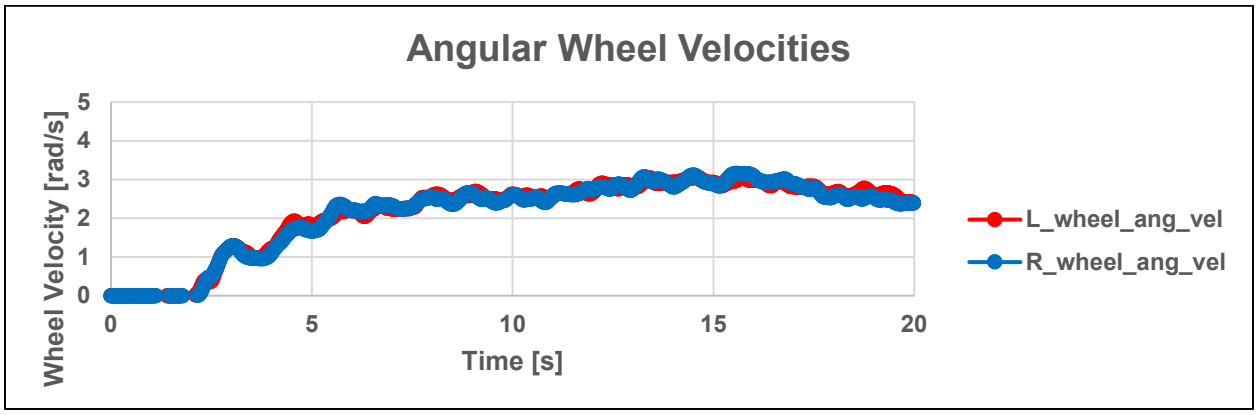

Multiplying the wheel torques and the wheel velocities together (element-by-element) results in the input power vectors, plotted below, for each motor:

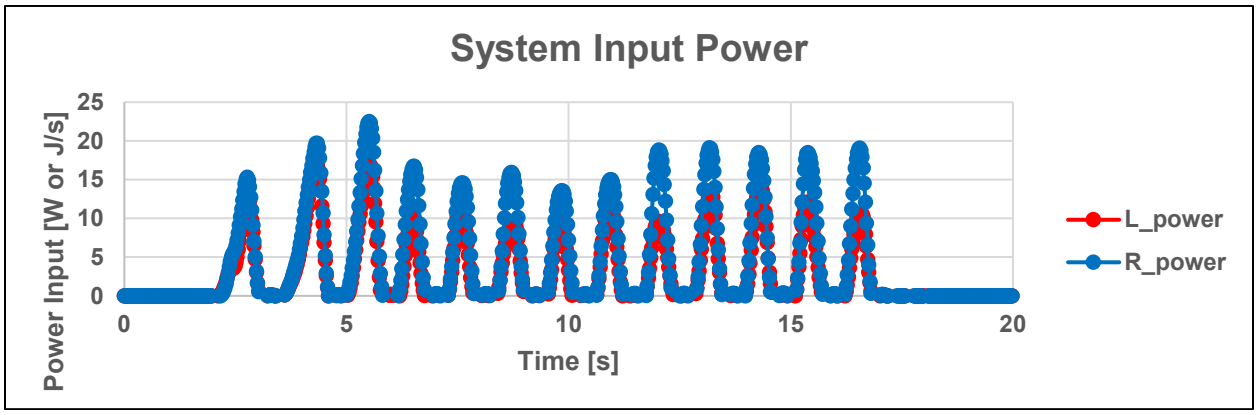

The cumulative area under the power curves represent the work supplied to each wheel by the motors. Integrating the left and right powers over time yields the work curves, and the summation represents the total energy or work supplied to the system at each timestamp:

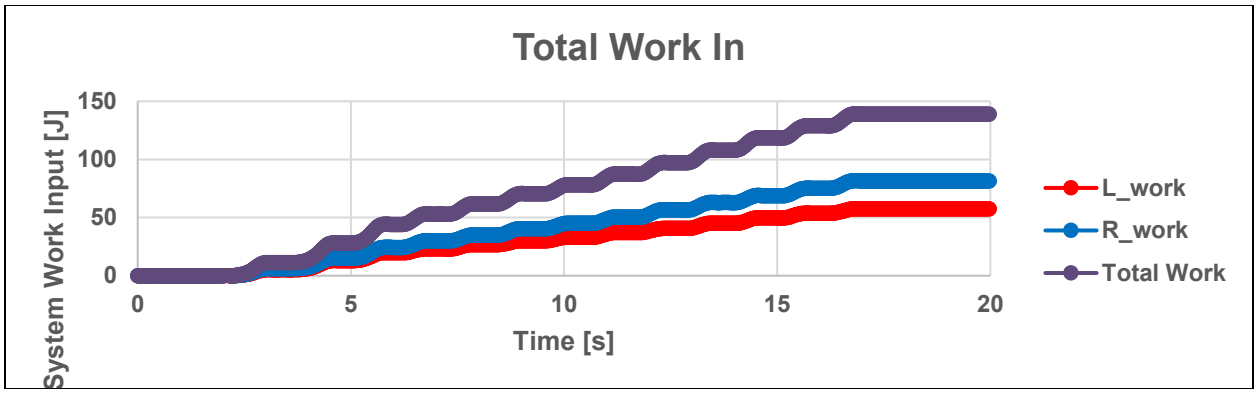

The cumulative work input can be segmented multiple ways. The work per push, for example, could be calculated based on the size of the 'step' in the total work curve. Work per phase would be segmented by determining either 'acceleration phase' and 'steady-state phase' parse-points, or even 'push phase' and 'coast phase' parse-points. However, there is no net change of work during the coasting periods between pushes because there are no torques being supplied to the push-rims.

2. 'Main' Propulsion Cost

- Equation:
  - $\frac{\int_{t_i}^{t_f}((\tau_L\omega_L)+(\tau_R\omega_R))\,dt}{\int_{t_i}^{t_f}(v_L+v_R)\,dt} = \frac{Work_{total}}{distance_{total}}$
- Requires:
  - Cumulative work (J)
  - Displacement of the center of mass (m for straight, rad for curvilinear)

As in the basic work calculation, filtered wheel torque is multiplied by the angular wheel velocity to get the filtered power input of each wheel. Integration of this 'power in' curve over time for each wheel yields the 'work in' curve for each wheel. Numerical integration of these curves uses cumulative summation via the trapezoidal method.

Distances traveled by each wheel are found by integrating the wheel velocities over the time duration of the maneuver. The linear velocities are found by multiplying the angular velocity plots by the radius of the wheel (typically around 12 inches, or 0.3048 m).

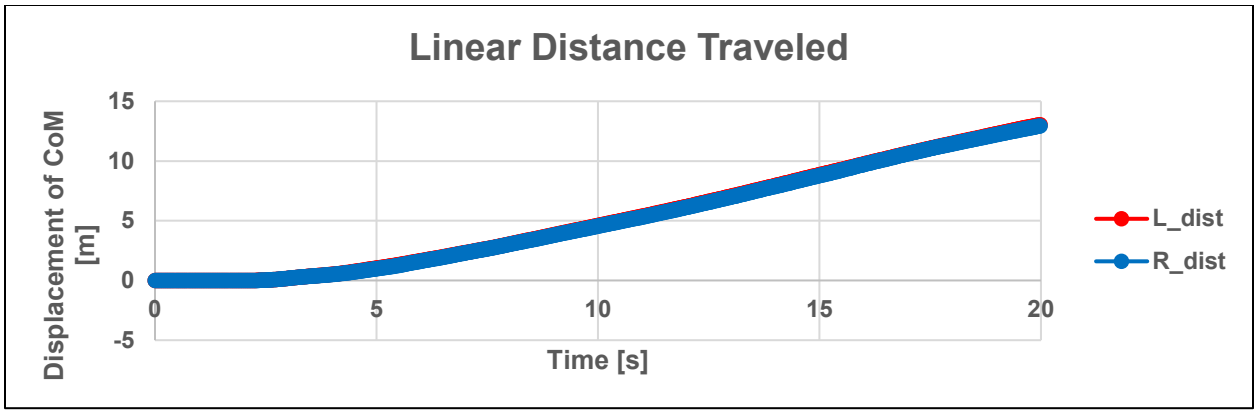

Propulsion cost is then defined as the ratio between the work supplied to the chair and the distance traveled by the chair. The element-wise division of main work and distance can be plotted against time.

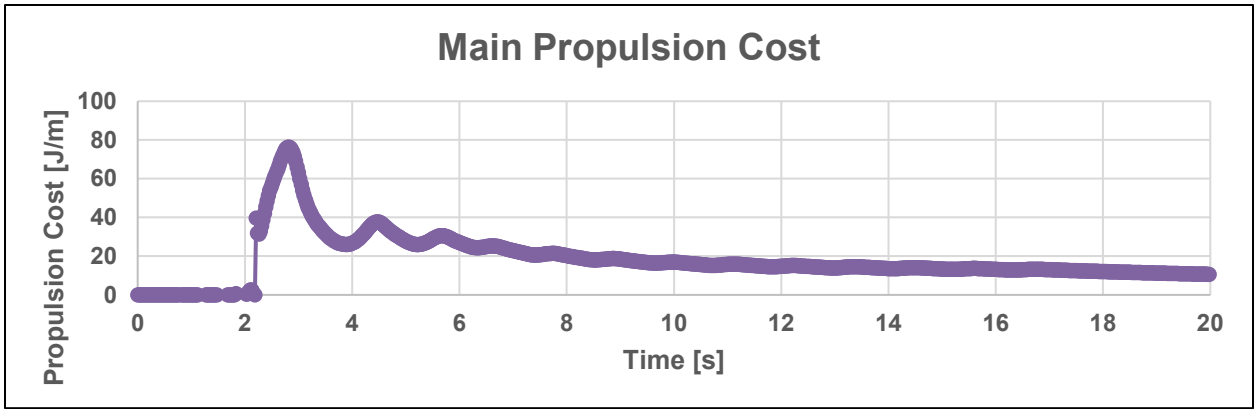

The curve itself does not have much significance. As the system is accelerating, there is a large amount of input work compared to the small amount of travel, so the cost appears significantly higher at the first peak than at the rest of the curve. The more important portion is the tail-end of the maneuver, when the pushes have concluded and the system is coasting to a stop. Propulsion cost is taken as a single value of the work at the end of the maneuver divided by the total distance traveled during the maneuver [71, 82]. With the velocity-based propulsion mode of the AMPS, the end was the start of the deceleration phase, just after the AMPS started to drop below the steady-state velocity (see Figure 11). In the newly-implemented torque mode, the end of the maneuver can be defined as the end of the final push as the applied torque drops back to 0 Nm, or after a pre-determined coasting time after the last push, or as the time when the chair coasts back to a rest.

In the above example, the 13-push maneuver propelled too far to let it coast completely to a stop, and thus the final cost was taken around 0.5 seconds after the final push concluded. Thus, the final cost of this particular example would be the value taken at 16.5 seconds (see the torque plots above), which yields an average propulsion cost of around 13.5 J/m. Truncating the maneuver here ensured that the distance traveled in the 'coasting' phase after the final push did not influence the propulsion cost, because some trials were allowed to coast farther before being manually restrained. However – this coasting is a direct result

of the input work, and it artificially inflates the cost of propulsion to exclude the total travel distance.

For the propulsion costs within the three study-based specific aims, propulsion cost was recorded as the value as soon as the chair coasted to a complete stop.

3. Propulsion Cost (by 'Phase')

- Equation:
  - $$\frac{\int_{t_{i,phase}}^{t_{f,phase}}((\tau_L\omega_L)+(\tau_R\omega_R))\,dt}{\int_{t_{i,phase}}^{t_{f,phase}}(v_L+v_R)\,dt} = \frac{Work_{phase}}{distance_{phase}}$$
- Requires:
  - Same torques and velocities as the 'Main Cost' parameter above, but segmented into Acceleration and Steady-State phases

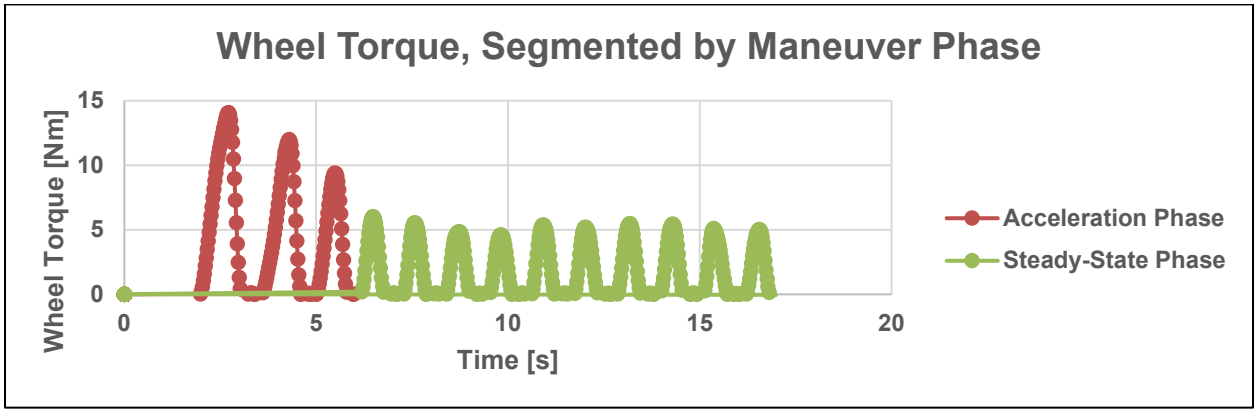

Splitting the propulsion cost by 'phase' of maneuver is much the same as the propulsion cost assessment in the previous method, except that each segment or phase of the maneuver has its own start and end points. In this basic 13-push straight example, the period of analysis terminates at the end of the last push with an added 0.5 seconds (approximately) for the coasting period. The torques of each phase are shown above.

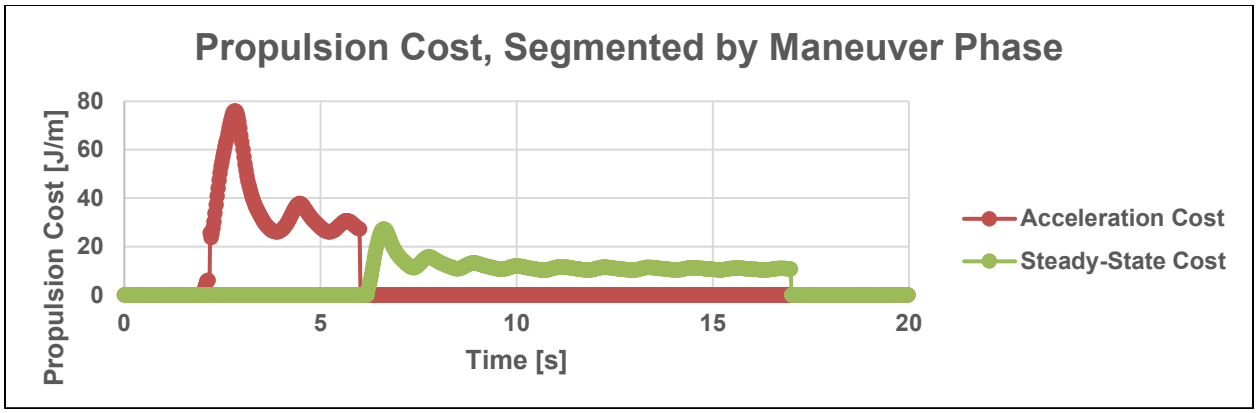

The cost of each phase would be determined by the last point in each phase. In this example, the Acceleration Cost is around 25 J/m, and the Steady-State Cost is around 13 J/m. The bump in the first push of the steady-state phase is because the cost is starting brand-new at the 7 second mark. What this means is that the new phase cost starts by taking the work and distance from the beginning of the phase. At and beyond the 7 second mark, the values are normalized by subtracting the values from the 7 second point. By 7.5 seconds, the cost still has not had time yet to normalize for the differences in the 'push' versus 'recovery' phases of the propulsion cycle.

4. Rate of Energy Loss

- Equation:
  - $$\frac{\int_{t_{i,phase}}^{t_{f,phase}}((\tau_L\omega_L)+(\tau_R\omega_R))\,dt-(KE_{f,phase}-KE_{i,phase})}{\int_{t_{i,phase}}^{t_{f,phase}}(v_L+v_R)\,dt}=\frac{Work_{phase}-\Delta KE_{phase}}{distance_{phase}}$$
- Requires:
  - Basic work input (J)
  - Total Kinetic Energy output (J)
  - Distance traveled by the CoM (m)

The concept of this analysis method is to represent the energy losses per meter directly, rather than including the conserved energy contained within the Kinetic Energy term. For example, in the acceleration phase, the AMPS starts from rest and reaches a speed of 0.8 m/s in the first three strokes, so the "Rate of Energy Loss" would take the total work in at the end of the acceleration phase, then subtract the system kinetic energy change (last point minus the first point), and finally divide this energy by the distance traveled.

Note that this is NOT the same as a 'propulsion cost.' This is a rate of energy loss. This metric is reflective of the energy purely expended without considering the energy that is used for motion. As such, it does not reflect the total amount of energy input required to move the wheelchair. A "cost" should incorporate all energy used to travel, not just the energy lost to non-conservative forces.

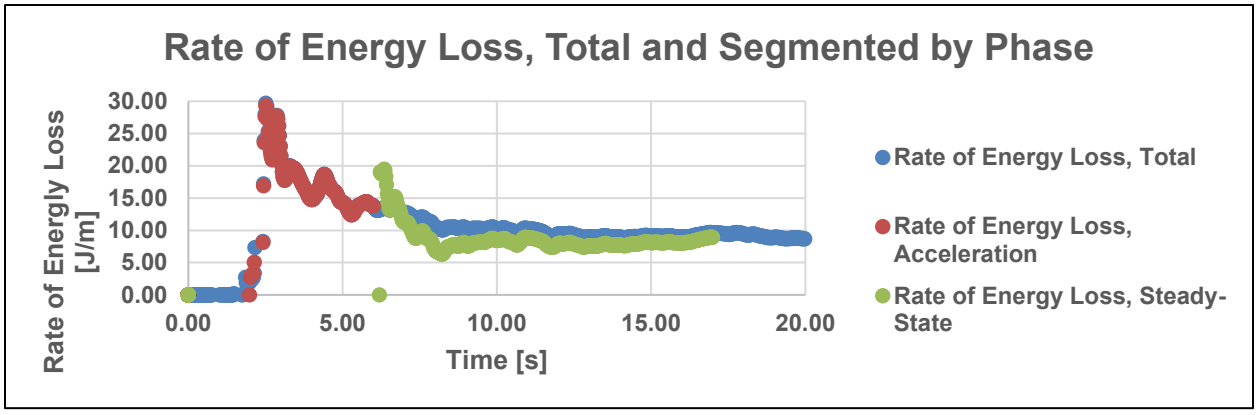

This plot shows that the total rate of energy loss yields roughly the same outcome as segmenting by phase. Ideally, the outcome parameter would be the last data point in each segment of the curve to normalize over as many data points as possible. In the example shown in the Rate of Energy Loss plot above, the Acceleration Phase has an energy loss rate of 13.78 J/m and the Steady-State Phase has a rate of 8.92 J/m. Within the steady-state phase, there is no net change in kinetic energy, which makes this assessment nearly equivalent to the main propulsion cost calculation.

5. Instantaneous Efficiency

- Equation:
  - $\frac{KE_i - KE_{i-1}}{((\tau_L \omega_L)+(\tau_R \omega_R)) * timestep} = \frac{\Delta KE_{per\ timestep}}{inst.\ Work_{input}} = \frac{"Energy\ Output"}{"Energy\ Input"}$
- Requires:
  - Torque, velocity, and mass of the system

Supplied power is calculated as in the other analyses above. In a broader sense, 'power' is defined as the average change in energy input to the system over a fixed time duration. This is typically integrated over the maneuver duration to find the total amount of work supplied to the system over the entire maneuver. Instead, if the power curve is multiplied by the timestep (25 ms, or 40 Hz), the result is an 'instantaneous work' curve representing the energy supplied to the system at each timestamp. In other words, it shows the quantity of work supplied in the span of the 25 ms between samples. This can be compared to the change in system energy (or kinetic energy, since there is no influence of potential energy along flat surfaces) at that moment in time to get a basic output-over-input-energy ratio.

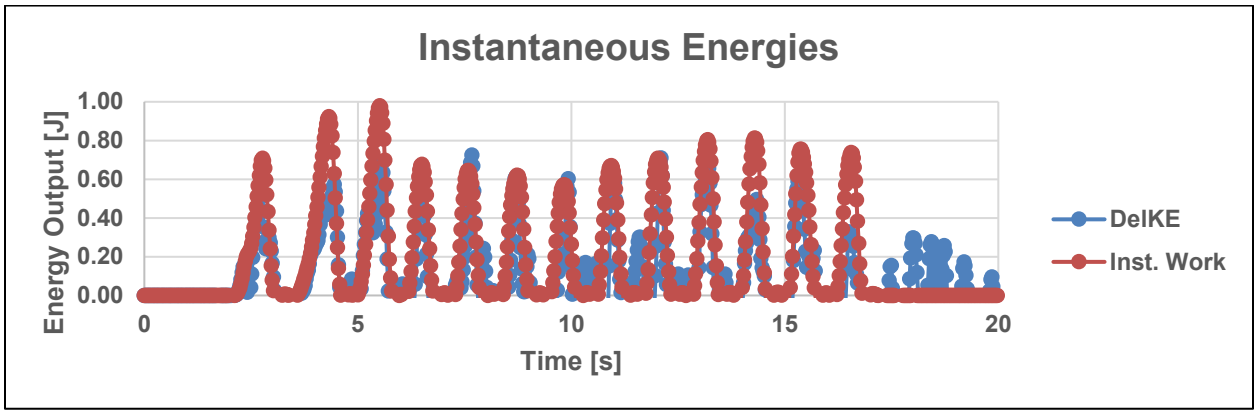

The change in kinetic energy (*DelKE*) is found by calculating the difference in kinetic energy between consecutive timestamps. The Instantaneous Work curve is found by multiplying the power curve by the timestep between each data point, a value of roughly 25 ms. Then, "Instantaneous Efficiency" is found by dividing the DelKE (the "output energy" of the system) by the instantaneous work ("input energy") at each point.

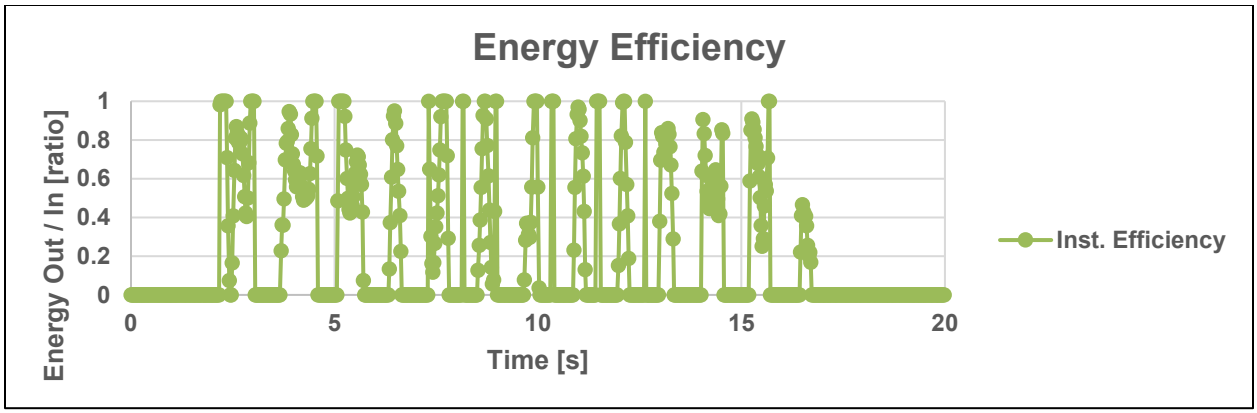

Instantaneous efficiency can then be averaged during the periods of active propulsion. The coasting phases would be excluded from the analysis because there is no energy supplied to the system. The plot is truncated at 0

6. Cost of Transport (Distance-based)

- Equation:
  - $CoT = \frac{Energy_{input}}{mass * gravity * displacement}$
- Requires:
  - Work input (J), which is used as the collective energy input numerator
  - Mass of the system (kg) and gravity (m/s^2) though some studies disregard the gravitational term
  - Displacement of the CoM (m) from the integral of the wheel velocities

Cost of transport [146, 147] is used in locomotion-based studies to compare relative energy efficiency between animals or vehicles. In this example, the numerator of 'energy input' is the work supplied by the motors, and the denominator of 'mass*gravity*displacement' are known or measured quantities of the system.

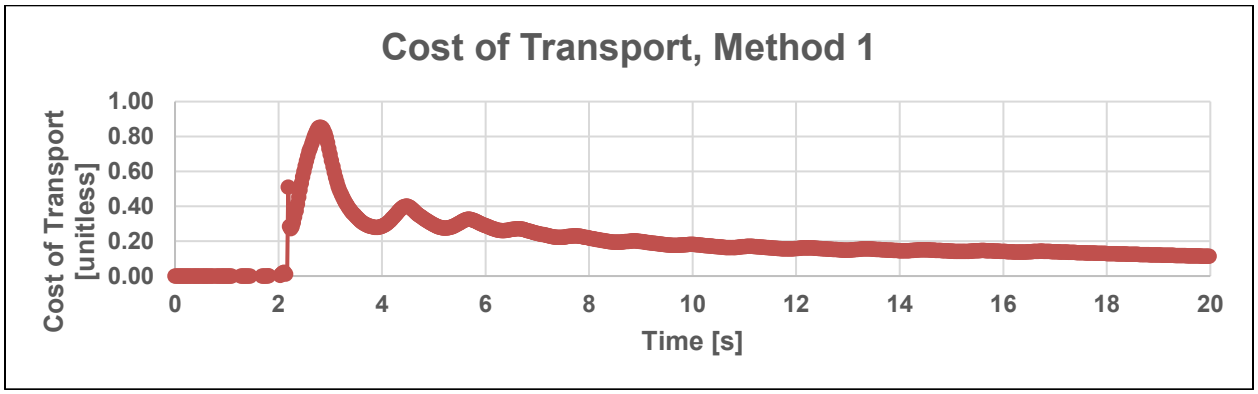

Note that the cost of transport curve using this method strongly resembles the shape of the "Main Cost" propulsion cost data above. Essentially, the established propulsion cost equation stemmed from the concept of cost of transport [71, 82], without the normalization

by system weight. The main difference is in the units – propulsion cost yields values similar to gas mileage in a car, that reflect the energetic expenditure the system requires to travel a certain distance, whereas cost of transport is unitless and more reminiscent of an efficiency parameter. This efficiency-like metric reduces the direct applicability of the outcome variable, because there is no physical representation of this efficiency. There is no clear way to represent a cost of transport of 0.21 versus 0.23, whereas propulsion cost differences can concisely be summarized by more energy expenditure per unit travel distance.

7. **Cost of Transport (Velocity-based)**

- Equation:
  - $CoT = \frac{Power_{input}}{mass * gravity * linear\ velocity}$
- Requires:
  - Power input to the system (W)
  - System mass (kg), gravitational constant (m/s^2), linear velocity of the CoM (m/s)

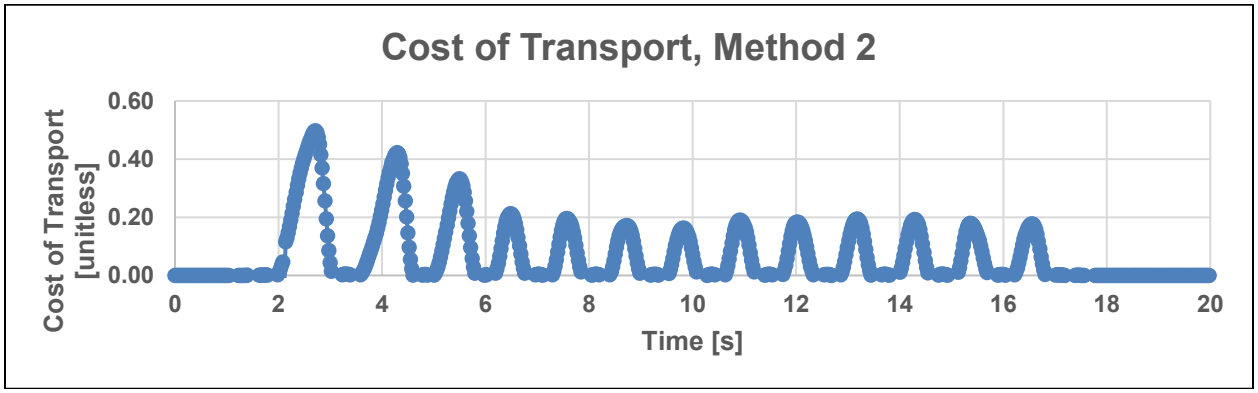

This second version of cost of transport uses the power input divided by the velocity term. Since these are both time-dependent and not cumulative like the work input plot, this outcome strongly resembles the shape of the Input Torque plot and goes to a value of 0 when there is no power supplied to the wheelchair. Consequently, this metric shows a relatively instantaneous reflection of chair efficiency, but no new knowledge is gained of the system after multiple pushes in steady-state, for example. After the fourth or fifth push, the trial might as well end, because the metric will not evolve with any further pushes.

Descriptive Statistics of Each Outcome

The data below shows the values from each of the described metrics for all of the incremental frame mass loading conditions using the extended 13-push straight maneuver over tile. The Main Cost values *do not* line up with those seen in CHAPTER 4 firstly because these examples were given 6 extra pushes in steady-state, and more importantly because the chair was not allowed to coast to a stop. The extra distance traveled by the

chair during the coast-down deceleration would have brought the Main Cost values here more closely aligned with those reported in the incremental frame mass study. Cost of transport values were excluded from the following table.

	Work	Propulsion Cost			Rate of Energy Loss			Other
	Basic Work In	Main (Total)	Accel. Phase	Steady-State Phase	Main	Accel. Phase	Steady-State Phase	Inst. Efficiency
Config.	(J)	(J/m)	(J/m)	(J/m)	(J/m)	(J/m)	(J/m)	(%)
0A	148.56 (±6.18)	13.06 (±0.17)	24.61 (±0.46)	10.65 (±0.17)	9.09 (±0.19)	6.83 (±0.48)	9.63 (±0.26)	63.11 (±2.20)
2A	142.61 (±6.41)	13.15 (±0.14)	24.56 (±0.24)	10.68 (±0.12)	9.32 (±0.36)	6.89 (±0.28)	10.16 (±0.36)	62.74 (±2.01)
4A	139.86 (±5.93)	13.21 (±0.16)	24.61 (±0.38)	10.76 (±0.14)	9.40 (±0.42)	6.99 (±0.44)	10.33 (±0.18)	59.99 (±2.18)
2F	145.54 (±6.86)	13.23 (±0.18)	24.72 (±0.40)	10.82 (±0.11)	9.37 (±0.31)	7.08 (±0.53)	10.10 (±0.28)	62.43 (±2.32)
4F	139.52 (±6.39)	13.37 (±0.17)	24.69 (±0.30)	10.89 (±0.17)	9.70 (±0.45)	7.11 (±0.55)	10.77 (±0.33)	60.50 (±3.56)

The Basic Work In parameter shows that the lightest chair harnesses more energy than the other configurations. This outcome is relevant because it shows that given the same torque application, the lighter chair goes faster, thus the "Power Input" values are greater and the integrated work values are higher.

Each outcome parameter has some benefit. Propulsion cost was selected as the most robust and ubiquitous metric of wheelchair performance. The units are relevant to the user as a representation of the required energy expenditure to travel a given distance, and the kinetic energy of the system is accounted for within the metric unlike the 'rate of energy loss' metric. Propulsion costs were measured over the entire maneuver rather than segmenting into the acceleration and steady-state phases because these partial costs are incomplete: acceleration cost excludes the kinetic energy remaining in the system that has not physically been expended by letting the system coast down, and the steady-state cost begins from a non-zero kinetic energy. These invalidate the concept of 'work in equals change in system energy' because the energy changes are unaccounted for. The total/main propulsion cost, on the other hand, starts from rest and ends at rest, so the net change in system energy is 0 and the work-energy relationship is maintained.

Deployment of Propulsion Cost Assessment

Generalized propulsion cost can get 'washed out' because the numerator (Work In) and denominator (distance traveled) both vary between chairs/maneuvers. The robustness of

the parameter is demonstrated by the fact that it can still see differences, yet they are much smaller differences than those seen in previous studies with propulsion cost where the distances were more defined and held constant between chairs.

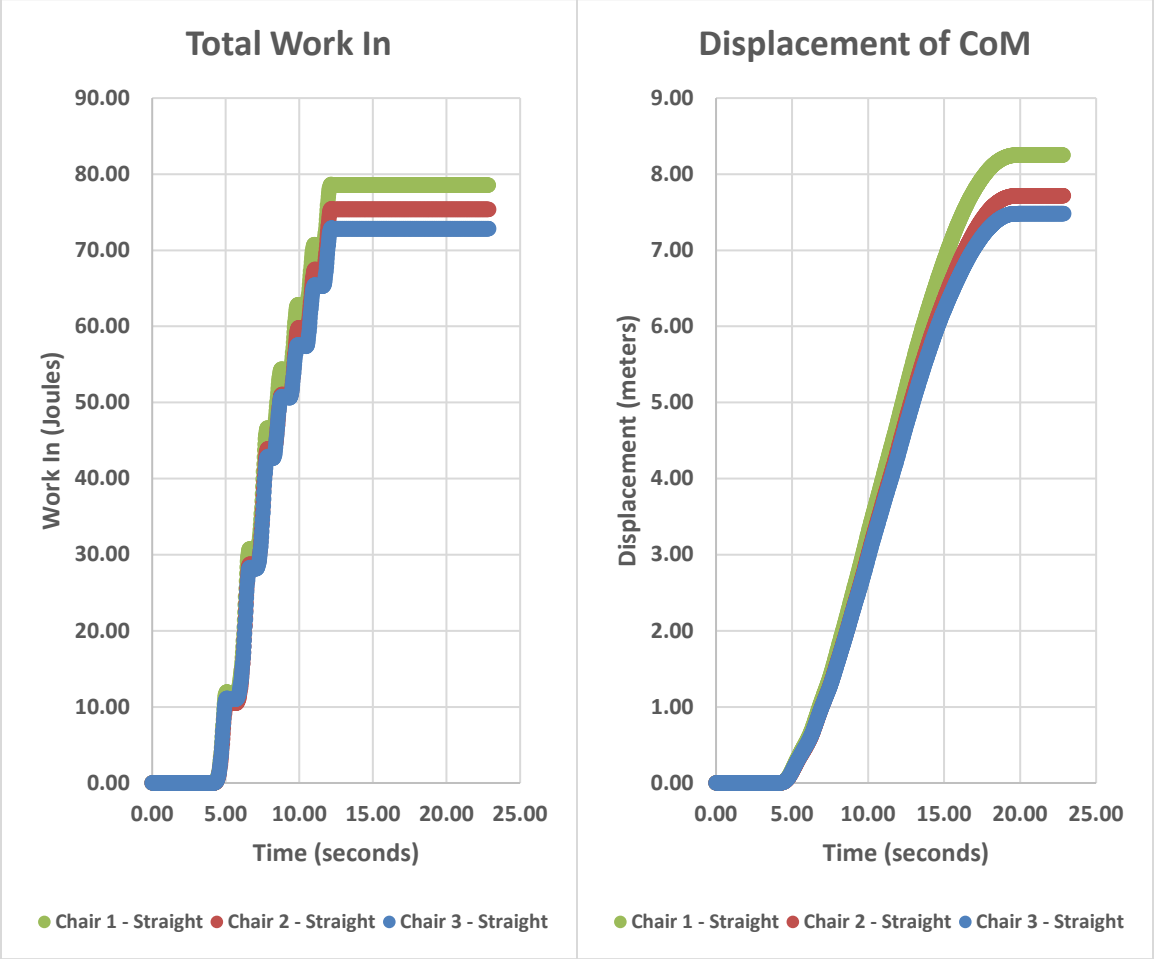

	Straight		
	Chair 1	**Chair 2**	**Chair 3**
Total Work (J)	78.54	75.36	72.83
Total Dist (m)	8.25	7.72	7.48
Cost (J/m)	9.52	9.77	9.73

Note: The Straight "Total Work (J)" row shows that Chair 1 has the highest work required to move the chair for the duration of the maneuver, yet it also has the highest distance traveled. Therefore, the propulsion cost of the chair is the lowest out of the three chairs.

APPENDIX C. ASSESSMENT OF MANEUVERABILITY VIA MOMENTUM

'Maneuverability' is a feature of the chair that is felt by the user, but it is difficult to objectively define. This appendix shows one method of assessing a representation of maneuverability via momentum. Momentum is defined as the combined magnitude and direction of the moving body as calculated by the product of the mass and velocity. The ability to rapidly change momentum was conceptually identified as one means of quantifying the illusive 'maneuverability' parameter, especially as it manifested within the slalom maneuver.

The equations used in this assessment were:

$$Linear\ Momentum = mass_{system} * velocity_{CoM}$$

$$Angular\ Momentum\ (simplified) = I_{ZZ,system} * yaw\ rate_{about\ CoM}$$

For the Straight maneuver, the momentum plot was dominated by the linear momentum, with only slight representation of rotation due to the rapid rolling of the wheels. Dashed vertical lines represent the beginning or end of a push or coast phase. The leftmost and rightmost lines indicate the start and end of the entire maneuver, respectively.

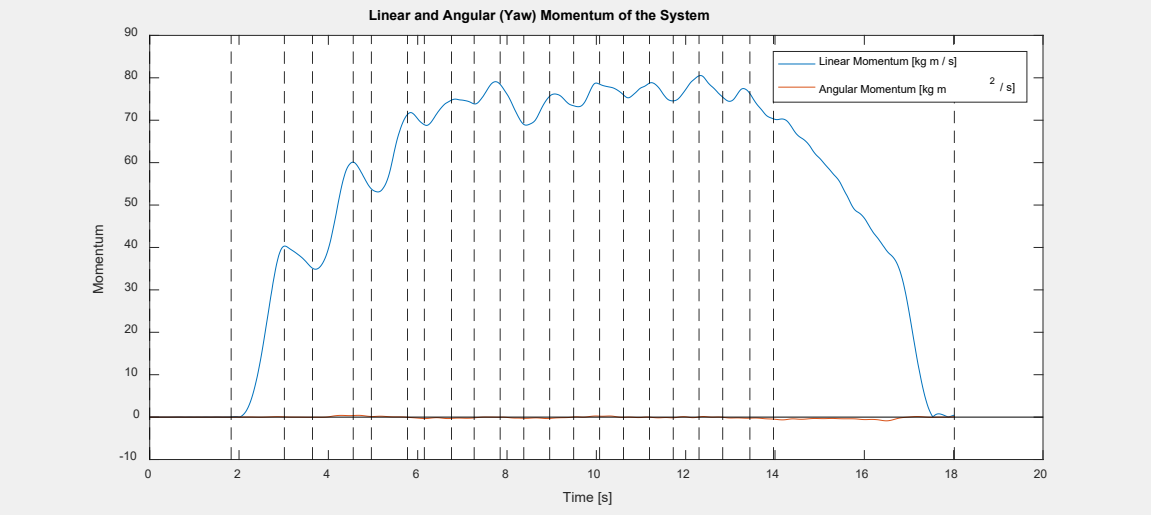

In the Slalom maneuver, the presence of the linear momentum component still dominated but the angular momentum component had a greater representation:

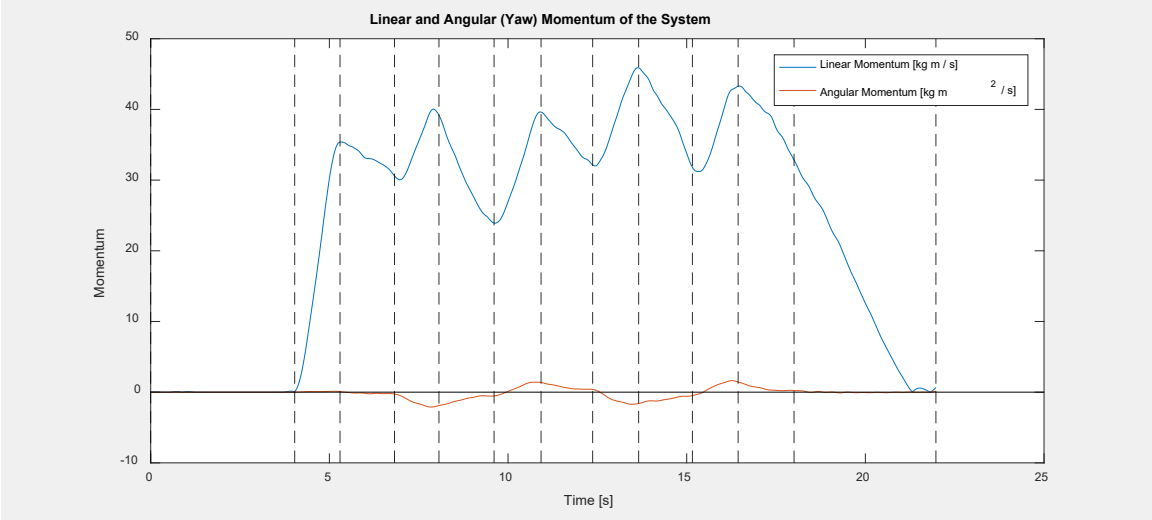

Note that the momentum calculation should be more complex to involve every form of rotation occurring in the system, but the complex calculation produced a much noisier signal due to the caster swivel calculations when the chair is mostly at rest.

$$Angular\ Momentum\ (complex) = \left(I_{ZZ,system} * \dot{\psi}_{frame}\right) + \left(I_{ZZ,LFLC} * \dot{\psi}_{LC\ swivel}\right) + \left(I_{ZZ,LFLC} * \dot{\psi}_{LC\ swivel}\right) + \left(I_{YY,LC} * \dot{\varphi}_{LC\ roll}\right) + \left(I_{YY,RC} * \dot{\varphi}_{RC\ roll}\right) + \left(I_{YY,LD} * \dot{\varphi}_{LD\ roll}\right) + \left(I_{YY,RD} * \dot{\varphi}_{RD\ roll}\right)$$

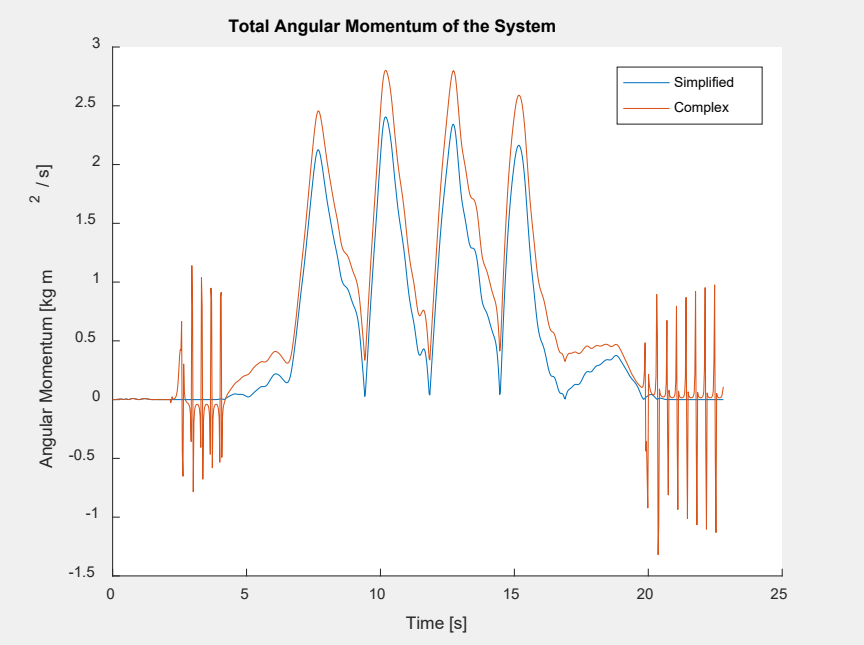

The general concept of this assessment would be to find the change in momentum per timestep for each maneuver and each configuration. Greater changes in momentum would indicate a greater response of the system to the same controlled input which would, in turn, represent a more maneuverable chair. The following plot shows the changes in momentum for the 13-push Straight maneuver:

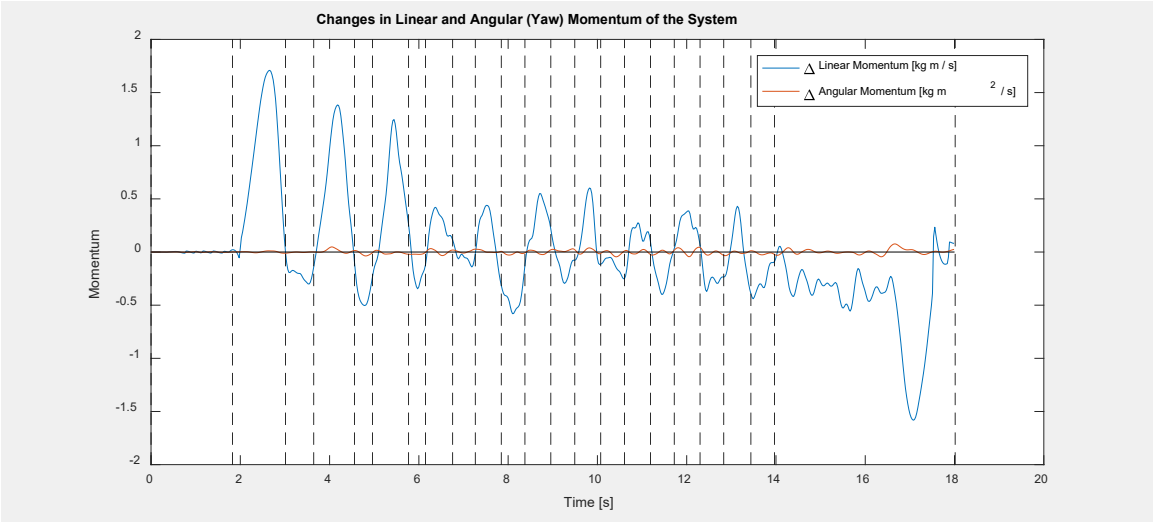

The next plot was generated from the Slalom maneuver on the same chair (the 0A configuration from the incremental frame mass study).

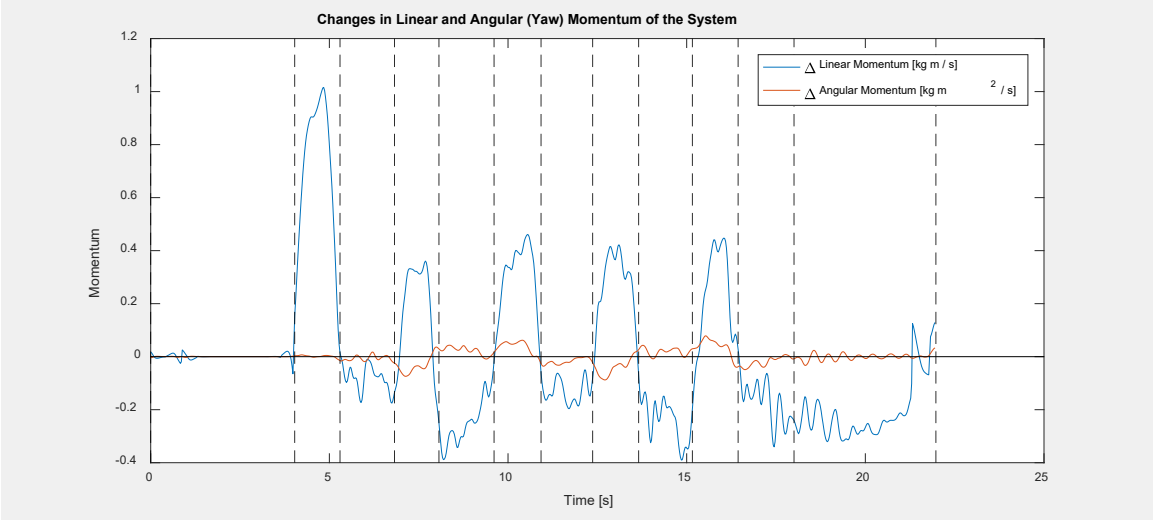

This assessment was discontinued due to lack of resolution. The variance for these data curves for a single configuration over five identical trials overshadowed the differences between the five loading configurations for the incremental frame mass study, and further time and energy were diverted from this line of analysis back to data collection for the other two studies. The framework for this assessment has been established and the analysis code is implemented in the data processing pipeline for future studies. Maneuverability was evaluated instead by inspecting the distance, kinetic energy, and angular yaw displacement for each configuration for the purposes of these studies.

REFERENCES

1. Brault, M.W., *Americans With Disabilities: 2010*, U.S. Department of Commerce, Editor. 2012, United States Census Bureau. p. 70-131.

2. Taylor, D.M., *Americans With Disabilities: 2014*, U.S. Department of Commerce, Editor. 2018, United States Census Bureau. p. 70-152.

3. Sonenblum, S.E., S. Sprigle, and R.A. Lopez, *Manual Wheelchair Use: Bouts of Mobility in Everyday Life.* Rehabilitation Research and Practice, 2012. **2012**.

4. Sonenblum, S.E. and S. Sprigle, *Wheelchair use in ultra-lightweight wheelchair users.* Disabil Rehabil Assist Technol, 2017. **12**(4): p. 396-401.

5. Levy, C.E., et al., *Use of power assist wheels results in increased distance traveled compared with conventional manual wheeling.* Am J Phys Med Rehabil, 2010. **89**(8): p. 625-34.

6. Oyster, M.L., et al., *Investigation of factors associated with manual wheelchair mobility in persons with spinal cord injury.* Arch Phys Med Rehabil, 2011. **92**(3): p. 484-90.

7. van der Woude, L.H., H.E. Veeger, and R.H. Rozendal, *Propulsion technique in hand rim wheelchair ambulation.* J Med Eng Technol, 1989. **13**(1-2): p. 136-41.

8. van der Woude LHV, et al., *Alternative modes of manual wheelchair ambulation: An overview.* Am J Phys Med Rehabil 2001. **80**: p. 765-777.

9. van der Woude LHV, et al., *Wheelchair ergonomics and physiological testing of prototypes.* Ergonomics, 1986. **29**(12): p. 1561-1573.

10. van der Woude LHV, et al., *Manual wheelchair propulsion: effects of power output on physiology and technique.* Med Sci Sports Exerc, 1988. **20**(1): p. 70-8.

11. Koontz, A.M., et al., *Manual wheelchair propulsion patterns on natural surfaces during start-up propulsion.* Arch Phys Med Rehabil, 2009. **90**(11): p. 1916-23.

12. Curtis, K.A., et al., *Shoulder pain in wheelchair users with tetraplegia and paraplegia.* Arch Phys Med Rehabil, 1999. **80**(4): p. 453-7.

13. Curtis, K.A., et al., *Effect of a standard exercise protocol on shoulder pain in long-term wheelchair users.* Spinal Cord, 1999. **37**(6): p. 421-9.

14. Boninger, M.L., et al., *Shoulder magnetic resonance imaging abnormalities, wheelchair propulsion, and gender.* Arch Phys Med Rehabil, 2003. **84**(11): p. 1615-20.

15. Boninger, M.L., et al., *Pushrim biomechanics and injury prevention in spinal cord injury: recommendations based on CULP-SCI investigations.* J Rehabil Res Dev, 2005. **42**(3 Suppl 1): p. 9-19.

16. Lin, Y.S., et al., *Effects of repetitive shoulder activity on the subacromial space in manual wheelchair users.* Biomed Res Int, 2014. **2014**: p. 583951.

17. Louis, N. and P. Gorce, *Surface electromyography activity of upper limb muscle during wheelchair propulsion: Influence of wheelchair configuration.* Clin Biomech (Bristol, Avon), 2010. **25**(9): p. 879-85.

18. van der Woude, L.H., et al., *Seat height: effects on submaximal hand rim wheelchair performance during spinal cord injury rehabilitation.* J Rehabil Med, 2009. **41**(3): p. 143-9.

19. Mulroy, S.J., et al., *Effect of fore-aft seat position on shoulder demands during wheelchair propulsion: part 1. A kinetic analysis.* J Spinal Cord Med, 2005. **28**(3): p. 214-21.

20. Boninger, M.L., et al., *Manual wheelchair pushrim biomechanics and axle position.* Arch Phys Med Rehabil, 2000. **81**(5): p. 608-13.

21. Hughes, C.J., et al., *Biomechanics of wheelchair propulsion as a function of seat position and user-to-chair interface.* Arch Phys Med Rehabil, 1992. **73**(3): p. 263-9.

22. Richter, W.M., *The effect of seat position on manual wheelchair propulsion biomechanics: a quasi-static model-based approach.* Med Eng Phys, 2001. **23**(10): p. 707-12.

23. Lin, J.T. and S. Sprigle, *The influence of operator and wheelchair factors on wheelchair propulsion effort.* Disabil Rehabil Assist Technol, 2020. **15**(3): p. 328-335.

24. Gorce, P. and N. Louis, *Wheelchair propulsion kinematics in beginners and expert users: influence of wheelchair settings.* Clin Biomech (Bristol, Avon), 2012. **27**(1): p. 7-15.

25. De Groot, S., et al., *Wheelchair propulsion technique and mechanical efficiency after 3 wk of practice.* Med Sci Sports Exerc, 2002. **34**(5): p. 756-66.

26. Center for Medicare and Medicaid Services, *Manual Wheelchairs Local Coverage Determination (LCD) and Policy*, Center for Medicare and Medicaid Services, Editor. 2019, Noridian Healthcare Solutions, LLC.

27. Watanabe, L., *Defining Ultralights: What the K0005 is and why it's the best answer for many complex clients*, in *Mobility Management*. 2019, 1105 Media, Inc.

28. Sawatzky, B., et al., *The need for updated clinical practice guidelines for preservation of upper extremities in manual wheelchair users: a position paper.* Am J Phys Med Rehabil, 2015. **94**(4): p. 313-24.

29. Veeger, H.E., L.A. Rozendaal, and F.C. van der Helm, *Load on the shoulder in low intensity wheelchair propulsion.* Clin Biomech (Bristol, Avon), 2002. **17**(3): p. 211-8.

30. Rimmer, J.H., et al., *Exercise intervention research on persons with disabilities: what we know and where we need to go.* Am J Phys Med Rehabil, 2010. **89**(3): p. 249-63.

31. Beekman, C.E., L. Miller-Porter, and M. Schoneberger, *Energy cost of propulsion in standard and ultralight wheelchairs in people with spinal cord injuries.* Phys Ther, 1999. **79**(2): p. 146-58.

32. de Groot, S., et al., *Effect of wheelchair stroke pattern on mechanical efficiency.* Am J Phys Med Rehabil, 2004. **83**(8): p. 640-9.

33. de Groot, S., R.J. Vegter, and L.H. van der Woude, *Effect of wheelchair mass, tire type and tire pressure on physical strain and wheelchair propulsion technique.* Med Eng Phys, 2013. **35**(10): p. 1476-82.

34. Sagawa, Y., Jr., et al., *Effects of wheelchair mass on the physiologic responses, perception of exertion, and performance during various simulated daily tasks.* Arch Phys Med Rehabil, 2010. **91**(8): p. 1248-54.

35. Stephens, C.L. and J.R. Engsberg, *Comparison of overground and treadmill propulsion patterns of manual wheelchair users with tetraplegia.* Disabil Rehabil Assist Technol, 2010. **5**(6): p. 420-7.

36. Koontz, A.M., et al., *Multisite comparison of wheelchair propulsion kinetics in persons with paraplegia.* J Rehabil Res Dev, 2007. **44**(3): p. 449-58.

37. Samuelsson, K.A., et al., *The effect of rear-wheel position on seating ergonomics and mobility efficiency in wheelchair users with spinal cord injuries: a pilot study.* J Rehabil Res Dev, 2004. **41**(1): p. 65-74.

38. Sauret, C., et al., *Respective contributions of the subject and the wheelchair to the total kinetic energy of manual wheelchair locomotion.* Computer Methods in Biomechanics and Biomedical Engineering, 2009. **12**(sup1): p. 227-228.

39. Schuring, D., *Energy loss of pneumatic tires under freely rolling, braking, and driving conditions.* Tire Science and Technology, 1976. **41**: p. 3-15.

40. Pacejka, H., *Tire and vehicle dynamics*. 2005: Elsevier.

41. Hofstad, M. and P.E. Patterson, *Modelling the propulsion characteristics of a standard wheelchair.* J Rehabil Res Dev, 1994. **31**(2): p. 129-37.

42. Gillespie, T.D., *Vehicle dynamics.* Warren dale, 1997.

43. Ellis, J.R., *Vehicle dynamics*. 1969: Random House Business.

44. Frank, T.G. and E.W. Abel, *Measurement of the turning, rolling and obstacle resistance of wheelchair castor wheels.* J Biomed Eng, 1989. **11**(6): p. 462-6.

45. Kauzlarich, J.J. and J.G. Thacker, *Wheelchair tire rolling resistance and fatigue.* J Rehabil Res Dev, 1985. **22**(3): p. 25-41.

46. Kwarciak AM, et al., *Evaluation of wheelchair tire rolling resistance using dynamometer-based coast-down tests.* Journal of Rehabilitation Research and Development, 2009. **46**(7): p. 931-938.

47. Gordon, J., J.J. Kauzlarich, and J.G. Thacker, *Tests of two new polyurethane foam wheelchair tires.* J Rehabil Res Dev, 1989. **26**(1): p. 33-46.

48. Kauzlarich, J.J., T. Bruning, and J.G. Thacker, *Wheelchair caster shimmy and turning resistance.* J Rehabil Res Dev, 1984. **21**(2): p. 15-29.

49. Sawatzky, B.J., W.O. Kim, and I. Denison, *The ergonomics of different tyres and tyre pressure during wheelchair propulsion.* Ergonomics, 2004. **47**(14): p. 1475-83.

50. Lin, J.T., M. Huang, and S. Sprigle, *Evaluation of wheelchair resistive forces during straight and turning trajectories across different wheelchair configurations using free-wheeling coast-down test.* J Rehabil Res Dev, 2015. **52**(7): p. 763-74.

51. Fallot, C., et al., *Manual wheelchair's turning resistance: swivelling resistance parameters of front and rear wheels on different surfaces.* Disabil Rehabil Assist Technol, 2019: p. 1-8.

52. Silva, L.C., et al., *Measurement of wheelchair contact force with a low cost bench test.* Med Eng Phys, 2016. **38**(2): p. 163-70.

53. de Groot, S., et al., *Mechanical efficiency and propulsion technique after 7 weeks of low-intensity wheelchair training.* Clin Biomech (Bristol, Avon), 2008. **23**(4): p. 434-41.

54. Gil-Agudo, A., et al., *Shoulder joint kinetics during wheelchair propulsion on a treadmill at two different speeds in spinal cord injury patients.* Spinal Cord, 2010. **48**(4): p. 290-6.

55. Cowan, R.E., et al., *Impact of surface type, wheelchair weight, and axle position on wheelchair propulsion by novice older adults.* Arch Phys Med Rehabil, 2009. **90**(7): p. 1076-83.

56. van der Woude, L.H., et al., *Measurement of wheelchair rolling resistance with a handle bar push technique.* J Med Eng Technol, 2003. **27**(6): p. 249-58.

57. Kotajarvi, B.R., et al., *The effect of seat position on wheelchair propulsion biomechanics.* J Rehabil Res Dev, 2004. **41**(3B): p. 403-14.

58. Freixes, O., et al., *Wheelchair axle position effect on start-up propulsion performance of persons with tetraplegia.* J Rehabil Res Dev, 2010. **47**(7): p. 661-8.

59. Lenton JP, et al., *Hand-rim forces and gross mechanical efficiency at various frequencies of wheelchair propulsion.* Int J Sports Med. , 2013. **34**(2): p. 158-64.

60. Cowan, R.E., et al., *Preliminary outcomes of the SmartWheel Users' Group database: a proposed framework for clinicians to objectively evaluate manual wheelchair propulsion.* Archives of Physical Medicine and Rehabilitation, 2008. **89**(2): p. 260-268.

61. van der Woude, L.H., et al., *Optimum cycle frequencies in hand-rim wheelchair propulsion. Wheelchair propulsion technique.* Eur J Appl Physiol Occup Physiol, 1989. **58**(6): p. 625-32.

62. Koontz, A.M., et al., *A kinetic analysis of manual wheelchair propulsion during start-up on select indoor and outdoor surfaces.* J Rehabil Res Dev, 2005. **42**(4): p. 447-58.

63. Limroongreungrat, W., et al., *An instrumented wheel system for measuring 3-D pushrim kinetics during racing wheelchair propulsion.* Res Sports Med, 2009. **17**(3): p. 182-94.

64. Kwarciak, A.M., et al., *Comparing handrim biomechanics for treadmill and overground wheelchair propulsion.* Spinal Cord, 2011. **49**(3): p. 457-62.

65. Corfman, T.A., et al., *Range of motion and stroke frequency differences between manual wheelchair propulsion and pushrim-activated power-assisted wheelchair propulsion.* J Spinal Cord Med, 2003. **26**(2): p. 135-40.

66. Sprigle, S., M. Huang, and J.T. Lin, *Inertial and frictional influences of instrumented wheelchair wheels.* J Rehabil Assist Technol Eng, 2016. **3**: p. 2055668316649892.

67. Sauret, C., et al., *Assessment of field rolling resistance of manual wheelchairs.* J Rehabil Res Dev, 2012. **49**(1): p. 63-74.

68. Bascou, J., et al., *Measurement of wheelchair adjustment effects on turning deceleration.* Comput Methods Biomech Biomed Engin, 2015. **18 Suppl 1**(sup1): p. 1882-3.

69. Sprigle, S. and M. Huang, *Impact of Mass and Weight Distribution on Manual Wheelchair Propulsion Torque.* Assist Technol, 2015. **27**(4): p. 226-35; quiz 236-7.

70. Liles, H., et al., *Design of a Robotic System to Measure Propulsion Work of Over-Ground Wheelchair Maneuvers.* IEEE Trans Neural Syst Rehabil Eng, 2015. **23**(6): p. 983-91.

71. Sprigle, S. and M. Huang, *Manual wheelchair propulsion cost across different components and configurations during straight and turning maneuvers.* J Rehabil Assist Technol Eng, 2020. **7**: p. 1-14.

72. Foster, J., J. Kortge, and M. Wolanin, *Hybrid III - A Biomechanically-Based Crash Test Dummy*. 1977, Society of Automotive Engineers.

73. Robinette, K.M., et al., *Civilian American and European Surface Anthropometry Resource (CAESAR)*. 2002, Society of Automotive Engineers.

74. International Standards Organization, *ISO 7176 Wheelchair Standards- Section 11: Test Dummies*. 2012, International Standards Organization,.

75. Robertson, R.N., et al., *Pushrim forces and joint kinetics during wheelchair propulsion.* Arch Phys Med Rehabil, 1996. **77**(9): p. 856-64.

76. van der Woude, L.H., et al., *Biomechanics and physiology in active manual wheelchair propulsion.* Med Eng Phys, 2001. **23**(10): p. 713-33.

77. Rozendaal LA, Veeger HE, and van der Woude LH, *The push force pattern in manual wheelchair propulsion as a balance between cost and effect.* J Biomech., 2003. **36**(2): p. 239-47.

78. Medola, F.O., et al., *Partitioning Kinetic Energy During Freewheeling Wheelchair Maneuvers.* Ieee Transactions on Neural Systems and Rehabilitation Engineering, 2014. **22**(2): p. 326-333.

79. Eicholtz, M.R., et al., *Test method for empirically determining inertial properties of manual wheelchairs.* J Rehabil Res Dev, 2012. **49**(1): p. 51-62.

80. Hou, Z., et al., *A new trifilar pendulum approach to identify all inertia parameters of a rigid body or assembly.* Mechanism Machine Theory, 2009. **44**(6): p. 1270-1280.

81. Sprigle, S., M. Huang, and J. Misch, *Measurement of rolling resistance and scrub torque of manual wheelchair drive wheels and casters.* Assist Technol, 2019: p. 1-13.

82. Huang, M., *Development of Component and System Level Test Methods to Characterize Manual Wheelchair Propulsion Cost*, in *Mechanical Engineering*. 2017, Georgia Institute of Technology: Atlanta, GA. p. 187.

83. Misch, J., M. Huang, and S. Sprigle, *Modeling manual wheelchair propulsion cost during straight and curvilinear trajectories.* PLoS One, 2020. **15**(6): p. e0234742.

84. Bascou, J., et al., *Assessment of power losses due to ground contact forces during usual manual wheelchair movements.* Comput Methods Biomech Biomed Engin, 2017. **20**(sup1): p. 7-8.

85. Crichlow, L.R., *Development of a Comprehensive Mathematical Model and Wheelchair Interface for Manual Wheelchair Simulation*, in *Institute of Biomaterials and Biomedical Engineering*. 2011, University of Toronto.

86. *AmpFlow A28-150 Motor Performance*, in *Three-Inch High-Performance Motors*. Powerhouse Engineering Inc.

87. Savić, V., *DC motor torque vs DC motor speed*, in *Zilsel Invent Blogspot*. 2016, Zilsel-Invent.

88. Keeping, S. *Voltage- and Current-Mode Control for PWM Signal Generation in DC-to-DC Switching Regulators*. Electronic Products, 2014.

89. Yao, H., *Modeling and Design of a Current Mode Control Boost Converter*, in *Electrical and Computer Engineering*. 2012, Colorado State University: Fort Collins, CO.

90. Liu, H. and H. Zhang, *A novel direct torque control method for brushless DC motors based on duty ratio control.* Journal of the Franklin Institute-Engineering and Applied Mathematics, 2017. **354**(10): p. 4055-4072.

91. Sheehan, R., *Understanding and Applying Current-Mode Control Theory*, in *Power Electronics Technology Exhibition and Conference*. 2007, National Semiconductor Corporation: Dallas, TX.

92. Wang, Z.Q., S. Yin, and T.H. Ma, *A New Three-Phase Current Modulation Method to Suppress the Commutation Torque Ripple of Brushless DC Motor.* Journal of Electrical Engineering & Technology, 2017. **12**(5): p. 1925-1933.

93. Shirvani Boroujeni, M., G.R.A. Markadeh, and J. Soltani, *Torque ripple reduction of brushless DC motor based on adaptive input-output feedback linearization.* ISA Trans, 2017. **70**: p. 502-511.

94. Lad, C.K. and R. Chudamani, *A simple overlap angle control strategy for reducing commutation torque ripple in a brushless DC motor drive.* Engineering Science and Technology-an International Journal-Jestech, 2017. **20**(4): p. 1406-1419.

95. Teran, E. and J. Ueda. *Evaluation of Wheelchair Rolling Resistance Using a Robotic Device*. in *Proceedings of the 2014 IEEE Workshop on Advanced Robotics and its Social Impacts (ARSO 2014)*. 2014. Evanston, IL.

96. Varenberg, M., et al., *Assessing workability of greased bearings after long-term storage.* Friction, 2019. **7**(5): p. 489-496.

97. Ueda, J., *Mechanisms*, in *ME 6407 - Robotics, Lecture 7*. 2019, Georgia Institute of Technology.

98. *A Dictionary of Physics*. 2009: Oxford University Press.

99. Maung, M.M., M.M. Latt, and C.M. Nwe, *DC Motor Angular Position Control using PID Controller with Friction Compensation.* International Journal of Scientific and Research Publications (IJSRP), 2018. **8**(11).

100. *Advanced Digital Motor Controller User Manual*, in *RoboteQ HDC-2460 User Manual*. 2019, Nidec Motor Corporation.

101. Asato, K.T., et al., *SMARTWheels: development and testing of a system for measuring manual wheelchair propulsion dynamics.* IEEE Trans Biomed Eng, 1993. **40**(12): p. 1320-4.

102. Guo, L., et al., *Validation of a biofeedback system for wheelchair propulsion training.* Rehabil Res Pract, 2011. **2011**: p. 590780.

103. Koontz, A.M., et al., *Comparison between overground and dynamometer manual wheelchair propulsion.* J Appl Biomech, 2012. **28**(4): p. 412-9.

104. Hurd, W.J., et al., *Wheelchair propulsion demands during outdoor community ambulation.* J Electromyogr Kinesiol, 2009. **19**(5): p. 942-7.

105. Cowan, R.E., *Manual Wheelchair Propulsion in Older Adults*, in *School of Health and Rehabilitation Sciences*. 2007, University of Pittsburgh.

106. Vegter, R.J., et al., *Variability in bimanual wheelchair propulsion: consistency of two instrumented wheels during handrim wheelchair propulsion on a motor driven treadmill.* J Neuroeng Rehabil, 2013. **10**: p. 9.

107. Ensminger, G.J., R.N. Robertson, and R.A. Cooper. *A model for determining 3-D upper extremity net joint forces and moments during wheelchair propulsion*. in *Proceedings of 17th International Conference of the Engineering in Medicine and Biology Society*. 1995.

108. Cooper, R.A., et al., *2-Dimensional Kinetic-Analysis of Manual Wheelchair Propulsion with an Improved Smart Wheel.* Proceedings of the Annual International Conference of the Ieee Engineering in Medicine and Biology Society, Vol 14, Pts 1-7, 1992. **14**: p. 1544-1545.

109. Ojeda, M. and D. Ding, *Temporal parameters estimation for wheelchair propulsion using wearable sensors.* Biomed Res Int, 2014. **2014**: p. 645284.

110. Wellek, S., *Testing statistical hypotheses of equivalence and noninferiority*. 2nd ed. 2010, Boca Raton: CRC Press. xvi, 415 p.

111. Snow, M.P., et al., *Comparing New Designs with Baselines.* Ergonomics in Design: The Quarterly of Human Factors Applications, 2016. **7**(4): p. 28-33.

112. Lui, J., et al., *Mechanical efficiency of two commercial lever-propulsion mechanisms for manual wheelchair locomotion.* J Rehabil Res Dev, 2013. **50**(10): p. 1363-72.

113. Pavlidou, E., et al., *Rolling resistance and propulsion efficiency of manual and power-assisted wheelchairs.* Medical Engineering & Physics, 2015. **37**(11): p. 1105-1110.

114. Hilbers, P.A. and T.P. White, *Effects of wheelchair design on metabolic and heart rate responses during propulsion by persons with paraplegia.* Phys Ther, 1987. **67**(9): p. 1355-8.

115. Bascou, J., et al., *A method for the field assessment of rolling resistance properties of manual wheelchairs.* Comput Methods Biomech Biomed Engin, 2013. **16**(4): p. 381-91.

116. Hoffman, M.D., et al., *Assessment of wheelchair drag resistance using a coasting deceleration technique.* American Journal of Physical Medicine & Rehabilitation, 2003. **82**(11): p. 880-889.

117. van der Slikke, R.M.A., et al., *Wheelchair Mobility Performance Enhancement by Changing Wheelchair Properties: What Is the Effect of Grip, Seat Height, and Mass?* Int J Sports Physiol Perform, 2018. **13**(8): p. 1050-1058.

118. Bednarczyk, J.H. and D.J. Sanderson, *Limitations of kinematics in the assessment of wheelchair propulsion in adults and children with spinal cord injury.* Phys Ther, 1995. **75**(4): p. 281-9.

119. Sprigle, S., *On "impact of surface type, wheelchair weight, and axle position on wheelchair propulsion by novice older adults".* Arch Phys Med Rehabil, 2009. **90**(7): p. 1073-5.

120. Alcoléa, V., et al. *Effect of Added Mass Location on Manual Wheelchair Propulsion Forces*. in *IHSED 2019*. 2020. Cham: Springer International Publishing.

121. Caspall, J.J., et al., *Changes in inertia and effect on turning effort across different wheelchair configurations.* J Rehabil Res Dev, 2013. **50**(10): p. 1353-62.

122. Cohen, J., *Statistical power analysis for the behavioral sciences*. 2nd ed. 1988, Hillsdale, NJ: Lawrence Earlbaum Associates.

123. Silva, L.C., et al., *A lateral dynamics of a wheelchair: identification and analysis of tire parameters.* Comput Methods Biomech Biomed Engin, 2017. **20**(3): p. 332-341.

124. Brubaker, C.E., *Wheelchair prescription: an analysis of factors that affect mobility and performance.* J Rehabil Res Dev, 1986. **23**(4): p. 19-26.

125. *2017 Part B National Summary Data File*, C.f.M.a.M. Services, Editor. 2017, American Medical Association: Baltimore, MD.

126. *2010 Part B National Summary Data File*, C.f.M.a.M. Services, Editor. 2010, American Medical Association: Baltimore, MD.

127. Watanabe, L., *Justify It! K0005 Manual Chairs*, in *Mobility Management*. 2014, 1105 Media, Inc.

128. *Cracking the Codes: Manual wheelchair definitions*, in *Mobility Management*. 2019, 1105 Media, Inc.

129. Parziale, J.R., *Standard V Lightweight Wheelchair Propulsion in Spinal-Cord Injured Patients.* American Journal of Physical Medicine & Rehabilitation, 1991. **70**(2): p. 76-80.

130. Loane, T.D. and R.L. Kirby, *Static rear stability of conventional and lightweight variable-axle-position wheelchairs.* Arch Phys Med Rehabil, 1985. **66**(3): p. 174-6.

131. Oliveira, N., et al., *Kinematics and pushrim kinetics in adolescents propelling high-strength lightweight and ultra-lightweight manual wheelchairs.* Disabil Rehabil Assist Technol, 2019. **14**(3): p. 209-216.

132. Bascou, J., et al., *Turning resistance of a manual wheelchair: a theoretical study.* Comput Methods Biomech Biomed Engin, 2014. **17 Suppl 1**(sup1): p. 94-5.

133. Chénier, F., P. Bigras, and R. Aissaoui. *A new dynamic model of the manual wheelchair for straight and curvilinear propulsion*. in *Rehabilitation Robotics (ICORR), 2011 IEEE International Conference on*. 2011. IEEE.

134. Cooper, R.A., *A systems approach to the modeling of racing wheelchair propulsion.* J Rehabil Res Dev, 1990. **27**(2): p. 151-62.

135. Hughes, B., B.J. Sawatzky, and A.T. Hol, *A comparison of spinergy versus standard steel-spoke wheelchair wheels.* Arch Phys Med Rehabil, 2005. **86**(3): p. 596-601.

136. Chan, F.H.N., et al., *The effect of caster types on global rolling resistance in manual wheelchairs on indoor and outdoor surfaces.* Assist Technol, 2018. **30**(4): p. 176-182.

137. Chenier, F. and R. Aissaoui, *Effect of wheelchair frame material on users' mechanical work and transmitted vibration.* Biomed Res Int, 2014. **2014**: p. 609369.

138. Fitzgerald, S.G., et al., *Comparison of fatigue life for 3 types of manual wheelchairs.* Arch Phys Med Rehabil, 2001. **82**(10): p. 1484-8.

139. Gebrosky, B., et al., *Comparing the performance of ultralight folding manual wheelchairs using standardized tests.* Disabil Rehabil Assist Technol, 2020: p. 1-10.

140. Sugawara, A.T., et al., *Abandonment of assistive products: assessing abandonment levels and factors that impact on it.* Disabil Rehabil Assist Technol, 2018. **13**(7): p. 716-723.

141. Kwarciak, A.M., R.A. Cooper, and S.G. Fitzgerald, *Curb descent testing of suspension manual wheelchairs.* J Rehabil Res Dev, 2008. **45**(1): p. 73-84.

142. Dziechciowski, Z. and M. Kromka-Szydek, *Vibration Transmitted to the Human Body during the Patient's Ride in a Wheelchair.* Archives of Acoustics, 2017. **42**(1): p. 137-148.

143. Hashizume, T., et al., *Study on the Wheelchair User's Body Vibration and Wheelchair Driving Torque when Wheelchair is Ascending/Descending the Boundary Curb between Pavement and Roadway.* 2008 Proceedings of Sice Annual Conference, Vols 1-7, 2008: p. 1214-+.

144. Garcia-Mendez, Y., et al., *Health risks of vibration exposure to wheelchair users in the community.* J Spinal Cord Med, 2013. **36**(4): p. 365-75.

145. Davis, R., et al., *The effects of whole body vibration on bone mineral density for a person with a spinal cord injury: a case study.* Adapt Phys Activ Q, 2010. **27**(1): p. 60-72.

146. Bramble, D.M. and D.E. Lieberman, *Endurance running and the evolution of Homo.* Nature, 2004. **432**(7015): p. 345-52.

147. Cunningham, C.B., et al., *The influence of foot posture on the cost of transport in humans.* J Exp Biol, 2010. **213**(5): p. 790-7.